A COMPREHENSIVE STUDY OF ESTERIFICATION AND HYDROLYSIS OF METHYL ACETATE IN SIMULATED MOVING BED SYSTEMS

YU WEIFANG

NATIONAL UNIVERSITY OF SINGAPORE

2003

A COMPREHENSIVE STUDY OF ESTERIFICATION AND HYDROLYSIS OF METHYL ACETATE IN SIMULATED MOVING BED SYSTEMS

YU WEIFANG
(B. Eng., Zhejiang University, China)

A THESIS SUBMITTED

FOR THE DEGREE OF DOCTOR OF PHILOSOPHY

DEPARTMENT OF CHEMICAL&ENVIRONMENTAL ENGINEERING

NATIONAL UNIVERSITY OF SINGAPORE

2003

Acknowledgements

With pleasure and gratitude I wish to express my appreciation to my research advisors, Prof. Ajay Kumar Ray and Prof. Kus Hidajat, for their enthusiasm, encouragement, insight, suggestions and support throughout the course of this research project.

I am always grateful to Prof. Massimo Morbidelli, the department of chemistry, ETH, Zurich, for his encouragement and invaluable advices and suggestions. Thanks also to the graduate students in his research group, who made my stay in ETH very enjoyable.

I am also thankful to Prof. Marc Garland and Prof. Sibudjing Kawi, the members of my Ph.D. committee, for rendering me suggestions and guidance. I wish to express my gratitude to Mdm. Chiang, Miss Ng, Mdm. Jamie, Mdm. Li Xiang, Mr. Boey, Mr. Mao Ning and the SVU team for their help with my experimental and computational work. I thank all my lab-mates and all my friends both in Singapore and abroad, who have enriched my life personally and professionally. The Research Scholarship from the National University of Singapore is also gratefully acknowledged.

I cannot find any words to thank my husband, Xu Jin, for his love, encouragement, patience, help and support through the years of my graduate study. Finally, to my parents goes my eternal gratitude for their boundless love, support and dedication.

Table of Contents

Summary

The simulated moving bed reactor (SMBR) in which chemical reaction and chromatographic separation take place concurrently is gaining significant attention in recent years. The coupling of two unit operations in SMBR may reduce the capital and operating costs of the process and enhance the conversion of equilibrium-limited reactions. Several studies show that substantial improvements in the process performance could be achieved in SMBR compared to fixed bed operation, and its application to some fine chemical and pharmaceutical industry is promising. However, due to the complexity of SMBR process, there is very few application of SMBR in the chemical industry. A more detailed understanding and criteria for the design and operating of SMBR are needed before successful implementation on industrial scale can be achieved.

In this research work, the reversible reaction of acetic acid and methanol catalyzed by Amberlyst 15 ion exchange resin was considered. The performance of SMBR was studied theoretically and experimentally for deeper insight into the behavior of the process. A new optimization and design strategy, multi-objective optimization, was proposed to improve the performance of SMBR and its modification, reactive Varicol, which adopts the non-synchronous shift of the inlet and outlet ports instead of the synchronous one used in SMBR, for the model reaction system.

The adsorption equilibrium constants, dispersion coefficients and kinetic parameters were first determined for the synthesis and hydrolysis of methyl acetate, corresponding to the different mobile phases, methanol or water. They were determined semi-empirically by fitting the experimentally measured breakthrough curves with the predictions from the single column chromatographic reactor model, which was developed based on equilibrium-dispersive model, quasi-homogeneous reaction kinetics and linear adsorption isotherm. Thereafter, The single column

chromatographic reactor model was extended to describe the behavior of SMBR unit by imposing the outlet concentration of one column as the inlet condition for the next column downstream, while incorporating the cyclic port switching and additional feed or withdrawal streams. The SMBR model predicted results for the synthesis of methyl acetate were verified experimentally at different operating conditions, and parametric analysis was carried out based on the verified model to systematically investigate the effects of process parameters on the performance of SMBR. The experimental as well as theoretical results clearly demonstrate that it is possible to obtain improved conversion and product purity for methyl acetate synthesis in SMBR, and it also reveals that there is a complex interplay of the operating parameters on the reactor performance. Some of the parameters act in conflicting ways. When one objective function is improved, the other is worsened.

Therefore, comprehensive multi-objective optimization study was performed for the synthesis and hydrolysis of methyl acetate using the experimentally verified model developed in this study to determine appropriate design and operating conditions for successful implementation of SMBR on industrial scale. The optimization problems were formulated both for the performance enhancement of an existing unit and the optimal design of a new plant. A robust, non-traditional global optimization technique known as Non-dominated Sorting Genetic Algorithm (NSGA) was used in obtaining the optimal solutions. The applicability of Varicol to reaction system was also investigated. It was found that reactive Varicol performs better than SMBR due to its increased flexibility in column distribution.

List of Tables

List of Figures

Nomenclatures

A	acetic acid
C	concentration in liquid phase
d	diameter
D	apparent axial dispersion coefficient; desorbent
E	methyl acetate; activation energy
F	error (objective) function
ΔG	change in Gibbs free energy of reaction
H	height equivalent of a theoretical plate
HOAc	acetic acid
ΔH	heat of adsorption
k	reaction rate constant, mass transfer coefficient
K	reaction equilibrium constant; adsorption constant; Langmuir parameter
L	length
m	flow rate ratio parameter
M	methanol
MeOAc	methyl acetate
MeOH	methanol
n	mole number; order of reaction
N	plate number; sorption capacity; number of switching; total number of columns
p	number of columns in section P
P	purity; section P
PrE	productivity of MeOAc at the raffinate port
PurE	purity of MeOAc at the raffinate port

PurW	purity of water at the extract port
Q	volumetric flow rate; section Q
q	concentration in polymer phase; swelling ratio; number of columns in section Q
r	number of columns in section R
R	reaction rate; resin particle radius; section R
s	number of columns in section S
S	section S, selectivity
t	time
T	temperature
ΔS	entropy change
u	superficial fluid phase flow rate
V	volume; velocity
W	water; weight
x	vector of fitted parameters; mole fraction
X	conversion
Y	yield
z	axial coordinate

Greek Symbols

α	fraction of feed
β	fraction of raffinate
χ	column configuration, dimensionless length
ε	void fraction
δ	phase ratio
ϕ	section
γ	fraction of desorbent

ζ	pseudo solid phase velocity
ν	stoichiometric coefficient of component
σ	relative carrying capacity
ρ	density of polymer resin

Subscripts and Superscripts

A	acetic acid
ap	apparent
b	backward
col	column
D	desorbent stream
e	equilibrium
E	methyl acetate; eluent
Ex	extract stream
exp	experiment
f	feed, forward
F	feed stream
g	gas, carrier
h	hydrolysis
HOAc	acetic acid
i	component i
j	jth data point; jth application; section j
k	M or W (mobile phase)
L	liquid phase
m	model; number of data points; mass transfer
M	methanol
MeOAc	methyl acetate

N	number, switching period
o	initial; standard; inlet
p	width of rectangular pulse; section P
P	polymer phase
q	section Q
r	section R
Ra	raffinate stream
s	synthesis; switching; section S; solid
w	water

Chapter 1 Introduction

Since separation process is indispensable for nearly every chemical manufacturing operation in order to obtain desired high purity products, integration of chemical reaction and separation into one single unit may significantly improve the economics and efficiency of process industries. Compared with the traditional process design of reaction and separation in series, the coupling of the two unit operations in one apparatus leads to lower capital investment and energy costs. Moreover, for reversible reactions, conversion can be enhanced beyond thermodynamic equilibrium by in-situ separation of the products resulting in better yield and selectivity.

The advantages of combining chemical reaction and separation have been exploited for a long time in the petrochemical industry with reactive distillation processes, and reactive distillation has now become the process of choice for a number of industry applications. However, one drawback of reactive distillation is that it is not applicable to the reaction system where the components involved are non-volatile or heat-sensitive, as this is the case in some fine chemical and pharmaceutical applications. An alternative integrated process for producing high purity products is chromatographic reactor, which couples chemical reaction with chromatographic separation. The driving force for chromatographic separation is the differences in adsorption affinity of the different components involved on the stationary phase. The utilization of chromatographic processes in reaction system is competitive to the use of other separation processes, such as membranes, extraction or crystallization, due to its superior separating power, versatility, relatively low cost and mild operating conditions. Additionally, if a chromatographic separation had been used for purification of the products before, lengthy work for screening a suitable adsorbent is omitted (Fricke et al., 1999a). Only the catalyst has to be chosen before the design of

the process. Consequently, the cost of process development is significantly reduced. Furthermore, chromatographic reactor seems especially attractive due to its potential applicability to life science products, which are considered to be the most promising market for the near future.

Since it was developed in the early 1960's, chromatographic reactor has been used for analytical purposes as well as for preparative applications in either batch or continuous operation. In the recent years, more attention has been focused on the continuous mode, which offers advantages of high efficiency in utilizing the stationary phase inventory and small amount of eluent consumption over the batch mode. Perhaps, the simplest way to realize an efficient continuous process would be a countercurrent flow of solid and fluid phase (true countercurrent moving bed reactor), which maximizes the average driving force. Both theoretical and experimental investigations have been carried out on the performance of true countercurrent moving bed chromatographic reactor (Viswanathan and Aris, 1974a, 1974b; Takeuchi and Uraguchi, 1976a, 1976b, 1977, 1979; Cho et al., 1982; Song and Lee, 1982; Petroulas et al., 1985a, 1985b; Fish et al., 1986, 1988, 1989). The conversion of reversible reaction much greater than equilibrium with high product purity was reported in these studies.

However, the actual movement of the solid phase in a true countercurrent moving bed chromatographic reactor causes a number of problems when scaling up to a large column diameter, such as mechanical difficulties of moving the solid, adsorbent attrition, fines removal, expansions of the bed, channeling in the reactor etc. In order to circumvent the problems associated with the handling of solids, the simulated moving bed technology (SMB), introduced by UOP in 1960s (Broughton and Gerhold, 1961) is used as a promising approach. In SMB technology, the countercurrent movement of the fluid phase toward the solid phase is mimicked by switching the introduction and

withdrawal ports periodically and simultaneously along a series of fixed columns in the direction of the fluid flow. For ease of operation, the columns are actually divided into sections (or zones). The number of columns within each section and total number of columns are adjustable depending on the design of the system for any particular applications. Recently, SMB was modified into Varicol process (Ludemann-Hombourger et al., 2000) for chiral separation by non-synchronously switching the inlet and outlet ports during a global switching period. Therefore, the column configuration (number of columns in any particular section) varies at different sub-time intervals in the Varicol process. This leads to more flexibility in operation in the Varicol process compared to more rigid conventional SMB process, and therefore, allows better utilization of the stationary phase. Varicol also provides opportunity for coupling reactions.

Several studies have been performed to evaluate the applicability of the simulated countercurrent moving bed chromatographic reactor to reaction systems (Hashimoto et al., 1983; Ray et al., 1990, 1992, 1994, 1995a, 1995b; Mazzotti et al., 1996b; Kawase et al., 1996; Meurer et al., 1996; Ching et al., 1997; Zhang et al., 2001b). These works show that the advantages of high product purity and favorable equilibrium shifts in a true countercurrent moving bed chromatographic reactor can be retained in SMBR and its application to some fine chemical and pharmaceutical industry is promising. Nevertheless, due to the complexity of SMBR process, there is very few application of SMBR in the chemical industry. A more detailed understanding and criteria for operating a SMBR is needed before successful implementation on industrial scale can be achieved. Especially, the optimal design and operating parameters are very essential to evaluate the economic potential of SMBR and therefore increase its competitive ability to other processes. Although a few studies have been reported on the optimization of SMBR (Migliorini et al., 1999b; Dunnebier

et al., 2000; Azevedo et al., 2001; Lode et al., 2001), they only involve single objective optimization except that reported by Zhang et al. (2002), which is usually not sufficient for the real-life design of complex SMBR system, since the operating variables influence the performance of SMBR usually in conflicting ways. This leads to any desirable change in one objective function results in an unfavorable change in another objective function. Therefore, the simultaneous optimization of multiple objective functions is very important for the design of SMBR process.

In principle, multi-objective optimization is very different from single objective optimization. In single objective optimization, one attempts to obtain the best solution, which is usually the global minimum or the global maximum. In the case of multiple objectives, there may not exist one solution that is best with respect to all objectives. The goal of multi-objective optimization is to obtain a set of equally good solutions, which are known as Pareto optimal solutions. In a set of Pareto solutions, no solution can be considered better than any other solutions with respect to all objective functions, since one solution is better than other in one objective, but is worse in the others. So the selection of any optimal solution from a Pareto set will depend on auxiliary information. However, by narrowing down the choices, the Pareto sets does provide decision makers with useful guidance in selecting the desired operating conditions (called the preferred solution) from among the (restricted) set of Pareto optimal solutions, rather than from a much larger number of possibilities.

In earlier years, multi-objective optimization problems were usually solved using a single scalar objective function, which was a weighted-average of the several objectives (‘scalarization’ of the vector objective function). This process allows a simpler algorithm to be used, but unfortunately, the solution obtained depends largely on the values assigned to the weighting factors used, which is done quite arbitrarily. An even more important disadvantage of the scalarization of the several objectives is that

the algorithm may miss some optimal solutions, which can never be found, regardless of the weighting factors chosen. This happens if the non-convexity of the objective function gives rise to a duality gap (Deb, 2001; Fonseca and Fleming, 1998). Several methods are available to solve multi-objective optimization problems, e.g., the e-constraint method (Chankong and Haimes, 1983), goal attainment method (Fonseca and Fleming, 1998) and the non-dominated sorting genetic algorithm (NSGA) (Goldberg, 1989, Srinivas and Deb, 1995; Deb, 1995). In this study we use NSGA to obtain the Pareto set. This technique offers several advantages (Bhaskar, 2000a; Deb 2001), as for example: (a) its efficiency is relatively insensitive to the shape of the Pareto optimal front, (b) problems with uncertainties, stochasticities, and with discrete search spaces can be handled efficiently, (c) the 'spread' of the Pareto set obtained is excellent (in contrast, the efficiency of other optimization methods decides the spread of the solutions obtained), and (d) it involves a single application to obtain the entire Pareto set (in contrast to other methods, e.g., the e-constraint method, which needs to be applied several times over).

In this dissertation, the performance of SMBR was investigated by numerical simulation as well as experimentally for the reversible reaction of acetic acid and methanol catalyzed by Amberlyst 15. The novel optimization and design strategy, multi-objective optimization using NSGA, was applied to improve the performance of SMBR and its modification, reactive Varicol for the model reaction system. The objective of this research work is to obtain deeper insight into the behavior of the process and propose a new optimization and design strategy to successfully implement SMBR on industrial scale.

This thesis is organized into eight chapters. In Chapter 2, the background and applications of chromatographic reactor are described. Several design strategies and optimization work on the simulated moving bed systems are reviewed.

Chapter 3 presents the determination of adsorption equilibrium constants, dispersion coefficients, and kinetic parameters for the synthesis and hydrolysis of methyl acetate catalyzed by Amberlyst 15. The adsorption and kinetic parameters were determined corresponding to two different mobile phases, methanol or water, which is required for the synthesis or hydrolysis of methyl acetate respectively. Experiments were conducted in a packed bed reactor in the temperature range 313-323 K using a rectangular pulse input. A mathematical model for the single column packed bed reactor was developed based on equilibrium-dispersive model, quasi-homogeneous reaction kinetics and liner adsorption isotherm. The adsorption and kinetic parameters were determined by tuning the simulation results to fit the experimentally measured breakthrough curves of acetic acid, water (or methanol) and methyl acetate using a state-of-the-art optimization technique, genetic algorithm. The mathematical model was further validated using the tuned parameters to predict experimental results at different feed concentrations and flow rates. The kinetics was obtained under conditions free of both external and internal mass transfer resistance. The computed parameters were found to predict experimental elution profiles for both batch and plug flow reactor reasonably well.

Chapter 4 covers the multi-objective optimization of SMBR for the synthesis of methyl acetate based on the numerical model reported by Lode et al. (2001). The performance of SMBR was optimized aiming at simultaneous maximization of productivity and purity, simultaneous maximization of productivity and minimization of desorbent consumption or simultaneous maximization of productivity and purity together with minimization of desorbent consumption. The optimal configuration of 5-column unit and the optimal acetic acid feed mole fraction in terms of maximum productivity and purity were determined. The effects of conversion constraint, reaction

rate constant and the eluent flow rate on the Pareto optimal solutions were also investigated.

In Chapter 5, the performance of SMBR for the synthesis of methyl acetate catalyzed by Amberlyst 15 was evaluated numerically and experimentally. A rigorous mathematical model was developed to describe the dynamic behavior of SMBR and was validated experimentally at different operating conditions. It was found that the model could predict experimental results quite well. The high yield and purity of methyl acetate and nearly complete conversion of the limiting reactant, acetic acid, could be achieved in SMBR by selecting proper operating conditions. The effect of various process parameters such as switching time, feed, eluent flow rate, etc. on the behavior of SMBR was also investigated systematically.

Chapter 6 aims at optimizing the performance of SMBR and its modification, Varicol process based on the experimentally verified mathematical model for the synthesis of methyl acetate ester illustrated in Chapter 5. Multi-objective optimization was first performed for an existing SMBR experimental setup and optimum results were verified experimentally. Thereafter, few other two and three objective optimization studies were performed for SMBR unit at the design stage. The applicability of Varicol to reaction systems, and the effect of variable feed flow rate on the optimum performance of SMBR were also investigated. It was observed that reactive Varicol performs better than SMBR due to its increased flexibility in column distribution.

In Chapter 7, the performance of SMBR and reactive Varicol process was optimized for the hydrolysis of methyl acetate. The optimization problems of interest in this application considered are a) simultaneous maximization of purity of raffinate and extract streams. b) maximization of yield of acetic acid in raffinate stream and yield of methanol (MeOH) in extract stream.

Finally, in Chapter 8 conclusion from the present work and recommendations for the future work are presented.

In this work, the adsorption equilibrium constants, dispersion coefficients and kinetic parameters were determined for the synthesis and hydrolysis of methyl acetate, corresponding to the different mobile phase, methanol or water. The mathematical model describing the dynamic behavior of the SMBR was developed and verified experimentally at various operating conditions. A comprehensive multi-objective optimization study of SMBR and reactive Varicol was performed for the synthesis and hydrolysis of methyl acetate using the validated model to determine the optimal design and operating parameters in order to successfully implement them on industrial scale. It was found that the optimal performance of reactive Varicol is better than that of SMBR.

Chapter 2 Literature Review

2.1 Introduction to Chromatography

Separation process is essential for nearly every chemical manufacturing operation in order to recover and purify the desired product. The process is difficult to achieve as it is the opposite of mixing, a process favored by the second law of thermodynamics. Consequently, in most cases, the efficiency of the separation process has a significant impact on both the quality and the cost of products. Distillation has become a reference operation against which alternative separation technologies compared, owing to its simplicity and extensive application. However, we often encounter situations involving separation of chemically similar components, especially amino acids, proteins, complex hydrocarbons and other heat sensitive substances. In such cases, the traditional separation methods based on the physiochemical properties such as distillation, crystallization and extraction are often not applicable. Adsorption offers a suitable approach in dealing with such difficult separations, due to the fact that adsorbents are known to be much more selective in their affinity for various materials than any known solvents.

Chromatography is a separation process driven by the differences in adsorption affinity of the different components involved. It was discovered in 1906 by the Russian botanist, Mikhail Tswett (1872-1919), who used this technique to separate various plant pigments by passing solutions of them through glass columns packed with calcium carbonate. The separated species appeared as colored bands on the column, and therefore Mikhail Tswett named this method as the combination of Greek chroma, meaning “color” and graphein, meaning “to write”. Chromatography can be defined as the unit operation where the separation of solutes occurs due to the differential migration of the solutes through a system of two phases, the mobile and the stationary

phase. Compared to other separation technologies, chromatography offers advantages of superior separating power, high selectivity, wide versatility, low energy cost and mild operating conditions and it is now widely used either for analytical purposes or on preparative scale. Apart from its widespread application to separation, chromatography also provides opportunity for coupling reactions.

Combination of chemical reaction and separation into one single unit may significantly improve the course of reaction and separation efficiency (Fricke et al., 1999a). In addition to financial benefits achieved through process intensification, the integrated reactor-separator also enhances conversions of reversible reactions beyond equilibrium limit by removing one or more of the products from the reaction zone and thus shifting the equilibrium. Moreover, the selectivity of a competitive reaction network can be increased greatly by separating the reactants that may lead to parasite products. The advantages of coupling chemical reaction and separation have been exploited for a long time in petrochemical industry with reactive distillation, which couples reaction and distillation in a single unit, and reactive distillation has become the choice for a number of applications. However, one drawback of reactive distillation is that it is not suitable for the reaction systems where the components involved are non-volatile or heat-sensitive, such as in some fine chemical and pharmaceutical applications. An alternative promising integrated process is chromatographic reactor, which couples chemical or biochemical reaction with chromatographic separation.

2.2 Batch Chromatographic Reactor

In the early 1960s, the idea of batch chromatographic reactor was developed by Roginskii et al. (1961, 1962) in the USSR and Magee (1963) in the USA. Figure 2.1 illustrates the operating principle of a batch chromatographic reactor for a reversible decomposition reaction ($A \leftrightharpoons B + C$). The column is packed with mixed catalyst and

adsorbent as the solid phase. Reactant A is introduced as a sharp pulse at one end of the reactor together with desorbent. As it migrates along the column, A reacts to form products B and C. The different adsorption affinities of component B and C on the stationary phase leads to different migration velocities and therefore the products are separated from each other. Separation of the products allows equilibrium limited reaction to proceed toward completion while at the same time obtaining products in high purity.

A + Desorbent B C

Figure 2.1 Operating principle of the batch chromatographic reactor (Fricke et al. 1999b)

Since its invention, the batch chromatographic reactor has been investigated both experimentally and theoretically by many researchers. Gore (1967) compared the performance of a chromatographic reactor under the condition of cyclic feed composition with a steady flow reactor based on simulation. He reported that chromatographic reactor gave a better conversion but needed more catalyst per unit feed flow than that for a steady flow reactor to reach equilibrium.

Langer and Patton (1973) defined chromatographic reactor as "a chromatographic column in which a solute or several solutes are intentionally converted, either partially or totally, to products during their residence in the column. A solute reactant or reactant mixture is injected into the chromatographic reactor as a pulse. Both conversion to product and separation take place in the course of passage

through the column; the device is truly both a reactor and a chromatography." They also defined (1969, 1973) and characterized a general ideal chromatographic reactor, which exhibits the following features:

i) a pulse of reactants reacts as it travels through the column, and the reaction products are instantaneously separated from the reactant and, in many cases, also from each other.

ii) the rates of mass transfer and adsorption are fast and not limiting. i.e. reaction is limiting

iii) the adsorption isotherms are linear.

iv) axial dispersion and band spreading are negligible.

v) the column is homogeneous in composition. i.e. the mobile phase is incompressible, and the stationary phase is uniformly packed.

vi) the column operates isothermally, and heat effects are negligible.

Chu and Tsang (1971) studied the behavior of a chromatographic reactor by use of Langmuir-Hinshelwood adsorption isotherm to account for the competitive adsorption on the catalyst surface.

Wetherold et al. (1974) investigated the liquid phase hydrolysis reaction of methyl formatted. Conversions in excess of equilibrium were achieved and their results were comparable with those obtained from numerical solutions of the mathematical model using Freundlich adsorption isotherm.

Schweich and Villermaux (1978) proposed a model assuming a fast reaction rate compared to the residence times of the components in the column and suggested that the optimal operating parameters maximizing the yield depend only on the reaction data obtained without any chemical reaction. They compared the experimentally measured conversion of dehydrogenation of cyclohexane with that calculated from the

mathematical model. It was shown (1980, 1982) that an accurate description of the adsorption isotherm and for gas phase reactions variation in volumetric flow rate due to chemical expansion has to be taken into account in order to improve the predictions of the model.

The batch chromatographic reactor has also been used for analytical purpose to determine reaction rate constants together with thermodynamic properties for the solute-solvent systems, when supported liquids are used as stationary phases. This is because it needs only small amount of reactants and requires less experimental time than the classic steady state procedures. A comprehensive review on the analytical application of batch chromatographic reactor has been reported by Langer and Patton (1969, 1973).

However, the batch operation of chromatographic reactors gives rise to several drawbacks, such as low throughput resulting from periodically injection of reactants, low efficiency in utilizing the stationary phase inventory and large eluent consumption leading to high dilution of the products. In order to overcome these problems, continuous chromatographic reactor was developed in the 1970s.

2.3 Continuous Chromatographic Reactor

Since the mid of 1970s, more attention has been paid to the continuous chromatographic reactor due to the inherent advantages of continuous operation, such as constant product quality, limited or no recycling, better utilization of the available mass transfer area. There are mainly two types of continuous chromatographic reactors examined till now, annular rotating chromatographic reactor and countercurrent chromatographic reactor.

2.3.1 Annular Rotating Chromatographic Reactor

Figure 2.2 shows a schematic diagram of the rotating cylindrical annulus reactor. The stationary phase is contained between the walls of two axially concentric cylinders. This unit is rotating about its axis while a continuous feed stream is introduced into it at a fixed point. The carrier is fed uniformly along the whole circumsection. Chemical reaction occurs in the stationary phase, and the reactant and products are swept in the axial direction by the carrier while the adsorbed components follow spiral paths of different pitch depending on their adsorption affinity. The more strongly adsorbed component travels longer time with the stationary phase and thus has larger angle compared to the fixed feed port. Therefore, different species can be collected at different angular position along the circumsection at the bottom of the cylinder.

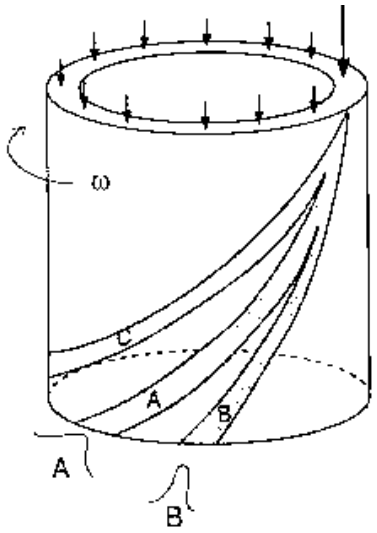

Figure 2.2 Schematic diagram of the rotating annulus reactor (Carr, 1993)

In 1949, Martin, who was the first one, proposed a design of rotating cylindrical annulus chromatography for continuous separation. In 1980s, Cho et al. (1980) applied

the rotating annulus chromatography to the hydrolysis of methyl formate. They found that conversion of the model reaction was significantly greater than the chemical equilibrium one and the developed numerical model predicted experimental results quite well, except when the experiment proceeds too long. They suggested that this discrepancy was due to the deactivation of activated charcoal. More recently, Sarmidi & Barker (1993a, 1993b) studied the saccharification of starch and the inversion of sucrose in the reactive rotating annulus chromatography.

Carr (1993) suggested several criteria for the selection of suitable reaction to be conducted in the rotating annulus chromatographic reactor. He stated that the reaction should be of the type A ⇋ B + C, and the forward reaction rate should be sufficient large to keep the reactor at reasonable length. Furthermore, the reaction equilibrium constant should be small enough to allow the significant improvement in yield. Finally, the adsorptions of A, B, and C should differ largely for good separation.

2.3.2 Countercurrent Chromatographic Reactor

2.3.2.1 True Countercurrent Moving Bed Reactor

In a true countercurrent moving bed chromatographic reactor (CMCR), the solid phase is introduced at the top of the reactor and moves downward under gravity, while the fluid phase is introduced at the bottom of the column and moves upward. The reactant is fed either at the bottom or in the middle of the reactor. By selecting appropriate operation parameters, the more strongly adsorbed chemical species involved in the process will travel downward with the solid phase while the less adsorptive species will elute upward with the mobile phase, thus separation is achieved while reaction proceeds.

A sketch of a typical configuration of a CMCR is shown in Figure 2.3. The unit is divided into four distinct sections by the inlet and outlet ports. Due to the

introduction of feed and withdrawal of products, the mobile phase flow rate changes abruptly between sections while remaining constant within an individual section. The solid phase travels down through the reactor and is recycled to the top of the column. The solvent is fed at the bottom of the column, flows countercurrent to the solid phase. An equilibrium limited decomposition reaction ($A \leftrightharpoons B + C$) is considered to illustrate the working principle of the CMCR. The feed stream containing reactant A, which is diluted by solvent D, is introduced in the middle of the column between section 2 and section 3. Upon entry the reactor, some of reactant A migrates to section 3 carried by the mobile phase, some of adsorbed reactant A is also carried to section 2 by the solid phase movement. The reversible reaction occurs both in section 2 and section 3. Therefore, the strongly adsorbed product B and less adsorptive product C present in both sections. In section 2, the less adsorbed product C is gradually desorbed by the rising mobile phase. By properly adjusting the flow rates in section 2, it is possible to completely remove C from the solid phase before reaching the Extract port without simultaneously removing all of the adsorbed B. Similarly, in section 3, as the solid moves downward, it adsorbs B from the bulk mobile phase. Thus by selecting the appropriate flow rates, the complete removal of product B from the fluid phase can be accomplished before it reaches the Raffinate while C is not completely adsorbed.

Moreover, the flow rates in sections 2 and 3 should be adjusted not only to fulfill the requirements for the separation but also to satisfy the needs for allowing sufficient time for reactant A to be completely consumed. In sections 1 and 4, under the conditions of complete conversion and separation no reaction takes place. The function of these two sections is to regenerate the adsorbent (by removing product B from solid phase) and clean the solvent (by removing product C from the fluid phase) in order to enable the recycling of adsorbent and solvent respectively.

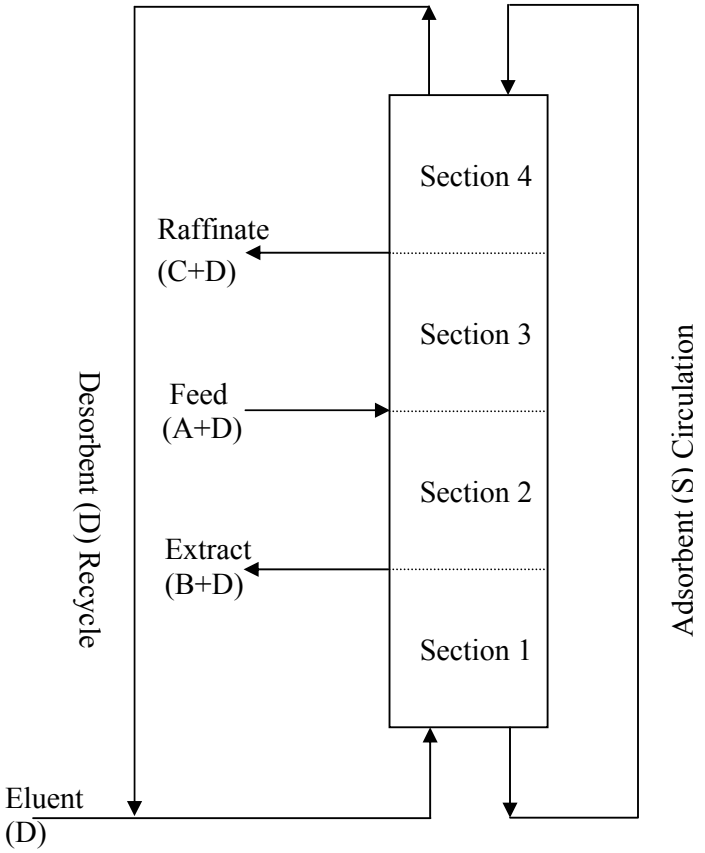

Figure 2.3 Typical configuration of a CMCR

The majority of the research to-date on the true countercurrent moving bed reactor has been concerned with the development of mathematical models. Table 2.1 summarizes the various investigations on the CMCR.

There are practical problems to be overcome in the design and operation of the CMCR. The actual movement of the solid phase in a CMCR causes a number of problems when scaling up to a large column diameter, such as mechanical difficulties of moving the solid, adsorbent attrition, fines removal, expansions of the bed, channeling in the reactor etc.

Table 2.1 Detailed description of the various investigations on CMCR

S.No.	System Investigated	Authors	Description of the work	Remarks
1	First order irreversible reaction	Viswanathan and Aris (1974a)	A mathematical model for CMCR was developed based on the assumption of isothermal operation, negligible dispersion, instantaneous desorption of the product, a Langmuir isotherm to describe adsorption of the reactant, and constant initial and boundary conditions. Under proper operating conditions, the model predicted complete conversion and pure product in a finite length of reactor.	A mathematical model for the prediction of CMCR performance was proposed. The steady state solutions and the development of steady state were studied by the method of characteristics.
		Viswanathan and Aris (1974b)	More general cases of finite adsorption rate and diffusion effect in the fluid phase were considered. The CMCR system could be described by one or two first order partial differential equations depending on whether the adsorption is at equilibrium or takes place at a finite rate.	Extensive mathematical study of the CMCR process was performed. The transient and steady state behavior of the solution were studied for the cases of finite adsorption rate and of adsorption equilibrium.
		Takeuchi and Uraguchi (1976a, 1976b)	A model for the prediction of CMCR performance was developed under the assumptions of isothermal operation, constant gas and solid velocity, sufficient long bed, linear adsorption isotherms, negligible axial dispersion and gas-solid mass transfer resistance. The separation conditions for a binary mixture and how they are affected by the presence of reaction were analyzed using the concept of the first absolute moment. The conversion in a CMCR fed from the bottom was found to be smaller than in a fixed bed of the same length.	In order to solve the model equations, a discontinuity was introduced arbitrarily for the product concentration profile at the top of the reactor. However, this assumption is not always true.

2	Reversible reaction	Song and Lee (1981)	A mathematical model was developed to describe the behavior of an isothermal CMCR for the hydrolysis of cellulose. The model predictions showed that yield was increased greatly (70%) compared with the maximum attainable (28%) in a tubular flow reactor at the same operating conditions. Yield and product concentration was observed to have inverse relationship.	Improvement in yields of hydrolysis of cellulose.
		Chou et al. (1982)	The idea model was defined as the isothermal, uniform flow, dispersionless adsorption equilibrium model. The separation effect of the reactor was found to be dependent on the carrying capacity of the solid phase relative to that of the fluid phase and the relative adsorption affinity of the components, as well as the feed conditions at the top and at the bottom of the column. The effects of axial dispersion and finite adsorption rates were also investigated. It was found that the overall conversion was enhanced by the dispersion effect as well as by the non-equilibrium adsorption for a sufficiently large value of the adsorption equilibrium constant. Both the axial dispersion and finite adsorption rate deteriorated product purity.	The work of Viswanathan and Aris was continued by Chou et al. to a reversible reaction of the type A? B with Langmuir adsorption isotherm for both A and B, other model assumptions remaining the same.

Petroulas et al. (1985a)	A modified CMCR process was proposed where the reactant was introduced on the side. The bottom part of the column could act as a stripping section to recover most of the reactant adsorbed on the solid phase. The modified CMCR performed better than a fixed bed reactor with respect to both product purity and conversion. The effects of finite adsorption rate and axial dispersion on the performance of CMCR were also investigated. Both finite adsorption rate and axial dispersion deteriorated product purity while conversion decreased when adsorption was slow but in the presence of axial dispersion it increased or decreased depending on the operating conditions.	CMCR was modified by introducing the feed on the side of the column.
Petroulas et al. (1985b)	Experimental study of hydrogenation of mesitylene to 1,3,5-trimethyl cyclohexane was carried out. Experimental apparatus: 7 ft long, ½ inch ID pyrex glass column, with a top and bottom reservoir for the solids. The feed position was varied to obtain different lengths for the reacting and rectifying section of he column. The experimental results showed products of higher purity than equilibrium prediction, and overall conversion comparable to a fixed bed reactor.	The performance of CMCR was investigated experimentally.
Fish et al. (1986)	Preliminary experimental results for the hydrogenation of 1,3,5-tryimethyl benzene were given. The design and construction of an improved countercurrent moving bed reactor was presented.	A new design of CMCR was reported.

Fish et al. (1988)	An experimental CMCR unit was interfaced with a laboratory microcomputer for data acquisition and computer control. The rapid, automated analysis of steady state concentration profiles for the CMCR gave information that can be compared with model predictions of reactor behavior.	Computer control and computer data acquisition for the CMCR.
Fish and Carr (1989)	The results of an experimental investigation of the performance of CMCR for the hydrogenation of 1,3,5-trimethylbenzene vapor at 190°C by Pt supported on 30–50 mesh Al_2O_3.was presented. The dependence of product purity and conversion on experimental conditions was investigated. A dispersionless, adsorption equilibrium model was presented for the two cases of a linear isotherm and a Langmuir isotherm. The trends of observed reactor behavior with changes in feed rate and feed position were satisfactorily accounted for by the models.	Experimental study of CMCR.
Takeuchi and Uraguchi (1978)	Mathematical models were developed for consecutive and reversible reactions in CMCR. The model predicted that the selectivity of consecutive reactions in CMCR could be improved compared with that in a fixed bed reactor and the conversion of reversible reaction could exceed that of chemical equilibrium.	Consecutive reactions were considered.

2.3.2.2 Simulated Countercurrent Moving Bed Reactor

In order to overcome the problems associated with the process of solid handling, the simulated moving bed technology (SMB), which has been successfully applied to petrochemical industry, is used as a promising approach. In the simulated moving bed technique, the countercurrent movement of the solid phase towards the fluid phase is mimicked by sequentially and simultaneously switching the inlet and outlet ports in the direction of the fluid phase. Therefore, In SMBR, the advantages of high product purity and favorable equilibrium shifts offer by the CMCR process are expected to be retained while a number of problems caused by the solid phase movement are avoided. There exist two main configurations of the SMBR process corresponding to the SMB system. One is the single column configuration, which employs one column subdivided into a number of interlinked compartments. The other one is the multiple column configuration, which consists of a number of columns connected in series. It was reported that the multiple configuration of the simulated countercurrent moving bed reactor is more suitable for laboratory investigations (Ray et al., 1990).

Recently, Adam et al. (1998) patented a novel separation process, Varicol, which showed a significant improvement over the SMB process without introducing any additional cost. In contrast with the SMB, Varicol process is based on a non-synchronous and unequal shift of the inlet/outlet ports. The operating principle of Varicol system was described, for the first time, in the work by Ludemann-Hombourger et al. (2000; 2002). The principle of (4-subinterval switching) Varicol operation during one switching period t_s is illustrated in Figure 2.4, together with an equivalent SMB operation for comparison.

Figure 2.4(a) depicts a 4-section 6-column setup, with 1/2/2/1 column configuration, meaning 1, 2, 2 and 1 column(s) in section I, II, III and IV, respectively. During a single switching period from 0 to t_s, in Figure 2.4(b), there is only one column configuration in the case of the SMB process. However, in Varicol operation, input/output ports may shift non-simultaneously and unequally, as shown in Figure 2.4(c) for a 4-subinterval Varicol process, where the column configuration changes from 1/2/2/1 ($0\sim t_s/4$) to 2/1/2/1 ($t_s/4\sim t_s/2$) by shifting extract port one column forward, then to 2/2/1/1 ($t_s/2\sim 3/4\ t_s$) by shifting feed port one column forward, and then to 1/2/1/2 ($3/4\ t_s\sim t_s$) by shifting extract, feed and raffinate ports one column backward. As a result, there can be 4 different column configurations for the four time intervals during one global switching period of the Varicol system. After the 4^{th} sub-interval, the column configuration reverts back to the original 1/2/2/1 configuration by shifting the eluent, extract and feed ports one column forward and the raffinate port two columns forward, and once again another global switching begins and the 4 sub-switching schedules repeated. Therefore, Varicol has more flexibility than SMB. SMB could be regarded as a special and also the most rigid case of Varicol, where the column configurations in all subintervals happen to be same.

In the open literature, only a couple of studies have been reported on Varicol process for the enantio-separation of 1, 2, 3, 4-tetrahydro-1-naphthol (Ludemann-Hombourger et al., 2000), the enantio-separation of SB-553261 (Ludemann-Hombourger et al., 2002), and for the separation of amino acids and sugars (Toumi et al., 2002). The potential of Varicol for coupling reaction and separation has not yet been reported so far.

In the last couple of decades, quite a few studies have been carried out to evaluate the applicability of SMBR. Various classes of important reactions, both

chemical and biochemical, have been studied using a SMBR. Table 2.2 gives a brief but comprehensive account of various reaction systems studied in a SMBR

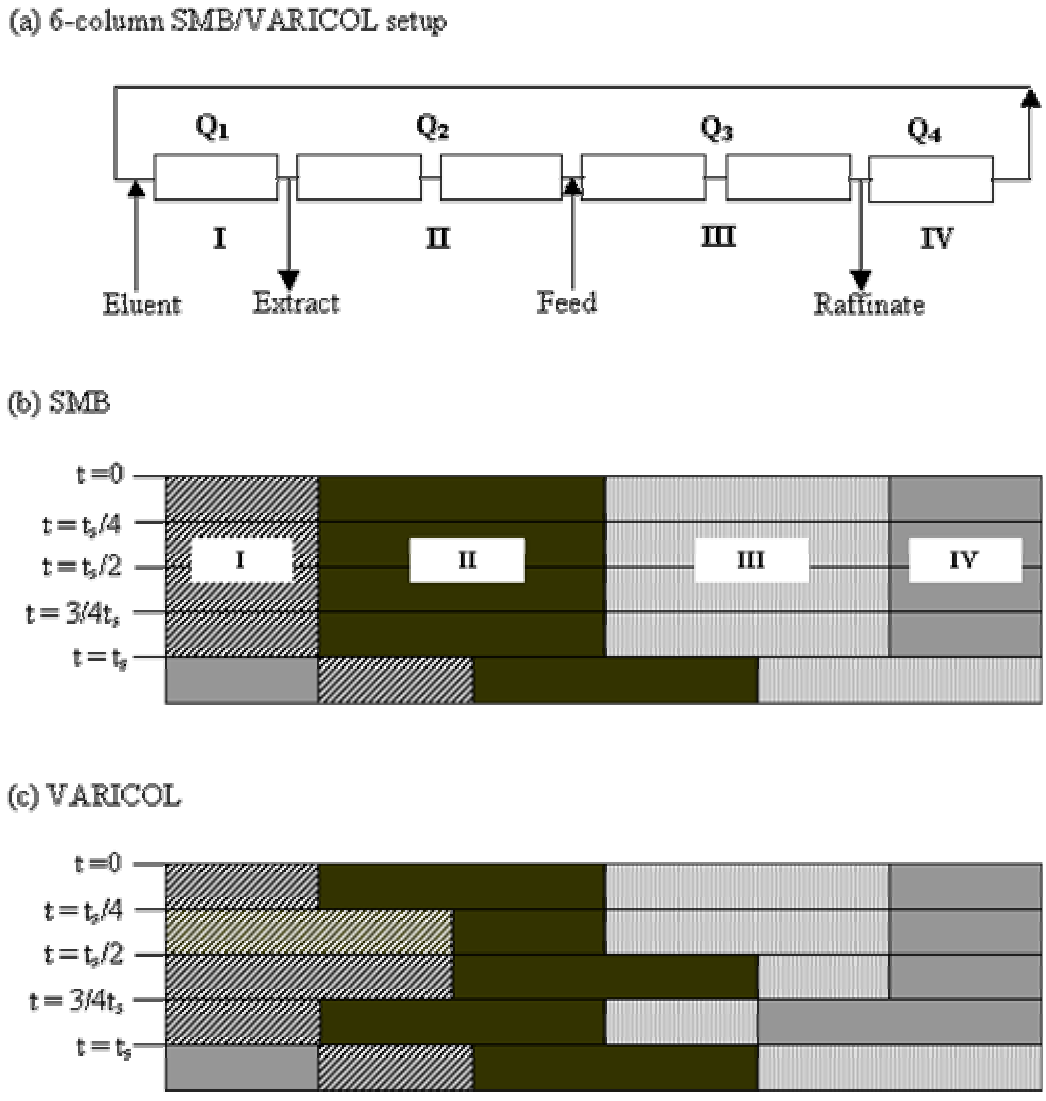

Figure 2.4 Comparison of 6-column SMB and 4-subinterval VARICOL

Table 2.2 Detailed description of the various Investigations on SMBR

S.No.	System Investigated	Authors	Details on the reactive SMB used	Description of the work	Remarks
1	Hydrogenation of mesitylene (reversible reaction)	Ray et al. (1990)	Two configurations were studied: 1. Single column – multi- ports for feed & product (Sorbex concept). 2. Multiple column- Series of columns inter-connected with inlet & outlet ports. Catalyst and adsorbent are mixed and packed together in the column(s).	The SMBR model was developed based on equilibrium stage model. Model calculations predicted very high purity & almost unit conversions for both configurations, though at 463K, X_{eq} = 62%.	Simulation studies on the performance of SMBR.
		Ray et al. (1994)	Single column – multi-ports for feed & product. Catalyst and adsorbent are mixed and packed together in the column.	Equilibrium stage model was considered for the SMBR. Simulation results showed that high purity and nearly complete conversion could be achieved in SMBR, though at 463K, X_{eq} = 62% Performance of the SMBR was compared with that of a long FBR.	Simulation studies on the performance of SMBR.
		Bjorklund & Carr (1995)	Series of columns inter-connected with inlet & outlet ports. Chromosorb 106 – adsorbent. 10% Pt/Al_2O_3 and 90% Chromosorb 106 – catalyst.	Though at 473K, X_{eq} = 40%, SMBR conversion was greater than 80%.	Applicability of SMBR for reversible reactions was verified.
		Ray & Carr (1995a)	5-columns SMBR (3 zones). 10% Pt/Al_2O_3 - catalyst Chromosorb 106 – adsorbent Catalyst and adsorbent are mixed and packed together in the columns.	Under proper operating conditions, SMBR conversion: exp-83%, pre-97% (At 473K, X_{eq} = 40%) Purity: exp-96%, pre-98%. Equilibrium stage model for SMBR was used for the model prediction. Results were compared with TMBR.	Evaluation & verification of the efficiency of SMBR and the study on the effects of various operating variables on reactor performance were performed.

		Ray & Carr (1995b)	4- or 5- columns SMBR. Catalyst and adsorbent are mixed and packed together in the columns.	PDEs solved by adaptive finite elements technique for simulations. SMBR Conversion ? 1 (X_{eq} = 62%, at 463 K); Purity 98-99%. Simulation results were qualitatively similar to the predictions by Equilibrium stage model for the SMBR.	A model for the prediction of SMBR behavior was proposed. Model predictions of concentration profiles were reported.
2	Oxidative Coupling of Methane (irreversible reaction)	Tonkovich et al. (1993)	4-section SMBR 1 reactor (high temperature) & 2 separator columns (low temperature) were used in each section. Samarium oxide - catalyst Activated charcoal - the adsorbent. Make up flows were introduced to reconcile the reversible elution order.	Ethane and Ethylene production was studied. The experimental results of the SMBR performance were reported. Effects of temperature, switch time & CH_4/O_2 feed ratio on the performance of SMBR were studied.	Improvement in yields of ethylene production in the industry.
		Tonkovich & Carr (1994a)	Same as that reported by Tonkovich et al. (1993)	Ethylene production was studied. Simple irreversible reaction kinetics followed. Micro-reactor trials with samarium oxide catalyst – 2 to 10% conversion in single pass. SMBR expts. showed: conversion – 60%, Yield – 50% and selectivity ≥ 90%. Effects of temperature, switch time & CH_4/O_2 feed ratio were studied.	Experiments were carried out to verify the applicability of SMBR for OCM.

Tonkovich & Carr (1994b)	Same as that reported by Tonkovich et al. (1993).	Ethane and Ethylene production was studied. Realistic and complex kinetics was not studied. Simple reversible reaction kinetics followed. SMBR equilibrium stage model was used for simulations. SMBR – more yields than conventional reactors. Switching time and makeup feed rate effects studied. Experimental and predicted values were compared. Occurrence of Opt. Switch time is observed.	A simple model for the prediction of SMBR behavior was proposed.
Bjorklund & Carr (1995)	Series of columns inter-connected with inlet & outlet ports. 4 reactors and 4 short and 2 long separators were used in the SMBR set-up. Samarium oxide was used as the catalyst and activated charcoal was used as the adsorbent.	Production of ethane & ethylene was studied experimentally. CH_4 oxidative coupling – 12-fold increase in conversion for this low per pass conversion reaction Yields are twice of that from conventional reactors.	Enhancement of the SMBR performance by modifying the configuration

		Kruglov et al. (1996)	4-section SMBR 1 reactor (high temperature – 700-850^{o}C) & 2 separator columns (low temperature – 100^{o}C) were used in each section.	Characterization of different adsorbents (activated charcoal, zeolite & hydrophobic CMS) to improve performance of the process was done. CMS was found to be the best. Sm_2O_3, $Y_1Ba_2Zr_3O_{9.5}$ and $Y_1Ba_2Ge_3O_{3.5}$ – three catalysts were used for the experimental studies in micro-reactors. $Y_1Ba_2Zr_3O_{9.5}$ was the best of all three. Effects of switching time and feed ratio were analyzed. Adaptive flow switching & uneven makeup feed was suggested to be the promising methods for further optimization of reactor.	Design of SMBR based on the sensitivity of its performance for changes in the operating parameters. Suitable catalysts and adsorbents for the model reaction system were also found.
		Bjorklund et al. (2001)	3 zones SMBR with only one reactor in the entire set-up and two adsorbers in each section. $YBa_2Zr_3O_{9.5}$ was used as the catalyst and activated charcoal was used as the adsorbent. High temperature reaction and low temperature adsorption scheme was followed.	Ethane and Ethylene combined yields were about 45% at optimum operating conditions. Experimental and Simulation results were in good agreement. Effects of the switching time and CH_4/O_2 feed ratio were studied. Axially dispersed plug flow model was used. Mass transfer kinetics involved linear driving force approximation. Langmuir isotherms were considered.	Modeling of the SMBR for OCM reaction system and verification of the model with experimental results.
3	Sucrose Inversion into Glucose and Fructose using the enzyme Invertase (irreversible reaction)	Ganetsos et al. (1993)	12 columns SMBR with calcium charged resin as the adsorbent.	Experimental results showed high purity of Glucose and Fructose and Enzyme productivity as well. Performing Sucrose Inversion in SMBR minimized substrate-inhibition-related problems.	Fructose – sweetener (food industry). A novel reactor-separator for the inversion of sucrose was proposed.

Meurer et al. (1996)	4 sections 8-column SMBR (2 columns each in the different sections). DOWEX 99/Ca Monosphere was used as the adsorbent. Invertase was used as the enzymatic catalyst.	Equilibrium dispersive model (SMBR) incorporating the LDF approximation for mass transfer effects was used for the model prediction. Dynamic simulation studies on the SMBR were performed and its performance was compared to that of conventional chromatographic processes. Optimization was done by rigorous modeling. Switching time, enzyme concentration and flow rates were the parameters.	Optimal design strategy of the SMBR by rigorous modeling.
Ching & Lu (1997)	3 zones SMBR. 1, 5 and 6 adsorbers in section I, II & III respectively.	Enzymatic Reaction takes place in fluid phase. Modeling & Simulation results for 3-zone type SMBR were reported. Axially dispersed plug flow model with LDF approximation for the mass transfer and linear isotherms were used.	SMBR performance evaluation & design based on rigorous modeling.
Azevedo & Rodrigues (2001)	Four sections SMBR – LICOSEP pilot plant (12 columns – 3, 2, 5 and 2 columns in sections I, II, III and IV respectively). DOWEX Monosphere 99/Ca cation exchange resin was used as the adsorbent.	Michaelis-Menten kinetic model was used. TMBR differential mass balance equations incorporating double linear driving force for mass transfer in pores and microparticles was considered. Both experimental and simulation results were reported. Optimization study involved minimization of column length and enzyme concentration for given feed flow rate– constrained by conversion >99% and purity >95% and also maximization of enzyme productivity. The effect of safety margin was also investigated.	Design of Bio-SMBR based on rigorous modeling and experimental verification.

		Dunnebier et al. (2000)	4 sections SMBR with 2 columns in each section was considered.	An optimization algorithm was developed to determine the optimal design of the SMBR focused on the operation costs. Five decision variables related to system flow rate (t_s, Ex, E, Q_4 and F), were optimized subjected to the constraints on product purities and maximum column flow rate. A standard successive quadratic programming (SQP) algorithm was used in obtaining the optimal operating conditions. SMBR model accounts for convection, axial dispersion, mass transfer resistances, particle diffusion and kinetics of adsorption. Eluent consumption was minimized indirectly. Savings in desorbent consumption up to 56.6% was realized.	A novel optimal design strategy for SMBR was proposed.
4	Isomerization of glucose into fructose (reversible reaction)	Hashimoto et al. (1983; 1993)	3 zones SMBR was used. Sections II and III had 4 adsorbers each. Section I had 8 adsorbers and 7 reactors placed alternately. Calcium ion form of Y zeolite was used as the adsorbent and glucose isomerase as the enzyme. There is no raffinate stream.	Two models (SMBR & TMBR) with LDF approximation for the mass transport and linear isotherms were considered. Higher fructose purity (65%) was obtained. Experimental and simulation results were in good agreement. Performance of the SMBR was compared to that of the conventional processes. The desorbent was required less than that for an equivalent fixed-bed batch process. Effect of Mg^{2+} on kinetics was also studied.	Fructose – sweetener and more soluble in water (used in food industry). A novel reactor-separator for the isomerization of glucose was proposed.

		Ching & Lu (1997)	3 zones SMBR was used. Sections I and II had 3 adsorbers each. Section III had 8 adsorbers and 7 reactors placed alternately. There is no raffinate stream.	Modeling & Simulation results for 3-zone type SMBR were reported. Axially dispersed plug flow model (TMBR) with LDF approximation for the mass transfer and linear isotherms were used.	SMBR performance evaluation & design based on rigorous modeling.
5	Methanol from Syngas (reversible reaction)	Kruglov (1994)	Two reactor configurations were compared. 1. Adiabatic FBR – catalyst & selective adsorbent mixed (4 columns). 2. Isothermal – catalyst & adsorbent alternately packed. (3 reactors and 5 adsorbers). Stripping section for recovery of residual reactants was incorporated in both configurations.	Synthesis using low-pressure catalyst $Cu/ZnO/Al_2O_3$. Axially dispersed plug flow (SMBR) model was used. Mass transport was limited only by diffusion of the product in the adsorbent pores. Both reactors could handle non-stoichiometric mixture of reactants. The heat production during the reaction determines the operating conditions. Conversion was greater than 97%.	Numerical Modeling of the SMBR.
6	Esterification of Acetic acid with ethanol (reversible reaction)	Mazzotti et al. (1996)	3 zones SMBR (8 columns – 2, 1 and 5 columns in the sections I, II and III respectively). Characterization of Amberlyst 15 (highly cross-linked sulphonic ion exchange resin) that acts as both catalyst and adsorbent was done in FBR.	Kinetic and adsorption data – from batch and fixed bed experiments. Ideal plug flow SMBR model was used (dispersionless and no mass transfer effects). Experimental results along with modeling were reported.	Development of a process based on SMBR unit. Modeling and experimental study of SMBR for a reversible reaction.

7	β-phenethyl acetate from AA and β-phenethyl alcohol. (reversible reaction)	Kawase et al. (1996)	4 zones SMBR (8 columns – 2, 2, 3 and 1 columns in sections I, II, III and IV respectively. Amberlyst 15 was used as catalyst and adsorbent.	Dispersionless plug flow model incorporating the LDF approximation for mass transfer effects and langmuir isotherms was used for model prediction. Experimental and simulation results were compared. The esterification reaction conversion was increased from the equilibrium value of 63% to more than 99%. Effects of reaction rate on SMBR performance were studied.	Essential oils & Fragrances contains this ester. Design of SMBR for esterification reaction system.
		Dunnebier et al. (2000)	4 zones SMBR (8 columns – 2, 2, 3 and 1 columns in sections I, II, III and IV respectively.	An optimization algorithm was developed to determine the optimal design of the SMBR based on the operation costs. SMBR model accounts for convection, axial dispersion, mass transfer resistances, particle diffusion and kinetics of adsorption. Eluent consumption was minimized indirectly. Purity constraints were imposed on these problems. Savings in desorbent consumption up to 58% was realized.	A novel optimal design strategy for SMBR was proposed.

8	Acetone + Phenol (solvent excess) = Bisphenol A. (reversible reaction)	Kawase et al. (1999)	SMBR of the 3 zones type was considered (3, 1 and 2 columns in the respective sections). Amberlyst 31 resin was used as the adsorbent and catalyst	Initial reaction rate proportional to acetone concentration. Batch experiments for adsorption isotherms and kinetics from fixed bed. Dispersionless, plug flow model incorporating the LDF approximation for the mass transfer effects and the langmuir isotherms was used for the model prediction. Problems associated with water adsorption that are encountered in the industry were overcome by SMBR.	Bisphenol A is used to produce a number of resins. Simulation study of the SMBR for reversible reactions was performed.
9	Lactose + Sucrose = lacto sucrose + glucose. (Reversible reaction)	Kawase et al. (2001)	Four sections SMBR was considered (12 columns – 2, 6, 2 and 2 columns in sections I, II, III and IV respectively. Amberlite CR-1310Na was used as the adsorbent and catalyst.	The reaction is uncompetitively inhibited by glucose and lactose. Mechanism of transfer reaction: bi-bi type. A simulation study showed that the reaction process was improved by product removal. Dispersionless plug flow model with LDF approximation for the mass transfer effects and linear isotherms was used for the simulation. Yield was improved from 50% to 80% by effective glucose removal. Experimental results for SMBR were reported. Hydrolysis near raffinate port reduces the yield below the optimum.	Lactosucrose is an artificial sweetener – suitable for low-calorie food. SMBR design and performance study.

10	Direct Synthesis of Methyl Tertiary Butyl Ether (MTBE) from Tertiary Butyl Alcohol (TBA) & Methanol (Reversible reaction)	Zhang et al. (2001b)	4 sections SMBR was considered. (8 columns) Amberlyst 15 was used as the catalyst and adsorbent.	Simulation results were reported for the SMBR performance and sensitivity of the process for the various operating variables was also reported. Equilibrium dispersive model with linear isotherms was used for the model prediction. Effects of switching time, solvent and the raffinate flow rates, the number of columns in sections S & P were studied. Conversion in SMBR ≥ 95% (X_{eq} = 85.24%, at 328 K) The operating parameters were observed to affect the system performance in conflicting way.	MTBE is used as an anti-knock in automobiles as a substitute for lead tetra-ethyl. Applicability of SMBR for MTBE synthesis was validated.
		Zhang et al. (2002, in press)	4 sections SMBR (5, 6, 7 or 8 columns). Amberlyst 15 was used as the adsorbent and catalyst.	Equilibrium dispersive model with linear isotherms was used for the model prediction. Multi-objective Optimization study was performed for the synthesis of MTBE. Objective functions included the purity and yield of MTBE, the eluent requirement, the conversion of TBA and the volume of the catalyst/adsorbent. Pareto-optimal solutions for the various problems were reported. Effects of switching time, solvent and the feed flow rates, the flow rate in section P, the length of the columns, the temperature and the number of columns in sections S & P on the pareto optimal solutions were studied.	Optimal Design Strategy for SMBR using non-traditional optimization method called Genetic Algorithm.

11	Methyl Acetate Synthesis from Acetic acid and Methanol. (Reversible reaction)	Lode et al. (2001,2003)	4 sections SMBR (10 columns – 3, 2, 3 and 2 columns in the sections I, II, III and IV respectively). Amberlyst 15 was used as the adsorbent and catalyst.	Kinetic and Adsorption isotherm (langmuir) parameters were determined in single column packed with Amberlyst 15 resin. Equilibrium dispersive model with LDF approximation for mass transfer effects and Langmuir isotherms was used for the model prediction. Simulation & Experimental results for the reaction in a SMBR were compared. Effect of the flow rates in different sections and the feed composition on the SMBR performance were studied and reported. The region for complete conversion and separation was determined. The effect of feed composition were investigated. Guidelines for SMBR optimization based on numerical simulation were proposed.	Design of SMBR based on rigorous modeling.
12	General	Meurer et al. (1997)	4 sections 8-column SMBR (2 columns each in the different sections). 9 columns SMBR (3 columns in section III, while 2 columns each in the other sections) was also considered for the reversible reaction. Both irreversible and reversible reactions of the type: A → B + C and	Equilibrium dispersive model (SMBR) incorporating the LDF approximation for mass transfer effects and adsorption isotherms for both adsorbent and catalyst was used for the model prediction. Dynamic simulation studies on the SMBR were performed and the performance was compared to that of conventional chromatographic processes. Effects of relative adsorptivities and portioning on the conversion were studied. Optimization was done by rigorous modeling.	Optimal design strategy of the SMBR by rigorous modeling.

Fricke et al. (1999)	4 sections SMBR (8 columns – 2 columns each in the different sections) was considered. Ester hydrolysis was studied.	Equilibrium dispersive model (SMBR) incorporating the LDF approximation for mass transfer effects and adsorption isotherms for both adsorbent and catalyst was used for the model prediction. Dynamic simulation studies on the SMBR and the performances of different reactor configurations were performed. Effect of the column packing – homogeneous or heterogeneous, the reactor length and column configurations were studied.	Design of SMBR based on simulations.
Fricke et al. (1999)	4 sections SMBR was considered (8 columns – 2 columns in each section).	Equilibrium dispersive model (SMBR) incorporating the LDF approximation for mass transfer effects and linear adsorption isotherms was used for the model prediction. The effects of the adsorption and the reaction constants on the reactor performance (based on the feed and eluent flow rates) were studied. Guidelines for enhanced performance of SMBR are given.	Design of SMBR based on simulations.

Migliorini et al. (1999)	4 sections SMBR was considered (8 columns – 2 columns in each section). Amberlyst 15 was used as the adsorbent and catalyst.	SMBR could be applied to the Esterification, trans-esterification, etherification, acetylation, isomerization, hydrogenation, enzymatic reactions. SMBR equilibrium dispersive model with linear adsorption equilibria was used for the model prediction. Analysis with respect to flow ratio m_j – simulations of ethyl acetate synthesis from acetic acid and ethanol on Amberlyst 15 was performed. Complete conversion/separation region is triangular similar to non-reactive SMB. Feed concentration – should be an optimization parameter. The triangle theory approach was also verified for the Sucrose Inversion reported by Ching & Lu (1997).	Behavior & design strategy based upon the knowledge about non-reactive SMB theory.
Huang & Carr (2001)	Irreversible and reversible reactions were studied. 1 reactor and 4 adsorbers were used. High temperature reaction and low temperature adsorption scheme was followed.	Algebraic material balance equations were used for model prediction. Simple algebraic expressions for the dependence of the reactor performance on per pass conversion, adsorption constants and reactant concentration are presented.	A novel but simple design approach for SMBR design was proposed.
Lode et al. (2003)	Comparison of true countercurrent and simulated moving bed reactor	An analytical solution of differential mass balance equations for the true moving bed reactor (linear adsorption isotherm) was developed. Criteria were derived for the optimum process design with respect to productivity and solvent consumption.	True moving bed reactor model does not apply to SMBT with a finite number of columns per section.

2.4 Design and Optimization Strategy for the Simulated Moving Bed Systems

2.4.1 Design Criteria Proposed by the Research Group at University of Minnesota

The theory of SMB proposed by the research group at university of Minnesota is presented here to provide a background for the design of SMBR. In order to understand SMB clearly, the operation of a True Moving Bed (TMB) is considered. Assuming one-dimensional flow of solid and fluid, instant adsorption equilibrium, and negligible axial dispersion and other mass transfer resistances, the overall differential transient mass balance for component i in any section is given by (Ray, 1992):

$$\varepsilon\frac{\partial C_i}{\partial t}+(1-\varepsilon)\frac{\partial q_i}{\partial t}+\varepsilon u_g\frac{\partial C_i}{\partial x}-(1-\varepsilon)u_s\frac{\partial q_i}{\partial x}=0 \tag{2.1}$$

Where u_s and u_g represent the velocities of the solid and the fluid phases in the respective section. Mobile phase concentration C_i is related to solid phase concentration q_i by the Langmuir isotherm:

$$q_i=\frac{NK_iC_i}{1+K_iC_i} \tag{2.2}$$

Applying the dimensionless parameters given below,

$$\gamma_i=K_iC_i;\alpha_i=\frac{1-\varepsilon}{\varepsilon}NK_i;\sigma_i=\alpha_i\frac{u_s}{u_g} \tag{2.3}$$

the mass balance equations were reduced to:

$$\left[1+\frac{\alpha_i}{(1+\gamma_i)^2}\right]\frac{\partial\gamma_i}{\partial t}+u_g\left[1-\frac{\sigma_i}{(1+\gamma_i)^2}\right]\frac{\partial\gamma_i}{\partial x}=0 \tag{2.4}$$

After rearrangement, the following equation was obtained:

$$-\frac{dx}{dt}=V_{i,s}=\frac{u_g\left[1-\frac{\sigma_i}{(1+\gamma_i)^2}\right]}{\left[1+\frac{\alpha_i}{(1+\gamma_i)^2}\right]} \tag{2.5}$$

$V_{i,s}$ is the velocity of a point of concentration γ_i, describing the location of a particular concentration as time proceeds. In other words, $V_{i,s}$ is the effective velocity with which a solute travels within the column and for a given set of operating conditions, it is a function of γ_i only. At low concentration, $\gamma_i << 1$, $V_{i,s}$ reduces to:

$$V_{i,s} = \frac{u_g\left(1-\sigma_i\right)}{\left(1+\alpha_i\right)} \tag{2.6}$$

The Equation 2.6 shows that for systems described by linear isotherm, the velocity of the species traveling through the column is independent of the concentration, but dependent on parameter σ_i which was first defined by Petroulas et al. (1985a. 1985b). If $\sigma_i<1$, $V_{i,s}$ will be positive and the species will always travel up the column in the direction of fluid flow regardless of concentration of the species. However, if $\sigma_i>1$, the species will travel down the column with the solid phase. Therefore, complete separation of binary mixtures A and B can be accomplished in the true moving bed system by adjusting the fluid flow rates in the four sections and solid phase flow rates u_s, such that for component A, $\sigma_A<1$ in section 1 and $\sigma_A>1$ in sections 2, 3 and 4; and for component B, $\sigma_B<1$ in sections 1, 2 and 3 and $\sigma_B>1$ in section 4.

The above example shows the principle of TMB operation for binary systems under ideal conditions where complete separation can be obtained. Same strategy is still valid in an equivalent SMB process, except that solid phase flow rate u_s in TMB should be replaced by the ratio between switching distance and switching time in SMB (L/t_s).

The same approach can be extended to the SMBR process. When $\sigma<1$, a component travels upward with the fluid phase, whereas when $\sigma>1$, a component travels downward at low concentration but upward at high concentration. For a reversible reaction of the type A ⇋ B, it was observed that when reactant A travels

downward ($\sigma_A>1$) and product B travels upward ($\sigma_B<1$), separation between reactant and product can enhance the conversion of reactant and the purity of product. Separation can be achieved by adjusting the fluid phase and pseudo solid velocities. Detailed description is available elsewhere (Ray, 1992)

2.4.2 Triangle Theory Proposed by the Research Group at ETH, Zurich

A novel triangle theory was proposed by the research group at ETH, Zurich, to determine the operating conditions of the SMB for a specific separation task (Storti et al., 1993; Mazzotti et al., 1997a). The complete separation region was identified as a triangle shape region in the (m_2, m_3) plane for linear or nonlinear isotherm, with or without mass-transfer resistance. It is now widely used for the SMB process design and hence, will be discussed in detail in this section due to its popularity.

The triangle theory is based on the analytical solution of an equivalent TMB model, which is used to predict the periodic steady state separation performances of SMB unit. These two systems, viz., the TMB & the SMB, have been proven to be equivalent if the following conversion rules are fulfilled:

$$V_\phi = N_\phi V_{col} \tag{2.7}$$

$$\frac{V_{col}}{t_s} = \frac{Q_s}{1-\varepsilon} \tag{2.8}$$

$$Q_\phi^{SMB} = \left[Q_\phi^{TMB} + \frac{Q_s \varepsilon}{1-\varepsilon} \right] \tag{2.9}$$

where V_ϕ and V_{col} are the volume of section ϕ of the TMB unit and that of a single column of the SMB unit, respectively; N_ϕ is the number of columns in section ϕ of the SMB unit; t_s is the switch time; ε is the bed void fraction; Q_s is the volumetric solid flow rate in the TMB unit; Q_ϕ^{SMB} and Q_ϕ^{TMB} are the volumetric flow rates of section ϕ in the SMB unit and in the equivalent TMB unit, respectively. For the SMB

unit, the design parameters are the internal flow rates, Q_ϕ^{SMB} and the switch time t_s; while Q_ϕ^{TMB} and solid flow rate Q_s, are those in an equivalent TMB unit according to above relationships.

An Equilibrium TMB model, neglecting axial dispersion and mass transport resistances, was considered first for binary system of A and B (with A being the more strongly adsorbed species). In section ϕ, the mass balance simplifies to:

$$\frac{\partial}{\partial \tau}\left[\varepsilon^* C_i + \left(1-\varepsilon^*\right) q_i\right] + \left(1-\varepsilon_p\right)\frac{\partial}{\partial \xi}\left[m_\phi C_i - q_i\right] = 0 \qquad \left(i = A, B\right) \tag{2.10}$$

$$m_\phi = \frac{net \quad fluid \quad flow \quad rate}{adsorbed \quad phase \quad flow \quad rate} = \frac{Q_\phi^{TMB} - Q_s \varepsilon_p}{Q_s\left(1-\varepsilon_p\right)} \tag{2.11}$$

where τ and ξ are the dimensionless time and space coordinates; $\varepsilon^* = \varepsilon + \varepsilon_p\left(1-\varepsilon\right)$ is the overall void fraction of the bed, whereas ε_p is the intra-particle porosity. The composition of component i in the adsorbed phase, q_i, is related to fluid phase composition C_i by either a linear or non-linear isotherm.

From the above relationships (Eqs. 2.10-2.11), in the case of given feed composition, the design of TMB or SMB unit needs to develop the criteria for the selection of the values of the m_ϕ parameters, which were defined as the ratio of the net fluid flow rate over the solid phase flow rate in each section of the TMB unit (Eqs. 2.11), or in terms of the operating parameters of the equivalent SMB unit using the conversion rules given by Eqs. 2.7-2.9:

$$m_\phi = \frac{Q_\phi^{SMB} t_s - V_{col}\varepsilon^*}{V_{col}\left(1-\varepsilon^*\right)} \tag{2.12}$$

The differential mass balance equations were solved and the analytical solutions were obtained under either linear or nonlinear type adsorption isotherm, and a

complete separation region mapped in the (m_2, m_3) plane (Storti et al., 1993; Mazzotti et al., 1994).

2.4.2.1 Linear Isotherm

Triangle theory was first explained with the systems described by the linear adsorption isotherm:

$$q_i = H_i C_i \quad (i = A, B) \tag{2.13}$$

where H_i is the Henry constant of the ith component. It was proven (Mazzotti et al., 1997a) that the necessary and sufficient conditions for complete separation are the following inequalities:

$$H_A < m_1 < \infty \tag{2.14a}$$

$$H_B < m_2 < H_A \tag{2.14b}$$

$$H_B < m_3 < H_A \tag{2.14c}$$

$$\frac{-\varepsilon_p}{(1-\varepsilon_p)} < m_4 < H_B \tag{2.14d}$$

An additional constraint, $m_3 > m_2$, required by positive feed flow rate, combines constraints on m_2 (Eq. 2.14b) and m_3 (Eq. 2.14c) into one:

$$H_B < m_2 < m_3 < H_A \tag{2.14e}$$

This inequality (Eqs. 2.14e) defines the projection of the four-dimensional region of complete separation zone to the (m_2, m_3) plane show in Figure 2.5 (a), if the constraints on m_1 (Eqs. 2.14a) and m_4 (Eqs. 2.14d) are fulfilled. The triangle-shaped region in the middle of the diagram indicates the complete separation region, where 100% purity products can be collected both in extract and raffinate. However, in the pure Extract region in Figure 2.5 (a), the constraint 3 is not fulfilled ($m_3 > H_A$),

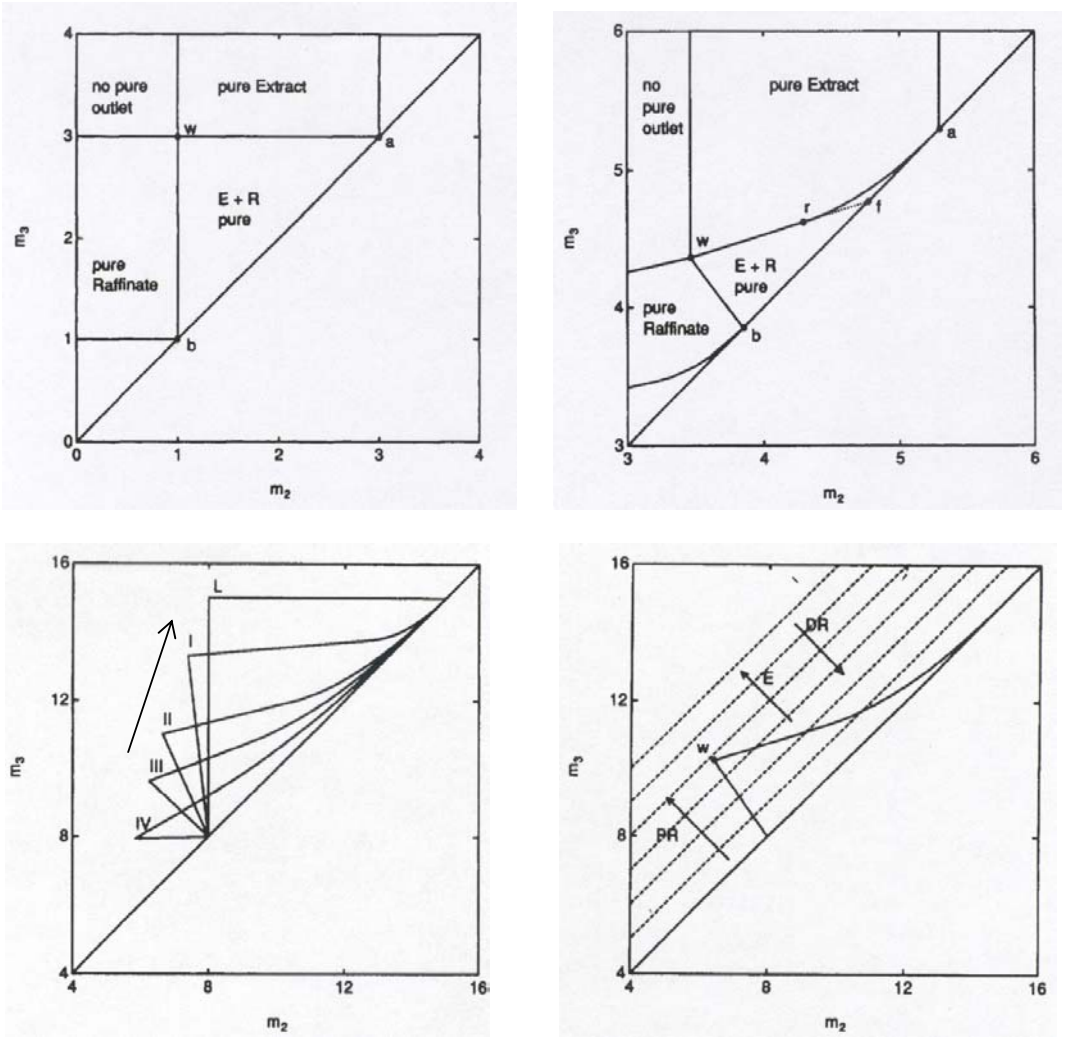

Figure 2.5 Triangle theory: Regions of the (m_2, m_3) plane with different separation regimes in terms of purity of the outlet streams

(Storti et al., 1993; Mazzotti et al., 1996a, 1997a)

(a) System described by a Linear Adsorption isotherm
(b) System described by a Langmuir adsorption isotherm
(c) Effect of the overall concentration of the feed mixture, $C_{T,\,f}$, on the region of complete separation in the (m_2, m_3) plane
(d) Application of Triangle theory to the design of optimal operating conditions

consequently, the strong component A is carried upwards from section 3 into section 4, thus contaminating the raffinate stream, whereas extract is still 100% pure. Similarly, in pure raffinate region, $m_2 < H_B$, only 100% pure raffinate can be obtained. The region in the top-left corner where both $m_3 > H_A$ and $m_2 < H_B$ corresponds to operating conditions under which none of the 100% pure products could be collected either in extract or in raffinate stream.

2.4.2.2 Nonlinear Isotherm

The triangle theory was further developed for non-linear systems, for which the adsorption equilibrium properties were described by means of the competitive non-stoichiometric Langmuir isotherm:

$$q_i = \frac{N_i K_i C_i}{1 + K_A C_A + K_B C_B} \qquad (i = A, B) \tag{2.15}$$

In derivation of the design conditions on the flow rate ratio m_ϕ to achieve complete separation, same equilibrium model equation (Eqs. 2.10) was used along with the above isotherm (Eqs. 2.15), and the following necessary and sufficient conditions were obtained for complete separation (Storti et al., 1993; Mazzotti et al., 1994, 1996a):

$$H_A = m_{1,\min} < m_1 < \infty \tag{2.16a}$$

$$m_{2,\min}(m_2, m_3) < m_2 < m_3 < m_{3,\max}(m_2, m_3) \tag{2.16b}$$

$$\frac{-\varepsilon_p}{1-\varepsilon_p} < m_4 < m_{4,\max}(m_2, m_3) = \frac{1}{2}\left\{H_B + m_3 + K_B C_{B,f}(m_3 - m_2) - \sqrt{\left[H_B + m_3 + K_B C_{B,f}(m_3 - m_2)\right]^2 - 4H_B m_3}\right\} \tag{2.16c}$$

where adsorptivity $H_i = N_i K_i$. The lower bound on m_1 and upper bound on m_4 were found to be explicit, whereas the latter is dependant on the flow rate ratio between m_2 and m_3. However, the implicit constraints on m_2 and m_3 define the complete separation

region in the (m_2, m_3) plane, which is also a triangle-shaped region shown in Figure 2.5 (b). It was also found that, in the case of nonlinear systems, the shape of the complete separation region depends on the feed concentrations, as expected. The effect of the overall concentration of feed mixture, $C_{T,f}(=C_{A,f}+C_{B,f})$, on the region of complete separation in the (m_2, m_3) plane, is shown in Figure 2.5 (c). As total feed concentration increases, the area of completely separation region decreases.

Similar procedure was extended to other nonlinear systems, for example, modified Langmuir isotherm (Charton and Nicoud, 1995; Mazzotti et al., 1997a) and bi-Langmuir isotherm (Gentilini et al., 1998). As a result, different sets of constraints on m_ϕ were obtained, which describes different shapes of complete separation region in (m_2, m_3) plane.

The procedures employed for binary separation was further applied to the design of multi-component systems, which were characterized by the Langmuir isotherm (Storti et al., 1993; Mazzotti et al., 1996a, b; Mazzotti et al., 1997b); to the design of SMB under non-ideal conditions, i.e., the effect of axial dispersion and mass transfer resistances were taken into account (Migliorini et al., 1999a; Biressi et al., 2000a).

With the objective of achieving a complete separation, the triangle theory was used to optimize SMB operation in terms of desorbent requirement, enrichment and productivity, which were defined as (Mazzotti et al., 1997a):

Desorbent requirement: $$DR=\frac{(E+F)C_d}{FC_{T,f}}=\frac{C_d}{C_{T,f}}\left(1+\frac{m_1-m_4}{m_3-m_2}\right) \tag{2.17}$$

Enrichment: $$E_A=\frac{C_{A,Ex}}{C_{A,f}}=\frac{m_3-m_2}{m_1-m_2},\ E_B=\frac{C_{B,Ra}}{C_{B,f}}=\frac{m_3-m_2}{m_3-m_4} \tag{2.18}$$

$$\text{Productivity: } PR = \frac{FC_{T,f}}{\left(1-\varepsilon^*\right)\rho_s V_T} = \frac{C_{T,f}\left(m_3 - m_2\right)}{\rho_s t^* \sum_{\phi=1}^{4} N_\phi} \tag{2.19}$$

where C_d, ρ_s and V_T are feed concentration of desorbent, density of adsorbent and total column volume.

Within the region of complete separation, operating conditions should be selected such that *DR* is minimized, whereas E_A, E_B and *PR* are maximized. The design procedure with triangle theory is illustrated in Figure 2.5 (d) for nonlinear systems described by Langmuir isotherm. By moving the operating point from the diagonal towards the vertex *w* inside the complete separation region across straight lines of unitary slope in the (m_2, m_3) plane, all these performance parameters (*DR*, *E* and *PR*) improve because of the increase in the difference (m_3-m_2). Therefore, the coordinates of the point *w* represent the optimal operating conditions for m_2 and m_3. Furthermore, desorbent requirement and enrichment of A and B improve if m_1 is small and m_4 is large. It follows that the optimal values of m_1 and m_4 coincide with their lower and upper bounds, respectively.

Triangle theory was also extended to the SMBR process. Migliorini et al. (1999b) and Lode et al. (2001) reported that sections 1 and 4 are regeneration sections where under complete conversion/separation conditions no reaction occurs and therefore the same criteria for non-reactive SMBs can be applied to the flow rate ratio in section 1 and 4. m_1 and m_4 must be larger and smaller than the corresponding critical values for complete regeneration of adsorbent and eluent, respectively. Once these conditions are fulfilled, the values of m_1 and m_4 have no effect on the SMBR performance in terms of conversion and purity. The flow rate ratios in sections 2 and 3 determine the separation performance. The complete conversion and separation region can be represented in the (m_2, m_3) plane and its shape and location depend on the feed

composition and residence time, and there is a lower bound on switching time, below which the residence time in the reactive zone of the SMBR is not sufficient to allow the reaction to occur to any significant extent. Same as in the SMB, the vertex of the region for complete conversion and separation In SMBR corresponds to the optimal operation conditions for maximum productivity.

2.4.3 Standing Wave Proposed by the Research Group at Purdue University

A research group in Purdue University, US, has proposed another novel design procedure, the Standing Wave Concept. They derived a series of explicit algebraic equations to link the product purity and recovery to axial dispersion and a lumped mass transfer coefficient, section lengths, linear fluid velocities and solid movement velocity. The standing wave method was explained by applying it to investigate the separation of Raffinose and Fructose (Ma and Wang, 1997), Fructose and Glucose (Mallmann et al., 1998), and Paclitaxel Separations (Wu et al., 1999).

The standing wave concept is based on the idea that each section should perform its own specific separation role to ensure product purities, by making certain concentration waves stand in a particular section. By proper choices of the four flow rates and solid movement velocity in TMB (or equivalent port switching time in SMB), the advancing front (or adsorption wave) of the fast migrating solute (B) can be made standing in section IV and its desorption wave standing in section II (Figure 2.3). The adsorption wave of the slow migrating solute (A) is made standing in section III and its desorption wave standing in section I, as shown in Figure 2.6 for linear systems with mass transfer resistance (Wu et al., 1999).

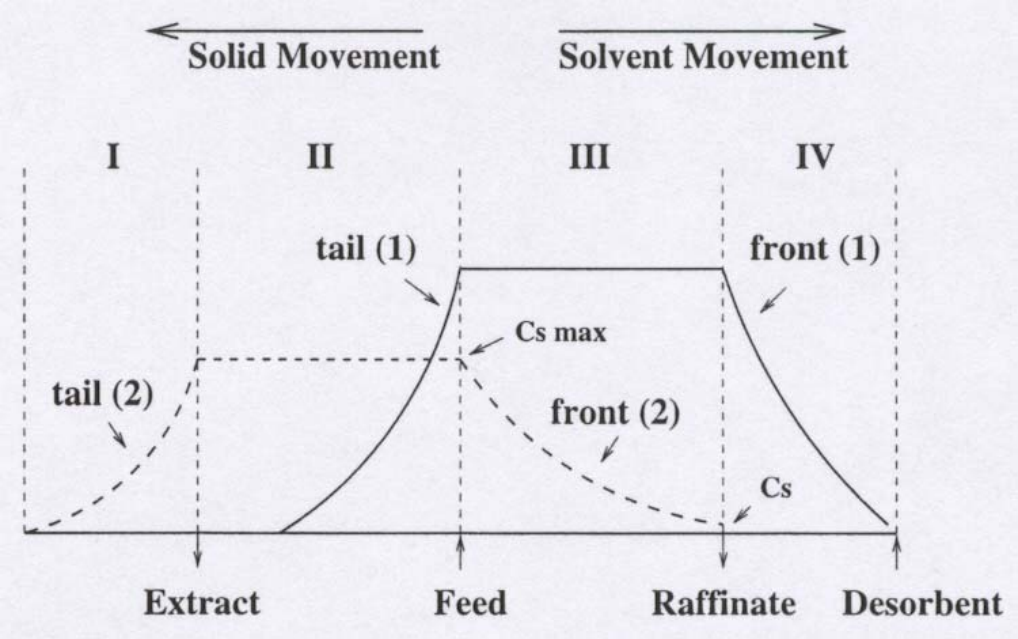

Figure 2.6 Standing Wave in a linear TMB system (Wu et al., 1999)

Like triangle theory, an equivalent true moving bed (TMB) model was also used to derive the standing wave equations. For example, in section I, the transport equations for a solute in the mobile phase and in the pore phase are:

$$\frac{\partial C_i}{\partial t} = E_i^I \frac{\partial^2 C_i}{\partial x^2} - u_1^{TMB} \frac{\partial C_i}{\partial x} - PK_{fi}^I \left(C_i - C_i^*\right) \tag{2.20}$$

$$\varepsilon_p \frac{\partial C_i^*}{\partial t} + \left(1-\varepsilon_p\right)\frac{\partial q_i^*}{\partial t} = K_{fi}^I \left(C_i - C_i^*\right) + u_s \varepsilon_p \frac{\partial C_i^*}{\partial x} + \left(1-\varepsilon_p\right) u_s \frac{\partial q_i^*}{\partial x} \tag{2.21}$$

where C_i, C_i^* and q_i^* are the mobile phase, average pore phase and solid phase concentrations of the ith component, respectively; P is the bed phase ratio, $\left(1-\varepsilon\right)/\varepsilon$; ε and ε_p are the bed and intra-particle void fraction, respectively; u_1^{TMB} and u_s are the interstitial linear mobile phase velocity in section I and the adsorbent movement velocity, respectively; E_i^I and K_{fi}^I are axial dispersion coefficient and lumped mass-transfer coefficient of component i in section I, respectively. The equivalent SMB interstitial velocity, u_1^{SMB}, is related to the TMB interstitial velocity u_1^{TMB} by:

$$u_1^{SMB} = u_1^{TMB} + u_s \tag{2.22}$$

2.4.3.1 Linear System without Axial Dispersion and Mass Transfer Resistance

The standing wave concept was first applied for linear systems, in which axial dispersion and other mass-transfer effects are negligible (Ma and Wang, 1997). The following equation was derived from Eqs.2.20 and 2.21:

$$\left(1+P\delta_i\right)\frac{\partial C_i}{\partial t} + \left[u_1^{SMB} - u_s\left(1+P\delta_i\right)\right]\frac{\partial C_i}{\partial x} = 0 \tag{2.23}$$

where $\delta_i = \varepsilon_p + \left(1-\varepsilon_p\right)K_i$; K_i is the linear equilibrium constant of component *i*.

From Eqs. 2.23, the linear velocity of the concentration wave of component *i*, u_{wi}, relative to the feed point is:

$$u_{wi} = -\frac{dx}{dt} = \frac{u_1^{SMB}}{1+P\delta_i} - u_s = u_{sol,i} - u_s \tag{2.24}$$

Therefore, u_{wi} is determined by two independent linear velocities: the solid movement velocity, u_s, and the solute migration velocity, $u_{sol,i}$. In order to have separation, the migration velocity wave of the more retained solute (A) should be less than u_s in section III and that of the less retained solute (B) should be less than u_s in section IV; the desorption wave of solute A should be greater than u_s in section I and that of solute B should be greater than u_s in section II. In conclusion, the following conditions for the velocities in each section were proposed to be satisfied for a complete separation:

Section I: $u_{sol,A} - u_s > 0$ (2.25a)

Section II: $u_{sol,B} - u_s > 0$ (2.25b)

Section III: $u_{sol,A} - u_s < 0$ (2.25c)

Section IV: $u_{sol,B} - u_s < 0$ (2.25d)

The following equations corresponding to the boundary values defined in Eqs.2.25a-d, were chosen as the optimum section flow rates, because they result in highest feed flow rate and lowest solvent flow rate for a given system:

$$u_1^{SMB} = (1+P\delta_A)u_s \tag{2.26a}$$

$$u_2^{SMB} = (1+P\delta_B)u_s \tag{2.26b}$$

$$u_3^{SMB} = (1+P\delta_A)u_s \tag{2.26c}$$

$$u_4^{SMB} = (1+P\delta_B)u_s \tag{2.26d}$$

These equations imply that the adsorption wave of solute A is standing still in section III. Separation occurs because the adsorption wave of solute B travels faster than that of solute A, moving past the raffinate port and entering section IV. Similarly, the desorption wave of solute B is standing still in section II and the desorption wave of solute A passes the extract port and enters section I, because the migration velocity of solute A is slower than that of solute B. Furthermore, the adsorption wave of solute B stands in section IV and the desorption wave of solute A stands in section I. As a result, the two concentration waves are confined in their respective sections, so as to prevent them from contaminating each other.

If one more condition, either the feed flow rate, F, or solvent flow rate, E, is given, all the fluid and solid phase movement velocities can be obtained from Eqs. 2.26a-d and one of the following mass balance equations:

$$\frac{F}{\varepsilon S} = u_3^{SMB} - u_2^{SMB} \tag{2.27a}$$

$$\frac{E}{\varepsilon S} = u_1^{SMB} - u_4^{SMB} \tag{2.27b}$$

where S is the bed cross section.

2.4.3.2 Linear System with Axial Dispersion and Mass Transfer Resistance

When mass transfer effects were taken into account, the authors used steady-state model to derive the analytical solutions, i.e., the time derivative term in the mass balance Eqs. 2.20 and 2.21 was omitted. After derivation and rearrangement (Ma and Wang, 1997; Wu et al., 1999), the following design equations were obtained:

$$\left(1 + P\delta_A\right)u_s - u_1^{SMB} = -\beta_A^I\left(\frac{E_A^I}{L^I} + \frac{Pu_s{}^2\delta_A^2}{K_{fA}^I L^I}\right) \tag{2.28a}$$

$$(1+P\delta_B)u_s - u_2^{SMB} = -\beta_B^{II}\left(\frac{E_B^{II}}{L^{II}} + \frac{Pu_s{}^2\delta_B^2}{K_{fB}^{II}L^{II}}\right) \quad (2.28b)$$

$$(1+P\delta_A)u_s - u_3^{SMB} = \beta_A^{III}\left(\frac{E_A^{III}}{L^{III}} + \frac{Pu_s{}^2\delta_A^2}{K_{fA}^{III}L^{III}}\right) \quad (2.28c)$$

$$(1+P\delta_B)u_s - u_4^{SMB} = \beta_B^{IV}\left(\frac{E_B^{IV}}{L^{IV}} + \frac{Pu_s{}^2\delta_B^2}{K_{fB}^{IV}L^{IV}}\right) \quad (2.28d)$$

Purity requirements were represented by parameter β, which defined the ratio of the highest concentration to the lowest concentration of the standing wave in one section. For example, $\beta_B^{III} = \ln\left(\frac{C_B\big|_{x=0}}{C_B\big|_{x=L^{III}}}\right)$ is the natural algorithm of the ratio of the concentration at the feed port to that at the raffinate port for solute B. L^{III} is the length of section III. The Eqs. 2.28a-d indicate the modification in the linear velocities (Eqs. 2.26a-d), and are related to the axial dispersion, E, the mass-transfer coefficients, K_f,, the section length, L, and product purity, β. The authors concluded that when axial dispersion and mass transfer resistance were significant, Eqs. 2.28a-d gave the highest throughput and lowest solvent consumption if the desired product purities (β^{III} and β^{IV}) and the feed flow rate (F) were specified for a given system.

The standing wave concept was further developed for nonlinear systems, but without mass-transfer effects (Mallmann et al., 1998).

It is obvious that triangle theory and standing wave concept, based on TMB model, are very convenient and effective for the systems that are described by a few relatively simple adsorption isotherms (such as linear, Langmuir or modified Langmuir isotherm) provided the mass transfer resistances are not significant. The results obtained from these design principles (based on TMB process) might deviate from what happens in real SMB process, especially when the total number of columns is

low. However, for real systems, triangle theory or standing wave concept can provide relatively close initial operating conditions in order to search for the optimal ones. A more reliable optimization strategy is needed for the design of SMB systems.

Chapter 3 Reaction Kinetics and Adsorption Isotherm Studies for Methyl Acetate Esterification and Hydrolysis

3.1 Introduction

Methyl acetate synthesis by esterification of acetic acid with methanol and the backward reaction, the hydrolysis of methyl acetate, have been considered as model reaction for reactive distillation (Fuchigami, 1990; Agreda et al., 1990; Han et al., 1997) and simulated moving bed reactor (Lode et al., 2001).

Methyl acetate is used as solvent for the production of coating materials, nitro-cellulose, cellulose acetate, cellulose ethers, and celluloid. It is also used with a wide variety of resins, plasticizers, lacquers and certain fats. Methyl acetate (MeOAc) is usually produced by the liquid-phase reaction of acetic acid (HOAc) and methanol (MeOH) catalyzed by sulphuric acid or a sulphonic acid ion exchange resin in the tempertaure range of 310-325 K and atmospheric pressure. The reaction is

$$CH_3COOH + CH_3OH \rightleftharpoons CH_3COOCH_3 + H_2O \qquad (3.1)$$

The hydrolysis of methyl acetate is also of importance as in the synthesis of polyvinyl alcohol, methyl acetate is formed, as byproduct, and acetic acid and methanol can be recycled in the process (Fuchigami, 1990).

Reactive distillation (DeGarmo et al., 1992; Doherty et al., 1992; Rev, 1992) has been found to be suitable for the methyl acetate reaction system for the two different processes mentioned above, namely, synthesis and hydrolysis of methyl acetate. Like reactive distillation, simulated moving bed reactor (Lode et al., 2001) can provide economic benefit for the above reversible reaction. In-situ separation of the products at the site of chemical reaction in the simulated moving bed reactor (SMBR) facilitates the reversible reaction to completion beyond thermodynamic equilibrium

and at the same time obtaining products of high purity. SMBR (Ray et al., 1990, 1994, 1995a, 1995b; Mazzotti et al., 1996b; Kawase et al., 1996, 2001; Lode et al., 2001) has recently received growing interest as an alternative for reactive distillation, especially in some fine chemical and pharmaceutical applications when the chemical species involved in the process are non-volatile or temperature sensitive. It is noted that the model reaction is a very good system to study the SMBR process, even though the SMBR for this model reaction is not competitive against the Eastman reactive distillation. This is always the case for adsorption-based processes that can be competitive only in the cases where distillation is too expensive. In order to investigate the performance of the SMBR for the above two different applications of the model reaction (Eqs. 3.1) catalyzed by ion exchange resin (Amberlyst 15), methanol or water has to be used as mobile phase depending on the application.

This Chapter describes the method of obtaining the adsorption equilibrium constants, dispersion coefficients and kinetic parameters for the two different application processes of methyl acetate reaction system, corresponding to the different mobile phases, methanol or water.

3.2 Reaction Kinetics and Adsorption Isotherm

Most reactions catalyzed by ion exchange resins can be classified either as quasi-homogeneous or as quasi-heterogeneous. The idealized homogeneous state requires complete swelling of the resin and total dissociation of the polymer-bound-SO_3H group, whereas the heterogeneous state is characterized by a direct interaction of the substrate with the polymer-bound-SO_3H group. In cases where the mass transfer resistance is absent and one of the reactants or solvent is highly polar, the rate of reaction can be expressed using a simple pseudo-homogeneous model (Chakrabarti and Sharma, 1993). The kinetics of this model reaction catalyzed by Amberlyst 15 has been

described in past investigations by both with a quasi-homogeneous or adsorption based heterogeneous model.

Xu and Chuang (1996) deduced a kinetic equation in the form of power law model from the Langmuir-Hinshelwood model for the esterification of acetic acid and methanol over Amberlyst 15 ion exchange resin, by assuming that the adsorption is weak for all the components. They concluded that although the resin is not completely swollen and the active polymer-bound group ($-SO_3H$) is not totally dissociated from the carrier, the reaction could still be considered as homogeneous as long as all the chemicals involved in the process are weakly adsorbed.

Mazzotti et al. (1996b) proposed a quasi-homogeneous kinetic model for a similar reaction system, esterification of acetic acid to ethyl acetate in the presence of Amberlyst 15 ion exchange resin catalyst. They assumed that the reaction occurs only in the polymer phase, and the bulk liquid and polymer phases are in constant equilibrium conditions. Instead of calculating the concentrations of adsorbed components by the Langmuir type adsorption isotherm (Rehfinger and Hoffmann, 1990), they used phase equilibrium model by equating the activities of the involved components in both liquid and polymer phases to relate the concentrations of components in the polymer phase to those in the bulk liquid phase. The activities were estimated using UNIFAC for the liquid phase and the extended Flory-Huggins model for the polymer phase. The parameters were fitted to adsorption equilibrium experimental results of four binary systems where no reactions were involved.

Song et al. (1998) developed a heterogeneous Langmuir-Hinshelwood/Hougen-Watson (LHHW) type reaction rate model for the synthesis of methyl acetate. They considered that adsorption effect should be taken into account to describe the reaction catalyzed by ion exchange resins, because more than 95% protons are inside the micro-

spheres and are only accessible to chemical species which are able to diffuse into the polymer matrix.

Pöpken et al. (2000) considered both pseudo homogeneous model and adsorption based model for acetic acid esterification with methanol and methyl acetate hydrolysis. They concluded that taking the liquid phase nonideality into account is not sufficient to describe the heterogeneous kinetics, and the interaction between the solid catalyst and the reactants has to be considered in the model.

In this work, either methanol or water is present in large excess concentration corresponding to the synthesis and hydrolysis of methyl acetate respectively. The polymer resin is initially saturated with either methanol or water, and therefore, it can be assumed that the ion exchange resin in contact with polar solvent (methanol or water) is completely swollen, the active sulfonic acid group is totally dissociated, and the solvated protons are evenly distributed in the polymer phase. This enables the chemical species participating in the reaction to penetrate the network of cross-linked polymer chains easily, and come in contact with the solvated protons. Therefore, the quasi-homogeneous model can be applied to describe the reaction in this study. However, when the concentration of methanol (or water) decreases, the polymer phase deviates much from the ideal homogenous state, an adsorption-based heterogeneous model would be more suitable. Moreover, the reaction is carried out in a large excess of methanol (or water) in this work, the concentration of methanol (or water) can be assumed to remain essentially unchanged in the course of the reaction. Based on the above assumptions, the quasi-homogeneous kinetic models, applicable to this work can be written as

$$R_s = k_{fs}\left[q_A - \frac{q_E q_W}{K_{es}}\right] \quad \text{for the synthesis of MeOAc} \tag{3.2}$$

$$R_{\mathrm{h}} = k_{\mathrm{bh}}\left[q_E - \frac{q_A q_M}{K_{eh}}\right] \quad \text{for the hydrolysis of MeOAc} \tag{3.3}$$

where R denotes the reaction rate, q_i is the concentration of component i in the polymer phase, k_f and k_b are the forward and backward reaction rate constant respectively, K_e is the reaction equilibrium constant, and the second subscript, s or h, stands for synthesis or hydrolysis. The concentration of the adsorbed component i (q_i) in the polymer phase is computed by assuming that the liquid and polymer phase are in constant equilibrium and using a linear adsorption isotherm (Henry's law), which is expressed as

$$q_i = K_{ij} C_i \tag{3.4}$$

where K_{ij} represents the adsorption equilibrium constant of component i (A, E, M or W) for the jth application (synthesis or hydrolysis). The linear adsorption isotherm is only valid when the concentrations of the adsorbed species are dilute in the bulk liquid phase, as is the case in this study. The assumption that adsorption equilibrium can be described through a liner relationship is rather weak, and in fact the proportionality constant for each species has to be modified whether one deals with synthesis or with hydrolysis.

3.3 Estimation of Reaction and Adsorption Parameters

3.3.1 Experimental Details

Methanol (purity > 99.9 wt %) and acetic acid (purity > 99.8 wt %) were obtained from Merck. Methyl acetate (purity > 99 wt %) was obtained from Riedel-de-Haën. They were used without further purification.

The macro-porous sulfonic acid ion exchange resin Amberlyst 15 Dry purchased from Rohm and Haas Company was chosen as the catalyst in this work. These are cross-linked 3-dimensional structures of polymeric material obtained by sulfonation of a copolymer of polystyrene and divinyl benzene. These resins are heat sensitive and will lose its activity above 393 K. Macro-porous resins are better catalyst compared to micro-porous resins, particularly in non-aqueous media where the latter resins do not swell appreciably. The main properties of the ion exchange resin are listed in Table 3.1. For the methyl acetate synthesis study in which methanol is used as solvent, the catalyst was first dried under vacuum at 363 K for 8 hours before usage. Drying at higher temperatures embraces the risk of losing catalyst capacity resulting from gradual desulfonation.

Table 3.1 Typical Properties of Amberlyst 15 Dry Ion Exchange Resin

Appearance	Hard, dry, spherical particle
Typical particle size distribution	% retained on US standard screens
16 mesh	2-5
16~20 mesh	20-30
20~30 mesh	45-55
30~40 mesh	15-25
40~50 mesh	5-10
through 50 mesh	1.0
Bulk density, lbs/ft^3	38 (608 g/l)
Moisture, by weight	Less than 1%
Hydrogen ion concentration, meq/g dry	4.7
Surface area, m^2/g	50
Porosity, ml pore/ml bead	0.36
Average pore diameter, Å	240

The experiments were conducted in a 0.25 m long HPLC column of inner diameter 0.0094m packed with Amberlyst 15. The column was immersed in a water bath filled with a 1:1 mixture of ethylene glycol and water, together with a temperature

controller to obtain desirable constant temperatures. A binary, series 200 LC pump from Perkin-Elmer was connected to the column to provide a rectangular pulse input of width $t_{p.}$ Effluent from the exit of the column was collected manually at fixed time intervals.

A HP 6890 gas chromatography equipped with 7683 Automatic Injector and FID was used to determine the concentration of methanol, methyl acetate, and acetic acid. A 30m×0.53mm×1μm OV-1 fused silica capillary column was used to separate the reaction mixture. Water concentration was measured using a volumetric Karl Fischer titrator with model 100-titration controller from Denver Instrument.

3.3.2 Experimental Procedure

Experiments were conducted at various temperatures (313, 318 and 323 K), feed concentrations and flow rates. The column was washed with mobile phase (methanol or water) until the effluent liquid was colorless to ensure removal of impurities when fresh catalyst/adsorbent was used. In the subsequent runs, the column was washed with methanol (or water) for about 30 minutes before feeding. A rectangular pulse input of width 5~10 minutes was introduced as feed to the packed bed reactor by switching on the LC pump connected with the feed reservoir. Afterwards, pure methanol (or water) was continuously fed to the column to wash off any chemical adsorbed on the catalyst.

Two types of experiments (non-reactive as well as reactive) were carried out in a single column packed bed reactor with either methanol or water as mobile phase. Adsorption parameters were determined from the non-reactive experiments while kinetic parameters were evaluated from the reactive experiments. When methanol was used as a carrier, a mixture of methyl acetate and water dissolved in methanol was used as feed for the non-reactive breakthrough experiments, while a binary mixture of acetic

acid and methanol was fed to the column in the reactive breakthrough experiments. When water was used as mobile phase, a binary mixture of methanol (or acetic acid) dissolved in water was used as feed for the non-reactive breakthrough experiments, while for the reactive breakthrough experiments, a binary mixture of methyl acetate and water was fed to the reactor. The elution (breakthrough) profiles of the various components from the exit of the column were monitored continuously. The samples were taken at 2 minutes intervals from the outlet of the column and the breakthrough curves of components involved in the process were obtained by plotting the concentration of each component with elution time.

3.3.3 Development of Mathematical Model

A mathematical model for the single column packed bed reactor was developed based on a quasi-homogeneous kinetics, which assumes the reaction in the polymer phase to be homogeneous considering the large excess of polar solvent (methanol or water) used in the reaction mixture. The behaviors of reactants and products in the fixed bed reactor were described by the equilibrium-dipersive model, which assumes that the mobile and the stationary phases are always in equilibrium, the contributions of all the non-equilibrium effects are lumped into an apparent axial dispersion coefficient, *D*, and the apparent dispersion coefficients of the solutes remain constant, independent of the concentrations of the components. Therefore the mass balance equation of component *i* for the reactive breakthrough system can be expressed as follows:

$$\frac{\partial C_i}{\partial t}+\left(\frac{1-\varepsilon}{\varepsilon}\right)\frac{\partial q_i}{\partial t}+\frac{u}{\varepsilon}\frac{\partial C_i}{\partial z}-\left(\frac{1-\varepsilon}{\varepsilon}\right)\upsilon_i R_j = D_{ik}\frac{\partial^2 C_i}{\partial z^2} \tag{3.5}$$

The initial and boundary conditions are given by

$$C_i\left[t=0\right]=C_i^0 \tag{3.6}$$

$$C_i\left|_{0<t<t_p}\right|_{Z=0} = C_{f,i} \tag{3.7}$$

$$C_i\left|_{t>t_p}\right|_{Z=0} = 0 \tag{3.8}$$

$$\left[\frac{\partial C_i(t)}{\partial z}\right]_{Z=0} = 0 \tag{3.9}$$

where u is the superficial mobile phase velocity, which is assumed to be constant, and the subscripts $i = A$ (HOAc), M (MeOH), E (MeOAc) or W (H_2O), $j = s$ (synthesis) or h (hydrolysis), and $k = M$ or W for mobile phase. Eqs. 3.5 is the overall mass balance equation of each component i in a single packed bed reactor in which the first two terms denote unsteady state term in the fluid and solid phase respectively, the third term represents the convective term, the fourth term stands for the reaction term, while the last term designates the diffusion term. In the case of non-reactive breakthrough system, the fourth term in the mass balance equation was set to zero. The apparent dispersion coefficient, D_{ik}, which is related to the height equivalent to theoretical plate (HETP) for the corresponding compound, is given by the following equation (Guiochon et al.1994):

$$D_{ik} = \frac{H_i u}{2} = \frac{Lu}{2N_{ap,i}} \tag{3.10}$$

In linear chromatography, HETP is related to the axial dispersion, adsorption equilibrium and the coefficients of resistance to mass transfer as described by Van Deemter et al. (1956). However, determination of the value of HEPT, H_i, or the apparent plate number, $N_{ap,i}$, is a tedious lengthy process. Hence, in this work, D_{ik} values were obtained by fitting the experimental elution profiles for each component to the solution of the above model equations (Eqs. 3.2-3.9). Due to experimental

limitations, an additional assumption is made that the apparent dispersion coefficient of acetic acid is equal to that of methyl acetate.

The PDE in Eqs. 3.6 together with the initial and boundary conditions (Eqs. 3.6-3.9), kinetic equations (Eqs. 3.2 or 3.3) and adsorption equilibrium (Eqs. 3.4) were solved using Method of Lines. In this technique the PDE is first discretized in space using Finite Difference Method (FDM) to convert it into a set of several-coupled ODE-IVPs. The numerical Method of Lines combines a numerical method for the initial value problems (IVPs) of ordinary differential equations (ODEs) and a numerical method for the boundary value problems (BVPs). The resultant stiff ODEs of the initial value kind was solved using the subroutine, DIVPAG (which is based on Gear's method), in the IMSL library. The breakthrough curves predicted by the model describing the concentration profiles of reactants and products are discussed later.

3.3.4 Parameter Estimation from Breakthrough Curves

In order to determine the kinetic and adsorption parameters, an error function was defined as the sum of square deviations of the component concentrations predicted by the model from the experimentally measured values. It is written as:

$$F(x) = \sum_{i=1}^{n} \sum_{j=1}^{m} \left[C_{ij,exp} - C_{ij,m} \right]^2 \tag{3.11}$$

where C_{ij} is the concentration of i^{th} component for j^{th} data point, x is the vector of the parameters tuned, and the subscripts exp and m denote experimentally measured and model predicted values respectively. Parameters need to be determined by tuning the model predicted values to the experimental breakthrough curves were obtained by minimizing the error function, F, using a state-of-the-art optimization technique, the genetic algorithm (GA). GA is a search technique developed by Holland (1975) based on the mechanics of natural selection and natural genetics, and has become quite

popular in recent years. A further understanding of genetic algorithm can be obtained elsewhere (Holland, 1975; Goldberg 1989; Bhaskar et al., 2000).

3.4 Results and Discussion

3.4.1 Synthesis of Methyl Acetate

3.4.1.1 Determination of Adsorption and Kinetic Parameters

The adsorption equilibrium constants and dispersion coefficients of methyl acetate and water were obtained by fitting the non-reactive breakthrough curves predicted by the model to those measured experimentally when a rectangular pulse input of a mixture of methyl acetate and water dissolved in methanol was fed to the column. The error function F in Eqs. 3.11 was minimized by tuning four parameters, x, namely, K_{Es}, K_{Ws}, D_{EM} and D_{WM} to match the predicted values with the experimental breakthrough curves. The single objective function optimization problem involving minimization of the error function was solved using genetic algorithm. A gene pool of 50 chromosomes was considered and GA operations were carried out for 50 generations, subsequent to which it was observed that all 50 chromosomes converged to a single global optimum point.

Figure 3.1 shows the experimental as well as the predicted breakthrough curves at three different temperatures (313, 318 and 323K). Separation of the two components takes place due to the difference in their adsorption affinities toward the adsorbent, and each component elutes from the column at different times. The figure shows that methyl acetate has less affinity towards the resin than water and there is some band broadenings. However, the model predicts quite well the experimentally measured breakthrough curves. The reasons for the broadening are manifold. Mass transfer resistance and axial dispersion are among the most important factors, which are lumped into one parameter, namely, apparent axial dispersion coefficient, D_{ik}.

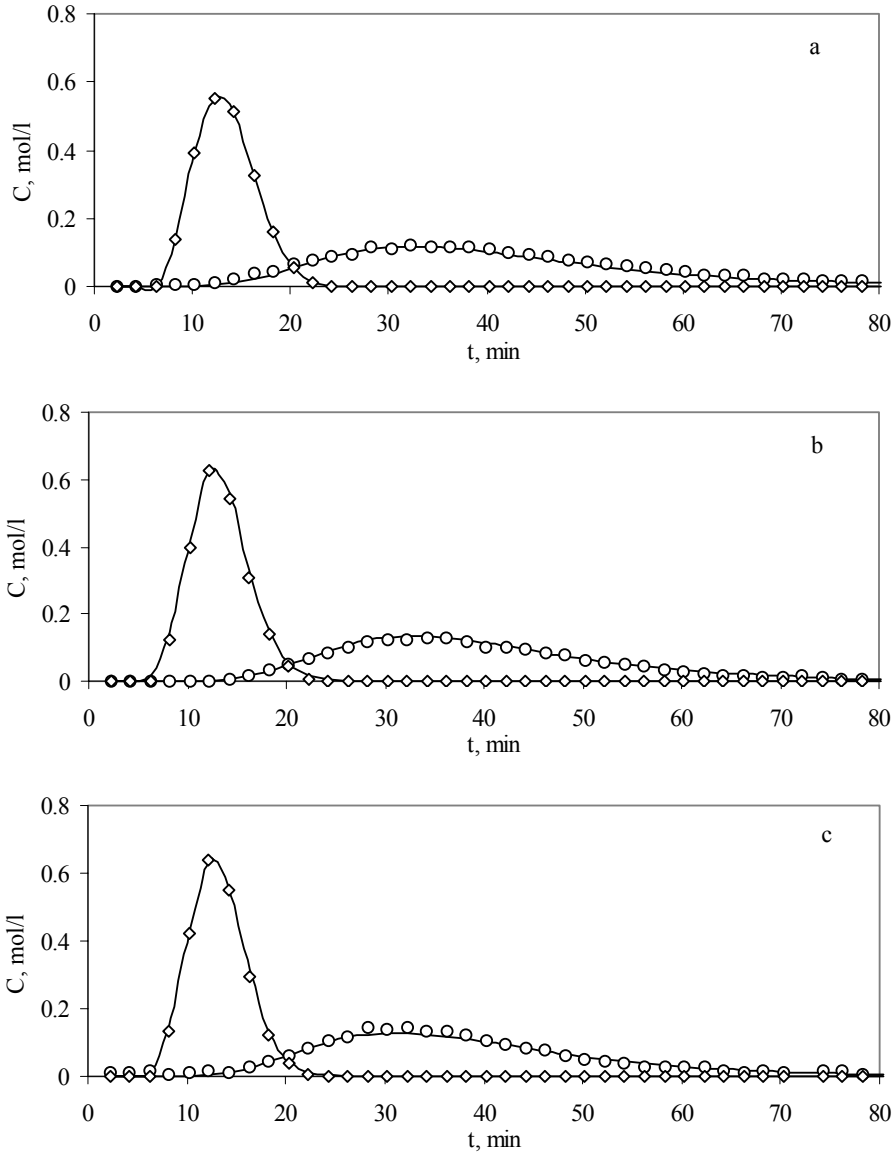

Figure 3.1 Effect of temperature on breakthrough curve of the MeOAc-H_2O system

Symbols: Experiment (◊ E; o W); Lines: Model prediction
Experimental conditions: Q = 1 ml/min, $[E]_f$ = 0.89 mol/l, $[W]_f$ = 0.81mol/l,
t_p = 5 min, solvent: M
(a) T = 313 K, (b) T = 318 K, (c) T = 323 K

The adsorption and dispersion parameters of methyl acetate and water for the synthesis reaction at different temperatures together with the error function values are given in Table 3.2. The numerical value of adsorption equilibrium constant of water is

much greater (7-8 times) than that of methyl acetate, which is expected since the polarity of water is much stronger than that of methyl acetate towards the resin and is also observed experimentally. Moreover, the calculated adsorption constants of water and methyl acetate decrease with the increase of temperature, which is also expected since adsorption is an exothermic process.

Table 3.2 Adsorption equilibrium constants and apparent dispersion coefficients for MeOAc and H_2O (methanol as mobile phase)

T K	K_{Es}	K_{Ws}	D_{EM} m^2/s	D_{WM} m^2/s	F mol^2/l^2
313	0.40	3.08	5.01×10^{-6}	14.6×10^{-6}	0.004
318	0.38	2.94	3.88×10^{-6}	11.2×10^{-6}	0.008
323	0.36	2.78	3.46×10^{-6}	11.0×10^{-6}	0.013

In order to investigate the validity of the computed parameters, the non-reactive breakthrough experiments were conducted at different feed compositions. Figure 3.2 shows the agreement between the experimental and theoretically predicted (using the parameter values listed in Table 3.2) breakthrough curves of methyl acetate and water when experiments were carried out either at the same feed concentration of Figure 3.1 but for varying length of pulse input (t_p) or at high feed concentrations. Figure 3.2 reveals that although the breakthrough curves calculated by the model are in good agreement with the experimental results for MeOAc, the prediction for H_2O is not so good due to the tailing effect and possibly a non-linear adsorption isotherm should be used.

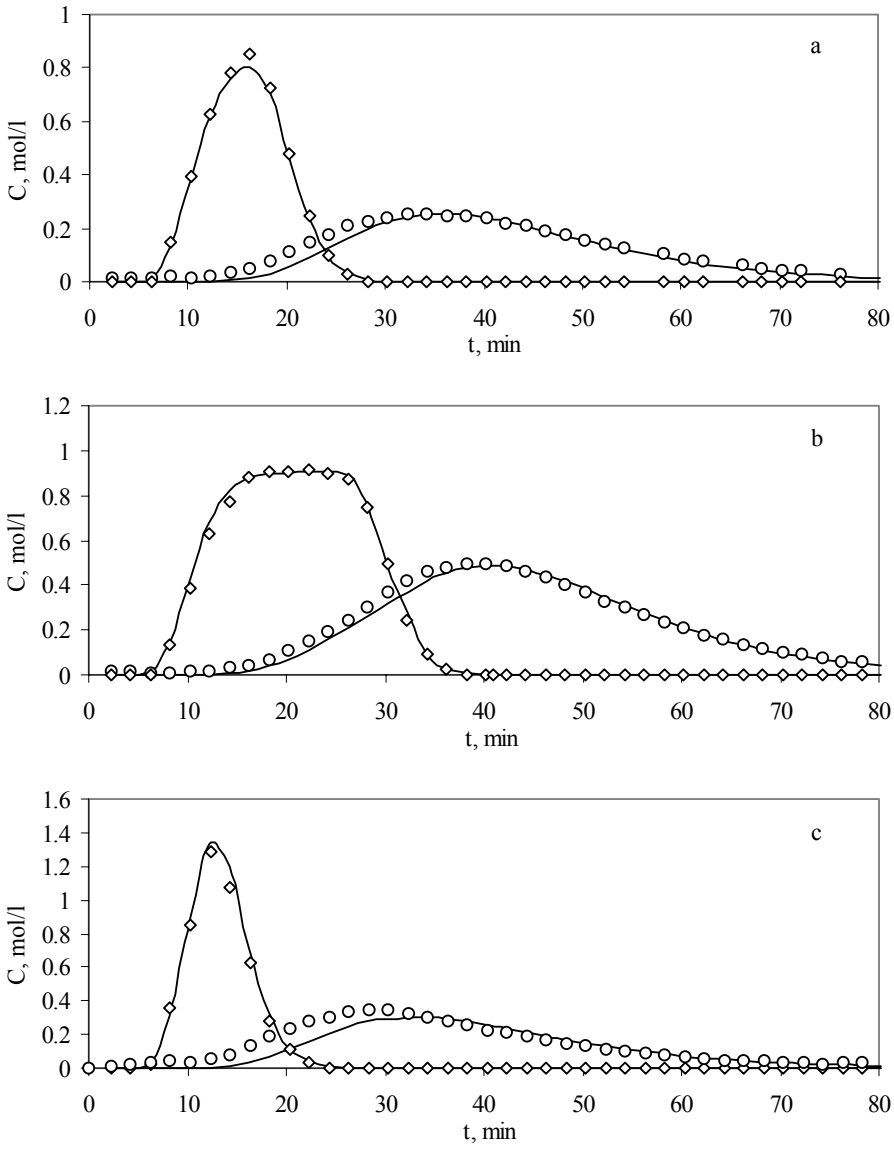

Figure 3.2 Effect of feed concentration on breakthrough curve of the MeOAc-H_2O system

Symbols: Experiment (◊ E; o W); Lines: Model prediction
Experimental conditions: Q = 1 ml/min, T = 318 K, solvent: M

(a) $[E]_f$ = 0.85 mol/l, $[W]_f$ = 0.81 mol/l, t_p = 10 min
(b) $[E]_f$ = 0.89 mol/l, $[W]_f$ = 0.81 mol/l, t_p = 20 min
(c) $[E]_f$ = 1.86 mol/l, $[W]_f$ = 1.99 mol/l, t_p = 5 min

In order to determine the adsorption equilibrium constant of acetic acid (K_{As}), the forward reaction rate constant (k_{fs}), and the reaction equilibrium constant (K_{es}) for the synthesis reaction at three different temperatures (313K, 318K and 323K), reactive breakthrough experiments were conducted by using a binary mixture of acetic acid and methanol as a pulse input. The three parameters (K_{As}, k_{fs}, K_{es}) were tuned keeping the other parameters (K_{Ws}, K_{Es}, D_{WM}, D_{EM}) determined from the non-reactive breakthrough results constant at the values listed in Table 3.2 , so that the error function in Eqs. 3.11 is minimum.

Figure 3.3 shows the experimental as well as model predicted results while the tuned values of the three parameters (K_{As}, k_{fs}, K_{es}) at different temperatures are listed in Table 3.3. The equilibrium conversion of HOAc, and yield and purity of MeOAc for three different temperatures are also summarized in Table 3.3. Once again, the proposed model can predict the experimental breakthrough curves reasonably well.

Table 3.3 Adsorption equilibrium constant, K_{As} and kinetic parameters, k_{fs} and K_{es} for the synthesis of MeOAc (methanol as mobile phase)

T K	K_{As}	k_{fs} s^{-1}	K_{es} mol/l	F mol^2/l^2	X_A	Y_E	P_E
313	0.48	1.42×10^{-2}	349	0.042	98.57%	98.57%	49.64%
318	0.43	1.77×10^{-2}	334	0.052	98.49%	98.49%	49.62%
323	0.38	2.40×10^{-2}	325	0.026	98.43%	98.43%	49.60%

*Calculation is based on $[A]_o$ = 2.0 mol/l. $X_A = 1 - [A]_{out} / [A]_o$; $Y_E = [E]_{out} / [A]_o$; $P_E = [E]_{out} / ([E]_{out} + [A]_{out} + [W]_{out})$.

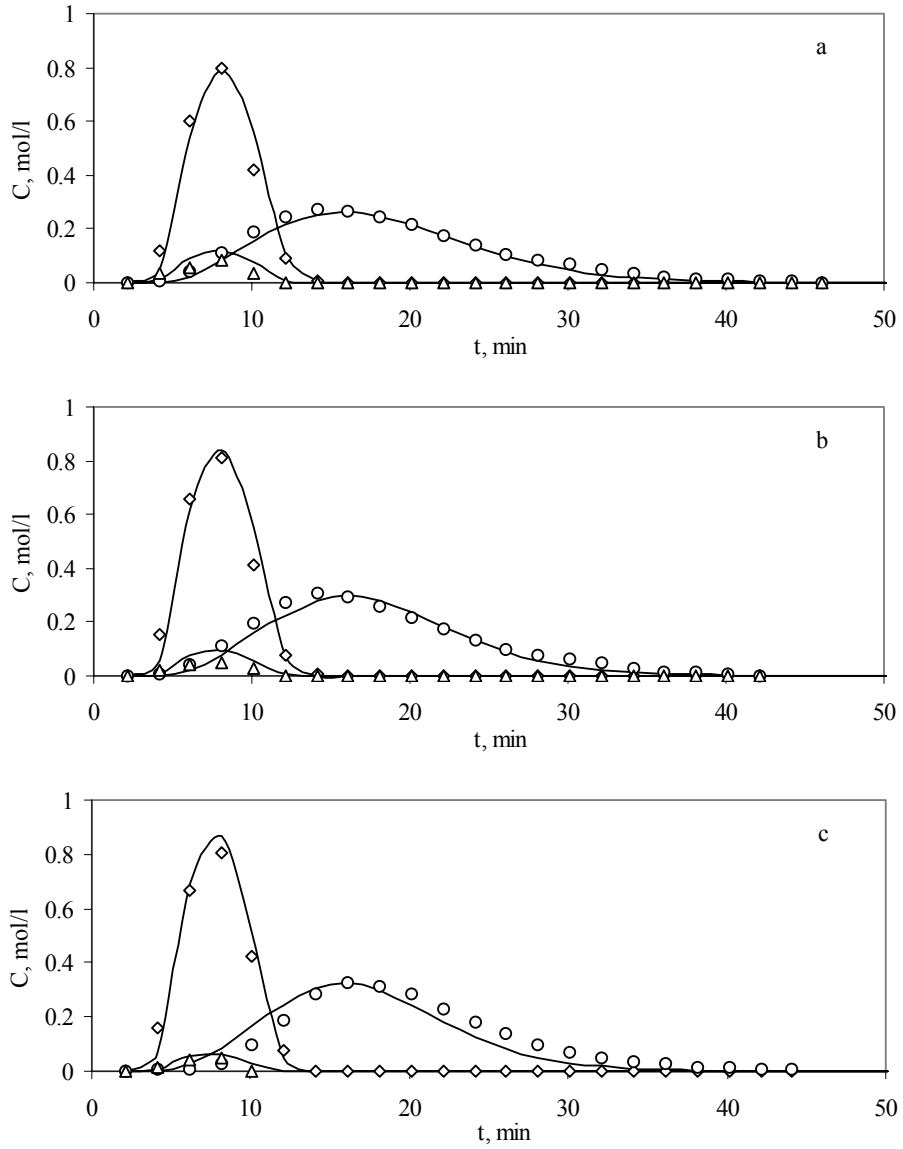

Figure 3.3 Effect of temperature on breakthrough curve of the HOAc -MeOAc-H_2O system

Symbols: Experiment (Δ A; ◊ E; o W); Lines: Model prediction
Experimental conditions: Q = 2 ml/min, $[A]_f$ = 0.95 mol/l, t_p = 5 min, solvent: M
(a) T = 313 K, (b) T = 318 K, (c) T = 323 K

In the heterogeneous reaction sequence, mass transfer of reactants first takes place from the bulk fluid to the external surface of the pellet. The reactants then diffuse from the external surface into and through the pores within the pellet. In order to determine intrinsic kinetic parameters, the effects of bulk diffusion resistance and pore diffusion resistance must be estimated first.

3.4.1.2 Estimation of Bulk (External) Diffusion Resistance

The Mear's criterion (1971), which uses the measured rate of reaction, helps to determine if external diffusion is limiting the reaction. Mear's criterion states that external mass transfer can be neglected if

$$\frac{\left(-r_A'\rho_b\right)R\,n}{k_c C_A} < 0.15 \tag{3.12}$$

where $(-r_A'\rho_b)$ is the measured rate of reaction, mol/m^3/s, R is the average particles radius (3.75×10^{-4} m), n is the order of reaction, C_A is the bulk concentration of the reactant (HOAc), mol/m^3, and k_c is the mass transfer coefficient, m/s. The measured initial rate of reaction can be determined from Eqs. 3.2 as 4.08 mol/m^3-cat bed/s, and the mass transfer coefficient, k_c, can be estimated from Dwivedi-Upadhyay mass transfer correlation (Dwivedi et al., 1977) as 4.13×10^{-5} m/s, which results in Mear's criterion parameter value of 3.79×10^{-3}, which is less than 0.15. Therefore, external mass transfer resistance can be neglected. Details of the above calculation are very similar to those reported by Zhang et al. (2001) and are not repeated here. It should also be noted that estimated kinetic parameters as reported in Table 3.3 can predict the breakthrough curves very well when experiments were performed at different flow rates (see later), confirming further that external mass transfer resistance is negligible.

3.4.1.3 Estimation of Pore Diffusion Resistance

In order to investigate the internal diffusion effect on the forward and backward reactions, commercial Amberlyst 15 was screened into several different particle sizes, and reaction kinetic experiments were conducted at 323K by using different sieved fractions of the catalyst particles in a batch reactor. Figure 3.4 clearly shows no observable effect of particle size on the forward (synthesis) as well as backward (hydrolysis) reaction kinetics. Therefore, the internal diffusion effect is negligible in this work. This was further confirmed that the plots of $\ln(k_{fs})$ vs $\ln(T)$ and $\ln(k_{bh})$ vs $\ln(T)$ show linear relationship indicating that the model reaction is kinetically controlled under our considered conditions, and also that the SMBR experimental results at various operating conditions are in good agreement with the model predictions using our determined kinetic parameters.

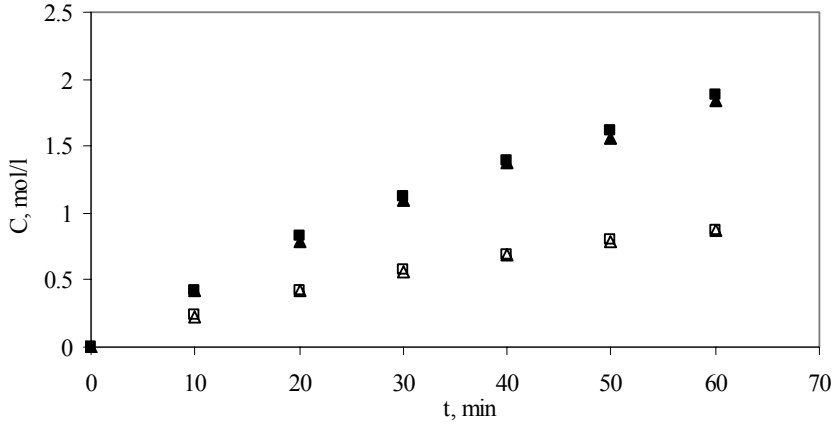

Figure 3.4 Effect of particle size on the reaction kinetics of synthesis and hydrolysis of MeOAc

Symbols □: d = 0.42-0.60mm; Δ: d = 0.85-1.00mm, open symbols: synthesis reaction, closed symbols: hydrolysis reaction. Experimental condition: T = 323 K, for synthesis reaction: initial mole number: n(HOAc) = 0.25, n(MeOH) = 4.80, mass of dry catalyst = 5.0 g; for hydrolysis reaction: initial mole number: n(MeOAc) = 0.70, $n(H_2O)$ = 10.50, mass of dry catalyst = 20.0 g. C: Concentration of MeOAc (synthesis reaction), Concentration of HOAc (hydrolysis reaction)

The tuned adsorption and kinetic parameters of the reaction system at three different temperatures were used next to verify the validity of the model by checking whether it could correctly predict experimental reactive breakthrough curves of the three components when experiments are performed at different flow rates and feed concentrations. Figure 3.5 and Figure 3.6 show the experimental as well as the predicted breakthrough curves at different initial concentrations and flow rates respectively. Figure 3.5 shows that the predicted breakthrough curves by the model fit the experimental results quite well when the feed is at low concentration as adopted in this work. Figure 3.6 shows that the model predicts experimental results reasonably well when flow rate is changed. These figures show that when adsorption and kinetic parameter values of Table 3.2 and 3.3 are used, the model can predict adequately the breakthrough curves for all three components.

From the figures, it is also apparent that when reaction occurs broadening of the elution peaks is less significant as the overall rate is controlled by kinetics (rate determining step) rather than by axial dispersion. The main reason for the small error is most likely that we have neglected the varied degrees to which the resin gets swollen when concentration changes inside the packed bed reactor. As a result, the local voidage will change, which subsequently changes the interfacial flow velocity. However, due to the low concentration range used in this work, the error caused by the swelling of resins can be considered to be insignificant.

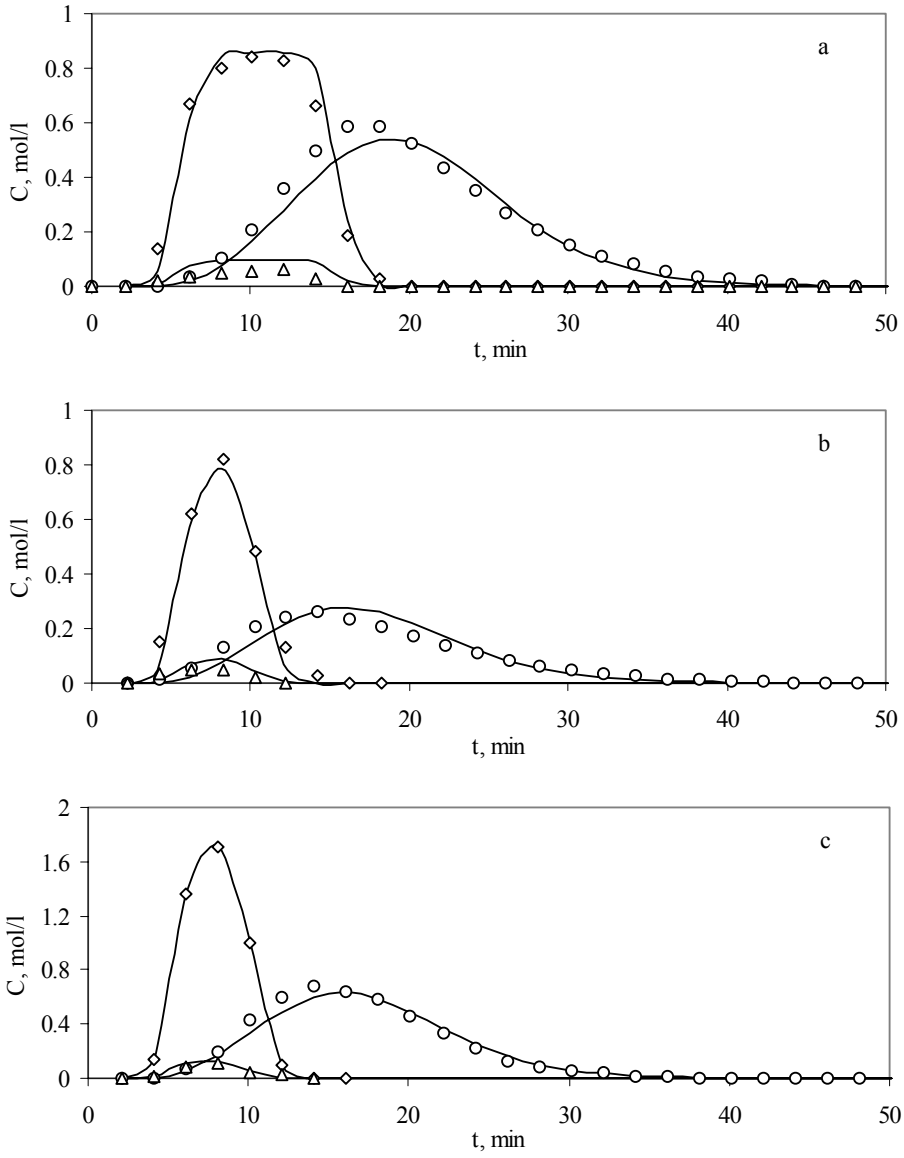

Figure 3.5 Effect of feed concentration on breakthrough curve of the HOAc-MeOAc-H_2O

Symbols: Experiment (Δ A; ◊ E; o W); Lines: Model prediction
Experimental conditions: Q = 2 ml/min, solvent: M

(a) $[A]_f$ = 0.95 mol/l, t_p = 10 min, T = 318 K
(b) $[A]_f$ = 0.89 mol/l, t_p = 5 min, T = 318 K
(c) $[A]_f$ = 1.86 mol/l, t_p = 5 min, T = 323 K

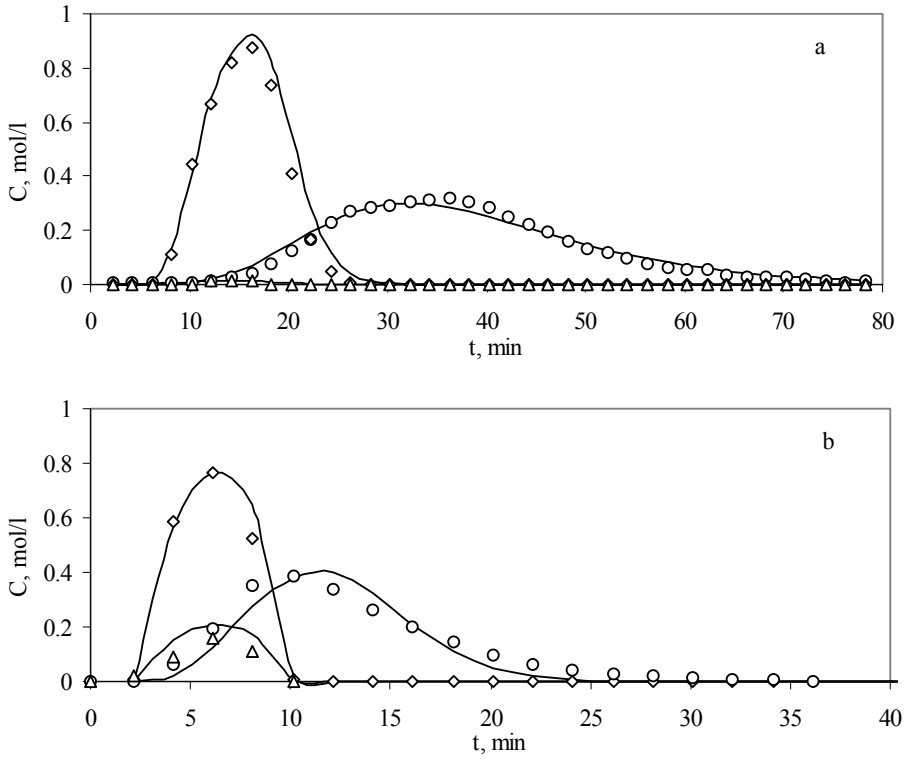

Figure 3.6 Effect of flow rate on breakthrough curve of the HOAc-MeOAc-H_2O system

Symbols: Experiment (Δ A; ◊ E; o W); Lines: Model prediction
Experimental conditions: T = 318 K, solvent: M
(a) Q = 1 ml/min, $[A]_f$ = 0.99 mol/l, t_p = 10 min
(b) Q = 3 ml/min, $[A]_f$ = 0.97 mol/l, t_p = 5 min

3.4.1.4 Effect of Temperature on the Adsorption and Kinetic Parameters

The temperature dependence of adsorption constants, K_{Es}, K_{Ws} and K_{As}, can be determined from the following Arrehenius equation:

$$K_{is} = K_{is}^{o} \exp\left[\frac{-\Delta H_{is}}{RT}\right], \qquad i = A, E, W \tag{3.13}$$

where ($-\Delta H$) is the heat of adsorption. The values of K_{is}^{o} and ($-\Delta H_{is}$) were obtained for each component (E, W and A) by least squares fit of Eqs. 3.13 to the data reported in Tables 3.2-3.3 and are given in Table 3.4. The heat of adsorption ($-\Delta H_{is}$) was found to be positive as it is an exothermic process and therefore, K_{is} decreases with the increase of temperature. The low values of ($-\Delta H_{is}$) indicate that the effect of temperature is not significant in the temperature range under study.

Table 3.4 Heat of adsorption, heat of reaction, activation energy and other thermodynamic values for the synthesis of MeOAc (methanol as mobile phase)

K_{is}^{0}			$-\Delta H_{is}$ kJ/mol			k_{fs}^{0} s^{-1}	E_{fs} kJ/mol	$\Delta S^{0}_{R,s}$ J/mol/K	$-\Delta H^{0}_{R,s}$ kJ/mol
A	E	W	A	E	W	From Eqs. 3.14		From Eqs. 3.15	
2.53×10^{-4}	1.21×10^{-2}	1.16×10^{-1}	19.6	9.10	8.53	3.26×10^{5}	44.2	30.0	5.83

Similarly, for forward reaction rate constant, k_{fs}:

$$k_{fs} = k_{fs}^{o} \exp\left[\frac{-E_{fs}}{RT}\right] \tag{3.14}$$

The reaction equilibrium constant, K_{es}, is related by

$$K_{es} = \left[\frac{k_{fs}}{k_{bs}}\right] = \left[\frac{k^o_{fs}}{k^o_{bs}}\right] exp\left[-\frac{(E_{fs}-E_{bs})}{RT}\right] = exp\left[-\frac{\Delta G^o_{R,s}}{RT}\right] = exp\left[\frac{\Delta S^o_{R,s}}{R}\right] exp\left[-\frac{\Delta H^o_{R,s}}{RT}\right] \quad (3.15)$$

The values of activation energy, E_{fs}, and pre-exponential factor, k^o_{fs} were obtained from least square fit of Eqs. 3.14 to the data given in Table 3.3 and the computed values are given in Table 3.4.

The $\Delta S^o_{R,s}\left[\equiv R\, ln\left(\frac{k^o_{fs}}{k^o_{bs}}\right)\right]$ and $\Delta H^o_{R,s}\left[\equiv (E_{fs} - E_{bs})\right]$ were also obtained by least square fit of Eqs. 3.15, and the values are given in Table3. 4.

3.4.2 Hydrolysis of Methyl Acetate

3.4.2.1 Determination of Adsorption and Kinetic Parameters

The non-reactive breakthrough experiments were carried out at three different temperatures (313, 318, and 323K) using acetic acid or methanol dissolved in water as a pulse input. Both the experimental and model predicted breakthrough curves at these three temperatures are shown in Figures. 3.7 and 3.8 for acetic acid and methanol respectively. The estimated adsorption and dispersion parameters of acetic acid and methanol using GA at different temperatures are tabulated in Table 3.5 and the figures show that the model predicts quite well the experimental results.

Table 3.5 Adsorption equilibrium constants and apparent dispersion coefficients for HOAc and MeOH (water as mobile phase)

T K	K_{Ar}	K_{Mr}	D_{AW} m^2/s	D_{MW} m^2/s	F mol^2/l^2
313	0.74	1.02	7.09×10^{-6}	6.30×10^{-6}	0.001
318	0.72	0.96	6.11×10^{-6}	6.49×10^{-6}	0.005
323	0.65	0.93	6.07×10^{-6}	6.30×10^{-6}	0.002

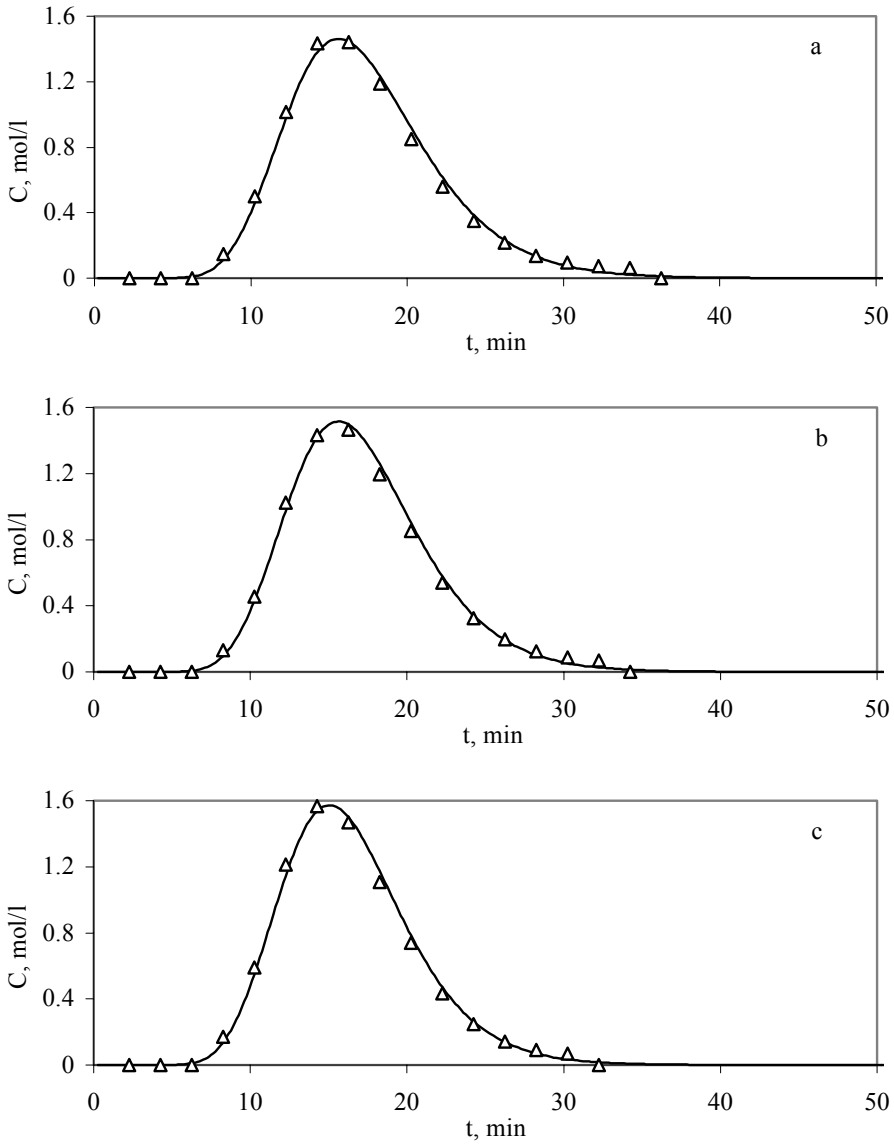

Figure 3.7 Effect of temperature on breakthrough curve of HOAc

Symbols: Experiment; Lines: Model prediction
Experimental conditions: Q = 1 ml/min, $[A]_f$ = 3.17 mol/l, t_p = 5 min, solvent: W
(a) T = 313 K, (b) T = 318 K, (c) T = 323 K

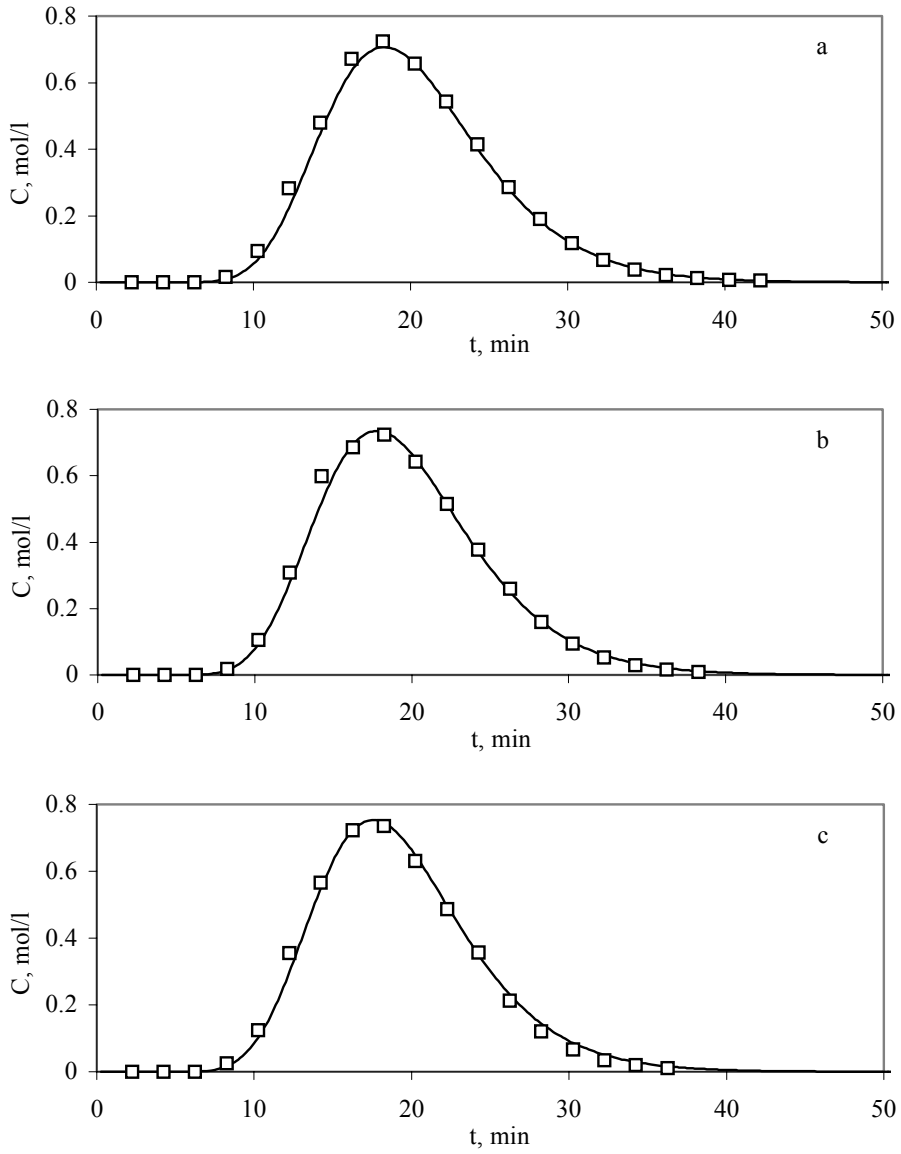

Figure 3.8 Effect of temperature on breakthrough curve of MeOH

Symbols: Experiment; Lines: Model prediction
Experimental conditions: Q = 1 ml/min, $[M]_f$ = 1.79 mol/l, t_p = 5 min, solvent: W
(a) T = 313 K, (b) T = 318 K, (c) T = 323 K

The adsorption constant of methyl acetate (K_{Eh}), the backward reaction rate constant (k_{bh}), and the reaction equilibrium constant (K_{eh}) were obtained by the same method as that described in section 3.4.1.1, except that a binary mixture of methyl acetate and water was fed as pulse input with water as mobile phase and the experimental results were fitted with kinetic expression given by Eqs. 3.3.

The experimental and model predicted elution profiles at three different temperatures are shown in Figure. 3.9, while the computed parameters (K_{Eh}, k_{fh} and K_{eh}) are listed in Table 3.6. Once again the reactive breakthrough experiments were conducted at different flow rates and feed concentrations in order to verify the robustness of the computed parameters. Figures 3.10 and 3.11 show experimental as well as model predicted results at different initial concentrations and flow rates respectively. The figures show that the predicted breakthrough curves are in good agreement with those obtained from experiments at different initial concentrations and flow rates.

Table 3.6 Adsorption equilibrium constant, K_{Eh}, and kinetic parameters, k_{fh} and K_{eh} for the hydrolysis of methyl acetate (water as mobile phase)

T, K	K_{Eh}	k_{fh} s^{-1}	K_{eh} mol/l	F mol^2/l^2	X_E	Y_M	P_M
313	7.05×10^{-1}	1.25×10^{-3}	8.89	0.025	90.25%	90.25%	47.44%
318	6.90×10^{-1}	1.87×10^{-3}	9.36	0.010	91.25%	91.15%	47.69%
323	6.86×10^{-1}	2.57×10^{-3}	9.54	0.026	92.16%	92.16%	47.96%

*Calculation is based on $[E]_o$ = 1.0 mol/l. $X_E = 1 - [E]_{out} / [E]_o$; $Y_A = [M]_{out} / [E]_o$; $P_A = [M]_{out} / ([E]_{out} + [A]_{out} + [M]_{out})$

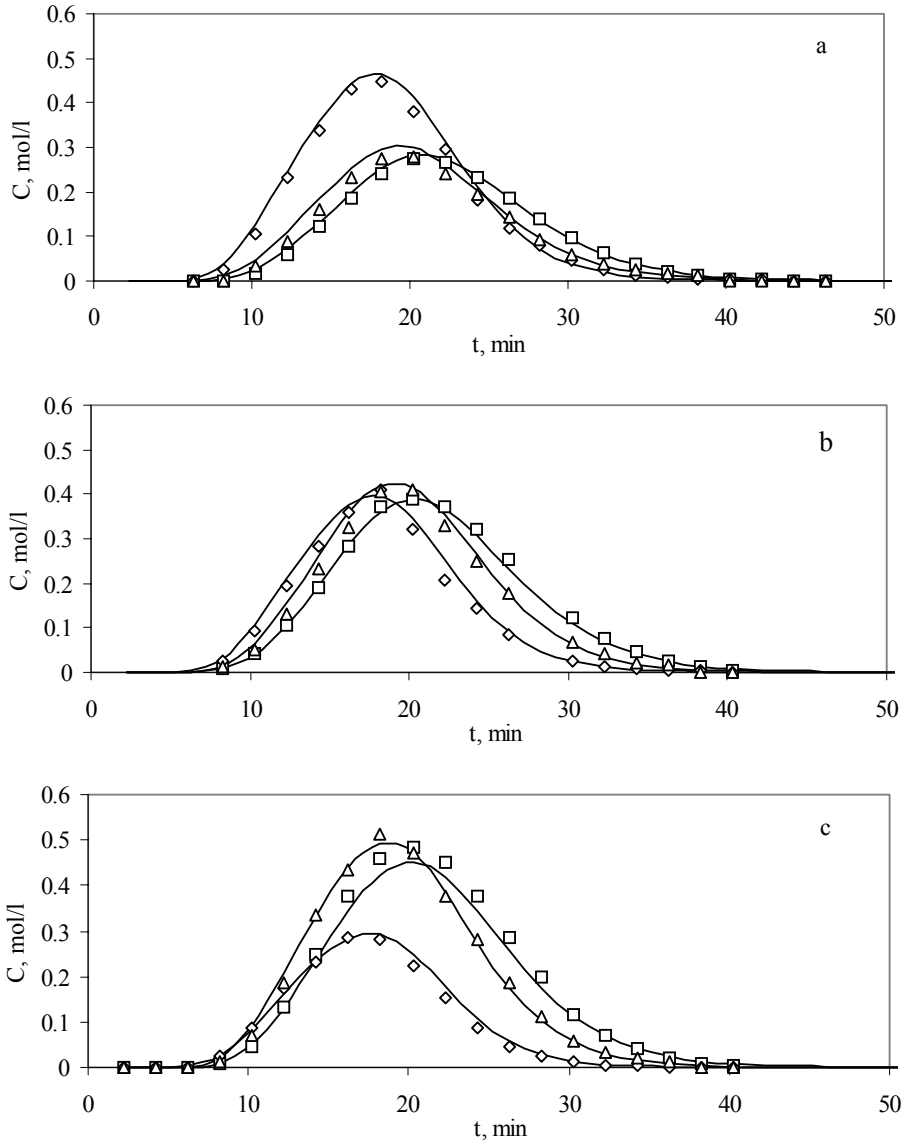

Figure 3.9 Effect of temperature on breakthrough curve of the MeOAc-HOAc-MeOH system

Symbols: Experiment (Δ A; ◊ E; □ M); Lines: Model prediction
Experimental conditions: Q = 1 ml/min, $[E]_f$ = 0.99 mol/l, t_p = 10 min, solvent: W
(a) T = 313 K, (b) T = 318 K, (c) T = 323 K.

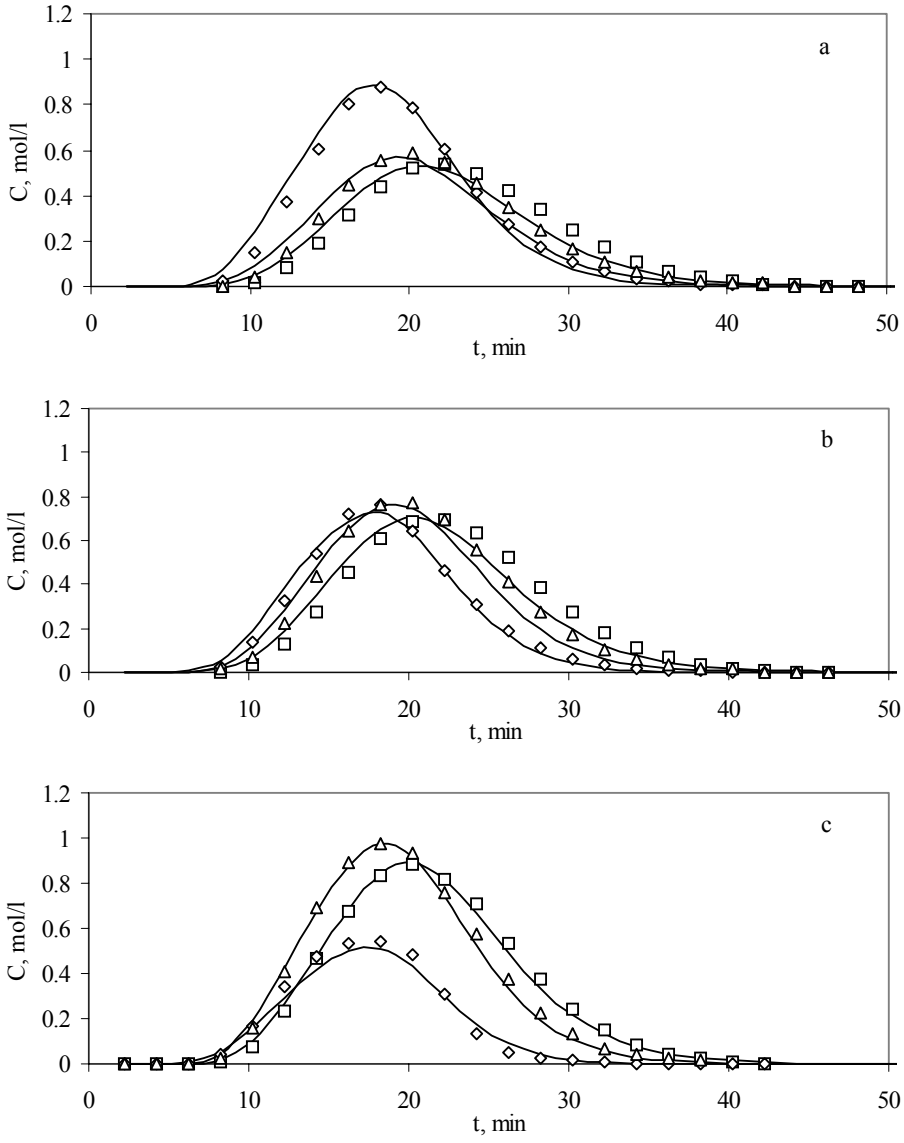

Figure 3.10 Effect of feed concentration on breakthrough curve of the MeOAc-HOAc-MeOH system

Symbols: Experiment (Δ A; ◊ E; □ M); Lines: Model prediction
Experimental conditions: Q = 1 ml/min, t_p = 10 min, solvent: W
(a) T = 313 K, $[E]_f$ = 1.87 mol/l
(b) T = 318 K, $[E]_f$ = 1.85 mol/l
(c) T = 323 K, $[E]_f$ = 1.82 mol/l

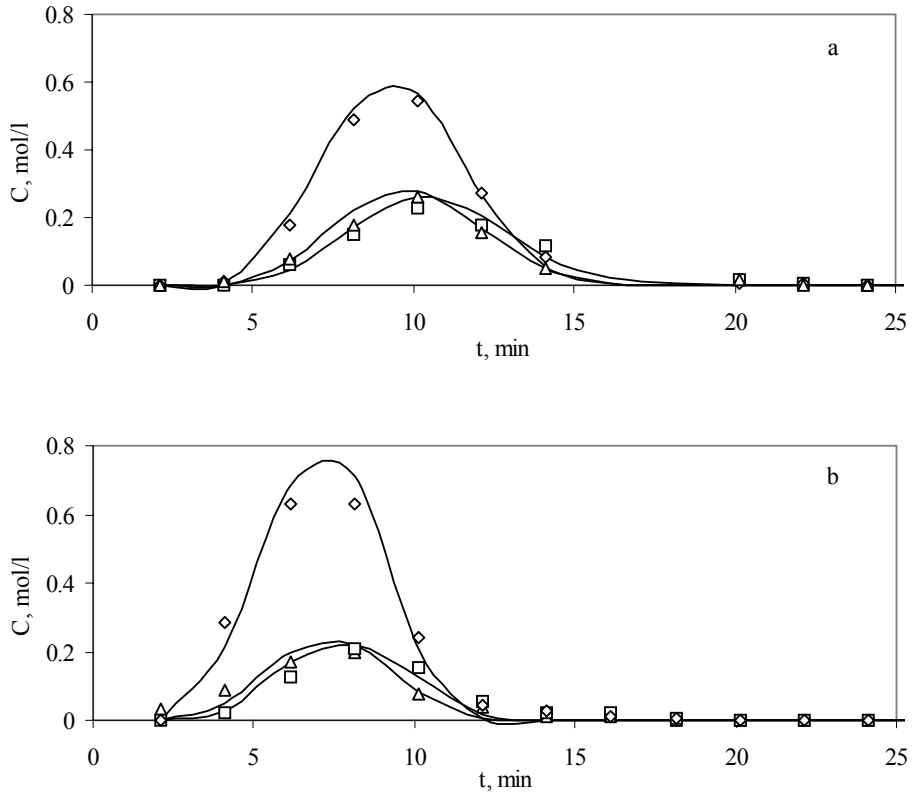

Figure 3.11 Effect of flow rate on breakthrough curve of the MeOAc-HOAc-MeOH system

Symbols: Experiment (Δ A; ◊ E; □ M); Lines: Model prediction
Experimental conditions: T = 318 K, $[E]_f$ = 0.97 mol/l, t_p = 5 min, solvent: W
(a) Q = 2 ml/min, (b) Q = 3 ml/min

3.4.2.2 Effect of Temperature on the Adsorption and Kinetic Parameters

The dependence of adsorption constants, K_{Ah}, K_{Mh}, K_{Eh}, on temperature were determined by least square fit of Eqs. 3.13 to the data reported in Tables 3.5-3.6. The values of K_{ih}^{o} and ($-\Delta H_{ih}$) are given in Table 3.7. Once again, the heat of adsorption was found to be positive ($-\Delta H_i > 0$) as it is an exothermic process and therefore, K_{ih} decreases with the increase of temperature. It was also observed that the effect of temperature is also not significant in the temperature range under study for the hydrolysis reaction. The dependence of reaction rate constant k_{bh} on temperature was determined from the Arrhenius equation (Eqs. 3.14) and the reaction equilibrium constants, K_{eh}, from Eqs. 3.15. The values of activation energy, E_{bh}, and pre-exponential factor, k_{bh}^{o}, were obtained from least square fit of Eqs. 3.14 while the values of $\Delta S_{R,h}^{o}$, $\Delta H_{R,h}^{o}$ were obtained by least square fit of Eqs. 3.15. The values are also given in Table 3.7.

Table 3.7 Heat of adsorption, heat of reaction, activation energy and other thermodynamic values for the hydrolysis of MeOAc (water as mobile phase)

K_{ih}^{o}			$-\Delta H_{ih}$ kJ/mol			k_{bh}^{o} s^{-1}	E_{bh} kJ/mol	$\Delta S_{R,h}^{o}$ J/mol/K	$-\Delta H_{R,h}^{o}$ kJ/mol
A	M	E	A	M	E	From Eqs. 3.16		From Eqs. 3.17	
0.013	0.053	0.290	10.54	7.69	2.30	1.65×10^{-7}	60.6	37.1	-5.91

3.4.3 Comparison of the Adsorption and Kinetic Parameters with those Reported in Literature

The adsorption and kinetic parameters calculated in our study do not match well with the reported results in literature (Song et al., 1998; Pöpken et al., 2000). In order to find out whether the discrepancy of results is due to the use of different types of Amberlyst 15, dry and wet, we carried out a reactive breakthrough experiment to compare the performance of Amberlyst 15 (dry) and Amberlyst 15 (wet). It was found that there is no significant difference between the two types of Amberlyst 15 when experiments were conducted with the wet Amberlyst 15 ion exchange resin vacuum dried for 10 hours at 353K.

Table 3.8 compares the adsorption equilibrium constants reported in literature with those obtained in this work. In our computed values, the adsorption constant of water was found to be about 7.7 times greater than that of methyl acetate and 6.4 times that of acetic acid. All our experimental studies showed that methyl acetate and acetic acid have very similar affinity towards the resin while water is strongly adsorbed on resin. However, the reported adsorption equilibrium values of Pöpken et al. (2000) reveals that the values of all three components are of similar magnitudes while that of Song et al. (1999) states that the adsorption constant of acetic acid is 3.9 times that of methyl acetate.

Table 3.8 Comparison of the computed adsorption equilibrium constants reported in literature with those obtained in this work at T = 313K

Parameters	Song et al. (1998)	Pöpken et al. (2000)	This work
K_{Es}	0.82	4.15	0.40
K_{Ws}	10.5	5.24	3.08
K_{As}	3.18	3.15	0.48
D_{EM}, m^2/s	23.5×10^{-6}	167×10^{-6}	5.01×10^{-6}
D_{WM}, m^2/s	167×10^{-6}	53.2×10^{-6}	14.6×10^{-6}

The adsorption equilibrium constants of the model reaction reported by Song et al. (1999) and Pöpken et al. (2000) were obtained from batch adsorption experiments. In order to compare the adsorption equilibrium constants of ours with literature reported values, the experimentally measured breakthrough curves were fitted with our model using the reported values of adsorption equilibrium constants in literature by adjusting the dispersion coefficients. The computed optimum values of dispersion coefficient are listed in Table 3.8. Figure 3.12 shows the comparison of the matching between experimental results and the predictions with our model using three different sets of parameter values listed in Table 3.8. The figure clearly shows that the model predicted breakthrough curves using the adsorption constants in literature are not in good agreement with the experimental results.

It is not possible to compare directly the kinetic parameters obtained in this work with that of Pöpken et al. (2000) due to the use of two different kinetic models. Pöpken et al. (2000) reported their results based on batch reactor while our experimental study is based on packed bed reactor. In order to compare the adsorption and kinetic parameters obtained in this study from the packed bed reactor experiments with that determined by Pöpken et al. (2000) from the batch reactor experimental results, two representative kinetic experiments of Pöpken et al. (2000), run number 32 and 42 (see Table 8 of (Pöpken et al., 2000) were repeated by us in a batch reactor. Figure 3.13 compares the experimental results obtained by us with that of the experimental results reported by them (Pöpken et al., 2000) together with our model predicted results. The figure shows that our kinetic model with the kinetic parameters obtained from a packed bed reactor can predict the experimental acetic acid concentration profile from a batch reactor reasonably well.

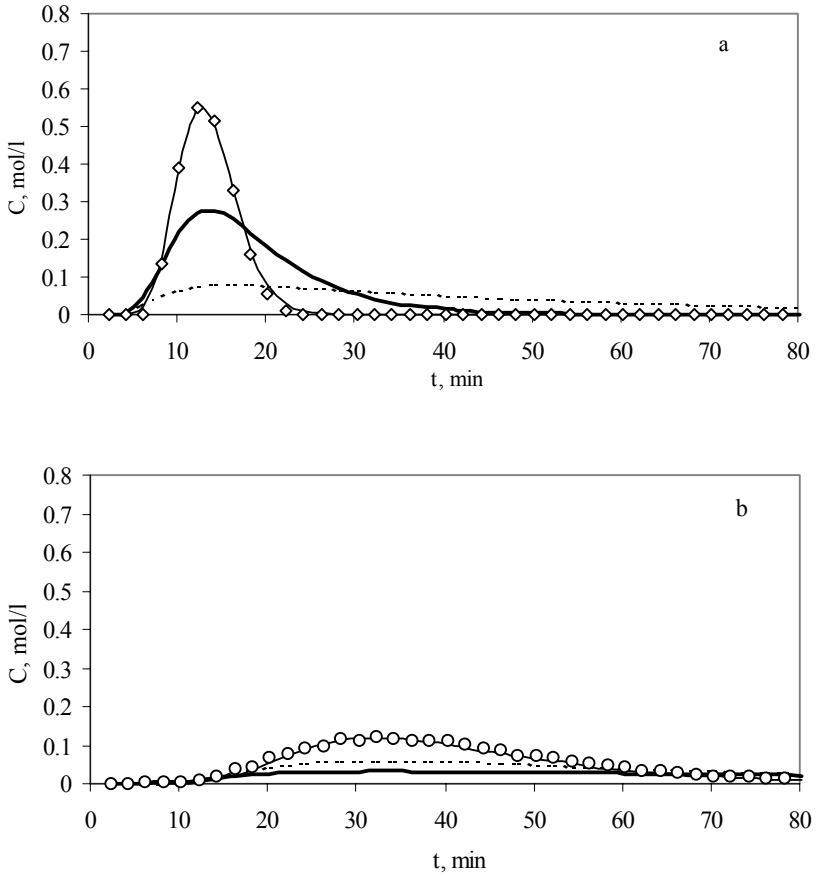

Figure 3.12 Comparison of model predicted results with experimental results for non-reactive breakthrough curves of (a) E and (b) W

Symbols: Experiment (◊ E; o W); Lines: Model prediction (——: this work; ▬▬ : Song et al. (1998);····· : Pöpken et al. (2000))
Experimental conditions: Q = 1 ml/min, T = 318 K, t_p = 5 min, solvent: M
(a) $[E]_f$ = 0.89 mol/l, (b) $[W]_f$ = 0.81 mol/l.

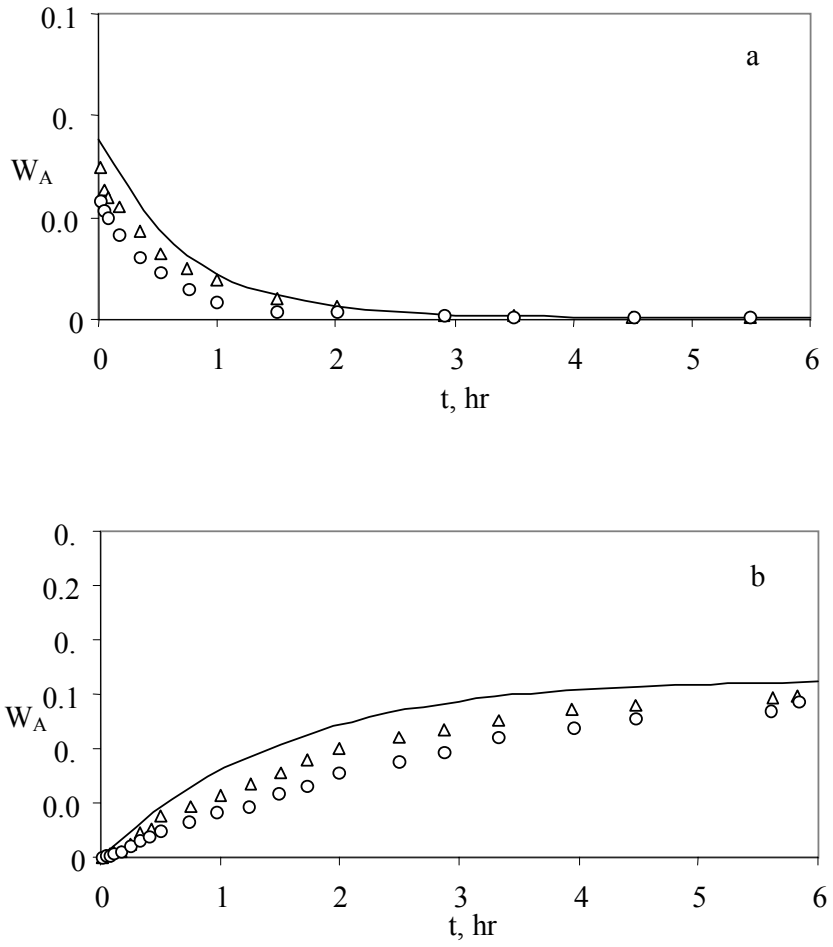

Figure 3.13 Comparison of experimental results of HOAc concentration profile reported by Pöpken et al. (2000) with our experimental and model predicted results in a batch reactor

Symbols: Experiment (Δ This work; o Pöpken et al. (2000)); Lines: our model prediction.
Experimental conditions:
(a) synthesis reaction, T = 323 K, mass of dry catalyst, W = 5.02 g, initial mole number n(HOAc) = 0.25 n(MeOH) = 4.76
(b) hydrolysis reaction, T = 318 K, mass of dry catalyst, W = 20.7 g, initial mole number n(MeOAc) =0.90 $n(H_2O)$ = 9.36

3.5 Conclusions

Reliable adsorption and kinetic parameters are very important for the design of reactors. This Chapter describes the method of obtaining the adsorption equilibrium constants, dispersion coefficients and kinetic parameters for the two different applications of the reversible reaction of acetic acid and methanol catalyzed by Amberlyst 15 ion exchange resin, namely, a) the synthesis of methyl acetate, b) and the hydrolysis of methyl acetate.

The quasi-homogeneous kinetic model and linear adsorption isotherm are applicable in this study, since the solvent, methanol or water, is present at a large excess concentration. A mathematic model was developed to predict the elution profiles of the components in breakthrough experiments.

The breakthrough curves of the reactants and products were experimentally measured at different temperatures, feed concentrations and flow rates. The adsorption and kinetic parameters were determined by minimizing an error function to fit the experimental results with the model predicted values using a state-of-the-art optimization technique, genetic algorithm.

It was found that under the experimental conditions used, both external and internal mass resistances are negligible. The accuracy of the proposed mathematical model was further verified when it was observed that the model could predict experimental results at different feed concentrations and flow rates quite well.

It was also found that with the increase of temperature, adsorption constants decrease, both the forward and backward reaction rate constants increase, and the reaction equilibrium constant for the forward reaction decreases while for the backward reaction increases.

The computed adsorption and kinetic parameters were compared with those reported in literature. It was found that the predicted breakthrough curves using the

adsorption constants reported in literature from batch adsorption experiment study could not match our experimental results from the packed bed reactor. However, our computed parameters obtained from a packed bed reactor can predict the experimental concentration profiles from a batch reactor reasonably well.

Chapter 4 Optimization of SMBR for MeOAc Synthesis

During the period of my PhD study, I had an opportunity to work in Professor Massimo Morbidelli's group at ETH, Zurich as an exchange research student. The optimization work that I carried out there is reported in this Chapter.

4.1 Introduction

The simulated countercurrent moving bed reactor, a novel device for carrying out chemical reaction and separation simultaneously in one single unit, has been investigated theoretically as well as experimentally in recent years by many researchers (see Table 2.2). The study of such an integrated reactor-separator is attractive not only because of lower economic cost resulting from the reduced need for any subsequent separation process, but also because of enhanced conversion of reversible reactions beyond thermodynamic equilibrium achieved by separating the products as soon as they are formed. In particular, the simulated moving bed reactor (SMBR) has recently received growing interests for some fine chemical and pharmaceutical applications, where reactive distillation process might not be suitable, since the chemical species involved are non-volatile and/or heat sensitive.

The concept of SMBR is developed from combining the true countercurrent moving bed reactor with the simulated moving bed (SMB) technology. A sketch of a typical configuration for a true countercurrent moving bed reactor is shown in Figure 4.1. The solid phase is introduced at the top while the fluid phase is introduced at the bottom of the column. The unit is divided into four distinct sections by the inlets and the outlets. Each of the four zones plays a specific role in achieving separation of the product streams at the site of reaction, and thereby attaining high conversion. For example, consider the equilibrium-limited reversible reaction of methyl acetate synthesis, A + M $\rightleftharpoons$ E + W. At the feed port, the limiting reactant A (acetic acid)

and excess amount of M (methanol), which is also used as solvent, is introduced (see Figure 4.1). Acetic acid and methanol react in presence of the catalyst (Amberlyst 15 ion exchange resin) to form products, E (methyl acetate ester) and W (water).

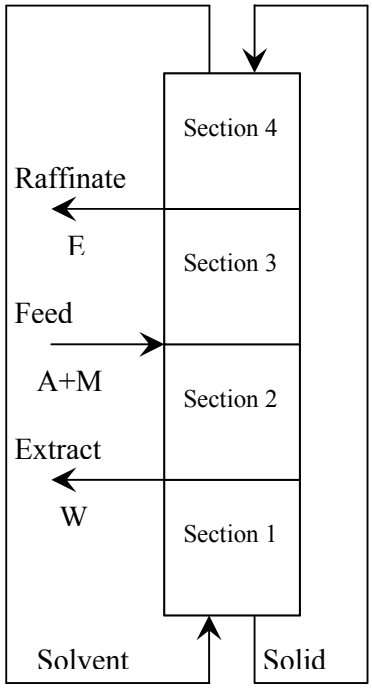

Figure 4.1 Schematic diagram of a true countercurrent moving bed reactor

The weakly adsorbed species E moves preferably with the carrier fluid and migrates to section 3 while the strongly adsorbed component W moves with the solid phase into section 2. By adjusting the flow rates in each section, one can fulfill not only the requirement of complete separation of product species but also to provide sufficient time for the limiting reactant A to be fully consumed. Hence, in this type of reactor, separation is achieved while reaction progresses and one can preferentially collect

weakly adsorbed component E at the raffinate port while the strongly adsorbed component W at the extract port.

However, the actual movement of the solid adsorbent in a true countercurrent moving bed reactor causes a number of problems, such as mechanical difficulties of moving the solids, adsorbent attrition, fines removal, flow channeling, etc. In order to alleviate the problems associated with the solid handling, the simulated moving bed technology is applied where the countercurrent movement of the solid phase with respect to the mobile phase is mimicked by sequentially switching the inlet and outlet ports in the direction of the fluid flow. Therefore, in the SMBR, the true countercurrent moving bed reactor advantages of high product purity and favorable equilibrium shift are retained while the problems associated with the solids movement are avoided.

Figure 4.2 shows a 4-section SMBR process in which all input/output ports shift by one column in the direction of fluid flow after a fixed interval (switching time, t_s). In order to achieve a good separation, each section should fulfill its own role, which is decided by the length and number of columns, fluid flow rates in each section, and switching time. Section 1 has the maximum flow rate, Q_1 to desorb W as well as E such that at least the first column of this section is clean before the next port switching is made. The difficulties for this task are due to insufficient fluid flow rate, Q_1, short switching interval, t_s, and long column length, L_{col}, as well as axial dispersion and tailing effect of the desorbing concentration front. The column flow rate in section 2, Q_2 is lower than Q_1 after withdrawing W as (extract) product at the rate of (Q_1-Q_2). However, Q_2 should be large enough to desorb E out of the section 2 to be mixed with feed as recycle to section 3. However, W should be retained in section 2. The difficulties for the task of this section is similar as those for section 1, however the influence of axial dispersion is more significant due to concentration shock caused by the introduction of feed at the end of section 2. The main task of section 3 is to retain

strongly adsorbed component W (adsorption of H_2O) so that it does not breakthrough at the raffinate port where ester, E, is collected as product. The possible difficulties in this section are due to large column fluid flow rate (Q_3), small section length, long switching time (t_s) and axial dispersion (D). Part of E flows into section 4, where the column flow rate Q_4 should be small enough to prevent E from breaking through into section 1. The primary roles of section 4 are, therefore, retention of E and regeneration of eluent, M.

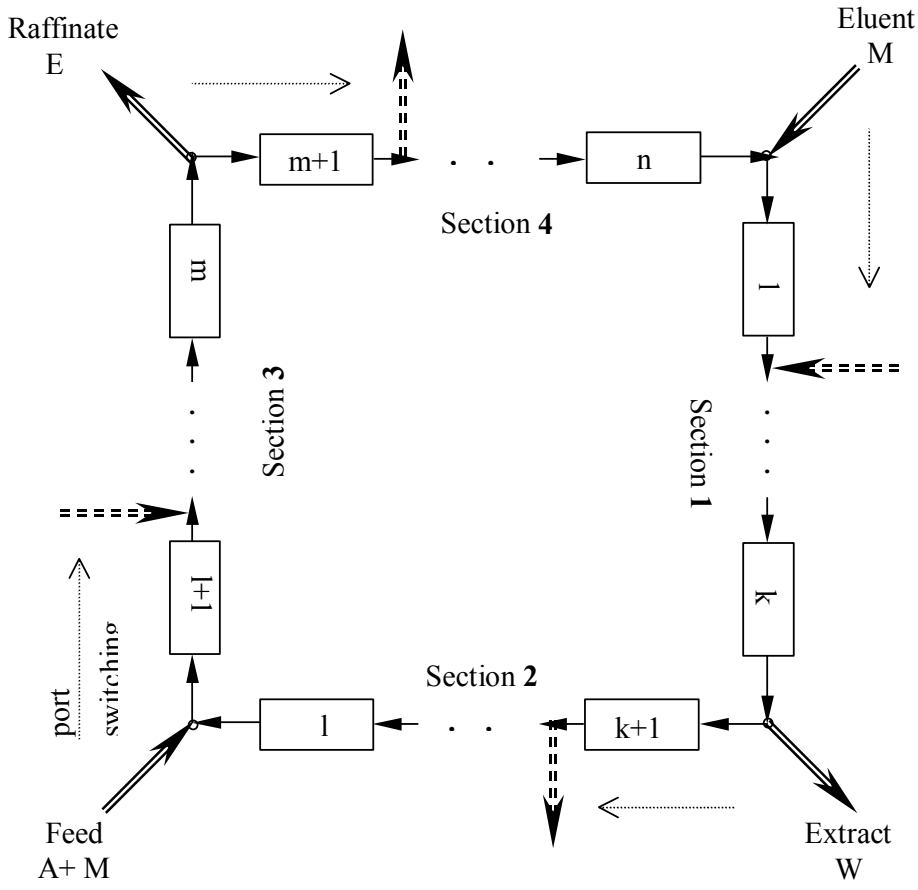

Figure 4.2 Schematic flow diagram of a SMBR unit

The length of sections 2 and 3 should be large enough to prevent W from breaking through into section 3 and at the raffinate port respectively as the primary objective for methyl acetate (E) synthesis is to maximize purity and yield of E. The roles of sections 1 and 4 are respectively to desorb W and retain E respectively. However, as the primary objective in methyl acetate synthesis is not necessarily to achieve high purity of W at the extract port, the length of these two sections could be small, and one column may be enough for each of these two sections. In general, when columns are of identical length (as required in the design of SMBR), it would be advantageous if they are of smaller lengths but larger in numbers so that columns can be distributed in each sections optimally to achieve a desired objective.

The effects of reaction and separation in SMBR are inter-related. On-site separation of two products E and W promotes the conversion of A, and near-complete reaction (high conversion) favors high purity of E at the raffinate port. If conversion of A is low, unconverted A is more likely to pollute purity of E at the raffinate port.

The successful implementation of SMBR on industrial scales will necessitate one to determine the optimal operating conditions and design parameters, such as the flow rates in the four sections, the feed composition, the switching time and the distribution of columns in each section, etc. leading to a comprehensive design of the unit. Although several studies have been reported on the design and optimization of SMBR (Migliorini et al., 1999b; Lode et al., 2001; Azevedo and Rodrigues, 2001), they only involved single objective optimization in terms of maximization of productivity, which is usually not sufficient for the real-life design of complex SMBR systems. This is due to the fact that the operating variables in a SMBR influence the productivity as well as other important objective functions, such as product purity and desorbent requirement, usually in conflicting ways. This leads to any desirable change in one objective function results in an unfavorable change in another objective

function. Therefore, in the design of SMBR units, it is very important that one performs simultaneous optimization of more than one objective functions or multi-objective optimization.

The principle of multi-criterion optimization with conflicting objectives is different from that of single objective optimization. Instead of trying to find the unique and best (global) optimum design solution, the goal of multi-objective optimization is to find a set of equally good solutions, which are known as Pareto optimal solutions. In a Pareto set, all solutions are equally good as no solution can be considered a better solution than any other solutions with respect to all the objective functions. When one moves from one solution to another, at least one objective function deteriorates. Hence, the selection of an optimal solution among the infinitely many solutions provided by the Pareto set will depend on additional information, which is usually non-quantifiable.

In this chapter, the multi-objective optimization for the synthesis of methyl acetate in a SMBR was performed using the Non-dominated Sorting Genetic Algorithm (NSGA) (see Appendix A) (Srinivas and Deb, 1995; Deb, 2001). Genetic Algorithm is a non-traditional search technique and optimization method based on the mechanics of natural genetics and natural selection. It has become quite popular in chemical engineering design in recent years (Bhaskar, et al., 2000a, 2000b, 2001; Rajesh et al., 2001). These works show that NSGA is a promising method and quite robust in obtaining global optimal solution for the simultaneous optimization of multiple objective functions. In the present work, three important objectives for the performance of SMBR were considered, namely, maximization of productivity and purity of methyl acetate using minimum desorbent. Efforts have been made to determine the optimal acetic acid feed mole fraction and the optimal distribution of columns in each section for a 5-column SMBR unit. The effects of conversion constraint, reaction rate constant and eluent flow rate on the Pareto optimal solutions

were also investigated. By performing multi-objective optimizations, we intend to deepen the understanding of the SMBR process and meanwhile generate a wider range of meaningful and useful optimal operating conditions for the decision makers.

4.2 Mathematical Modeling of SMBR

A detailed mathematical model was developed to describe the dynamic behavior of a SMBR, where the interphase mass transfer resistance and the change in the sorbed phase volume during the course of the reaction are taken into account. The model used in this work is modified from that reported by Lode et al. (2001). The differential mass balance equations for component *i* in section *j* are given by

$$\varepsilon \frac{\partial C_i^L}{\partial t} + u_j \frac{\partial C_i^L}{\partial z} + (1-\varepsilon) k_m (C_{i,eq}^P - C_i^P) = 0 \tag{4.1}$$

$$\frac{\partial C_i^P}{\partial t} = k_m (C_{i,eq}^P - C_i^P) + v_i R \tag{4.2}$$

The liquid and solid phase concentrations are represented by C_i^L and C_i^P respectively while the subscripts '*eq*' represents equilibrium concentration in polymer phase. u_j represent the superficial liquid phase velocity in section *j* (j = 1, 2, 3, 4), k_m is the characteristic coefficient for interphase mass transfer, v_i is the stoichiometric coefficient of the i^{th} component, r denotes the reaction rate per unit volume of the sorbed phase, and ε represents the overall bed void fraction. The adsorption isotherm is expressed based on the empirical multi-component Langmuir model as follows:

$$C_{i,eq}^P = \frac{(\rho/q) N_i K_i x_i^L}{\sum_{j-1}^{N} K_j x_i^L} \tag{4.3}$$

where ρ refers to the density of the dry polymer resin, q represents the average swelling ratio, which is assumed to be 1.61 (Lode et al., 2001). N_i is the sorption capacity per unit mass by the dry resin when immersed into a pure liquid, K_i is the Langmuir parameter, and x_i^L denotes the mole fraction in the liquid phase.

The reaction kinetics for this reversible esterification reaction are given by

$$r = k_f C_A^P C_M^P \left[1 - \frac{x_W^P x_E^P}{x_A^P x_M^P K_{eq}} \right] \tag{4.4}$$

where k_f and K_{eq} denote the reaction rate constant and the reaction equilibrium constant respectively. The subscripts A, M, W and E represent acetic acid, methanol, water and methyl acetate ester, respectively.

The above model equations are solved using the method of lines based on the backward finite differences together with the following initial and boundary conditions:

$$C_i(0,z) = C_i^0 \tag{4.5}$$

$$Q_1 C_i(t,0^+) = Q_4 C_i(t,z_4^-) + Q_D C_{i,D} \tag{4.6}$$

$$C_i(t,z_1^+) = C_i(t,z_1^-) \tag{4.7}$$

$$Q_3 C_i(t,z_2^+) = Q_2 C_i(t,z_2^-) + Q_F C_{i,F} \tag{4.8}$$

$$C_i(t,z_3^+) = C_i(t,z_3^-) \tag{4.9}$$

Here, z_j (j = 1, 2, 3, 4) denotes the axial position of the outlet from section j while the superscripts + and – denote the position before and after the inlet and outlet

port at z_j respectively. Q_j (j = 1, 2, 3, 4) represents the volumetric flow rate in section j while the subscripts D and F denote the desorbent and feed respectively.

4.3 Optimization of SMBR

4.3.1 Definition of the Objective Functions

In order to characterize the performance of SMBR at optimal conditions for the synthesis of methyl acetate, a set of objective functions need to be defined. In here, we have used the following as objective functions.

The productivity of methyl acetate ester (PrE) is defined as amount of methyl acetate collected at the raffinate port per unit time per unit volume of resin as follow:

$$\mathrm{PrE} = \frac{Q_{Ra} C_{E,Ra}}{(1-\varepsilon) V_{unit}} = \frac{(m_3 - m_4) C_{E,Ra}}{t_s \; n \times 1000} \times 3600 \tag{4.10}$$

Where V_{unit} and n represent the total volume of the reactor and the total number of columns, respectively, t_s is the switching time, the subscript Ra denotes raffinate stream while m_j represent the flow rate ratios of the liquid phase to the solid phase in section j and is given by

$$m_j = \frac{Q_j \, t_s - V_{col} \varepsilon}{V_{col}(1-\varepsilon)}, \quad \mathrm{j} = 1, 2, 3, 4 \tag{4.11}$$

The desorbent requirement (D) is defined as the moles of eluent consumed per unit moles of the desired product E at the raffinate port as follows

$$\mathrm{D} = \frac{Q_D C_{M,D} + Q_F C_{M,F}}{Q_{Ra} C_{E,Ra}} = \frac{(m_1 - m_4) C_{M,D} + (m_3 - m_2) C_{M,F}}{(m_3 - m_4) C_{E,Ra}} \tag{4.12}$$

The conversion of acetic acid (X_A), the purity of methyl acetate ester (PurE) at the raffinate port and the purity of water (PurW) at the extract port are defined as follow:

$$X_A = 1- \frac{Q_{Ra}C_{A,Ra} + Q_{Ex}C_{A,Ex}}{Q_F C_{A,F}} \tag{4.13}$$

$$\text{PurE} = \frac{C_{E,Ra}}{C_{A,Ra} + C_{E,Ra} + C_{W,Ra}} \tag{4.14}$$

$$\text{PurW} = \frac{C_{W,Ex}}{C_{A,Ex} + C_{E,Ex} + C_{W,Ex}} \tag{4.15}$$

4.3.2 Complete Conversion and Separation Region

It is well known that the separation performance of non-reactive SMB depends only on the flow rate ratios of the fluid phase to the solid phase within the two central sections (m_2, m_3), provided that m_1 and m_4 are chosen properly for successful regeneration of solid and purification of eluent respectively, and the complete separation conditions are identified in the (m_2, m_3) plane by the triangle shaped region (Storti et al., 1993). In the case of a reactive unit, the complete conversion and separation region in the operating parameter space was found to have a triangular shape similar to that for the non-reactive SMB, and its shape and location depend on the feed composition (Migliorini et al., 1996b) and switching time (Lode et al., 2001). In addition, there is a lower limit for switching time, below which the residence time in the reactive zone of the SMBR is not sufficient to allow the reaction to proceed to any significant extent.

4.3.3 Case 1: Maximization of Productivity and Purity of Methyl Acetate

In recent years, a great deal of attention has been devoted to SMBR as a promising technology for fine chemical and pharmaceutical industries, where productivity and purity of product are the most important factors. However, the operating and design variables of SMBR, especially the flow rate ratios in the four sections (m_j), the switching time (t_s), the feed composition ($x_{i,F}$) and the column configuration (χ), influence productivity and purity in conflicting ways, leading to a trade-off relationship between the two objectives. That is, the high product purity is obtained at the expense of productivity and vice versa. Therefore, the multi-objective optimization for the SMBR is of considerable interest to determine the optimal operating and design parameters. In this section, the multi-criterion optimization with productivity (PrE) and purity of ester (PurE) at the raffinate port (Eqs. 4.10 and 4.14) as objective functions were performed using NSGA. In order to obtain the optimal results within reasonable computation time, a 5-column SMBR unit instead of the 10-column unit reported by Lode et al. (2001) was considered for the synthesis of MeOAc in this work, since its performance is comparable with the 10-column unit as shown in Table 4.1.

Table 4.1 Comparison of the performance of a 5-column SMBR with that of a 10-column unit

Configuration	t_s min	PrE mol/h/l	D mol/mol	PurE (-)	X (-)
1-1-2-1	7.57	11.6	8.38	98.8	98.7
3-2-3-2	6.67	11.2	8.50	99.5	99.5

4.3.3.1 Case 1a: Optimal Column Distribution

For a given 5-column SMBR unit, there exist four possible configurations, namely, χ_1 (2-1-1-1), χ_2 (1-2-1-1), χ_3 (1-1-2-1) and χ_4 (1-1-1-2). Among them, which one is the optimal configuration that makes the best use of the solid phase volume is an interesting topic, since the good utilization of the resin leads to high productivity. Hence, the performance of SMBR was first optimized using the numbers of possible configurations for 5-column unit, the switching time, and the flow rate ratios in the four sections as decision variables (see Table 4.2 Case 1a). The constraint on the purity of water at the extract port was imposed to ensure high yield of methyl acetate and nearly complete separation. The adsorption and kinetic parameters used are shown in Table 4.3.

Table 4.2 Formulation of the optimization problem solved in Case 1

Case #	Objective Function	Constraints	Decision Variables	Fixed Parameters
1a	Max PrE Max PurE	$X_A \geq 95\%$ $PurW \geq 95\%$	$300 \leq t_s \leq 1500$ s $0.5 \leq m_1 \leq 4.0$ $0.01 \leq m_2 \leq 1.0$ $0.5 \leq m_3 \leq 2.0$ $-0.5 \leq m_4 \leq 0.5$ $\chi_1 \leq \chi \leq \chi_4$	L = 0.3 m, d = 0.025 m $\varepsilon = 0.616$ $x_{A,F} = 1.0, x_{M,D} = 1.0$ N, K, k_m, k_f, K_{eq} (see Table 4.3)
1b	Same as 1a	Same as 1a	Same as 1a $0.1 \leq x_{A,F} \leq 1.0$	Same as Case 1a except χ is fixed at χ_3 and $x_{A,F}$ is varied
1c	Same as 1a	$X_A \geq y\%$ $PurW \geq y\%$ y = 85, 90, 98	Same as 1a $60 \leq t_s \leq 1500$ s	Same as Case 1a except χ is fixed at χ_3 and lower bound of t_s was decreased.
1d	Same as 1a	Same as 1a	Same as 1a	Same as Case 1a except χ is fixed at χ_3 and k_f (10^{-6} m^3 /s/mol) = 0.5, 5, 5000

Table 4.3 Kinetic and adsorption parameters used in the optimization problems

Component	N, mol/g	K
A	4.32×10^{-3}	0.243
M	9.28×10^{-3}	0.565
E	3.23×10^{-3}	0.060
W	26.20×10^{-3}	1.000
k_m	6.67×10^{-2} s^{-1}	
k_f	5×10^{-6} m^3 /s/mol	
K_{eq}	35.0	

Figure 4.3a shows the Pareto optimal solutions as it can be observed that when we move (left to right) from one point to another productivity increases but purity decreases. The optimal column configuration obtained was χ_3, which corresponds to the 1-1-2-1 configuration for a 5-column SMBR unit. The result is expected since section 3 is the main reactive section and for the model reaction system studied in this work, the additional column should be placed in this section due to the very small difference between the Henry-coefficients of acetic acid and methyl acetate. Therefore by increasing the overall length of section 3, one can either increase PrE for a given PurE or increase PurE for a given PrE.

It is shown by Figure 4.3b that the switching time is the key parameter in shaping the Pareto and it has a minimum value, below which the constraint on PurE and conversion (see Figure 4.3g) are not satisfied due to the insufficient residence time in the reactive section that allows the reaction to proceed. The maximum productivity is restricted by the minimum switching time, which is limited by the constraint on conversion.

It can be observed from Figure 4.3c that m_1 is scattered, but it tends to be greater than some specific value. This value may be the critical value of the flow rate ratio in section 1 to ensure successful regeneration of the solid adsorbent (resin), below which the strongly adsorbed product (W) cannot be completely removed, which

subsequently contaminates the ester product at the raffinate port. Similarly, as shown in Figure 4.3f, m_4 is scattered, but it tends to be smaller than some specific value, which may be the maximum flow rate ratio in section 4 satisfying the purification of the eluent. Nevertheless, it seems that the flow rate ratios in sections 1 and 4 have very little effect on the productivity and the purity of the ester at the raffinate port once they fulfill the basic criteria for regeneration of the solid adsorbent and the eluent for recycling respectively.

Figure 4.3d and Figure 4.3e show that m_2 and m_3 are essentially constant. The point (m_2, m_3) could be the vertex of the triangular region for complete conversion and separation represented in the (m_2, m_3) plane.

From Figure 4.3h, it is found that the desorbent requirement is insensitive in obtaining the Pareto. However, the eluent consumption is a very important factor in determining not only the process economic costs but also less eluent flow may lead to higher enrichment of ester product at the raffinate port. Hence, it may be more sensible to consider three objective function optimization in which the productivity and purity of the ester product is maximized using minimum desorbent consumption. This problem has been considered later in Case 3 (4.3.5).

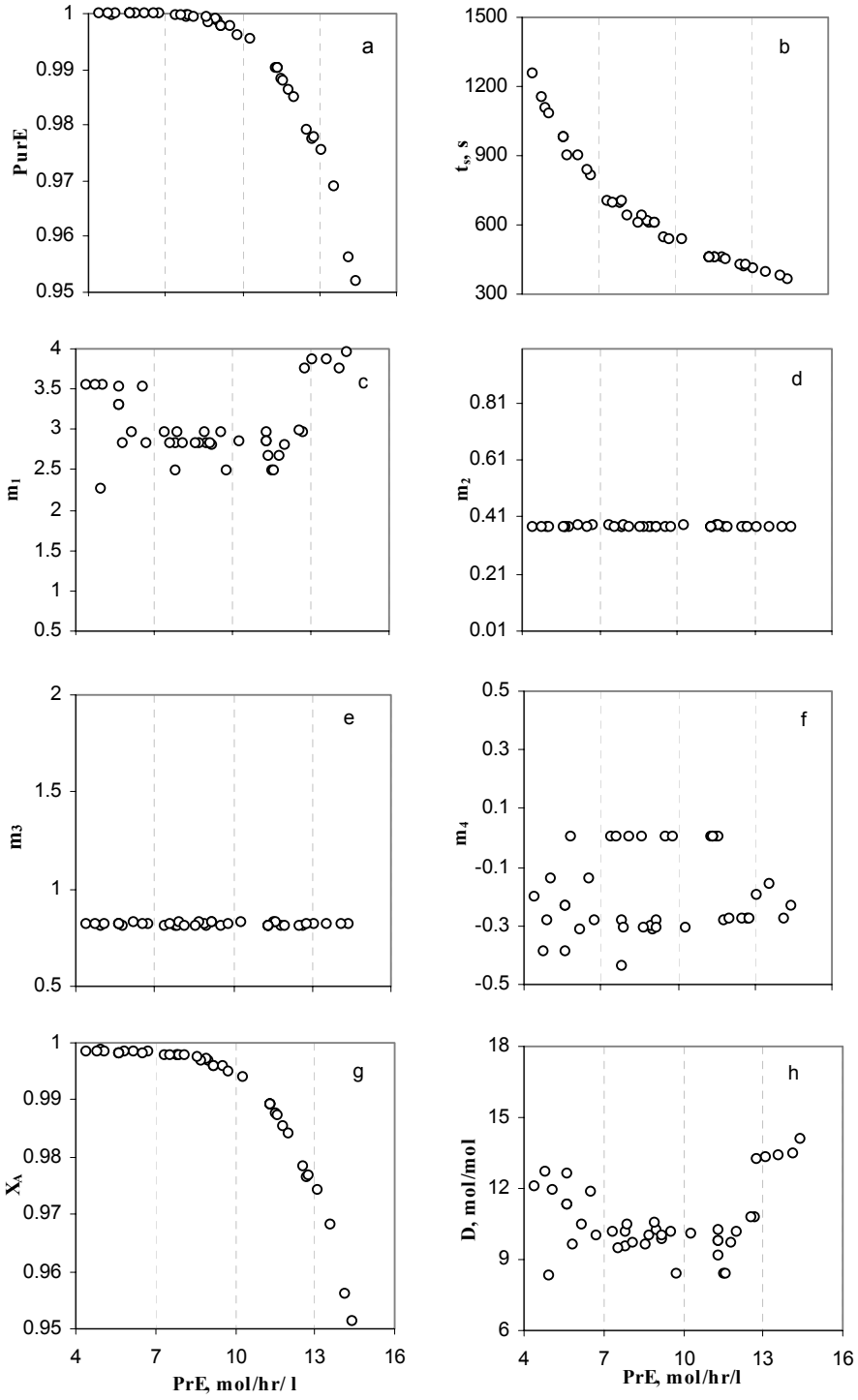

Figure 4.3 Optimal column distribution

4.3.3.2 Case 1b: Optimal Feed Composition

The feed composition plays an important role in the performance of SMBR (Migliorini et al. 199b). Lode et al. (2001) reported that the triangular region of complete conversion and separation is enlarged when additional solvent (methanol) is fed together with the limiting reactant (acetic acid) in between the central sections. Accordingly, the distance of its vertex from the diagonal becomes larger. In addition, there exists a lower bound on the flow rate ratio in section 2 when the feed stream containing pure acetic acid is introduced at higher flow rate. Hence, if m_2 is too low at large feed flow rates with only acetic acid is introduced at feed port, methanol will be completely consumed in Section 2 and therefore, reaction would stop in section 3 due to the lack of the reactant methanol. In order to relax the limit on m_2 and overcome the poor utilization of the reactor volume, it would be appropriate to introduce additional methanol with acetic acid at the feed port. Therefore, the mole fraction of acetic acid in the feed becomes a key parameter for process optimization.

In Case 1b, the multi-objective optimization problem was solved in which an additional decision variable, the mole fraction of acetic acid in the feed, was used. The optimization problem is described in Table 4.2 and is depicted as Case 1b. In this optimization problem, the reactor configuration was fixed as χ_3 (1-1-2-1), which was found out to be the optimum configuration for a 5-column SMBR unit in Case 1a.

The Pareto optimal solutions are shown in Figure 4.4a. The optimal mole fraction of acetic acid in the feed was found out to be 0.79 (Figure 4.4h). From Figure 4.4c and 4.4f, it can be observed that m_1 and m_4 are scattered as before and they show the same trend as discussed earlier for case 1a. Once again Figure 4.4d and 4.4e, show that the flow rate ratios in sections 2 and 3 are essentially constant, which correspond to the vertex of the triangle for the complete conversion and separation region in the (m_2, m_3) plane. It is to be noted that the optimal operating point (m_2, m_3) for Case 1b in

which optimum $x_{A,F}$ was determined is different from that of Case 1a in which pure acetic acid was used as feed. Comparing Figure 4.4d with 4.3d, it can be seen that the optimal flow rate ratio, m_2, for Case 1b is significantly smaller than that of Case 1a.

In order to check the validity of the optimal feed composition, the Pareto optimal solutions were also determined for the acetic acid feed mole fraction of 0.7 and 0.9. The four Paretos for different feed composition ($x_{A,F}$) are compared in Figure 4.5, one can observe that the productivity for the optimal acetic acid feed concentration is the highest among the four feed compositions for the same purity requirement. The flow rate ratios (m_2, m_3) corresponding to the four different acetic acid feed mole fractions are compared in Table 4.4. It shows that (m_2, m_3) are different for different feed composition and the optimal flow rate ratio in section 2, m_2 becomes smaller when the feed concentration is smaller.

Table 4.4 Optimal flow rate ratios (m_2, m_3) for different acetic acid mole faction in the feed

$x_{A,F}$	m_2	m_3
1.0	0.377	0.813
0.9	0.348	0.828
0.79*	0.289	0.801
0.7	0.260	0.949

* Optimum $x_{A,F}$

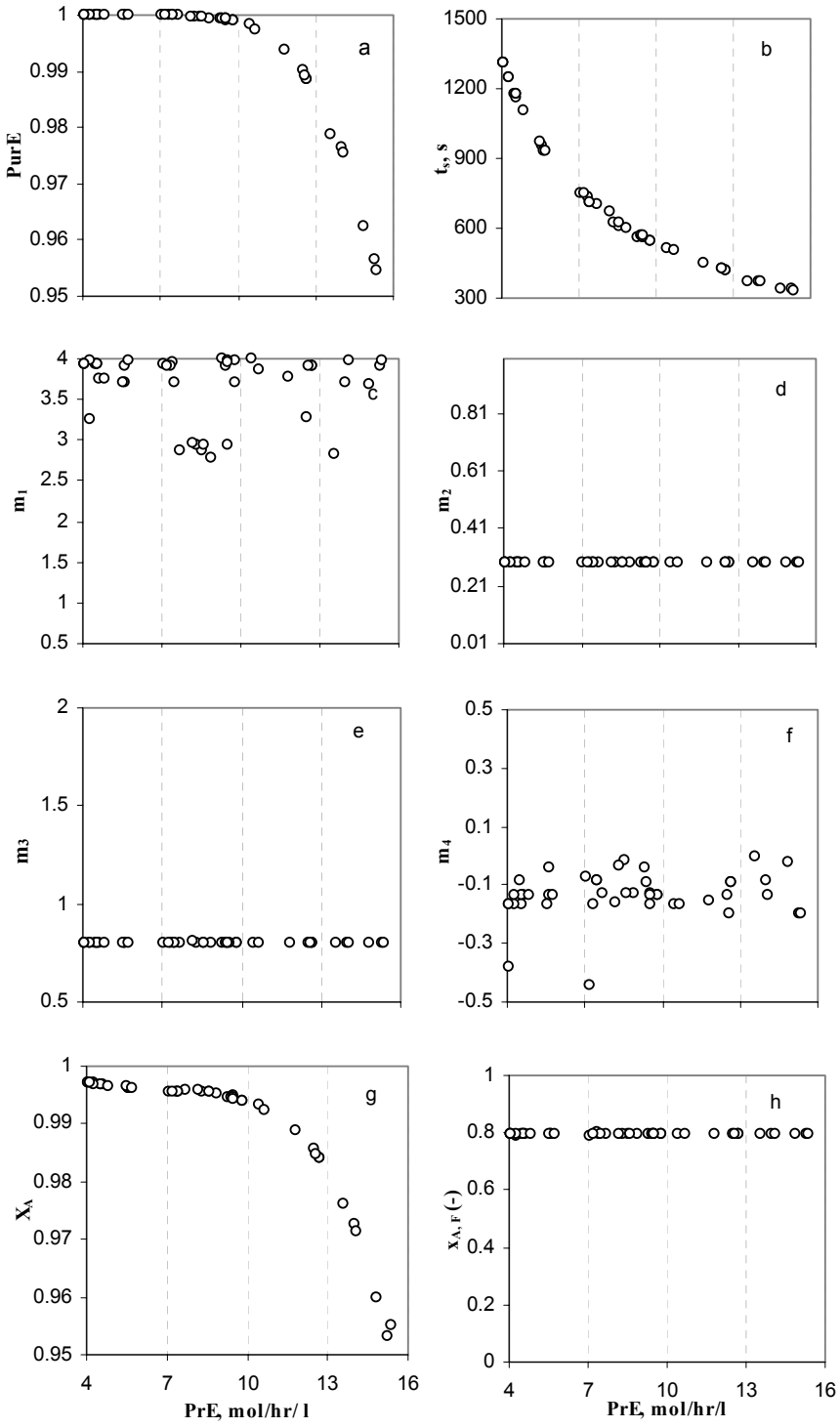

Figure 4.4 Optimal feed composition

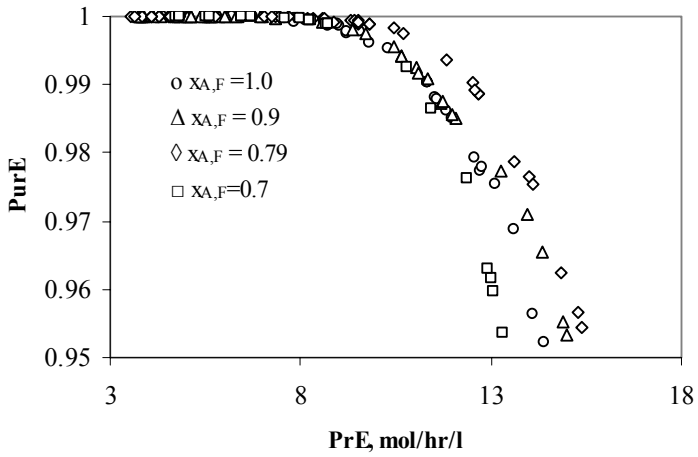

Figure 4.5 Comparison of Paretos for different acetic acid feed mole fractions

4.3.3.3 Case 1c: Effect of Constraint on Conversion

The multi-objective optimization of SMBR has been performed for different values of constraint on the conversion of acetic acid (X_A) to examine how the Pareto and the optimal values of the associated decision variables shift. The optimization formulation for Case1c is described in Table 4.2.

Figure 4.6a, clearly demonstrates that when the desired conversion constraint is lowered (i) the productivity of ester (PrE) is higher for a given purity of ester (PurE), and (ii) the maximum productivity obtainable increases. The corresponding switching time responsible for the Pareto set is given in Figure 4.6b. One can see that the required minimum switching time for carrying out the reaction to satisfy the conversion constraint can reach smaller value when the conversion requirement is smaller. The optimal flow rate ratios in the central sections for Case 1c optimization problem are shown in Table 4.5. It is to be noted that the above results were obtained by using inequality constraints on the conversion.

Table 4.5 Optimal flow rate ratios (m_2, m_3) for different conversion constraints

X_A	m_2	m_3
≥ 0.98	0.381	0.828
≥ 0.90	0.369	0.800
≥ 0.85	0.319	0.691

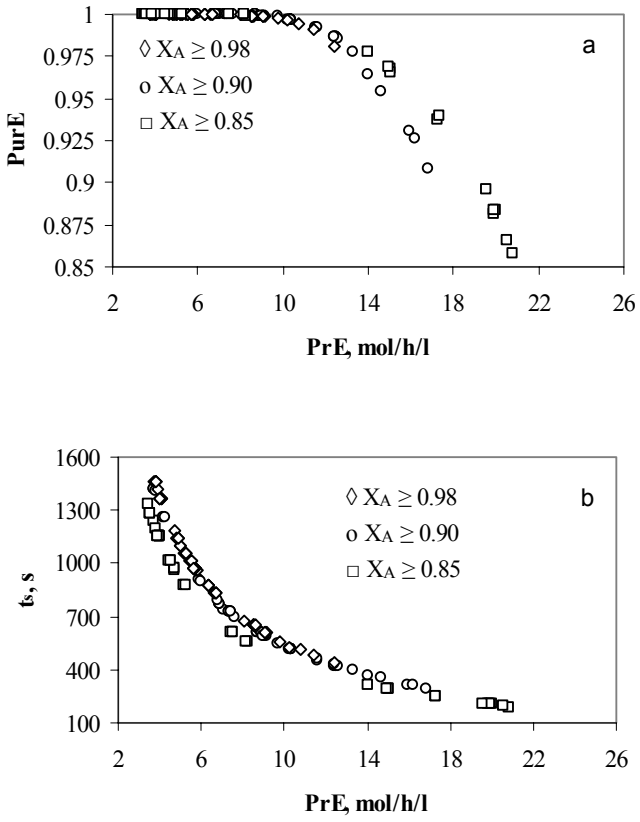

Figure 4.6 Effect of conversion constraint on Paretos and corresponding decision variables

4.3.3.4 Case 1d: Effect of Reaction Rate Constants

The reaction rate constant (k_f) is a key parameter to relate the simulated moving bed reactor to the non-reactive SMB systems. In the case of very fast (instantaneous)

reaction, the behavior of a SMBR becomes similar to the pure separation unit, since the reaction can be completed very close to the feed port and the rest of the reactive section will essentially carry out separation of the products. Fricke et al. (1999b) has analyzed the effect of the reaction rate constant on the performance of a SMBR for a reversible decomposition reaction (A $\rightleftharpoons$ B+C). They reported that the feed flow rate increases and approaches a limiting value with increasing reaction rate constant, and this limiting value is given by the corresponding feed flow rate of the SMB separation between B and C.

By performing the multi-objective optimizations with three different reaction rate constants in this work, we intend to see if the optimal flow rate ratios in sections 2 and 3 approach the optimal operating point (m_2, m_3) for a non-reactive SMB when the reaction is instantaneous, as well as how the Pareto solutions are influenced by the reaction rate constant. The formulation of the optimization problem is described in Table 4.2.

Figure 4.7 shows comparison of the Paretos for different reaction rate constants, k_f. It is found that the productivity of ester (PrE) for a fixed ester purity (PurE) requirement increases with the increase of k_f. This is due to the fact that less residence time is needed to fulfill the constraint on conversion when reaction is instantaneous. The optimal flow rate ratios in sections 2 and 3 (m_2, m_3) are shown in Table 4.6. It shows that m_2 and m_3 values when the reaction rate constant is very large still deviate significantly from the optimal values obtained for non-reactive SMB (m_2 = 0.115, m_3 = 1.885) (Storti et al., 1993). This can be explained by the concentration profiles of the four species (A, M, E and W) at the end of a switching period.

Figure 4.8 shows the profiles for the following conditions: t_s = 300 s, m_1 = 3.825, m_2 = 0.115, m_3 = 1.885, m_4 = -0.235, χ = 1-1-2-1, and $k_f = 5000\times10^{-6}$ m^3 /s/mol while the other parameter values are same as reported for Case 1d in Table 4.2. We

have selected the value of m_2 and m_2 as the optimal values for pure separation unit while m_1 and m_4 are fixed at values that ensure complete regeneration of the solid adsorbent and eluent flow respectively. It can be seen in Figure 4.8 that methanol (M) is almost completely consumed in most part of section 3. Hence, no reaction takes place in a large portion of section 3. This leads to very low conversion (X_A = 25.7%) and purity of ester at the raffinate (PurE = 20.2%). For the methyl acetate esterification reaction, it appears that m_2 and m_3 are also controlled by the availability of the reactant methanol in the reactive section when pure acetic acid is used as feed. The maximum feed flow rate would thus be smaller than that in the case of pure separation of methyl acetate and water.

Table 4.6 Optimal flow rate ratios (m_2, m_3) for different values of reaction rate constant

k_f m^3 /s/mol	Symbol*	m_2	m_3
0.5×10^{-6}	◊	0.258	0.520
5×10^{-6}	○	0.377	0.813
5000×10^{-6}	Δ	0.377	0.831

* Symbols used in Figure 4.7

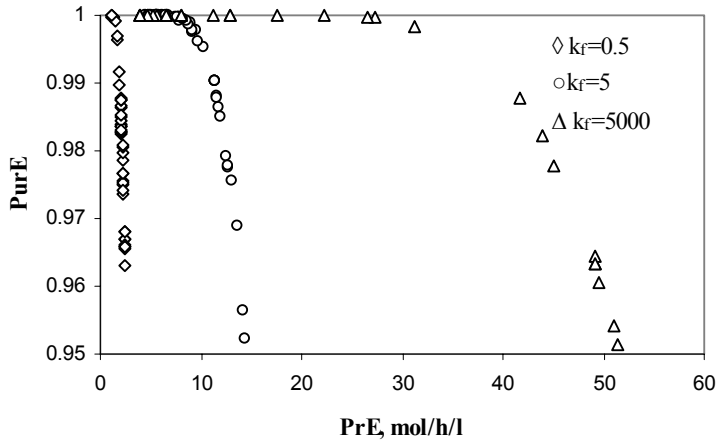

Figure 4.7 Effect of reaction rate on the Paretos for maximization of productivity and purity

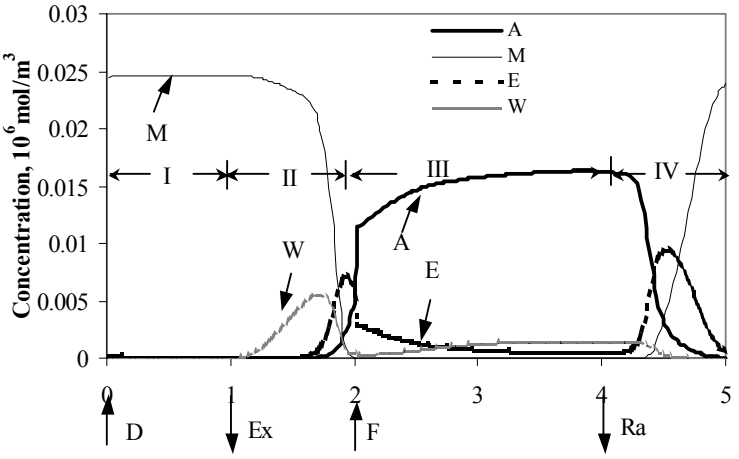

Figure 4.8 Periodical steady state concentration profiles of A, M, E and W at the end of a switching cycle

4.3.4 Case 2: Maximization of Productivity & Minimization of Desorbent Requirement

In the SMBR applications, productivity of desired product and eluent (desorbent) consumption are important factors in the determination of process economic costs. Therefore, the optimal design of the SMBR process that aims at maximizing productivity using minimum desorbent was investigated next. The multi-objective optimization problem formulated is described in Table 4.7.

Table 4.7 Formulation of the optimization problem solved in Case 2 and Case 3

Case #	Objective Function	Constraints	Decision Variables	Fixed Parameters
2	Max PrE Min D	$X_A \geq 95\%$ PurW $\geq 95\%$	$300 \leq t_s \leq 1500$ s $0.01 \leq m_2 \leq 1.0$ $0.5 \leq m_3 \leq 2.0$	L = 0.3 m, d = 0.025 m, $\varepsilon = 0.616$ $m_1 = 2.5$, $m_4 = 0$, χ = 1-1-2-1 $x_{A,F} = 1.0, x_{M,D} = 1.0$ N, K, k_m, k_f, K_{eq} (see Table 4.3)
3	Max PrE Min D Max PurE	$X_A \geq 98\%$ PurE $\geq 98\%$ PurW $\geq 98\%$	$300 \leq t_s \leq 1500$ s $0.5 \leq m_1 \leq 4.0$ $0.01 \leq m_2 \leq 1.0$ $0.5 \leq m_3 \leq 2.0$ $-0.5 \leq m_4 \leq 0.5$	L = 0.3 m, d = 0.025 m, $\varepsilon = 0.616$ χ = 1-1-2-1, $x_{A,F} = 1.0, x_{M,D} = 1.0$ N, K, k_m, k_f, K_{eq} (see Table 4.3)

In this case study, only three decision variables, namely, the flow rate ratios in the two central sections (m_2 and m_3) and the switching time (t_s) were used. In order to simplify the optimization problem, the flow rate ratios in sections 1 (m_1) and 4 (m_4) were kept constant at appropriate values to ensure complete regeneration of the solid adsorbent and eluent. However, the effect of m_1 on the shift of Pareto is investigated later. The column configuration of SMBR is also fixed at the previously obtained optimum value of χ = 1-1-2-1.

Figure 4.9 shows the Pareto optimal solution and the corresponding decision variable plots for Case 2. It can be observed that the improvement in productivity of ester at the raffinate port (PrE) can only be achieved at the expense of more eluent (D) consumption. Once again it was found that the optimal flow rate ratios in the two central sections (m_2 and m_3) are almost constant (Figure 4.9b-c), which may correspond to the vertex of the complete separation in (m_2 and m_3) plane and the optimal switching time (t_s) is the variable responsible (Figure 4.9d) for the Pareto in Figure 4.9a. Moreover, the switching time has a minimum value (330 s) below which the constraint on conversion would be violated due to insufficient residence time in the reactive section that allows the reaction to proceed.

Effect of Flow Rate Ratio in Section 1

The effect of flow rate ratio in section 1 (m_1) on the optimal solutions is investigated next. When m_1 is reduced from 2.5 to 1.6, the maximum productivity (PrE) that can be obtained decreased from 14.7 to 10.5 mol/hr/l and the minimum switching time satisfying the constraints on X_A and PurW increases from 330 to 600 s (Figure 4.10a). When m_1 is increased from 2.5 to 4, the maximum productivity (PrE) improves marginally to 15.8 mol/hr/l (Figure 4.10c) and the minimum switching time required satisfying the constraints decreases to 279s. It seems that when m_1 is small, the maximum productivity can be greatly improved at the expense of eluent flow. But when m_1 is large, increasing the eluent flow cannot significantly increase productivity.

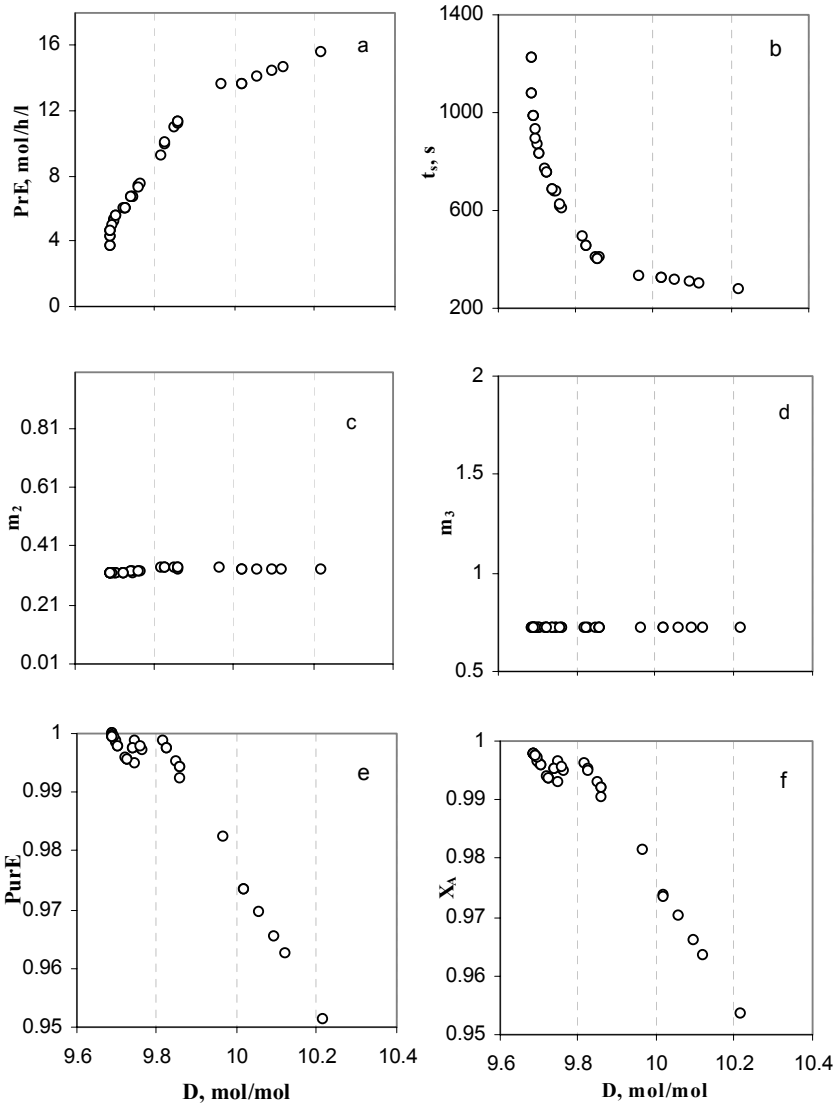

Figure 4.9 Maximum productivity and minimum desorbent requirement

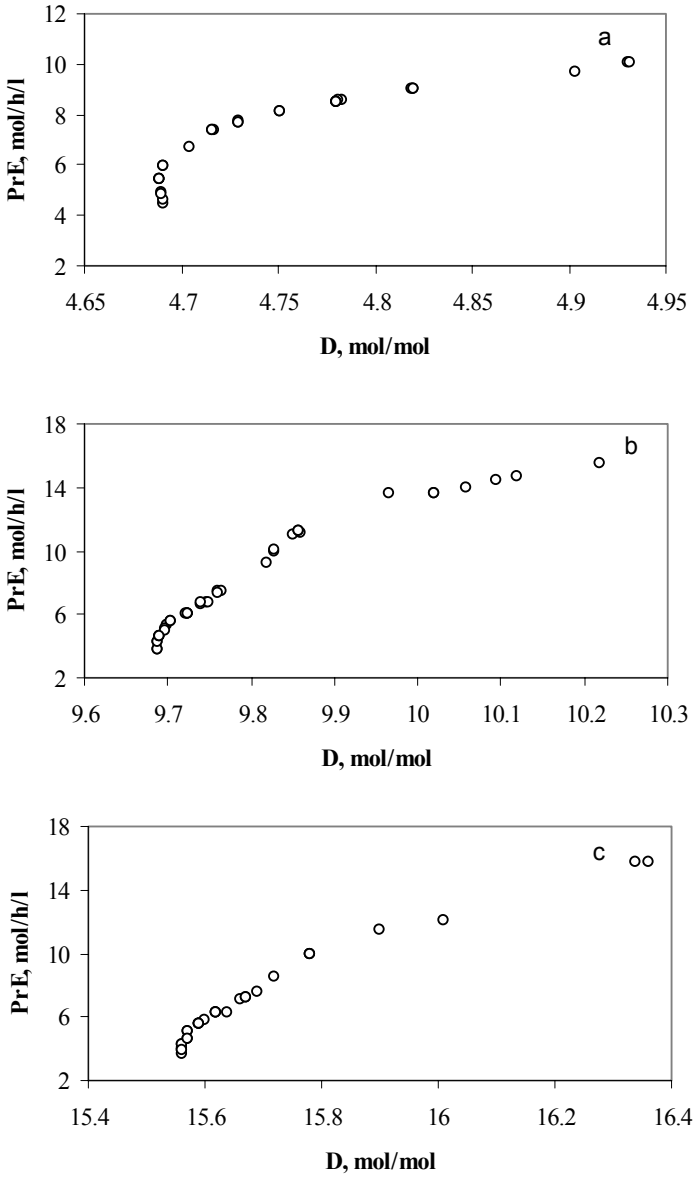

Figure 4.10 Effect of m_1 on the Pareto optimal solutions

a) $m_1 = 1.6$; b) $m_1 = 2.5$; c) $m_1 = 4$

4.3.5 Case 3: Maximization of Productivity & Purity with Minimization of Desorbent Requirement

Unlike the previous two cases that involved optimization of two objective functions, in this case we considered simultaneous optimization of three objective functions, namely, maximization of the productivity and purity of the ester product at the raffinate port while at the same time the consumption of desorbent is minimized. This problem is a more realistic optimization problem for the design of a SMBR, since as shown in Figure 4.3h, when only the productivity and the purity was maximized, the desorbent requirement plot was quite scattered. Certainly, minimum consumption of the desorbent for a fixed desired productivity and purity would be of economic benefit. The optimization problem formulation is described in Table 4.7.

For the convenience of analysis, the Paretos were plotted in two dimensions. Figure 4.11a shows that the productivity increases with decreasing purity while Figure 4.11b shows that the desorbent consumption increases when desired purity requirement increases. However, when purity reaches a value very close to 100%, it could hardly be improved any further as the desorbent requirement increases exponentially. From Figure 4.11d and 4.11g , it was observed that m_1 and m_4 are not scattered but follows a trend in contrast to what was obtained earlier for Case 1. While, Figure 4.11e and 4.11f show that m_2 and m_3 are still essentially constant. Figure 4.11c shows that the switching time is still the key parameter for the Pareto and it must be increased to a very high value to achieve conversion close to 100% (see Figure 4.11h).

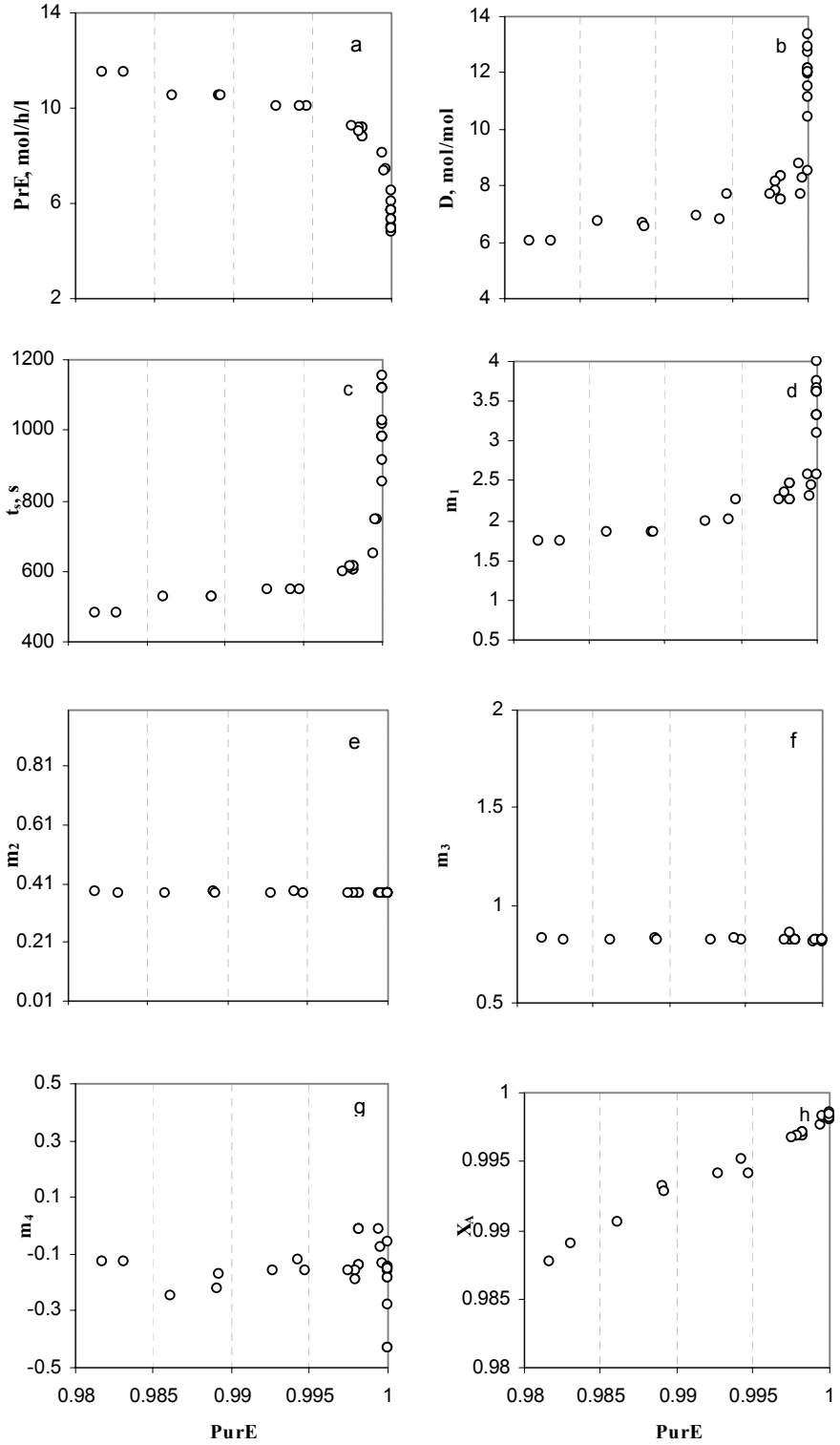

Figure 4.11 Maximization of productivity and purity together with minimization of desorbent requirement

4.6 Conclusions

The multi-objective optimization study for the synthesis of methyl acetate ester in simulated moving bed reactor (SMBR) was performed using non-dominated sorting genetic algorithm (NSGA). Several two-objective functions and a three objective functions optimization were carried out to characterize the performance of SMBR.

It was found that productivity and purity of ester product at the raffinate port does not result in a global optimum solution instead a series of non-dominated (Pareto optimal) solutions were obtained. In all cases, switching time was the key parameter resulting in the Paretos while there exist unique optimal values for flow rate ratios m_2 and m_3. The optimal configuration for a 5-column SMBR unit was found to be 1-1-2-1, while the optimum mole fraction of acetic acid in the feed to be 0.79. Subsequently, the effects of conversion constraint and reaction rate constant on the Pareto optimal solutions was investigated. With the same purity requirement, the productivity is higher when the conversion constraint is lower, and the maximum productivity increases when the conversion requirement decreases. When the reaction rate constant increases, the productivity with the same purity requirement also increases. It was also found that the flow rate ratios in section 2 and section 3 control the available reactant (methanol) in the reactive section when pure acetic acid is used as feed. When the effect of m_1 on the performance of SMBR was investigated, it was found that when m_1 is small, the maximum productivity could be greatly improved at the cost of eluent flow.

The three objective functions optimization results show that the productivity increases with decreasing purity and the desorbent consumption increases exponentially in order to achieve near 100% pure product. The objective of this work was to provide a more sensible and rigorous approach using multi-objective optimization technique towards a realistic design of SMBR.

Chapter 5 Modeling, Simulation and Experimental Study of SMBR for MeOAc Synthesis

5.1 Introduction

In this chapter, the synthesis of methyl acetate (MeOAc) ester catalyzed by Amberlyst 15 was considered to investigate the performance of SMBR for deeper insight into the behavior of the process. Mathematical model was developed, which was solved using experimentally determined kinetic and adsorption parameters reported in Chapter 3. The SMBR model predicted results were verified experimentally and finally parametric sensitivity studies were performed to investigate the effects of various parameters on the performance of the integrated reactor-separator.

5.2 Synthesis of MeOAc in SMBR

The esterification reaction can be described by the following equation:

$$CH_3COOH + CH_3OH \rightleftharpoons CH_3COOCH_3 + H_2O \quad (5.1)$$

In the reactor methanol is used as carrier solvent, and is present in excess. Its concentration varies very little in the entire reaction process, and therefore, can be regarded as constant. The breakthrough curves of the reactants and products from a single packed column were experimentally measured at different temperatures, feed concentrations and flow rates. Experimental results show that H_2O travels slower than MeOAc (less strongly adsorbed), the reaction rate increases with an increase in reaction temperature. The adsorption equilibrium constants, dispersion coefficients and reaction kinetic parameters together with its dependence on temperature were determined experimentally and reported in Chapter 3.

A schematic diagram of a SMBR unit is illustrated in Figure 5.1. The two incoming streams (Feed and Eluent) and the two outgoing streams (Raffinate and Extract) divide the system into four sections, namely P, Q, R and S, each of which consisting of p, q, r and s columns respectively. The flow rate in section P, Q_p, was chosen as the reference flow rate based on which all other flow rates were described. The ratios of the feed flow rate, F, the raffinate flow rate, R, the eluent flow rate, D to that in section P (Q_p) were designated as α, β, γ respectively. By advancing the introduction and withdrawal ports simultaneously, column by column, in the direction of fluid flow at a predetermined time interval (switching time, t_s), the simulation of countercurrent movement of the solid phase toward the fluid phase is achieved. In SMBR, switching time and column configuration (the number of columns in each section) are decided a priori and is kept constant throughout the entire operation.

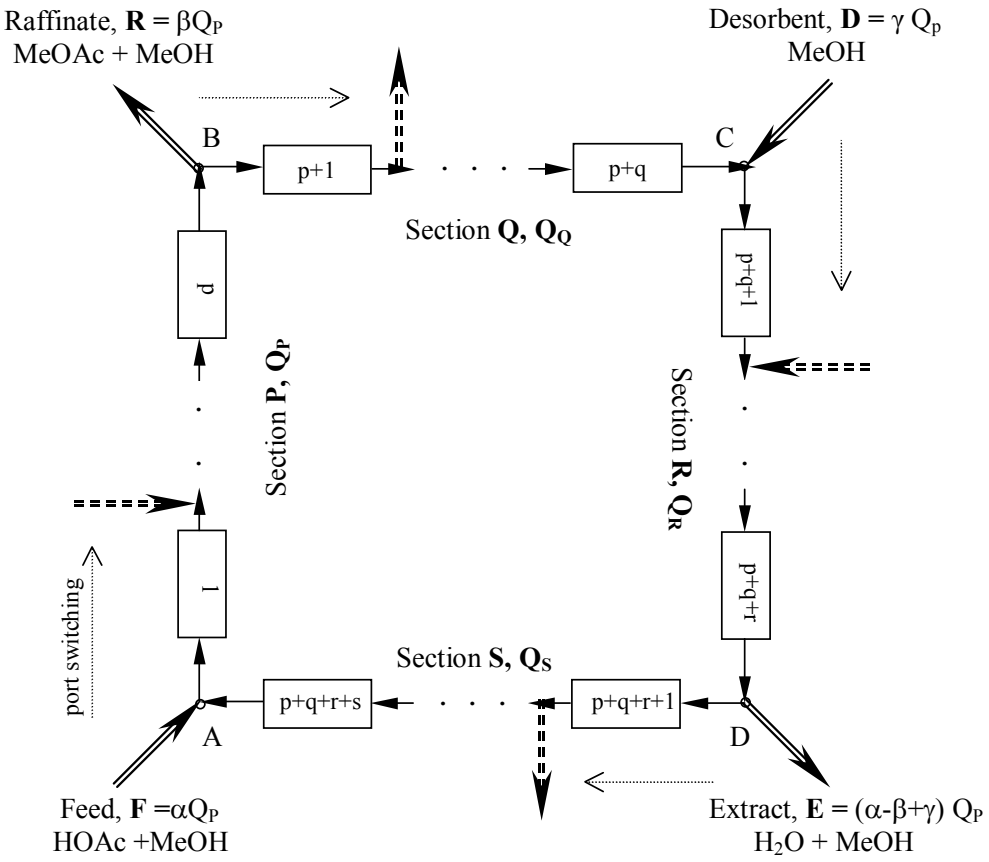

Figure 5.1 Schematic diagram of a SMBR system for MeOAc synthesis

The inlets and outlets divide the entire system into four sections: P, Q, R, and S with respectively p, q, r and s number of columns. The flow rates in each section is given by $Q_Q = (1-\beta)\ Q_P$, $Q_R = (1-\beta+\gamma)\ Q_P$, and $Q_S = (1-\alpha)\ Q_P$, where α, β, γ are given by F/Q_P, R/Q_P, D/Q_P.

5.3 Mathematical Model

A comprehensive analysis of the performance of SMBR will be difficult only with experimental study due to the complexity of the process. Particularly, length and number of columns in each section, flow rates of different streams and switching time are impossible to decide in advance without a detailed mathematical or optimization study. Consequently, a dynamic mathematical model was developed not only to acquire deeper understanding of the behavior of the reactor, but also to enable one to design an experimental setup, and perform experiments efficiently.

The concentration of methanol remains essentially unchanged in the course of reaction since methanol acts as both reactant and carrier solvent and is present in large excess. The reaction rate equation is described by quasi-homogeneous kinetic model and is written as

$$R = k_f \left[q_{HOAc} - \frac{q_{MeOAc} q_{H_2O}}{K_e} \right] \tag{5.2}$$

where R denotes the reaction rate, q_i is the concentration of component i (*MeOAc*, H_2O, or *HOAc*) in the solid phase, k_f is the forward reaction rate constant, and K_e represents the reaction equilibrium constant. The concentration of adsorbed species i in the solid phase is computed by assuming that the local liquid and solid phases are in equilibrium and liner adsorption isotherm is applicable. So it is expressed as

$$q_i = K_i C_i \tag{5.3}$$

where K_i and C_i are the adsorption equilibrium constant and liquid phase concentration of component i respectively. It should be noted that the linear isotherm is only valid when the concentration of the adsorbed components are dilute in the bulk

liquid phase, as is the case in this study. When the concentrations of the reactants and products are not sufficiently low, non-linear adsorption models, such as Langmuir model, should be considered in order to describe adsorption process accurately.

Based on the proposed reaction kinetics and adsorption isotherms, the dynamic model for a fixed-bed chromatographic reactor corresponding to each single column in the SMBR unit was developed by adopting equilibrium-dispersive model. Mass balance equations for each component i are written as follows:

$$\frac{\partial C_i}{\partial t}+\left(\frac{1-\varepsilon}{\varepsilon}\right)\frac{\partial q_i}{\partial t}+\frac{u}{\varepsilon}\frac{\partial C_i}{\partial z}-\left(\frac{1-\varepsilon}{\varepsilon}\right)\upsilon_i R = D_{iM}\frac{\partial^2 C_i}{\partial z^2} \tag{5.4}$$

The initial and boundary conditions are:

$$C_i[t=0] = C_i^0 \tag{5.5a}$$

$$C_i\ (0 < t < t_p)_{z=0} = C_{f,i} \tag{5.5b}$$

$$C_i\ (t > t_p)_{z=0} = 0 \tag{5.5c}$$

$$\left[\frac{\partial C_i(t)}{\partial z}\right]_{z=0} = 0 \tag{5.5d}$$

The kinetic, adsorption constants and diffusion coefficients of each component involved in the process are listed in Tables 3.2-3.3. They were determined semi-empirically by fitting the experimentally measured breakthrough curves with model predictions obtained by solving the above mass balance equations.

SMBR unit resembles a fixed-bed chromatographic reactor except at the instant of column rotating. Therefore, the dynamic behavior of the SMBR unit can be described by the mathematical model of a single reactive chromatographic column

while incorporating the cyclic port switching and additional feed or withdrawal streams. The modified mass equations are given by

$$\frac{\partial C_{ij}^{(N)}}{\partial t}+\left(\frac{1-\varepsilon}{\varepsilon}\right)\frac{\partial q_{ij}^{(N)}}{\partial t}+\frac{u_\phi}{\varepsilon}\frac{\partial C_{ij}^{(N)}}{\partial z}-\left(\frac{1-\varepsilon}{\varepsilon}\right)\nu_i R_j^{(N)}=D_{iM}\frac{\partial^2 C_{ij}^{(N)}}{\partial z^2} \tag{5.6}$$

for the component i in the j^{th} column during the N^{th} switching period, u_ϕ denotes superficial flow rate in section ϕ (where ϕ = P, Q, R, S), and the reaction rate expression and adsorption isotherms are given by

$$R_j^{(N)}=k_f\left[q_{HOAc,j}^{(N)}-\frac{q_{MeOAc,j}^{(N)}\cdot q_{H_2O,j}^{(N)}}{K_e}\right] \tag{5.7}$$

$$q_{ij}^{(N)}=K_i C_{ij}^{(N)} \tag{5.8}$$

The initial and boundary conditions are:

Initial condition:

When $N=0$, $C_{ij}^{(0)}=C_{ij}^{Initial}=0$ (5.9a)

When $N\geq 1$,

$$C_{ij}^{(N)}=C_{i,j+1}^{(N-1)} \qquad for \quad j=1\sim(N_{col}-1) \tag{5.9b}$$

$$C_{ij}^{(N)}=C_{i1}^{(N-1)} \qquad for \quad j=N_{col} \tag{5.9c}$$

Boundary conditions:

Feed entry point (point A in Figure 5.1)

$$C_{i1}^{(N)}\Big|_{z=0} = (1-\alpha)\, C_{i,N_{col}}^{(N)}\Big|_{z=L} + \alpha\, C_{i,f} \tag{5.10a}$$

Raffinate take-off point (point B in Figure 5.1)

$$C_{i,p+1}^{(N)}\Big|_{z=0} = C_{i,p}^{(N)}\Big|_{z=L} \tag{5.10b}$$

Eluent inlet point (point C in Figure 5.1)

$$C_{i,p+q+1}^{(N)}\Big|_{z=0} = \left[\frac{1-\beta}{1-\beta+\gamma}\right] C_{i,p+q}^{(N)}\Big|_{z=L} \tag{5.10c}$$

Extract take-off point (point D in Figure 5.1)

$$C_{i,p+q+r+1}^{(N)}\Big|_{z=0} = C_{i,p+q+r}^{(N)}\Big|_{z=L} \tag{5.10d}$$

The mass balance (Eqs. 5.6), initial (Eqs. 5.9) and boundary conditions (Eqs. 5.10), kinetic equation (Eqs. 5.7) and adsorption isotherm (Eqs. 5.8) completely define the SMBR system. The PDEs were solved using Method of Lines. The PDEs were first discretized in space using Finite Difference Method (FDM) to convert it into a set of several-coupled ODE-IVPs and the resultant stiff ODEs of the initial value kind were solved using the subroutine, DIVPAG, in the IMSL library. Since periodic switching is imposed on the system, the reactor works under transient conditions. Whenever switching is performed a new initial value problem must be solved. However, a cyclic (periodic) steady state with a period equal to the switching time is eventually attained. After each switching, column numbering was redefined according to Eqs. 5.11 so that feed is always introduced into the first column.

Before switching *After switching*

Column1 Column N_{col}

Column j Column j -1 $j = 2, 3, \ldots, N_{col}$ (5.11)

The concentration profiles were obtained from the solution of the above equations (Eqs. 5.6-5.11). The objectives of this work are to see whether we can achieve higher conversion and improve product purity for MeOAc synthesis in SMBR. Therefore, the design of SMBR configuration and operating conditions to be used therein must be set such that conversion of the limiting reactant HOAc (X_{HOAc}), and yield (Y_{MeOAc}), and purity (P_{MeOAc}) of the desired product (MeOAc) are maximized at the raffinate port. The four quantities are defined as

$$X_{HOAc} = \frac{(\text{HOAc fed} - \text{HOAc collected at raffinate and extract})}{\text{HOAc fed}}$$

$$= \frac{\alpha \cdot C_{HOAc,f} \cdot t_s - \left[\beta \cdot \int_0^{t_s} C^{(N)}_{HOAc,p}\Big|_{z=L_{col}} dt + (\alpha + \gamma - \beta) \int_0^{t_s} C^{(N)}_{HOAc,p+q+r}\Big|_{z=L_{col}} dt \right]}{\alpha \cdot C_{HOAc,f} \cdot t_s} \quad (5.12)$$

$$Y_{MeOAc} = \frac{\text{MeOAc collected in raffinate}}{\text{HOAc fed}} = \frac{\beta \cdot \left[\int_0^{t_s} C^{(N)}_{MeOAc,p}\Big|_{z=L_{col}} dt \right]}{\alpha \cdot C_{HOAc,f} \cdot t_s} \quad (5.13)$$

$$P_{MeOAc} = \frac{\text{MeOAc collected in raffinate}}{\left[\text{MeOAc} + \text{H}_2\text{O} + \text{HOAc}\right]\text{collected in raffinate}}$$

$$= \frac{\int_0^{t_s} C^{(N)}_{MeOAc,p}\Big|_{z=L_{col}} dt}{\int_0^{t_s} \left(C^{(N)}_{MeOAc,p} + C^{(N)}_{H_2O,p} + C^{(N)}_{HOAc,p} \right)\Big|_{z=L_{col}} dt} \quad (5.14)$$

$$S_{MeOAc} = \frac{\text{MeOAc collected in raffinate}}{\left[\text{MeOAc} + \text{H}_2\text{O}\right]\text{collected in raffinate}} = \frac{\int_0^{t_s} C_{MeOAc,p}^{(N)}\Big|_{z=L_{col}} dt}{\int_0^{t_s} \left(C_{MeOAc,p}^{(N)} + C_{H_2O,p}^{(N)}\right)\Big|_{z=L_{col}} dt} \quad (5.15)$$

In order to achieve separation between the components, the internal flow rates of the fluid phases within the four sections, and the switching time (which defines the hypothetical solid phase velocity) have to be specified appropriately. Petroulas et al. (1985) defined for true countercurrent moving bed chromatographic reactor (CMCR) a parameter, σ_i, called relative carrying capacity of the solid relative to the fluid stream for any component *i* as

$$\sigma_i = \frac{1-\varepsilon}{\varepsilon} NK_i \frac{u_S}{u_g} = \delta_i \frac{u_S}{u_g} \quad (5.16)$$

They showed that to achieve countercurrent separation between two components, one must set σ greater than 1 for one and less than 1 for the other. Later, Fish et al. (1986) verified the above fact experimentally. Fish et al. (1986) also defined V_i, the net velocity at which component i travels (or the concentration front moves) within the column, which for linear isotherm is given by

$$V_i = \frac{u_g\left[1-\sigma_i\right]}{\left[1+\delta_i\right]} \quad (5.17)$$

Therefore, when $\sigma_i < 1$, $V_i > 0$ (species move with the fluid phase), and when $\sigma_i > 1$, $V_i < 0$ (species move with the solid phase). When $\sigma = 0$, it represents fixed bed.

Ray et al. (1990, 1994) re-defined the above parameter, σ, for SMBR by replacing the solid-phase velocity, u_s, in CMCR by a hypothetical solid phase velocity, ζ, defined as $\zeta = L/t_s$ for SMBR. They found, both theoretically (1995a) and experimentally (1995b), that simulation of the countercurrent movement between two

components can be achieved when redefined σ's were set such that it is greater than 1 for one and less than 1 for the other component.

Hence, in the present study if we set σ properly, the more strongly adsorbed component (H_2O) will move with the imaginary solid (resin) stream, and can be collected at the extract port (point D in Figure. 5.1), while at the same time the less strongly adsorbed component (MeOAc) will travel with the fluid stream, and can be collected at the raffinate port (point B in Figure 5.1).

5.4 Experimental Details

An experimental investigation of the SMBR would prove valuable for testing the model predictions. Theoretical analysis of model of SMBR has shown that if equilibrium-limited reaction occurs on the solid surface, then under certain operating conditions the chemical reaction process and the adsorption process interact to break the local thermodynamic equilibrium limitation and it is possible to obtain improved conversions and product purity than would be obtained in a traditional fixed-bed reactor (Ray et al., 1994). The aim of the experimental investigation is to achieve four goals. The first is to see whether the SMBR can produce pure product at a higher conversion than the fixed-bed reactor for a given reactor length, switching time and eluent flow rates, as predicted by the model. The second is to compare experimental results with that of the model and to determine how good the model is. The third is to characterize the effect of changing variables on overall performance of the SMBR and to ascertain robustness of the model. This would also verify whether the adsorption and kinetic parameters obtained experimentally earlier were correct. Finally, experiments would be performed at optimal operating conditions to determine whether optimization results are meaningful and attainable experimentally.

For laboratory-scale experimental studies, the most convenient way to configure the SMBR is to design a reactor configuration consisting of a series of packed columns with provision for feed entry and product withdrawal from the ends of each column and with an appropriate sequence of column switching to simulate a countercurrent flow system. An important design decision is the length and number of columns in each section. This must be determined from a reliable model followed by systematic optimization study. Hence, in this work the model is first being used to evaluate the parameters and conditions for running such reactor by sensitivity analysis, and thereby to guide reactor design. This is followed by computer aided experimental characterization of the reactor performance to evaluate and validate the mathematical model. Subsequently, systematic optimization study is performed using multiple objectives followed by experimental verification of the optimization results.

Figure 5.2 shows a schematic diagram of the experimental setup of SMBR, which consists of four-jacketed stainless steel columns (0.25m long × 0.0094m ID) packed with Amberlyst 15 ion exchange resin. Each column is connected to four rotary valves actuated by the control system. The four rotary valves correspond to the positions of feed, raffinate, extract and desorbent streams respectively, and it allows either delivery of feed/desorbent into the column or withdrawal of raffinate/extract streams from the column as required. The rotary valves are switched in tandem periodically after a preset interval (switching period) moving the positions at which the various streams enter and leave. A shift in the positions of feed and withdrawal, in the direction of mobile phase flow through the bed, mimics the movement of the solids in the opposite direction. It should be noted that in the experimental study in this work only four columns were used although the experimental set-up is very flexible since columns can be added or removed as desired without any major difficulty. The columns are arranged in a bank with the last column connected to the first so that

switching of feed, desorbent and product streams can cycle continuously. The feed and desorbent streams were fed by HPLC pumps (Jasico, PU-1580) into the SMBR unit. The extract stream is controlled by a mass flow controller (Fisher Rosmount, QUANTIM). The raffinate stream is kept free for all the experiments in order to achieve periodic steady state within a reasonable experimental time.

All experiments were carried out at 318 K. During the experiment, samples from the raffinate and extract ports were collected during a switching time interval and their average concentrations were analyzed by a HP 6890 gas chromatography equipped with 7683 automatic injector and FID. Water concentration was measured using a volumetric Karl Fisher titrator with model 100-titration controller from Denver Instrument.

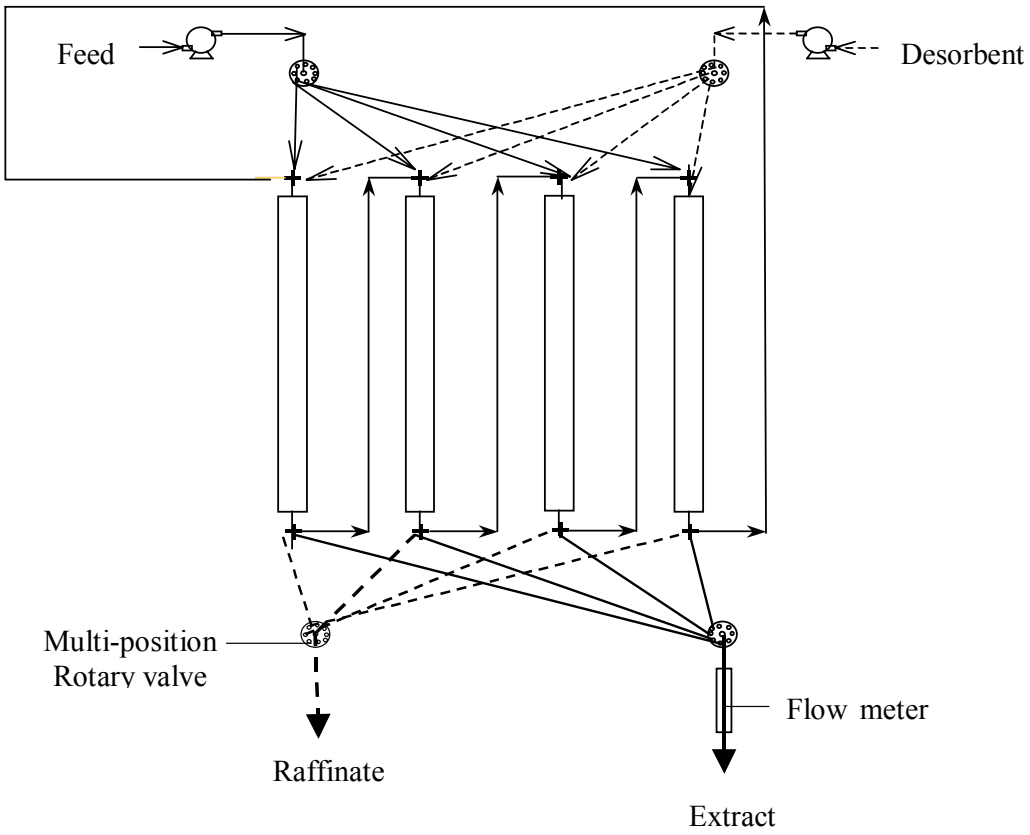

Figure 5.2 Schematic diagram of a 4-column experimental apparatus

5.5 Results and Discussion

Experiments were carried out at different switching time, feed and desorbent flow rates and flow rate in section P (feed section). The concentration profiles for the limiting reactant (HOAc) and products (MeOAc and H_2O) within the columns were obtained from the solution of the model equations (Eqs. 5.6-5.11) and the performances of the SMBR were compared based on the performance criteria defined in Eqs. 5.12-5.15.

5.5.1 Effect of Switching Time

Switching time plays a key role in determining the performance of SMBR unit. The effect of switching time on the behavior of SMBR was investigated both theoretically and experimentally. In Figure 5.3, results are compared for four different values of switching time. The figure reveals that the experimental results are in good agreement with the model predictions except that the conversion of the limiting reactant (X_{HOAc}) obtained from experiment was always higher than that predicted by the mathematical model. This is expected since the breakthrough concentration profiles of the reaction system from the single-column studies in Chapter 3 always over-predicted the outlet concentration of acetic acid.

Figure 5.3 also reveals that purity of MeOAc (P_{MeOAc}) at the raffinate port deviates from the model predicted value when switching time is small. This is most likely due to the non-linear adsorption behavior of the strongly adsorbed component, water. As a result, the adsorbent requires longer time to be completely regenerated and the remaining water in adsorbent will eventually appear in the product stream leading to lower P_{MeOAc}. The effect of tailing of water concentration front on the performance of SMBR becomes particularly obvious when switching time is small.

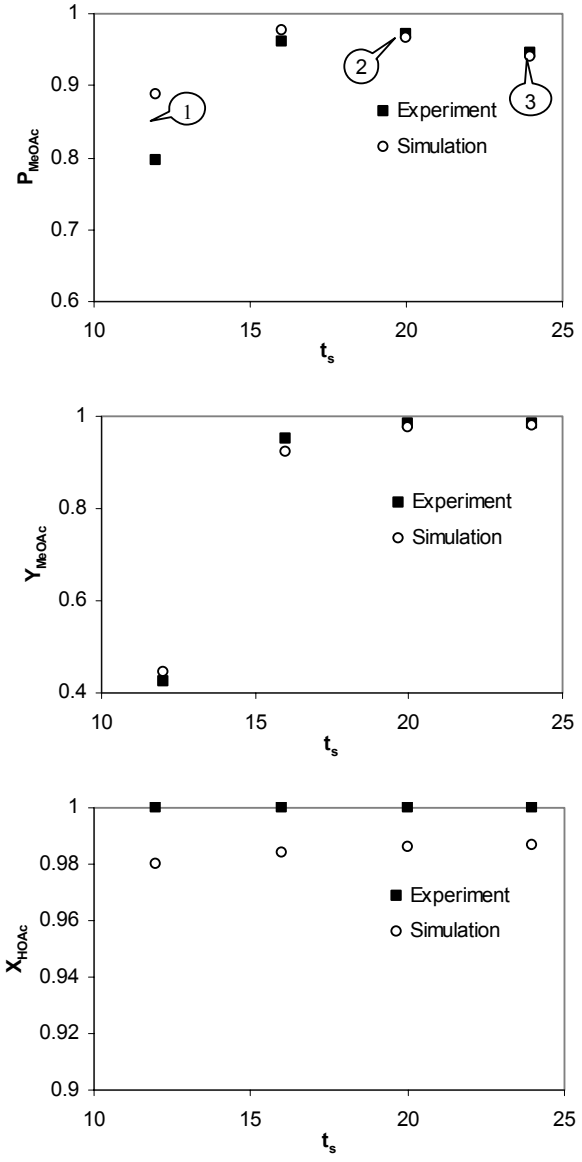

Figure 5.3 Effect of switching time on the performance of SMBR

Q_p = 1ml/min, α = 0.2, β = 1.0, γ = 3.0, C_{HOAc} = 2mol/l

When the switching time was reduced from 20 min (point 2 in Figure 5.3) to 12 min (point 1 in Figure 5.3), the experimentally measured yield of MeOAc (Y_{MeOAc}) decreased from 98.2% to 42.3% while P_{MeOAc} decreased from 97% to 79.7% respectively. The reduction of switching time increases the solid phase pseudo-velocity, and therefore, all components travel at a much faster rate with the solid phase. This in turn reduces the residence time of reactant and products in each section. Reduction in residence time deteriorates the performance of section R, which is responsible for desorbing strongly adsorbed component (water) from the solid adsorbent.

The above observation can be explained from the values of σ and V, defined in Eqs. 5.16-5.17, and reported in Table 5.1. The table shows that countercurrent separation ($\sigma_{MeOAc} < 1$, $\sigma_{H2O} > 1$) is achieved in sections P and S for all three points shown in Figure 5.3. Desorption of H_2O is better in section R (σ_{H2O} decreases while V_{H2O} increases) as t_s increases. This can be seen from the decreasing value of σ_{H_2O} from 0.85 to 0.51 and the increasing value of V_{H_2O} from 0.30 cm/min to 0.98 cm/min in section R as shown in Table 5.1. As a result, more water will remain in section R at the end of the switching period for point 1 due to insufficient regeneration and eventually contaminate the product stream at the raffinate port. Purity is poor when t_s = 12 min is primarily due to poor regeneration of section R.

Moreover, the increased solid phase pseudo-velocity deteriorates as well the performance of section S, which is responsible for desorbing weakly adsorbed component (MeOAc) and recycle it back to feed section P. This can be explained by the lower value of V_{MeOAc} (= 1.09) for point 1 compared to the value for point 2 (= 1.39). Consequently, more MeOAc tends to be retained in section S at the end of a switching period for point 1, and it will appear at the extract port instead of the

raffinate port during the next switching period since section S becomes section R after the switch, resulting in lower Y_{MeOAc}.

In contrast, when switching time was increased to 24 min (point 3 in Figure 5.3), the experimentally obtained P_{MeOAc} was decreased a little to 94.6% while Y_{MeOAc} was slightly increased to 99.7%. The pseudo solid-phase velocity is reduced when switching time is increased, and therefore, all components moved faster with the fluid phase than with the solid phase. The net separation of the concentration fronts of the two products, MeOAc and H_2O in sections P and S was decreased (ΔV decreased from 2.2 cm/min to 2.11 cm/min in section P and from 1.88 cm/min to 1.79 cm/min in section S), thereby deteriorating the effective separation of the two components. Consequently, water will breakthrough from section P and contaminate the product stream. However, the smaller solid phase pseudo velocity is beneficial for desorbing MeOAc in section S, resulting higher yield of MeOAc. This is expected from the increased value of V_{MeOAc} from 1.39 to 1.47 in section S. In this situation, separation factors in sections P and S become more important, as regeneration of column in section R is no longer a factor. Slight decrease in ΔV (degree of separation) in sections P and S reduces purity of MeOAc.

This can also be observed when concentration profiles at the cyclic steady state are compared for the three different switching times as shown in Figure 5.4. To summarize, purity and yield is poor when t_s is 12 min is primarily due to poor regeneration of section R. When t_s is increased to 20 min, sufficient time for regeneration of section R and recycle of MeOAc to section P improves purity and yield. However, when t_s is increased further to 24 min, separation factor in section P and S becomes more important as regeneration of column in section R is no longer a factor. Slight decrease in ΔV (degree of separation) in section P and S reduces pucrity of MeOAc in raffinate.

Table 5.1 Comparison of σ and V (cm/min) of the two components in different sections for various operating conditions

Effect of	Point in figure	Section P				Section R				Section S			
		σ_{MeOAc}	σ_{H2O}	V_{MeOAc}	V_{H2O}	σ_{MeOAc}	σ_{H2O}	V_{MeOAc}	V_{H2O}	σ_{MeOAc}	σ_{H2O}	V_{MeOAc}	V_{H2O}
t_s	1 in Fig. 3	0.33	2.55	1.55	-1.03	0.11	0.85	6.15	0.30	0.41	3.19	1.09	-1.17
	2 in Fig. 3	0.20	1.53	1.85	-0.35	0.07	0.51	6.45	0.98	0.24	1.91	1.39	-0.49
	3 in Fig. 3	0.16	1.28	1.93	-0.18	0.05	0.43	6.53	1.15	0.20	1.59	1.47	-0.32
γ	1 in Fig. 5	0.20	1.53	1.85	-0.35	0.13	1.02	3.00	-0.02	0.24	1.91	1.39	-0.49
	2 in Fig. 5	0.20	1.53	1.85	-0.35	0.10	0.77	4.15	0.31	0.24	1.91	1.39	-0.49
	3 in Fig. 5	0.20	1.53	1.85	-0.35	0.05	0.38	8.76	1.64	0.24	1.91	1.39	-0.49
α	1 in Fig. 7	0.20	1.53	1.85	-0.35	0.07	0.51	6.45	0.98	0.22	1.70	1.62	-0.42
	2 in Fig. 7	0.20	1.53	1.85	-0.35	0.07	0.51	6.45	0.98	0.33	2.55	0.93	-0.62
Q_P	1 in Fig. 9	0.39	3.06	0.70	-0.69	0.13	1.02	3.00	-0.02	0.49	3.83	0.47	-0.75
	2 in Fig. 9	0.10	0.77	4.15	0.31	0.03	0.26	13.36	2.98	0.12	0.96	3.23	0.05
Desired		< 1	> 1	> 0	< 0	< 1	< 1	> 0	> 0	< 1	> 1	> 0	< 0
		Retention of H_2O				Desorption of H_2O				Desorption of MeOAc			

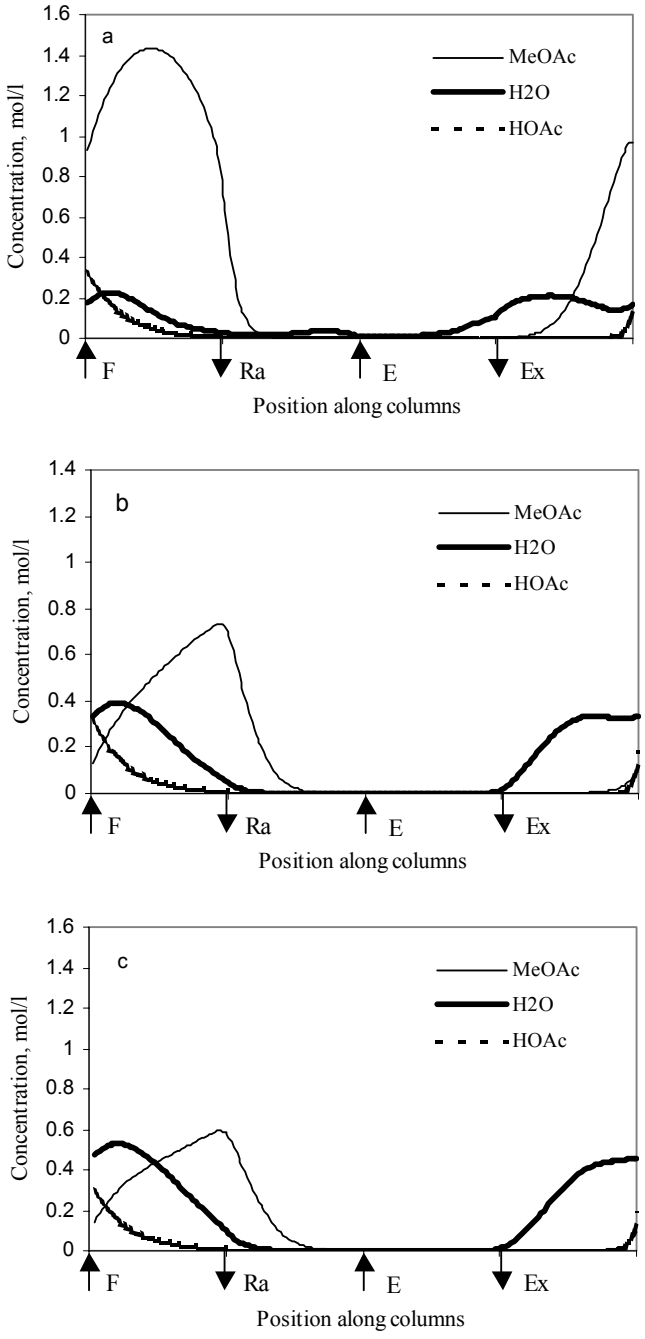

Figure 5.4 Effect of switching time on the cyclic steady state concentration profiles of MeOAc-H_2O-HOAc

(Model predictions)

Q_p = 1ml/min, α = 0.2, β = 1.0, γ = 3.0

a) t_s = 12 min b) t_s = 20 min c) t_s = 24 min

5.5.2 Effect of Desorbent Flow Rate

The complete regeneration of solid adsorbent is crucial for the successful separation of the products. With a smaller switching time, water will not be completely desorbed from section R due to the tailing of its concentration front and MeOAc will show up at the extract port because there is not enough time for MeOAc to be desorbed from section S to be recycled back to section P. On the contrary, with a longer switching time, water will breakthrough from section P and contaminate the product stream. Therefore, the only way to further improve the separation performance is to completely regenerate (purge) at least one column in section R by increasing the desorbent (solvent) flow rate.

Figure 5.5 shows the effect of desorbent flow rate (γ) on the performance of SMBR. It is obvious that the model can predict experimental results quite well at different desorbent flow rates. The model over-predicts experimental results for P_{MeOAc} at lower desorbent flow rates while under-predicts at higher flow rates. This is possibly due to the non-linear adsorption behavior of the strongly adsorbed component, water. In order to achieve the same regeneration performance, higher desorbent flow is required than that predicted from the linear model. The prediction for Y_{MeOAc} is very good in the range of solvent flow rates studied. However, model predicted X_{HOAc} is always lower than the experimental values, which shows that complete conversion of HOAc is possible in SMBR.

It is observed that P_{MeOAc} at the raffinate port was improved with higher eluent flow although Y_{MeOAc} is hardly changed. This can be explained by comparing the steady state concentration profiles for γ equal to 1.5, 2.0 and 4.0 shown in Figure 5.6. When γ is 1.5, a considerable amount of water breaks through at the raffinate port due to inadequate desorption of water (purging) in Section R ($\sigma_{H_2O} > 1$ (Table 5.1), water still

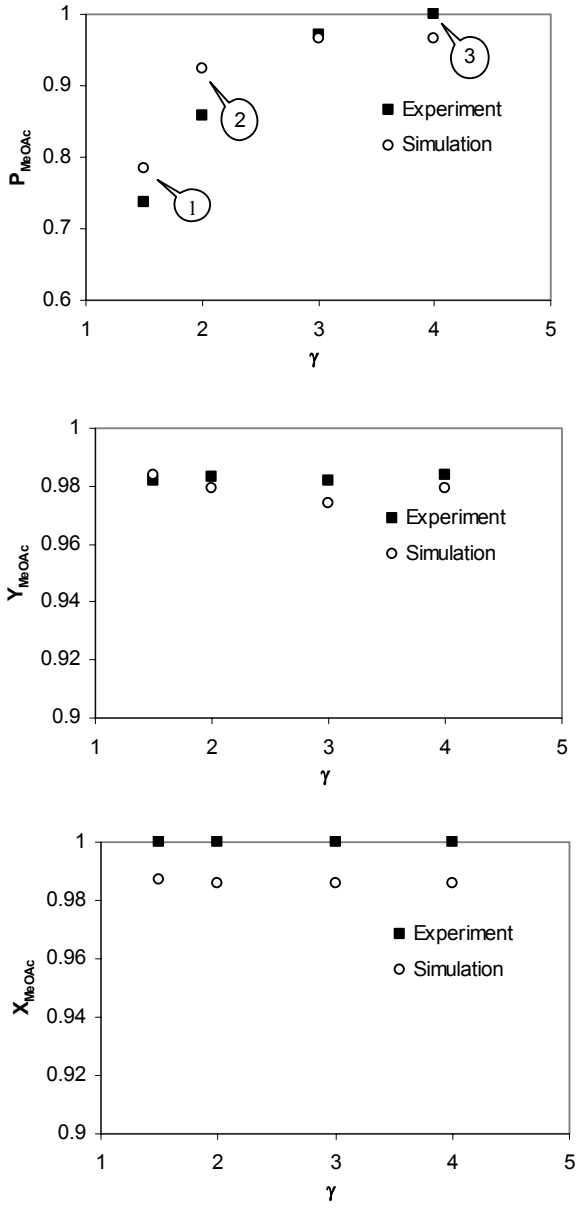

Figure 5.5 Effect of eluent flow rate on the performance of SMBR

Q_p = 1ml/min, α = 0.2, β = 1.0, t_s = 20 min, C_{HOAc} = 2mol/l

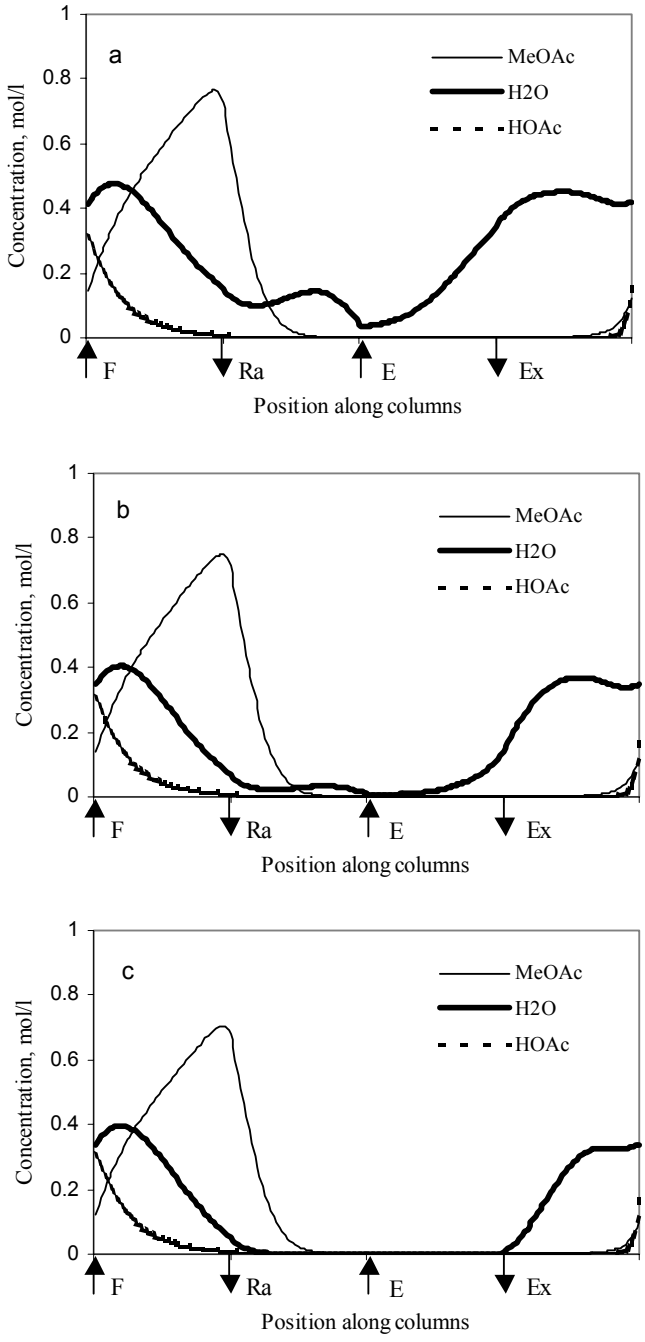

Figure 5.6 Effect of eluent flow rate on the cyclic steady state concentration profiles of MeOAc-H_2O-HOAc

(Model predictions)

Q_p = 1ml/min, α = 0.2, β = 1.0, t_s = 20 min
a) γ = 1.5 b) γ = 2.0 c) γ = 4.0

moves with the solid phase). This is indeed found out to be true as when γ is increased to 2, P_{MeOAc} increased significantly due to the better regeneration of the solid phase in section R (σ_{H_2O} = 0.77) at the end of a switching period. When γ is further increased to 4.0, hardly any water appears at the raffinate port since at this high eluent flow rate section R is almost completely free of water (σ_{H_2O} = 0.38). Therefore, increase of γ keeping all the other parameters fixed improves regeneration of section R (decreasing σ_{H2O} and increasing V_{H2O}) resulting in better purity. It is to be noted that the improvement of P_{MeOAc} becomes less significant when the desorbent flow rate becomes sufficiently large.

5.5.3 Effect of Feed Flow Rate

The effect of feed flow rate on the performance of SMBR is illustrated in Figure 5.7. It was found that purity and yield of MeOAc decreased while increasing feed flow rate, α.

Since the flow rate in section P (Q_P) is fixed, the increase of feed flow rate leads to the reduction of fluid flow rate in section S since Q_S is equal to $(1-\alpha)Q_P$. The smaller fluid phase velocity in section S deteriorates its performance in desorbing MeOAc as can be seen in Table 5.1 the V_{MeOAc} was decreased from 1.62 to 0.93, which is equivalent to increasing solid-phase pseudo-velocity by reducing switching time. More MeOAc and unreacted HOAc will be retained in section S at the end of a switching period and the remaining components will breakthrough at the extract port during the next switching period when section S becomes section R.

As the feed flow rate was increased, the P_{MeOAc} in raffinate was slightly decreased. Since more water is likely to be produced at higher feed flow rate, the performance of adsorbent regeneration deteriorates unless desorbent flow rate is

increased. This will be more due to the nonlinear behavior of the strongly adsorbed component, water. The remaining water in adsorbent will eventually appear at the raffinate port leading to lower product purity. Moreover, as α was increased from 0.1 to 0.4 keeping all other parameter values constant, ΔV (effective separation factor) in section S reduces significantly from 2.04 to 1.55 (see Table 5.1) lowering both purity and yield. This can be illustrated by comparing the steady state concentration profiles for two different feed flow rates as shown in Figure 5.8.

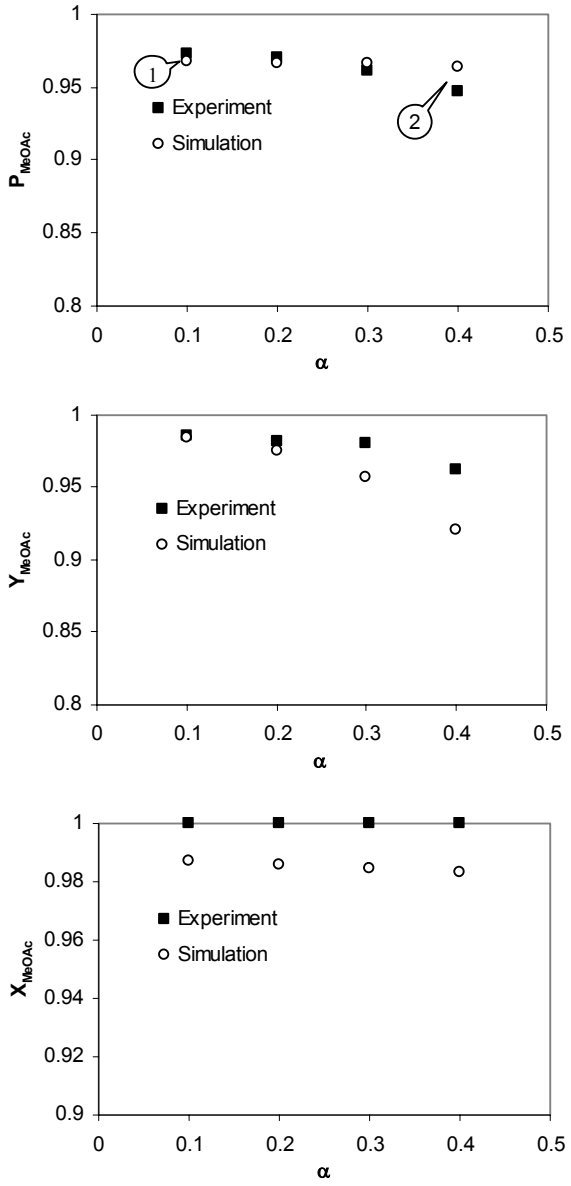

Figure 5.7 Effect of feed flow rate on the performance of SMBR

Q_p = 1ml/min, β = 1.0, γ = 3.0, t_s = 20 min, C_{HOAc} = 2mol/l

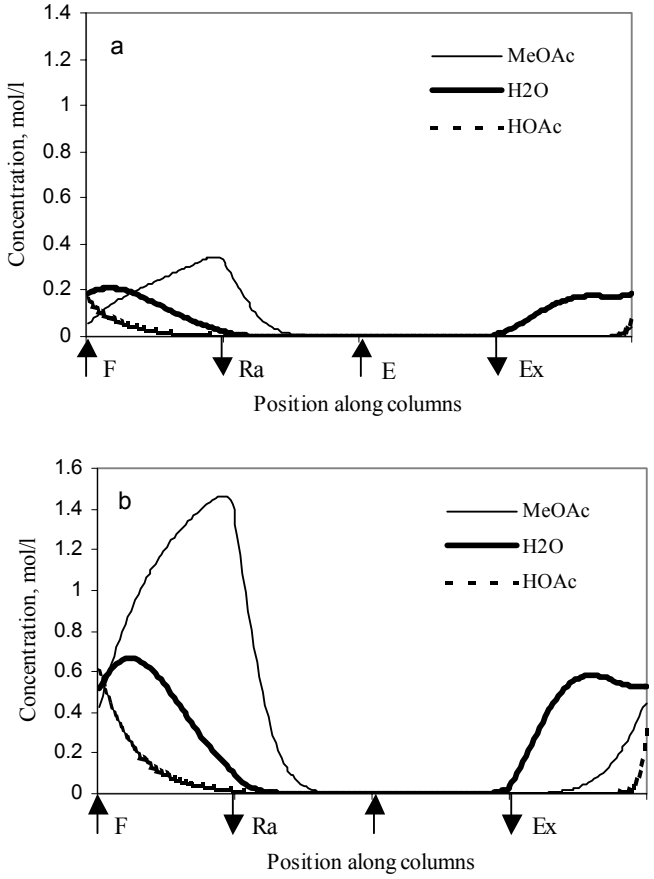

Figure 5.8 Effect of feed flow rate on the cyclic steady state concentration profiles of MeOAc-H_2O-HOAc

(Model predictions)

Q_p = 1ml/min, β = 1.0, γ = 3.0, t_s = 20 min

a) α = 0.1; b) α = 0.4

5.5.4 Effect of Flow Rate in Section P

The effect of flow rate in section P on the behavior of SMBR is demonstrated in Figure 5.9. The fluid phase velocity in each section is increased with the increased flow rate in section P (Q_P). The higher fluid phase velocity is beneficial for the performance of section R and section S, which are responsible for desorbing water and MeOAc respectively. However the increased fluid phase flow rate deteriorates the performance of section P, which plays the central role for reaction and separation of the products for the MeOAc synthesis in SMBR. On one hand, when the fluid phase flow rate is increased, the residence is not enough for acetic acid to be completely consumed. Hence, the unconverted acid will breakthrough from the raffinate port due to its similar adsorption affinity towards resin as MeOAc, and therefore, the product stream would be contaminated. On the other hand, if Q_P is small water tends to breakthrough from at the raffinate port.

When the flow rate in section P was decreased from 1 ml/min to 0.5 ml/min, the P_{MeOAc} and Y_{MeOAc} were decreased significantly from 97% and 98.2% to 62.3% and 26.9% respectively. This is probably because of the decrease of ΔV (degree of separation) from 2.2 to 1.39 (see Table 5.1) in section P and from 1.88 to 1.22 in section S respectively. Moreover, desorption of water in section R ($\sigma_{H_2O} > 1$, water still moves with the solid phase), and desorption of methyl acetate in section S (V_{MeOAc} decreased from 1.39 to 0.47) is poor due to the decreased fluid phase velocity. This can also be seen when the concentration profiles are compared as shown in Figure 5.10a and Figure 5.4b. At low Q_P, large amount of water is retained in section R ($\sigma_{H_2O} = 1.02$), which eventually pollutes the product stream at the raffinate port (see Figure. 5.10a). MeOAc and unconverted HOAc are kept in section S at the end of a

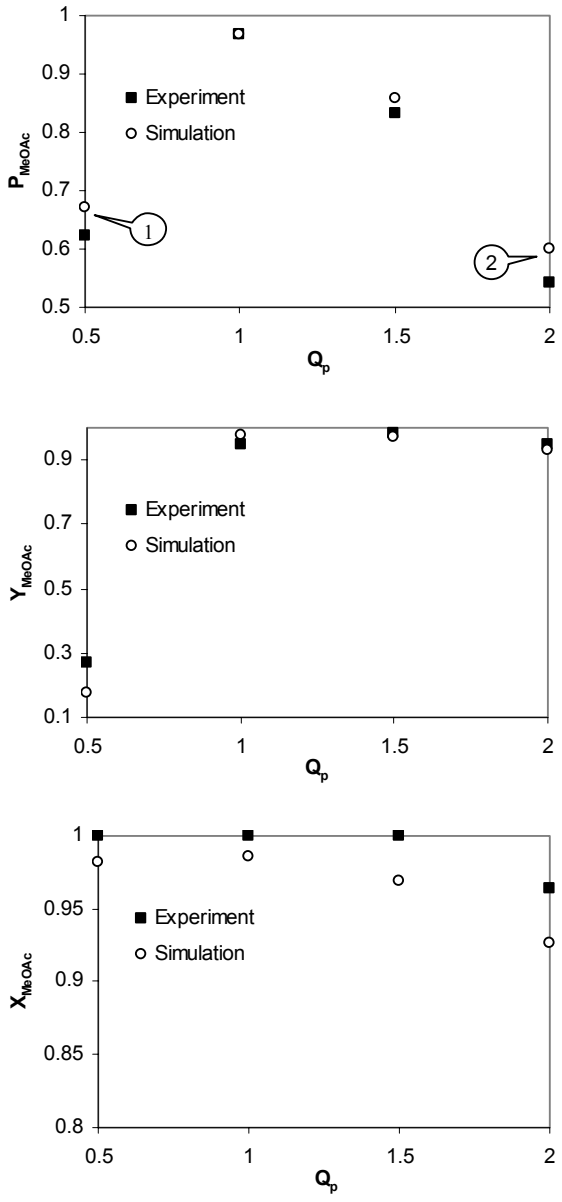

Figure 5.9 Effect of flow rate in section P on the performance of SMBR

$\alpha = 0.2$, $\beta = 1.0$, $t_s = 20$ min, $\gamma = 3.0$, $C_{HOAc} = 2$mol/l

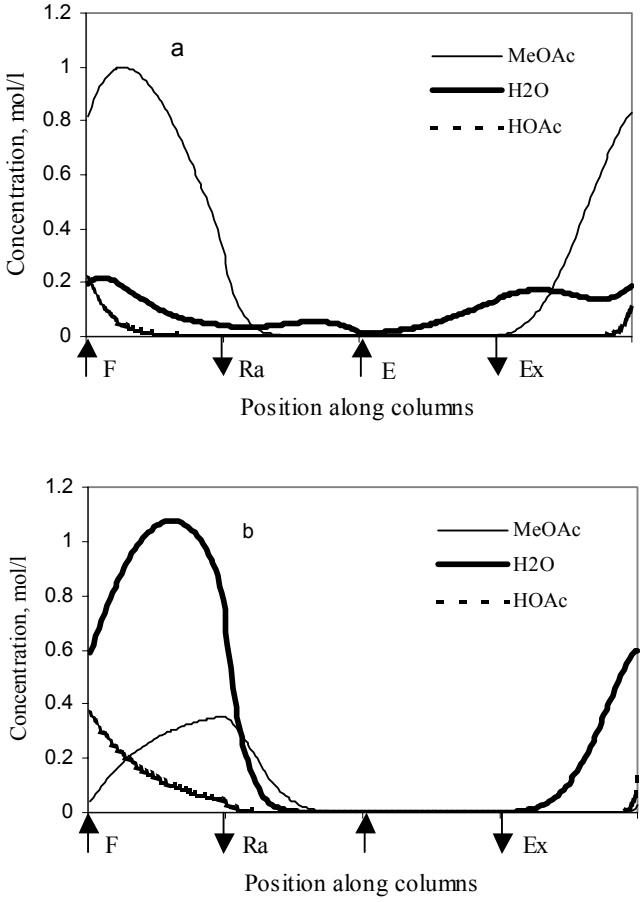

Figure 5.10 Effect of flow rate in section P on the cyclic steady state concentration profiles of MeOAc-H_2O-HOAc

(Model predictions)

$\alpha = 0.2$, $\beta = 1.0$, $t_s = 20$ min, $\gamma = 3.0$
a) $Q_p = 0.5$ ml/min b) $Q_p = 2.0$ ml/min

switching period, which will ultimately be lost with the extract stream during the next switching period lowering the Y_{MeOAc}.When the flow rate in section P was increased to 2 ml/min, the P_{MeOAc} once again decreased drastically from 97% to 54%, while the Y_{MeOAc} decreased slightly. As shown in Figure 5.10b and Figure 5.4b, when the fluid flow rate is increased in section P, water tends to breakthrough from the raffinate port lowering purity significantly ($\sigma_{H_2O} < 1$ in both section P ($\sigma_{H_2O} = 0.77$) and S ($\sigma_{H_2O} = 0.96$) when Q_p is 2 ml/min, and therefore, water moves with the fluid phase co-currently and not counter-currently) unless the switching time is changed. The reduced residence time also lowered conversion of acetic acid and the unconverted acetic acid will elute with the fluid phase at the raffinate port leading to lower product purity, P_{MeOAc}. Although ΔV in section S increases from 1.88 to 3.28 when Q_p is increased to 2.0 ml/min, yield decreases slightly due to $\sigma_{H_2O} < 1$, $V_{H_2O} > 1$ in section S.

5.6 Sensitivity Study

The experimental as well as theoretical model clearly demonstrates that it is possible to obtain improved conversions and product purity for methyl acetate synthesis in SMBR. In addition, it was found that the model adequately predicts experimentally observed overall performance of the reactor for changing values of various operating variables. This also verifies that the adsorption and kinetic parameters obtained experimentally earlier were correct and the model is quite robust and reliable.

An important design decision for SMBR is the appropriate length (L_{col}) and number of columns (N_{col}) in each section, and various flow rates. This must be determined from a systematic optimization study. The effects of switching time, desorbent and feed flow rate, and flow rate in section P on the performance of SMBR

Table 5.2 Sensitivities of process parameters for the synthesis of MeOAc

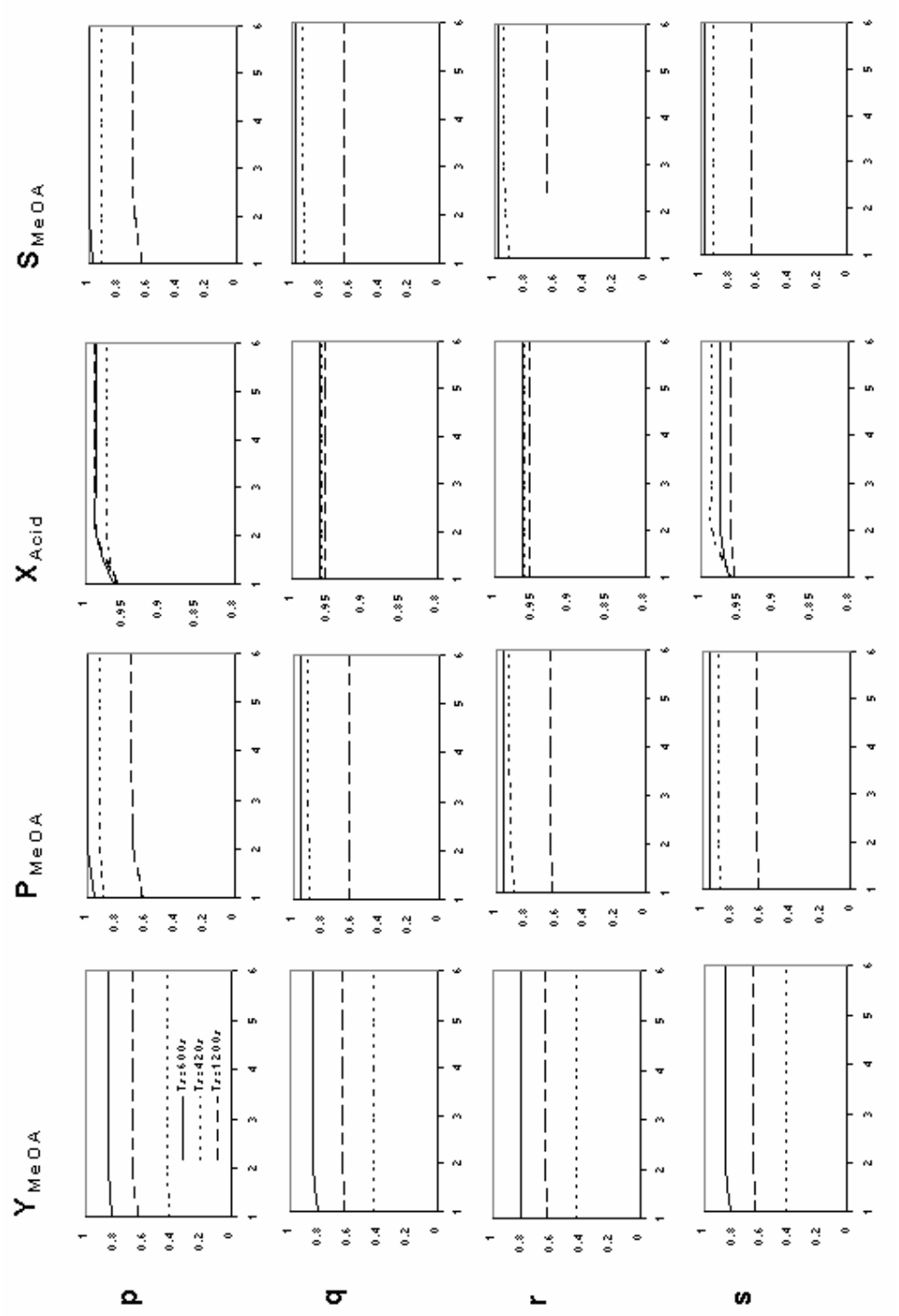

Reference: P=1.O=1.R=1.S=1. O_n=2 ml/min. L=25cm. ε=0.4. $C_{HOAC\ F}$ = 2mol/l. α=0.5. β=0.5. γ=2.0

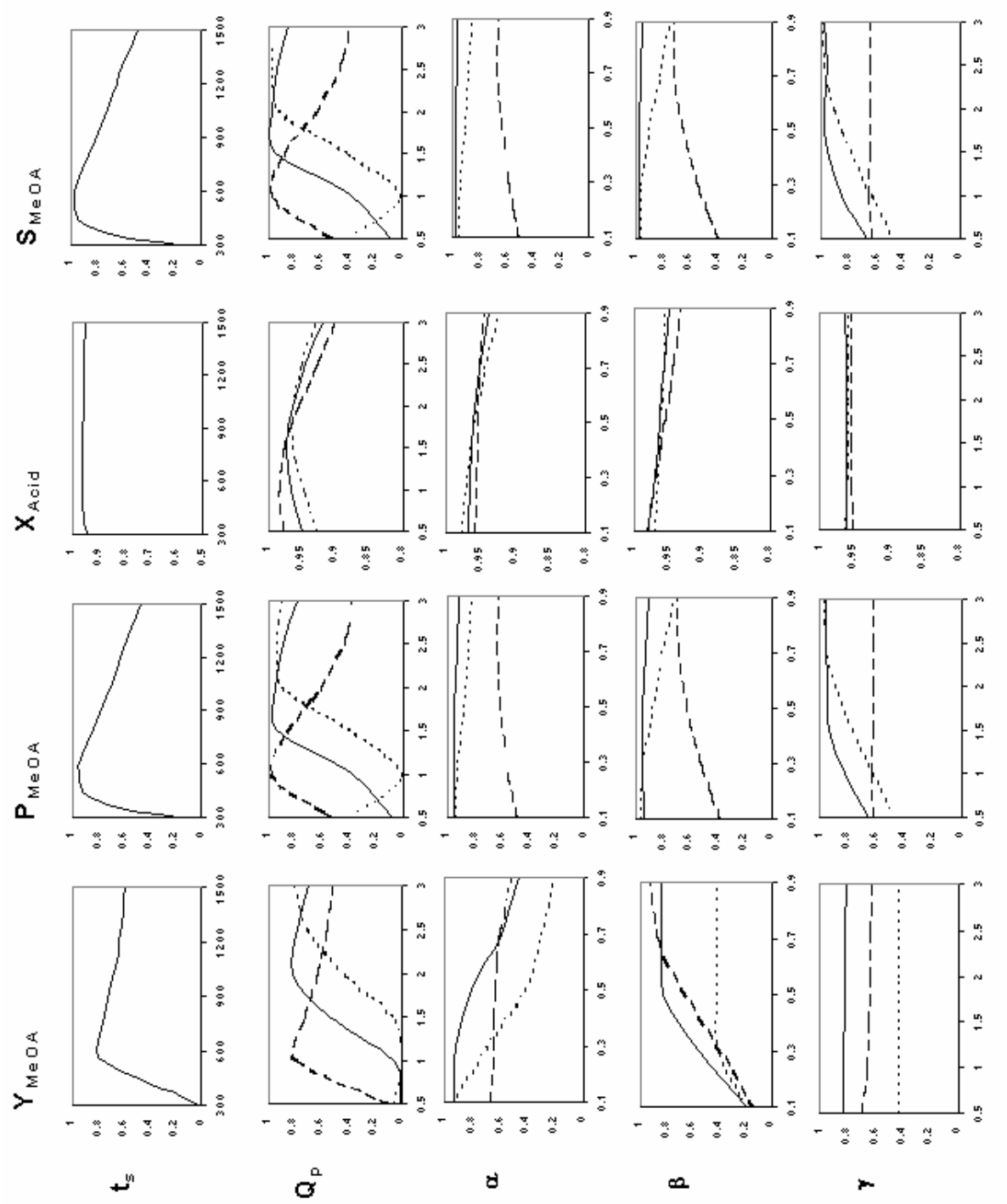
Y_{MeOA}
P_{MeOA}
X_{Acid}
S_{MeOA}
t_s
Q_p
α
β
γ

reveal that there is a complex interplay of all these operating parameters on X_{HOAc}, Y_{MeOAc}, S_{MeOAc} and P_{MeOAc}. A close scrutiny of all the figures clearly reveals that if we want to maximize one (for example, Y_{MeOAc}), another one (for example, P_{MeOAc}) worsens (see, for example, Figure 5.5). Therefore, comprehensive parametric sensitivity study must be conducted in order to acquire a thorough understanding of the SMBR system.

Sensitivity analysis was carried out by changing only one process parameter at a time while fixing the other operating parameters fixed at a reference set of values. Table 5.2 shows the results of sensitivity study. Effects of switching time (t_s), flow rates of feed (α), raffinate (β), desorbent (γ), in section P (Q_P), and number of columns (p, q, r and s) in sections P, Q, R and S respectively on the several performance criteria, Y_{MeOAc}, P_{MeOAc}, X_{HOAc} and S_{MeOAc} as defined in Eqs. 5.12-5.15 are shown. The parameters on the left column of Table 5.2 denote x-axis variable for the respective row and the effect of each parameter on Y_{MeOAc}, P_{MeOAc}, X_{HOAc} and S_{MeOAc} are shown for reference values of other parameters in the four subsequent columns. The effect of switching time, t_s, is shown in the diagrams in the first row. Subsequently, three values of t_s (420s, 600s and 1500s) were used to show the influence of a particular parameter on Y_{MeOAc}, P_{MeOAc}, X_{HOAc} and S_{MeOAc}.

It was found that q and r, which represents numbers of columns in section Q and R, respectively, have little effect on the performance of the process, when each of them was varied between 1 to 6. Some parameters, such as β and γ, influence the Y_{MeOAc}, P_{MeOAc}, X_{HOAc} and S_{MeOAc} in conflicting ways. Moreover, the effects of α, β, γ and p are quite different depending on the switching time. The influence of switching time is particularly complex as its optimum value depends not only on the distribution of columns, but also on the values of α, β and γ. A close look at Table 5.2 reveals that

there is an intricate relationship of all these parameters on Y_{MeOAc}, P_{MeOAc}, X_{HOAc} and S_{MeOAc}. If we want to maximize one the other one worsens. Optimum SMBR configuration (number and length of columns), and operating conditions (such as t_s, β, γ, etc.) differ depending on which variable we want to maximize among Y_{MeOAc}, P_{MeOAc}, X_{HOAc} and S_{MeOAc}, and it may not be possible to maximize all at the same time. One may also get infinite optimal solutions, or Pareto optimal solution, when one performs multi-objective optimization of SMBR. Pareto optimal solution is usually obtained when one or more of the decision variables are conflicting in nature. This is indeed found out and is discussed in the next chapter.

5.7 Conclusions

The synthesis of methyl acetate (MeOAc) in a simulated moving bed reactor (SMBR) was investigated by numerical simulation as well as experimentally. A rigorous mathematical model was developed to describe the dynamic behavior of SMBR and comparing the experimental results obtained at various operating conditions further validated the model. It was observed that experimental results were in good agreement with that predicted from the model. The high yield and purity of MeOAc and near complete conversion of the limiting reactant, acetic acid, could be achieved in SMBR by selecting proper operating conditions.

Parametric analysis was carried out based on the verified model to systematically investigate the effects of the process parameters on the performance of SMBR. It was found that there is a complex interaction of all these parameters on the reactor performance. Some of the operating parameters not only influence the purity, yield and selectivity of MeOAc significantly but also act in conflicting ways. This makes extremely difficult to select length and number of columns in various sections, switching time and flow rates in different sections since desirable change in one

performance criteria results in an unfavorable change in another desired variable. Therefore, one must carry out systematic multi-objective optimization study using the experimentally verified model developed in this study to determine appropriate design and successful implementation of SMBR on industrial scale.

Chapter 6 Optimization of Reactive SMB & Varicol Process for MeOAc Synthesis

6.1 Introduction

The simulated moving bed (SMB) (Magee, 1961) is a practical way to implement continuous countercurrent operation of chromatographic separation processes. In SMB technology, the countercurrent movement of the fluid phase toward the stationary phase is mimicked by switching the introduction and withdrawal ports periodically and simultaneously along a series of fixed columns in the direction of the fluid flow. For ease of operation, the columns are actually divided into sections (or zones). The number of columns within each section and total number of columns are adjustable depending on the design of the system for any particular applications. One of the limitations of the SMB is that during most of the operation, the stationary phase in few columns are either completely free of solutes or contains only product so that their separation capacity is reduced. This is primarily due to synchronous switching of all the inlet and outlet ports. Recently, SMB was modified into Varicol process (Ludemann-Hombourger et al., 2000) for chiral separation in which several non-synchronous switching (shifting) of the inlet and outlet ports were made during a global switching period. Therefore, the column configuration (number of columns in any particular section) varies at different sub-time intervals in the Varicol process. This leads to more flexibility in operation in the Varicol process compared to more rigid conventional SMB process, and therefore, allows better utilization of the stationary phase.

SMB and its modification also provide opportunities for coupling reactions (Ray et al., 1990), which allow higher conversion for equilibrium-limited reversible

reactions by on-site separation of the products, which leads to better yield and selectivity compared with typical fixed-bed processes. Additionally, the combination of two unit operations in one single apparatus reduces capital and operating cost. However, such integration of chemical reaction and separation complicates the process design and plant operation. The optimal design and operating parameters, such as switching time (and sequence), flow rates in each section, length of each column and its distribution, are therefore essential to evaluate the economic potential of the process and to successfully implement the reactive SMB and Varicol processes on industrial scale.

The modeling, simulation and experimental study of SMBR for the synthesis of methyl acetate (MeOAc) have been carried out, details of which are reported in Chapter 5. A rigorous numerical model was developed to describe the dynamic behavior of SMBR for the synthesis of MeOAc, and comparing the experimental results with model predictions validated the model. Thereafter, a parametric sensitivity study was performed to investigate the effects of several design and operating parameters, such as switching time, number of columns in each section and inlet and outlet flow rates, on the performance of SMBR. It was found that there is a complex interplay of these parameters and some of the operating variables not only influence the yield, selectivity and purity of MeOAc significantly but also act in conflicting ways. This leads to any desirable change in one objective function results in an unfavorable change in another objective function. For example, it is not possible to improve yield and purity of MeOAc simultaneously, as when one is improved, the other worsened. Although several studies (Migliorini et al., 1999b; Dunnebier et al., 2000; Lode et al., 2001; Azevedo and Rodrigues, 2001; Zhang et al., 2002) have been reported on the design and optimization of SMBR, they only involved single objective

optimization except that reported by Zhang et al., 2002, which is usually not sufficient for the real-life design of complex reactive SMB systems. Therefore, a more realistic approach, multi-objective optimization (Bhaskar et al., 2000) is proposed in this study for the design of reactive SMB and Varicol process for the methyl acetate synthesis. This is the first time multi-objective optimization has been studied systematically for the reactive Varicol process.

The principle of multi-criterion optimization with conflicting objectives is different from that of single objective optimization. Instead of trying to find the best design solution, the goal of multi-objective optimization is to obtain a set of equally good solutions, which are known as Pareto optimal solutions. In a set of Pareto solutions, no solution can be considered better than any other solutions with respect to all objective functions, since one solution is better than other in one objective, but is worse in the others. So the selection of any optimal solution from a Pareto set will depend on auxiliary information. However, by narrowing down the choices, the Pareto set does provide decision makers with useful guidance in selecting the desired operating conditions (called the preferred solution) from among the (restricted) set of Pareto optimal solutions, rather than from a much larger number of possibilities.

In this Chapter, a comprehensive multi-objective optimization study of reactive SMB and Varicol processes is reported. The Non-dominated Sorting Genetic Algorithm (NSGA) (Deb, 2001) was applied in obtaining Pareto optimal solutions. Genetic Algorithms are non-traditional search and optimization methods based on the mechanics of natural genetics and natural selection. It has become quite popular in recent year in chemical reactor design. Literature reported results in chemical reactor design (Rajesh et al., 2000; Bhaskar et al., 2000a, 2000b, 2001; Oh et al., 2001; Zhang

et al., 2002), which show that NSGA is a very promising method for the simultaneous optimization of multiple objective functions.

Initially, the optimal solutions in terms of maximization of purity and yield of MeOAc for an existing SMBR experimental unit were obtained. Subsequently, experiments were performed at the predicted optimal operating conditions and the performance of the reactor was compared. This not only demonstrates that the model is robust, but also shows that optimization results can be duplicated experimentally. The effects of constant and non-uniform feed flow rate, raffinate flow rate, flow rate in section P and total number of columns on the Pareto optimal solutions for few different combinations of two and three objective functions were also investigated. Moreover, the applicability of Varicol to reaction systems was evaluated and optimal results were compared with that of the SMBR. To the best of our knowledge, this is the first attempt to extend the concept of Varicol process to reactive systems. This paper illustrates a new more realistic approach toward the optimal design and operation of reactive SMB and Varicol processes.

6.2 SMBR and Reactive Varicol Systems

In contrast to conventional SMBR, reactive Varicol process is based on non-simultaneous and unequal shift of the inlet and outlet ports. Figure 6.1 illustrates the principles of operation of a 6-column Varicol based on a four sub-interval switching period and compares it with an equivalent 6-column SMBR. Figure 6.1(b) illustrates a typical sequence of column configuration within a global switching period, t_s,

First sub-interval, $0 < t < t_s/4$: 2/1/1/2

Second sub-interval, $t_s/4 < t < t_s/2$: 2/1/2/1

Third sub-interval, $t_s/2 < t < 3t_s/4$: 1/1/2/2

Last sub-interval, $3t_s/4 < t < t_s$: 1/2/1/2

The configuration 2/1/1/2 implies that there are two columns in section P, one each in sections Q and R while two columns in section S, respectively. In the second sub-interval, the configuration of columns changes to 2/1/2/1 by shifting the extract port by exactly one column forward keeping all other fixed. For the next sub-interval, a forward shift of the feed port by one column changes the configuration to 1/1/2/2. In the last sub-interval, the eluent port shifts forward by one column to change the column configuration to 1/2/1/2. Finally, the column configuration gets reverted back to original configuration 2/1/1/2 at the end of the global switching period. Consequently, for a four-subinterval Varicol process, there are four different column configurations corresponding to the four subintervals, which is due to the local switching within a global switching period. Though the number of columns in any section varied within a global switching time, the number of columns in each section returned back to its initial value at the end of each cycle. For the case mentioned above, the time-averaged number of columns per section in a global switching time is equivalent to the configuration 1.5/1.25/1.5/1.75. It should be noted that it is always possible for any port to shift more than once, either forward or backward, during a global switching period. Hence, location of input and output ports in Varicol systems is quite diverse compared to that of SMBR and allows taking advantage of collecting a particular component at any port for longer (or shorter) duration. As a result, Varicol system endows more flexibility compared to the SMBR, and therefore, SMBR can be considered to be the most rigid specific case of a Varicol system.

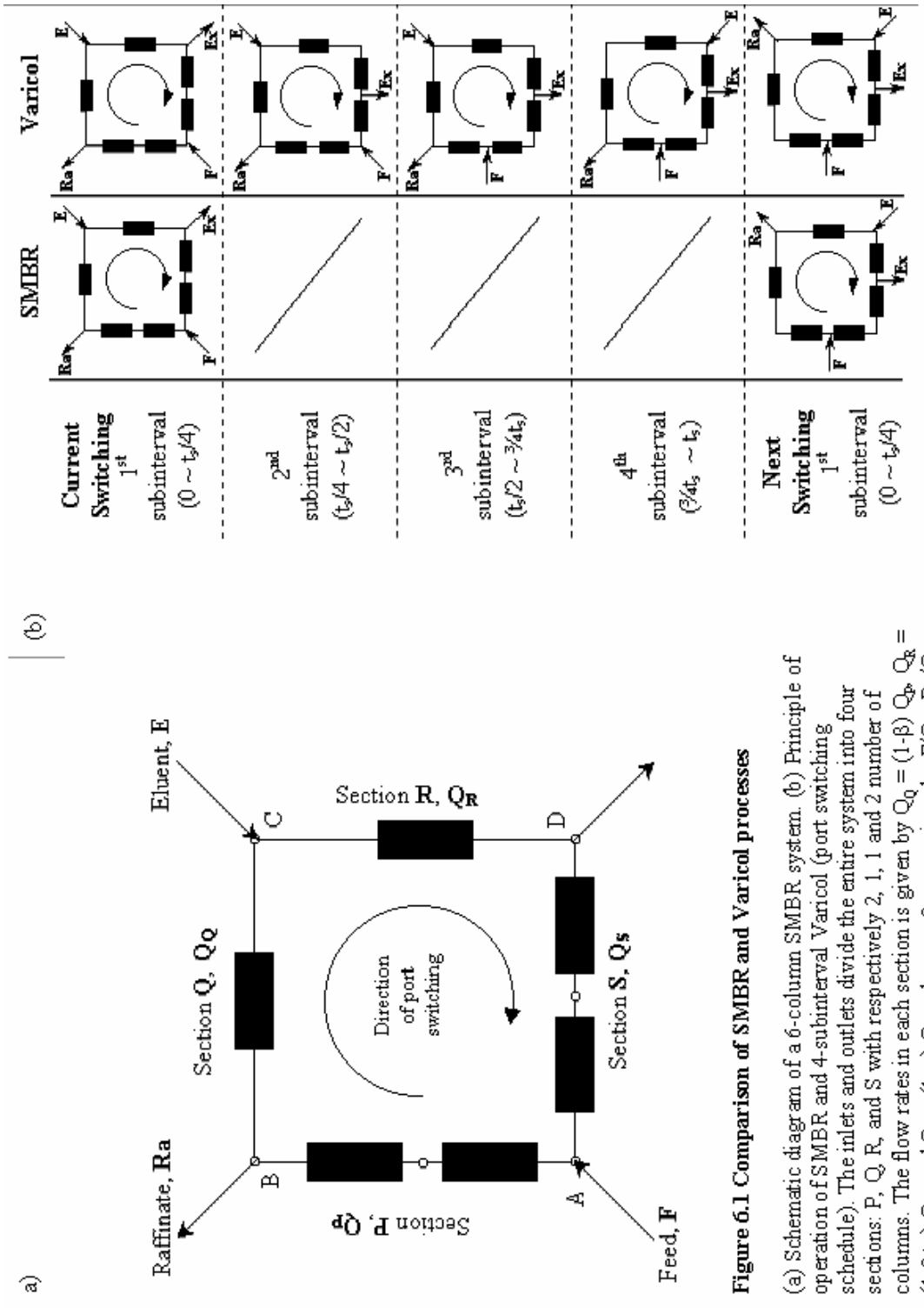

Figure 6.1 Comparison of SMBR and Varicol processes

(a) Schematic diagram of a 6-column SMBR system. (b) Principle of operation of SMBR and 4-subinterval Varicol (port switching schedule). The inlets and outlets divide the entire system into four sections: P, Q, R, and S with respectively 2, 1, 1 and 2 number of columns. The flow rates in each section is given by $Q_Q = (1-\beta)\ Q_P$, $Q_R = (1-\beta+\gamma)\ Q_n$, and $Q_s = (1-\alpha)\ Q_n$, where α, β, γ are given by F/Q_n, Ra/Q_n,

6.3 Mathematical Model

The experimentally verified mathematical model describing the dynamic behavior of SMBR for the synthesis of MeOAc was described in Chapter 5, the same are not included here for brevity. The model can predict the concentration profiles of the limiting reactant (HOAc), and products (MeOAc and H_2O). It was observed that enhancement of conversion of HOAc and purity of MeOAc is possible in the SMBR due to the separation of the products at the site of reaction.

The dynamic model for reactive Varicol can be easily derived by incorporating the sub-time interval switching in the SMBR model. A set of objective functions examined in this chapter are defined as follows:

$$X_{HOAc} = \frac{\text{(HOAc fed – HOAc collected at Raffinate and Extract)}}{\text{HOAc fed}}$$

$$= \frac{\alpha \cdot C_{HOAc,F} \cdot t_s - \left[\beta \cdot \int_0^{t_s} C^{(N)}_{HOAc,p}\Big|_{z=L_{col}} dt + (\alpha+\gamma-\beta) \int_0^{t_s} C^{(N)}_{HOAc,p+q+r}\Big|_{z=L_{col}} dt \right]}{\alpha \cdot C_{HOAc,F} \cdot t_s} \quad (6.1)$$

$$Y_{MeOAc} = \frac{\text{MeOAc collected in raffinate}}{\text{HOAc fed}} = \frac{\beta \cdot \left[\int_0^{t_s} C^{(N)}_{MeOAc,p}\Big|_{z=L_{col}} dt \right]}{\alpha \cdot C_{HOAc,F} \cdot t_s} \quad (6.2)$$

$$P_{MeOAc} = \frac{\text{MeOAc collected in raffinate}}{\left[\text{MeOAc} + \text{H}_2\text{O} + \text{HOAc}\right]\text{collected in raffinate}}$$

$$= \frac{\int_0^{t_s} C^{(N)}_{MeOAc,p}\Big|_{z=L_{col}} dt}{\int_0^{t_s} \left(C^{(N)}_{MeOAc,p} + C^{(N)}_{H_2O,p} + C^{(N)}_{HOAc,p} \right)\Big|_{z=L_{col}} dt} \quad (6.3)$$

$$V_{solid} = N \times \pi/4 \times (d_{col})^2 \times (1-\varepsilon) \quad (6.4)$$

6.4 Optimization of SMBR and Reactive Varicol Systems

The effects of switching time (t_s), number of columns (p, q, r and s) in sections P, Q, R and S respectively, and feed (α), product (β), solvent (γ) and reference (Q_P) flow rates were studied on the yield, selectivity, purity of MeOAc and conversion of the limiting reactant HOAc. From the sensitivity study (Table 5.2), it was found that some of the process parameters not only alter the yield, selectivity and purity of MeOAc profoundly, but also act in conflicting manner. For example, parameters, such as β and γ have conflicting influence on the yield and purity (or selectivity) of MeOAc. Furthermore, depending on t_s, the effects of α, β, γ and p are quite different. The influence of t_s is particularly complex. Its optimum value depend not only on the distribution of columns in sections P and S, but also on the value of α, β and γ. It is not possible to maximize yield and purity (selectivity) simultaneously. One must perform multi-objective optimization to determine optimal conditions and configuration of SMBR. It is also to be noted that optimum process design for SMBR is almost impossible (and time consuming) just by simulation due to a large number of parameters, which are interrelated but conflicting. A systematic optimization study not only provide optimum operating conditions for the desired objectives, but also will be helpful in understanding the roles of each parameter in the SMBR system.

The optimization problems of SMBR and Varicol process may be classified into two main categories, namely, the performance enhancement of an existing unit and the optimal design of a new plant. The process can be optimized for different objectives, which may include minimization of fixed cost (e.g., equipment such as total number of columns or volume of stationary phase) or operating cost (e.g., reactants or desorbent), and/or maximization of throughput (feed) or product quality (e.g., purity of product streams). However, cost data is site (and time) specific, and therefore, may not

always be a meaningful objective function. In SMBR, unlike SMB process for separation only, there is usually only one desired product, which is withdrawn either from the raffinate or the extract port. Therefore, in SMBR (as well as in Varicol), objectives usually include maximization of yield, purity or selectivity of the desired product and/or the conversion of the limiting reactant. One can also consider objective function such as maximization of throughput (capacity) or minimization of desorbent (eluent). It is possible to consider all these objective functions together, but it may be difficult to analyze the optimum solutions, as one has to consider multi-dimensional surfaces.

For the synthesis of MeOAc in SMB and Varicol, the decision variables can be classified as (a) *fixed cost parameters*: total number of columns (N_{col}), and length (L_{col}) and diameter (d_{col}) of each column; (b) *operating cost parameters*: temperature (T), eluent flow rate (γ), and maximum flow rate of the carrier (Q_p), which is related to the maximum pressure drop in the system; (c) throughput *parameters*: feed flow rate (α) and product flow rate at the raffinate port (β); and (d) *process parameters*: switching time (t_s), distribution of number of columns in sections P, Q, R and S (p, q, r, s) and in Varicol system, switching sequence.

In this chapter, we considered few two and three objective optimization problems associated to both existing and design stage. In all the considered optimization problems, decision variables were chosen in relatively narrow range in order to save computation time by narrowing down the search space. These was justified that the determined optimal decision variable values are neither hitting the upper nor the lower bounds.

6.5 Case1: Existing Set-up: Maximization of Purity and Yield of Methyl Acetate

In this section, the optimal operating parameters were determined using NSGA with respect to simultaneous maximization of purity and yield of methyl acetate ester for an existing set-up. Thereafter, experiments were performed at the obtained optimal operating conditions to verify the performance predicted by the optimization package. The first multi-objective optimization problem (Case 1) solved is described mathematically (see Table 6.1) as

$$\text{Maximize } I_1 = P_{MeOAc}(t_s, \gamma) \tag{6.5a}$$

$$\text{Maximize } I_2 = Y_{MeOAc}(t_s, \gamma) \tag{6.5b}$$

Subject to

$$P_{MeOAc} \geq 90\%;\ Y_{MeOAc} \geq 90\% \tag{6.6}$$

$$5\ (\text{min}) \leq t_s \leq 40\ (\text{min});\ 1 \leq \gamma \leq 4 \tag{6.7}$$

$$Q_p = 1\ \text{ml/min};\ \alpha = 0.2;\ \beta = 1;\ C_{HOAc}^{feed} = 2\ \text{mol/l} \tag{6.8a}$$

$$L = 25\ \text{cm};\ d_{col} = 0.94\text{cm};\ N_{col} = 4,\ p = q = r = s = 1 \tag{6.8b}$$

The choice of the two objective functions, I_1 and I_2, in Eqs. 6.5 enables the simultaneous maximization of yield and purity of the desired product, MeOAc. These two objective functions were chosen, as the primary goal of MeOAc synthesis in SMBR is to maximize yield and purity (or selectivity) of MeOAc. This model reaction is not severely equilibrium limited, as the equilibrium conversion of acetic acid in a non-separative reactor can reach as high as 98.5% at 318K when the feed concentration of HOAc is 2 mol/l and methanol is in large excess (see Table 3.3) and in SMBR, even higher conversion can be achieved if the operating conditions are set properly. Two

Table 6.1 Description of the multiobjective optimization problems solved together

With constraints, bounds of decision variables, and fixed parameters

Case	Objective function	Constraint	Decision variables	Fixed parameters
1 Existing	Max Y_{MeOAc} Max P_{MeOAc}	$Y_{MeOAc} \geq 90\%$ $P_{MeOAc} \geq 90\%$	$5 \leq t_s \leq 40$ min $1 \leq \gamma \leq 4$ [-]	$\alpha = 0.2$, $\beta = 1.0$, $Q_p = 1$ ml/min, T = 318 K $L_{col} = 25$ cm, $d_{col} = 0.94$ cm, $N_{col} = 4$, $C_{HOAc,f} = 2$ mol/l p = q = r = s = 1,
1a Existing Variable α	Max Y_{MeOAc} Max P_{MeOAc}	$Y_{MeOAc} \geq 90\%$ $P_{MeOAc} \geq 90\%$	$1 \times 10^{-5} \leq \alpha_1, \alpha_2, \alpha_3 \leq 0.5$ [-]	Same as case 1 except $\gamma = 3.79$, $t_s = 18$ min, $\alpha_4 = 4\,\alpha - (\alpha_1 + \alpha_2 + \alpha_3)$
2 Design Stage	Max P_{MeOAc} Min V_{solid}	$Y_{MeOAc} \geq 90\%$ $P_{MeOAc} \geq 90\%$	$1 \leq t_s \leq 40$ min $1 \leq \gamma \leq 2.5$ [-] $10 \leq L \leq 100$ cm	$\alpha = 0.1$, $\beta = 0.6$, $Q_p = 2$ ml/min, T = 318 K $d_{col} = 0.94$ cm, $N_{col} = 4$, p = q = r = s = 1,
3 Design Stage	Min γ Min V_{solid}	$Y_{MeOAc} \geq 80\%$ $P_{MeOAc} \geq 98\%$	$1 \leq t_s \leq 40$ min $0.8 \leq \gamma \leq 4$ [-] $10 \leq L \leq 150$ cm χ (see Table 6.4)	$\alpha = 0.1$, $\beta = 0.6$, $Q_p = 2$ ml/min, T = 318 K $d_{col} = 0.94$ cm, $C_{HOAc,f} = 2$ mol/l $N_{col} = 4$, 5 or 6
4	Max Y_{MeOAc} Max P_{MeOAc} Min γ	$Y_{MeOAc} \geq 80\%$ $P_{MeOAc} \geq 80\%$	$1 \leq t_s \leq 20$ min $0.1 \leq \beta \leq 0.9$ [-] 0.2 $1 \leq \gamma \leq 4$ [-] χ (see Table 6.4)	$\alpha = 0.1$, $Q_p = 2$ ml/min, T = 318 K, $C_{HOAc,f} = 2$ mol/l $N_{col} = 5$, $L_{col} = 10$ cm, $d_{col} = 0.94$ cm

decision variables were used for Case 1 optimization study. These are switching time (t_s) and the eluent flow rate (γ) since in sensitivity analysis it was found that these two parameters are most influential.

The Pareto optimal solutions in terms of maximizing purity and yield of MeOAc and the corresponding operating variables are shown in Figure 6.2. It was found that if purity of MeOAc is improved, yield of MeOAc is worsened and switching time plays the key role in determining the optimal solutions. This can be explained by comparing the concentration profiles of two different optimal points in the Pareto set as shown in Figure 6.3. It is obvious that when switching time increases, water will breakthrough from section P contaminating the raffinate stream, leading to lower purity of ester, but on the other hand, longer switching time seems to be beneficial for the performance of section S, which is responsible for desorbing MeOAc, so that most of the ester and un-reacted acid can be recycled to section P at the end of a switching period, resulting in higher yield. Likewise, when switching time decreases, water is retained in section P resulting in higher P_{MeOAc}. The decrease of switching time deteriorates the performance of section S, as more ester and un-reacted acid tend to be retained in Section S and they appear at the extract port instead of the raffinate port during the next switching period, since Section S becomes Section R after the switch. Therefore, lower Y_{MeOAc} is expected. Figure 6.2c reveals that the eluent flow rate has less significant effect on the performance of the process, as it is sufficiently large for the complete regeneration of the adsorbent.

Experiments were carried out at optimal operating conditions corresponding to five optimal points in the Pareto set shown in Figure 6.2. Table 6.2 compares the experimental results with that of the optimal solutions. It was found out that optimal predicted solution can be achieved experimentally except when optimal P_{MeOAc} is very

high (points 4 and 5). This is in agreement with our earlier study of the effect of switching time on the performance of SMBR. It was found that the experimental results deviate much from the model predictions when switching time is small. This is presumably due to the non-linear behavior (long tail) of the water (strongly adsorbed

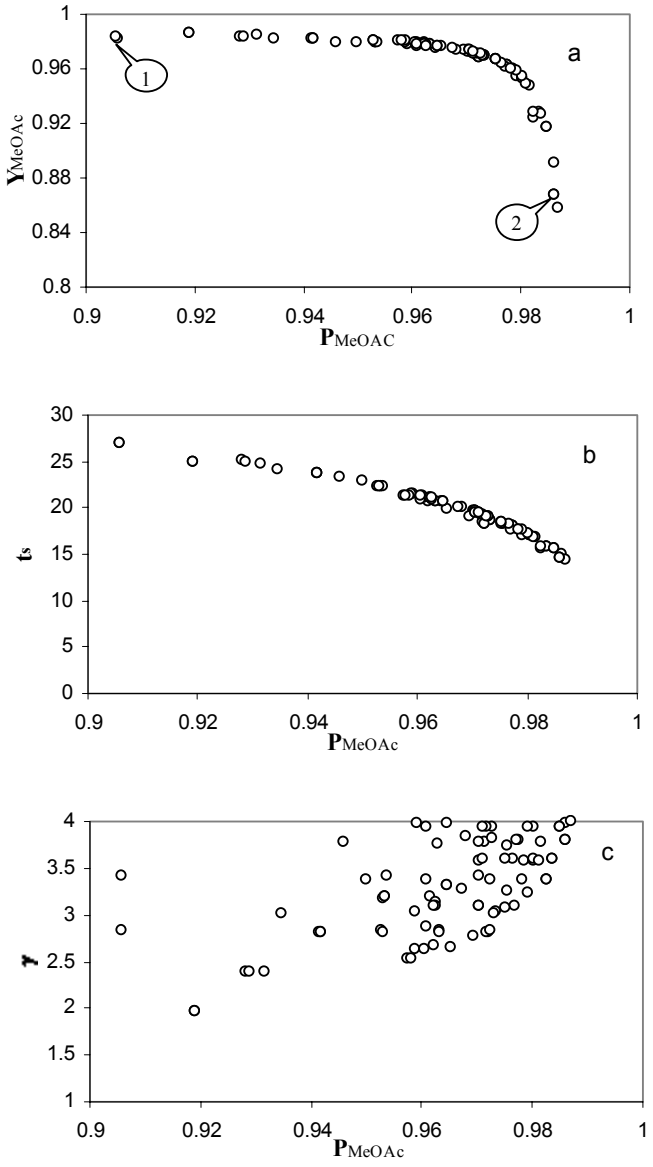

Figure 6.2 Optimal solutions and corresponding operating variables for maximization of purity and yield of MeOAc

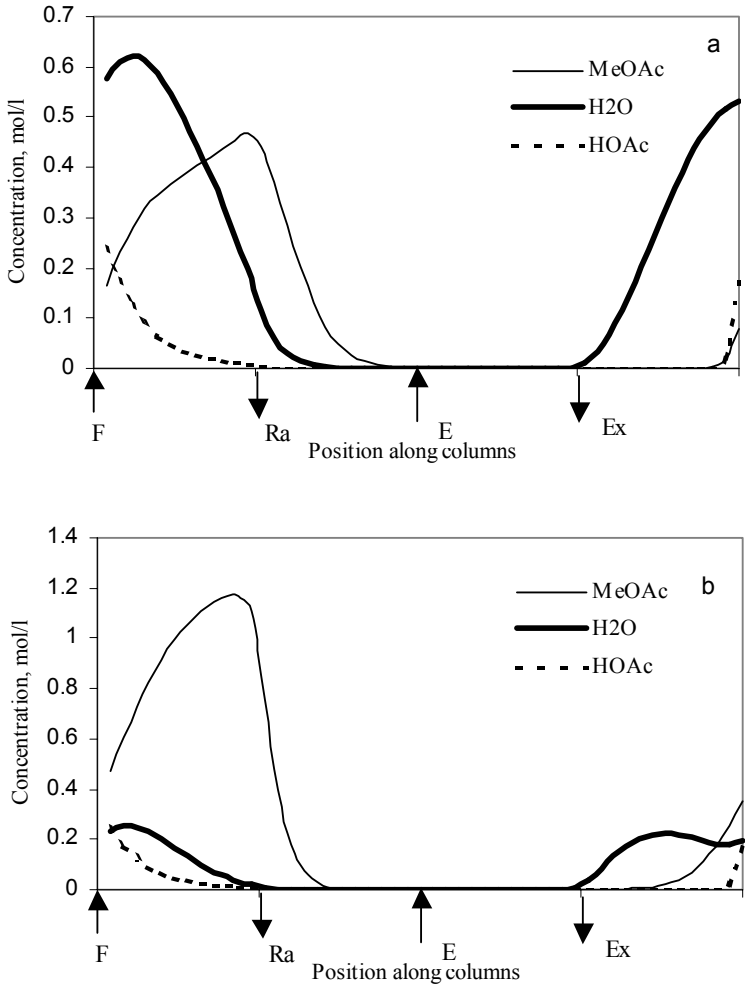

Figure 6.3 Concentration profiles of MeOAc-H_2O-HOAc at the end of 100 switching

a) Corresponding to point 1 in Figure 6.2
b) Corresponding to point 2 in Figure 6.2

component) concentration front towards the resin. At low switching time, there is not enough time for complete regeneration of the solid adsorbent. Hence, water breaks through at the product port in the next cycle thereby lowering the purity value obtained experimentally. This certainly can be improved if competitive non-linear adsorption is used in the model.

Table 6.2 Comparison of optimal predictions with experimental results

Experimental conditions: Q_p = 1 ml/min; α = 0.2; β = 1; C_{HOAc}^{feed} = 2 mol/l, L = 25 cm; d_{col} = 0.94 cm; N_{col} = 4, p = q = r = s = 1

Set No.	t_s [min]	γ [-]	Optimum solutions		Experimental results	
			P_{MeOAc} [%]	Y_{MeOAc} [%]	P_{MeOAc} [%]	Y_{MeOAc} [%]
1	25	2.98	92.1	98.2	93.0	98.3
2	21	3.13	96.5	97.6	95.9	98.2
3	18	3.79	97.7	96.3	97.1	96.7
4	15.5	3.43	98.1	93.1	94.6	95.2
5	14.5	3.79	98.6	86.8	93.5	90.4

6.5.1 Effect of Distributed Feed

One of the limitations of the SMB is that during much of the operation, the stationary phase in some of the columns are either completely free of solutes, or contains only product so that the separation capacity is significantly reduced. One way to improve SMB efficiency is to use non-synchronous switching like in Varicol, which is considered later. Alternative option that could improve the effective utilization of adsorbent phase would be to vary the feed flow rate during a global switching interval. In order to evaluate the efficacy of this approach, and to determine the extent to which the performance of SMBR could be improved by using variable feed flow rate, the

following optimization problem for the SMBR with four sub-feed interval was formulated and solved:

$$\text{Maximize } I_1 = P_{MeOAc}(\alpha_1, \alpha_2, \alpha_3) \tag{6.9a}$$

$$\text{Maximize } I_2 = Y_{MeOAc}(\alpha_1, \alpha_2, \alpha_3) \tag{6.9b}$$

Subject to

$$P_{MeOAc} \geq 90\%;\ Y_{MeOAc} \geq 90\% \tag{6.10}$$

$$1 \times 10^{-5} \leq \alpha_1, \alpha_2, \alpha_3 \leq 0.5 \tag{6.11a}$$

$$\alpha_4 = 4\alpha - (\alpha_1 + \alpha_2 + \alpha_3) \tag{6.11b}$$

$$Q_p = 1 \text{ ml/min};\ t_s = 18 \text{ min};\ \alpha = 0.2;\ \beta = 1;\ \gamma = 3.79;\ C_{HOAc}^{feed} = 2 \text{ mol/l} \tag{6.12a}$$

$$L = 25 \text{ cm};\ d_{col} = 0.94\text{cm};\ N_{col} = 4;\ p = q = r = s = 1. \tag{6.12b}$$

The operating conditions for the above problem is identical to the optimum solution obtained corresponding to set number 3 in Table 6.2 except that the feed flow rate was not kept constant at $\alpha = 0.2$ for the entire switching interval instead allowed to vary according to Eqs. 6.11a. Eqs. 6.11b is used to ensure that total feed flow rate is same as that of the constant feed flow case (set 3 in Table 6.2), and therefore, the optimum results can be compared.

Figure 6.4 compares the optimal solution, and it is evident from the figure that by varying the feed flow rate (although keeping the total feed flow rate constant), both of the purity and yield of MeOAc can be improved. Table 6.3 compares the objective function values and the corresponding optimal feed flow rates at the four sub-time

intervals for three optimal points with the reference point 4 (same as set 3 listed in Table 6.2) shown in Figure 6.4.

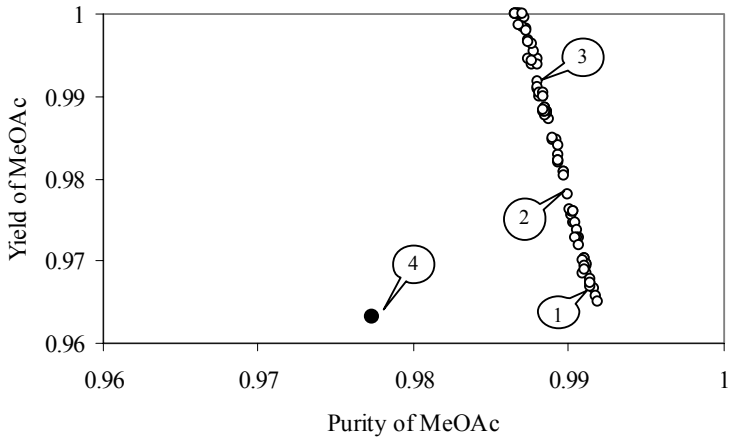

Figure 6.4 Comparison of optimal results for constant and variable feed flow rates

●: Constant feed flow rate ○: Variable feed flow rate

Table 6.3 Comparison of objective function values for constant and variable feed flow rate

Point in Figure 6. 4	P_{MeOAc} [%]	Y_{MeOAc} [%]	α_1	α_2	α_3	α_4
1	99.1	96.7	9.0×10^{-4}	0.198	0.397	0.204
2	99.0	98.1	6.0×10^{-5}	0.256	0.399	0.146
3	98.8	99.2	2.0×10^{-4}	0.338	0.400	0.0623
4	97.7	96.3	$\alpha = 0.2$			

It was observed that the distribution of the feed flow rate for all the optimal solutions represents a uniform cyclic (periodic) behavior. The feed flow rate (α_1) is extremely small during the first sub-interval, increases to a higher value for the second and the third time interval, and finally decreases to a lower value at the last time interval. The advantage of this particular cyclic behavior for the performance of SMBR can be illustrated by comparing the concentration profiles for constant (point 4) and variable (point 3) feed flow rate at the end of each of the four sub-time intervals as shown in Figure 6.5. The figure shows that the concentration front of water moves faster toward the raffinate port and tends to breakthrough form section P during the last time interval when the feed flow rate is constant. This gives rise to lower purity of ester (P_{MeOAc}) compared to variable feed flow. Likewise, the smaller feed flow rates in the first and last time interval help to improve the yield of ester (Y_{MeOAc}). Since Q_p is fixed, the flow rate in section S [$Q_s = (1-\alpha)Q_P$] increases as the feed flow rate (α_1 and α_4) decreases, the performance of section S becomes better, which leads to higher yield as discussed earlier. The forced periodic feed flow rate could improve the performance of SMBR for other operating conditions also and the extent improvement vary depending on the specific reaction system, column configuration, and numbers of sub-time intervals employed. It is noted that the strategy of varying feed flow rate is general to any system, however the cyclic behavior of the distribution of feed flow rate during each sub-feed interval may not be the same for different systems.

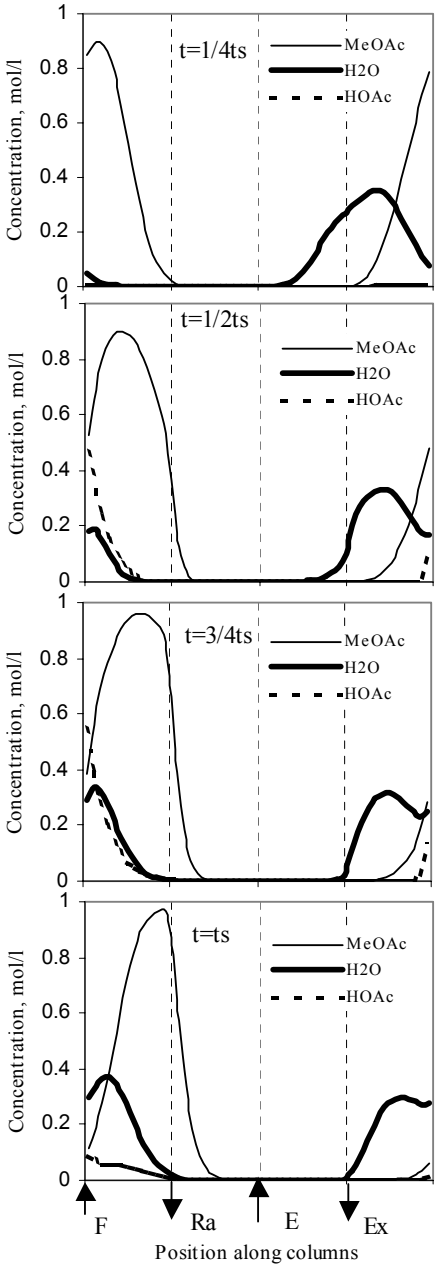

Fig. 6.5a

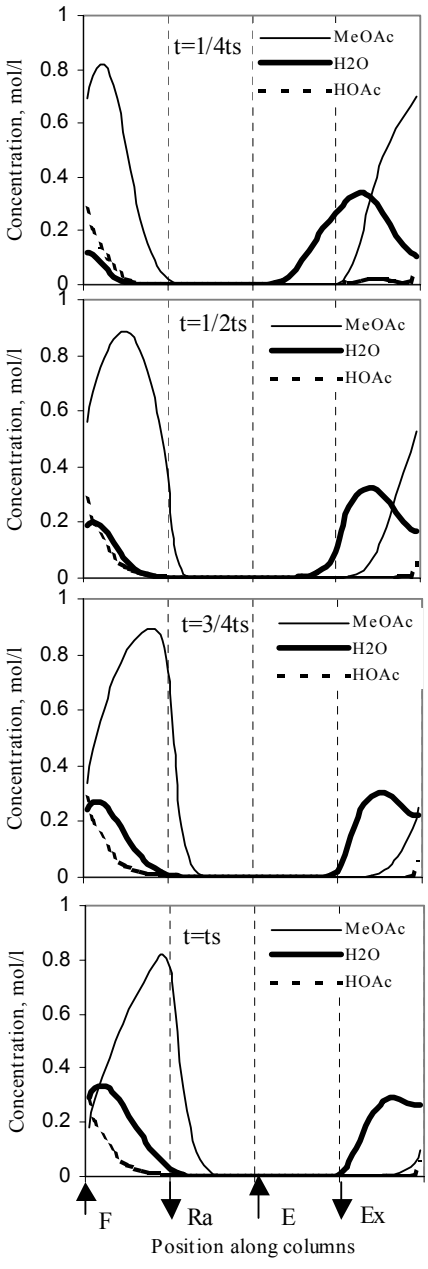

Fig. 6.5b

Figure 6.5 Concentration profiles for constant and variable feed at the end of each sub-time interval

a): Variable feed flow rate (point 3 in Figure 6.4)
b): Constant feed flow rate

6.6 Case 2: Design-stage Optimization: Maximization of Purity of MeOAc and Minimization of Volume of Solid

The performance of SMBR process was next optimized at design-stage to determine the optimal length of each column for a 4-cloumn SMB unit in order to minimize the total amount of adsorbent (V_{solid}) required while at the same time producing as high purity product as possible. The optimization problem solved in this case is described in Table 6.1, Case 2.

Figure 6.6a shows that to obtain higher P_{MeOAc} total adsorbent volume (V_{solid}) must be increased. To achieve very high purity, the length of each column (L_{col}) as well as switching time must be increased significantly.

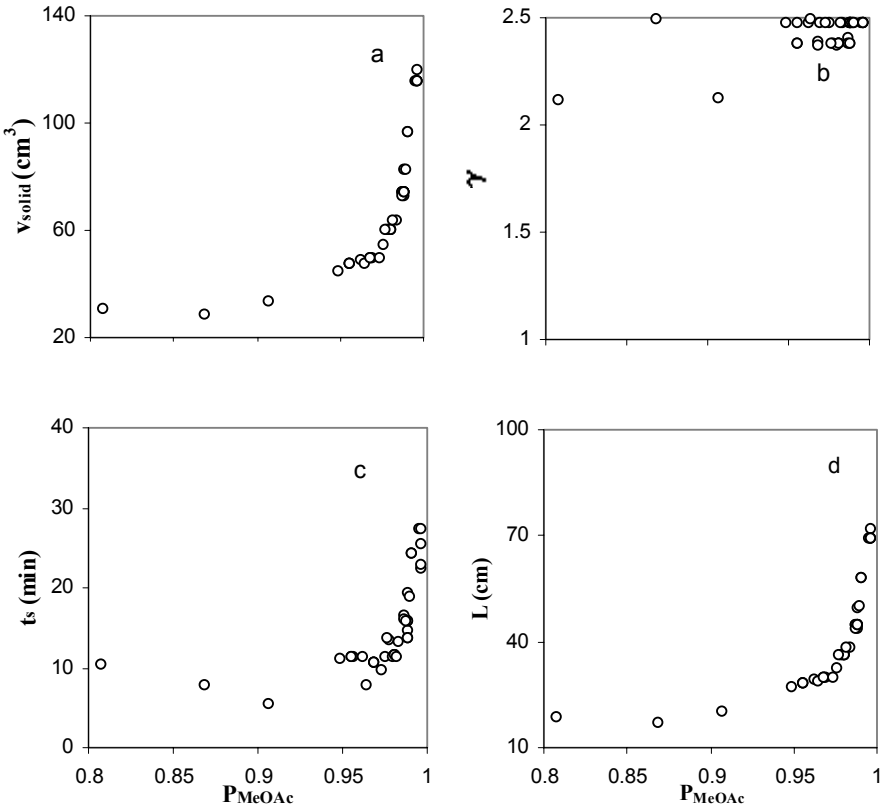

Figure 6.6 Pareto optimal solutions and corresponding values of decision variables for maximum P_{MeOAc} and V_{solid}

However, the improvement on product purity is insignificant when column length is sufficient long. From Figure 6.6b, it can be observed that eluent flow rate tends to reach upper bound, especially in the high purity region as complete regeneration of adsorbent in section R leads to high product purity. Figure 6.6c and 6.6d show that there exists an optimal switching time corresponding to any specific optimal length of each column.

6.6.1 Effect of Feed Flow Rate, α

The effect of feed flow rate (α) on the Pareto was investigated by comparing the optimal solutions for different values of α (α = 0.1, 0.4 and 0.6) keeping all other values fixed at the same value depicted for Case 2 in Table 6.1 (reference run). Figure 6.7a shows that more adsorbent is required to achieve the same purity level as α increases. With the flow rate in section P (Q_p) being kept constant, the increase of α leads to the decrease of the flow rate in section S [$Q_s = (1-\alpha)\ Q_p$], which deteriorates the performance of section S (lowers effective degree of separation) and results in lower Y_{MeOAc}. Section S is responsible for desorbing MeOAc so that it can be carried by the fluid phase to section P towards the raffinate port. When Q_s becomes smaller, MeOAc tends to be kept longer in section S, which becomes section R in the subsequent switch, and the remaining MeOAc will be elute at the extract port instead of the raffinate port. Therefore, t_s has to be increased to improve the performance of section S due to the constraint on yield. However, the increase of t_s is detrimental for section P, since water will breakthrough from section P and contaminate MeOAc in the raffinate stream. This leads to increase of column length to retain water in section P for the same purity requirement.

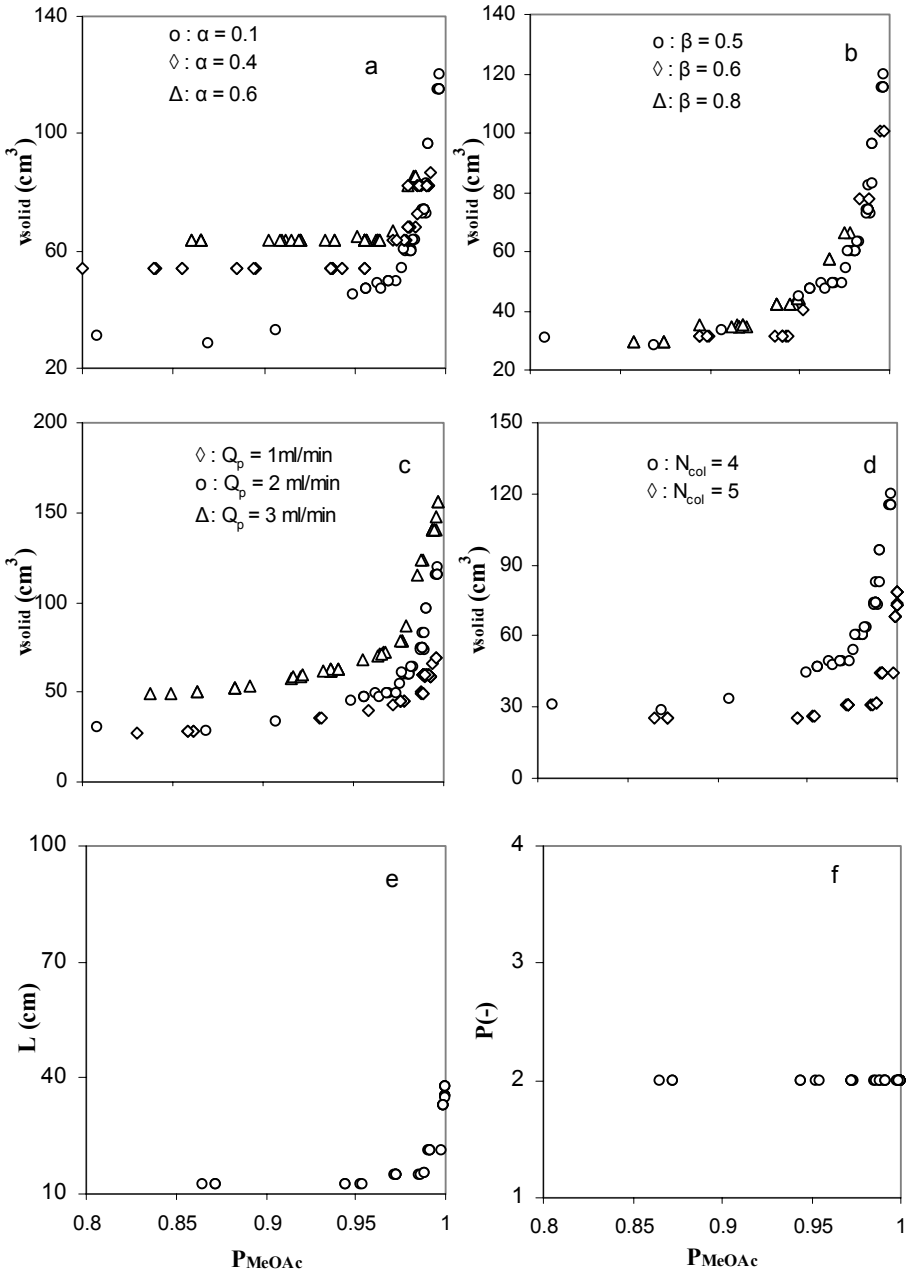

Figure 6.7 Effect of (a) α, (b) β, (c) Q_p and (d) N_{col} on the Pareto optimal solution

Figure 6.7e and 6.7f show optimum length and number of columns corresponding to Pareto solution for N_{col} = 5 in Figure 6.7d

6.6.2 Effect of Raffinate Flow Rate, β

Figure 6.7b compares Pareto optimal solution for different β when all other values are kept fixed at the reference value. The figure shows that the effect of β is less significant compared to α. When β increases, the flow rates in section Q [$Q_Q = (1-\beta) Q_p$] and in section R [$Q_R = (1-\beta+\gamma) Q_p$] both decrease. The decrease of Q_Q is favorable, since the role of section Q is to retain MeOAc. However, the decrease of Q_R will hinder in complete regeneration of column in section R. Hence, t_s has to be increased in order to improve the performance of section R, otherwise the remaining water in the adsorbent will eventually pollute the ester product at raffinate port. Likewise, as discussed in the effect of feed flow rate section, the length of column has to be increased to retain water in section P.

6.6.3 Effect of Flow Rate in Section P, Q_P

Figure 6.7c shows the effect of reference flow rate, Q_P. Amount of adsorbent requirement increases with the increase of Q_p for the same desired product purity. In this case, with the increase of Q_p, L_{col} has to be increased to provide sufficient residence time for reaction to proceed, otherwise the unconverted acetic acid will contaminate the purity of the ester at the raffinate port, particularly when conversion is low since acetic acid travels with the ester product due to their similar adsorption affinity toward the solid adsorbent.

6.6.4 Effect of Total Number of Columns, N_{col}

Figure 6.7d compares Pareto optimal solution when total number of columns (N_{col}) was increased to 5. It was found that the total adsorbent requirement for a 5-column unit is less than that of a 4-column unit for the same purity requirement. This is due to the fact that the optimum L_{col} to achieve the same product purity is small (see

Figure 6.7e compared to Figure 6.6d owing to more flexibility. Each section in SMB plays a specific role in achieving in-situ countercurrent separation of the reactants and products. Sections P and S are primarily responsible for reaction and separation while the functions of sections Q and R are to regenerate eluent and adsorbent respectively. Since in this case we intend to maximize purity, section P is most important, as reactive section will control the optimum length of column. Therefore, by placing the additional column in the reactive section, the total V_{solid} could be reduced. Figure 6.7f shows that the optimum column configuration is indeed 2/1/1/1.

6.7 Case 3: Design Stage Optimization: Minimization of Volume of Solid and Desorbent Consumption

Since adsorbent requirement and eluent consumption are usually the key factors to decide the capital and operating cost of a SMBR plant, it is worth considering a problem intended to obtain specified purity and yield of MeOAc with minimal eluent flow and adsorbent requirement. In this case, in addition to t_s, L_{col} and γ, column configuration (χ) is used as decision variable. The optimization formulation is described in Table 6.1, Case 3. In order to obtain a smooth Pareto within reasonable computation time, we intentionally increased the constraint for purity of MeOAc to a higher value, 98%.

The Pareto optimal solutions obtained for the SMBR as well as Varicol systems for different N_{col} are illustrated in Figure 6.8a. It can be observed that 6-column SMBR requires the least amount of adsorbent and eluent for the desired task of obtaining more than 98% purity and 80% yield of MeOAc. The 5-column Varicol was found to perform better than an equivalent 5-column SMBR in terms of demanding less amount of adsorbent at similar eluent flow rate or less eluent for same total V_{solid}. This is due to

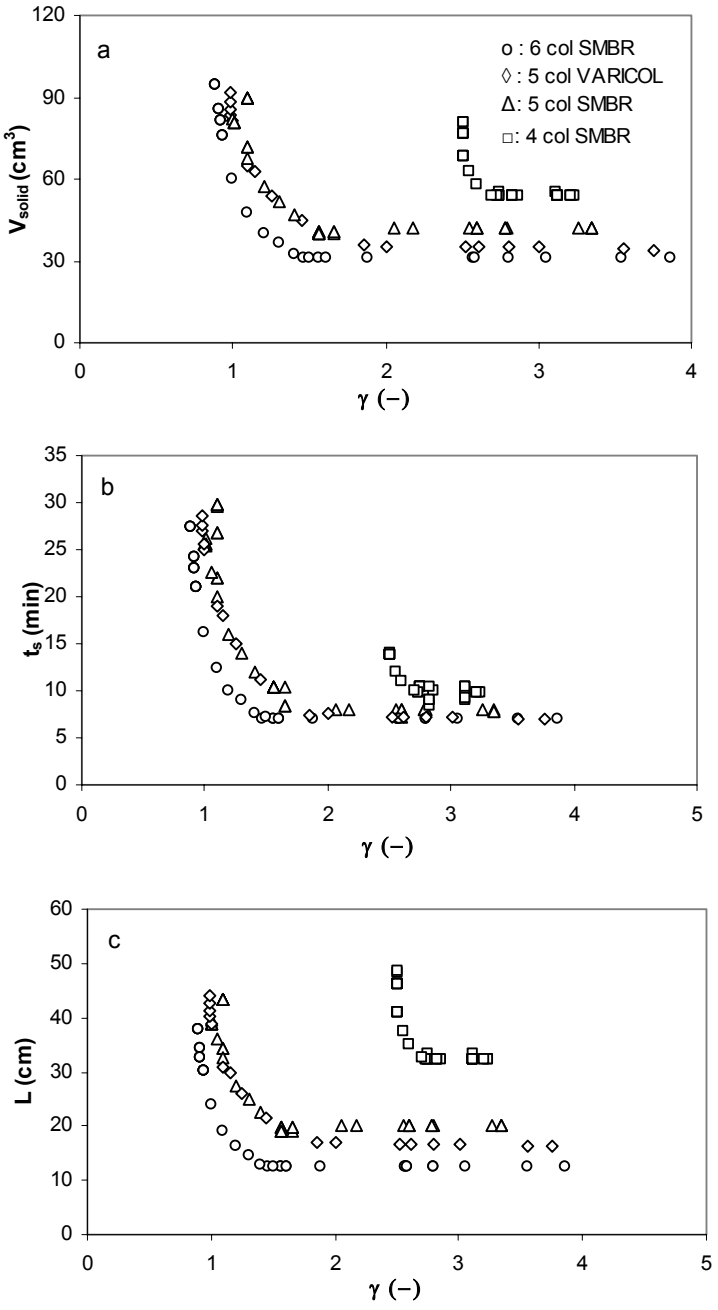

Figure 6.8 Optimal solutions for minimization of adsorbent volume and eluent consumption and corresponding decision variables

the increased flexibility in Varicol leading to better utilization of the stationary phase. For the same eluent consumption, the 6-column SMBR required less adsorbent volume as against the 4-, 5- column SMBR and Varicol. This is due to the fact that the minimum length of column required to achieve the same product purity can be reduced when introducing more columns into the reactive sections (P, S), and also because the increase of the number of columns in SMBR set-up leads to true moving bed behavior and hence the improvement in performance. Likewise, when adsorbent volume is the same, 6-column SMBR consumed less eluent compared to 4- or 5-column SMBR and Varicol. The optimum column configuration of 5- and 6- column SMBR is 2/1/1/1 and 3/1/1/1 respectively. The optimal column distribution for reactive Varicol was found to be χ = D-A-A-A (in Table 6.4). The corresponding switching time and column length are shown in Figure 6.8b and Figure 6.8c respectively.

Table 6.4 Possible column configurations (distribution) for N_{col} = 5 and 6

N_{col} = 5			
χ	Column configuration[#]	χ	Column configuration
A	2/1/1/1	C	1/1/2/1
B	1/2/1/1	D	1/1/1/2
N_{col} = 6			
χ	Column configuration	χ	Column configuration
A	1/1/2/2	F	2/2/1/1
B	1/2/1/2	G	3/1/1/1
C	1/2/2/1	H	1/3/1/1
D	2/1/1/2	I	1/1/3/1
E	2/1/2/1	J	1/1/1/3

Column distribution 2/1/1/1 implies 2 columns in section I and one column each in sections II to IV.

6.8 Case 4: Maximization of Purity and Yield of MeOAc and Minimization of Desorbent Consumption

So far we focused on optimizing two objective functions simultaneously. However, the operation of SMBR is considerably influenced by quite a number of operating parameters sometimes it is not sufficient if one tries to optimize only two objective functions concurrently. Hence, solving a triple optimization problem will be a better approach to provide further insight in the design and operation of reactive SMB and Varicol process. In this section, a typical triple optimization problem in terms of maximization of purity and yield of MeOAc together with the minimization of eluent consumption were considered for a 5-column reactive SMB and Varicol unit. The length of each column (L_{col}) was fixed as 10 cm based on the 5-column optimal solutions in Case 2. The problem is described in Table 6.1, Case 4.

For the convenience of analysis, the Pareto solutions are plotted in two dimensions. Figure 6.9a shows that Y_{MeOAc} decreases as P_{MeOAc} increases for both reactive SMB and Varicol systems and the performance of reactive Varicol is better than reactive SMB in terms of higher yield for the same purity requirement. From Figure 6.9b, it can be observed that the increase of P_{MeOAc} is at the cost of more eluent consumption for both reactive SMB and Varicol unit and the required eluent consumption is less in reactive Varicol than that in reactive SMB for the same desired purity requirement, especially in the high purity region. The optimal column distribution for reactive Varicol was also found to be χ = D-A-A-A compared to χ = A for reactive SMB system (see Table 6.4). The above column distribution refers to placement of additional column in section S in the first sub-interval followed by in section P for the rest of the switching period in the Varicol system. The better performance of reactive Varicol results in its flexibility in column distribution, leading

to better utilization of adsorbent. It is noted that NSGA is not perfect yet and it can only give near global optimal solutions. It takes much longer computation time to get smooth Pareto solutions by varying the operators in the algorithm. However, in most cases, the improvement is insignificant. A more powerful optimization package is needed in order to obtain a smooth Pareto within reasonable computation time.

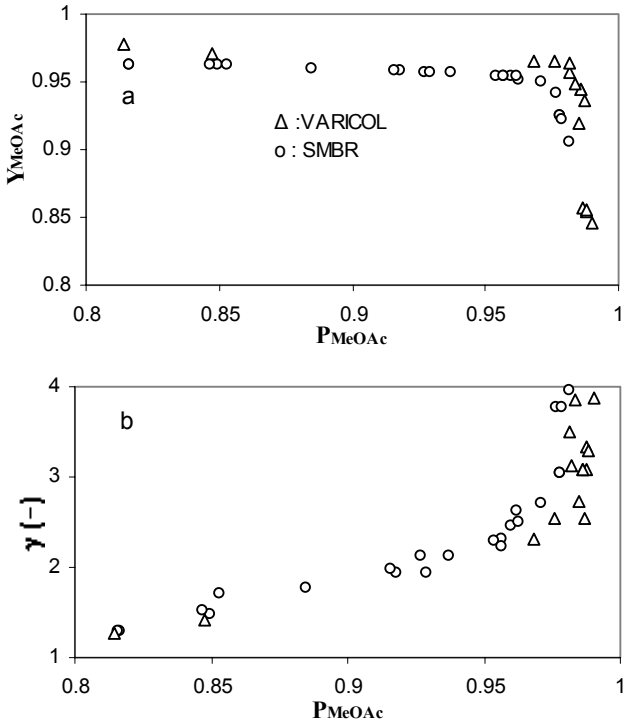

Figure 6.9 Comparison of Pareto optimal solution between SMBR and Varicol

6.9 Conclusions

The multi-objective optimization of reactive SMB and Varicol process for the synthesis of MeOAc were performed using NSGA. The optimal solutions in terms of maximization of purity and yield of MeOAc for the existing experimental setup were compare with the experimental results obtained by running the unit at the optimal operating conditions. The variation of feed flow rate during a global switching period on the performance of SMBR was investigated. It was found the both the purity and yield of MeOAc could be improved compare to the constant feed flow process. The effects of flow rates and total number of columns on the performance of reactive SMB were investigated. The applicability of Varicol to reaction systems is also evaluated by comparing the optimal results with that of SMBR. It was found that the performance of reactive Varicol could be better than that of reactive SMB due to the increased flexibility.

Chapter 7 Optimization of Reactive SMB & Varicol Processes for MeOAc Hydrolysis

7.1 Introduction

In order to obtain more valuable compound, large amount of by-product, methyl acetate (MeOAc), is usually hydrolysed to methanol (MeOH) and acetic acid (HOAc) in industrial polyvinyl alcohol plant, which are recycled to the methanolysis reaction of polyvinyl acetate and the synthesis of vinyl acetate respectively. However the conversion of MeOAc is low in the traditional process consisting of a packed bed reactor followed by a series of distillation columns for the separation of components, due to the equilibrium limitation (Fuchigami, 1990; Han et al., 1997).

Combination of chemical reaction and separation in a single apparatus could enhance the conversions of thermodynamic equilibrium-limited reactions and simultaneously obtain products of high purity. This is achieved by separating products when they are formed, which in turn shifts the equilibrium toward the desired products. The simulated moving bed reactor (SMBR) is such an integrated reactor-separator that could be employed to enhance the conversion of hydrolysis of MeOAc, leading to less energy cost and higher efficiency of the process.

The optimal design and operating parameters are essential to evaluate the economic potential of SMBR and reactive Varicol processes and to successfully implement them on industrial scale. In this Chapter, a comprehensive multi-objective optimization study of SMBR and reactive Varicol processes for the hydrolysis of MeOAc is reported. The Non-dominated Sorting Genetic Algorithm (NSGA) is applied to obtain Pareto optimal solutions. The multi-objective optimization problems are formulated aiming at a) simultaneous maximization of purity of both raffinate and

extract streams, b) maximization of yield of HOAc in raffinate stream and MeOH in extract stream. By performing multi-objective optimizations, we are able to deepen the understanding of the SMBR and reactive Varicol processes and meanwhile generate a wider range of alternative optimal operating conditions as the guidance for decision makers.

7.2 Mathematical model

In this application, water is present in large excess concentration. The polymer resin is initially saturated with water, and therefore, the quasi-homogeneous model can be applied to describe this reaction kinetics in this work. However, when the concentration of water decreases, the polymer phase deviates much from the ideal homogenous state, an adsorption-based heterogeneous model would be more suitable. As the reaction is carried out in a large excess of water in this study, the concentration of water can be assumed to remain essentially unchanged in the course of the reaction. Based on the above assumptions, the quasi-homogeneous kinetic models, applicable to this work can be written as

$$R = k_b \left[q_{MeOAc} - \frac{q_{HOAc} q_{MeOH}}{K_e} \right] \tag{7.1}$$

where R denotes the reaction rate, q_i is the concentration of component i (MeOAc, MeOH, or HOAc) in the solid phase, k_b is the reaction rate constant, and K_e represents the reaction equilibrium constant.

The concentration of adsorbed species i in the solid phase is computed by assuming that the local liquid and solid phases are in equilibrium and liner adsorption isotherm is applicable. So it is expressed as

$$q_i = K_i C_i \tag{7.2}$$

where K_i and C_i are the adsorption equilibrium constant and liquid phase concentration of component i respectively. It should be noted that the liner isotherm is only valid when the concentration of the adsorbed components are dilute in the bulk liquid phase, as is the case in this study. When the concentrations of the reactants and products are not sufficiently low, non-liner adsorption models, such as Langmuir model, should be considered in order to describe adsorption process accurately.

Based on the proposed reaction kinetics and adsorption isotherm, the dynamic models for SMBR unit and reactive Varicol are the same as that described in Chapter 6, except that the kinetic equation is written as:

$$R_j^{(N)} = k_b \left[q_{MeOAc,j}{}^{(N)} - \frac{q_{HOAc,j}{}^{(N)} \cdot q_{MeOH,j}{}^{(N)}}{K_e} \right] \tag{7.3}$$

A set of objective functions examined in this Chapter are defined as follows:

$$X_{MeOAc} = \frac{\text{(MeOAc fed – MeOAc collected in Raffinate and Extract)}}{\text{MeOAc fed}}$$

$$= \frac{\alpha \cdot C_{MeOAc,f} \cdot t_s - \left[\beta \cdot \int_0^{t_s} C_{MeOAc,p}^{(N)} \Big|_{z=L_{col}} dt + (\alpha + \gamma - \beta) \int_0^{t_s} C_{MeOAc,p+q+r}^{(N)} \Big|_{z=L_{col}} dt \right]}{\alpha \cdot C_{MeOAc,f} \cdot t_s} \tag{7.4}$$

$$Y_{MeOH} = \frac{\text{MeOH collected in Extract}}{\text{MeOAc fed}} = \frac{\beta \cdot \left[\int_0^{t_s} C_{MeOH,p+q+r}^{(N)} \Big|_{z=L_{col}} dt \right]}{\alpha \cdot C_{MeOAc,f} \cdot t_s} \tag{7.5}$$

$$Y_{HOAc} = \frac{\text{HOAc collected in Raffinate}}{\text{MeOAc fed}} = \frac{(\alpha + \gamma - \beta) \cdot \left[\int_0^{t_s} C_{HOAc,p}^{(N)} \Big|_{z=L_{col}} dt \right]}{\alpha \cdot C_{MeOAc,f} \cdot t_s} \tag{7.6}$$

$$P_{MeOH} = \frac{\text{MeOH collected in Extract}}{[\text{MeOH} + \text{MeOAc} + \text{HOAc}]\text{collected}} = \frac{\int_0^{t_s} C_{MeOH,p+q+r}^{(N)} \Big|_{z=L_{col}} dt}{\int_0^{t_s} \left(C_{MeOH,p+q+r}^{(N)} + C_{MeOAc,p+q+r}^{(N)} + C_{HOAc,p+q+r}^{(N)} \right) \Big|_{z=L_{col}} dt} \tag{7.7}$$

$$P_{HOAc} = \frac{\text{HOAc collected in Raffinate}}{[\text{MeOH} + \text{MeOAc} + \text{HOAc}]\text{collected}} = \frac{\int_0^{t_s} C_{HOAc,p}^{(N)} \Big|_{z=L_{col}} dt}{\int_0^{t_s} \left(C_{MeOH,p}^{(N)} + C_{MeOAc,p}^{(N)} + C_{HOAc,p}^{(N)} \right) \Big|_{z=L_{col}} dt} \tag{7.8}$$

7.3 Sensitivity Study

Before formulating optimization problems, it would be desirable to conduct a comprehensive parametric sensitivity study in order to acquire a thorough understanding of the SMBR system. Sensitivity analysis was carried out by changing only one process parameter at a time while fixing the other operating parameters at a reference set of values. Effects of switching time (t_s), flow rates of feed (α), raffinate (β), desorbent (γ), and number of columns (p, q, r and s) in sections P, Q, R and S respectively on the several performance criteria, X_{MeOAc}, Y_{MeOH}, Y_{HOAc}, P_{MeOH} and P_{HOAc}, as defined in Eqs. 7.4-7.8 are shown in Table 7.1. The parameters on the first row of Table 7.1 denote x-axis variable for the respective column and the effect of each parameter on X_{MeOAc}, Y_{MeOH}, Y_{HOAc}, P_{MeOH} and P_{HOAc} is shown for reference values of other parameters in the five subsequent rows.

It can be seen from Table 7.1 that q and r, which represents numbers of columns in section Q and R, respectively, have little effect on the performance of the process, when each of them is varied between 1 to 5. However other parameters influence the Y_{HOAc}, P_{HOAc}, Y_{MeOH} and P_{MeOH} in conflicting ways. Table 7.1 shows that there is a complex interplay of all these parameters on X_{MeOAc}, Y_{MeOH}, Y_{HOAc}, P_{MeOH} and P_{HOAc}. If we want to maximize one, the other one worsens. Optimum SMBR configuration (number and length of columns), and operating conditions (such as t_s, β, γ, etc.) differ depending on which variable we want to maximize among X_{MeOAc}, Y_{MeOH}, Y_{HOAc}, P_{MeOH} and P_{HOAc}, and it may not be possible to maximize all at the same time. Therefore, multi-objective optimization is essential for improving the performance of SMBR.

7.4 Optimization of SMBR and Varicol

7.4.1 Case1: Maximization of Purity of Both Raffinate and Extract Streams

In industrial polyvinyl alcohol plant, both of the products (MeOH and HOAc) from the hydrolysis of MeOAc are desirable, since they can be recycled to the methanolysis reaction of polyvinyl acetate and the synthesis of vinyl acetate respectively. Therefore, it is meaningful to formulate the optimization problem aiming at simultaneous maximization of purity of P_{HOAc} in raffinate stream and P_{MeOH} in extract stream. In addition, since the cost of the adsorbent is always one of the key factors in evaluating the economic potential of SMBR plants, the performance of SMBR is therefore first optimized at the design stage to determine the optimal length of column for a 7-column SMBR unit in order to maximize P_{HOAc} in raffinate stream while at the same time producing as high purity of MeOH in extract as possible. This type of optimization problem can be described mathematically as follow:

Maximize	$J_1 = P_{HOAc}\,(t_s, L, \beta, \gamma, q, r, s)$	(7.9a)
Maximize	$J_2 = P_{MeOH}\,(t_s, L, \beta, \gamma, q, r, s)$	(7.9b)
Subject to	$X_{MeOAc} \geq 90\%$	(7.10a)
	$P_{MeOH} \geq 80\%$	(7.10b)
	$P_{HOAc} \geq 80\%$	(7.10c)
Decision variables	$30 \leq t_s \leq 60$ min; $3 \leq \gamma \leq 5$; $0.1 \leq \beta \leq 0.9$; $20 \leq L \leq 100$ cm	
	$1 \leq s \leq 3$; $1 \leq q \leq 2$; $1 \leq r \leq 2$	(7.11)
Fixed parameters	$d_{col} = 0.94$ cm, $N_{col} = 7$	(7.12a)
	$Q_p = 1$ ml/min, $\alpha = 0.1$	(7.12b)
	$C_{HOAc}^{feed} = 1$ mol/l, T = 318 K	(7.12c)

Table 7.1 Sensitivities of process parameters for the hydrolysis of MeOAc

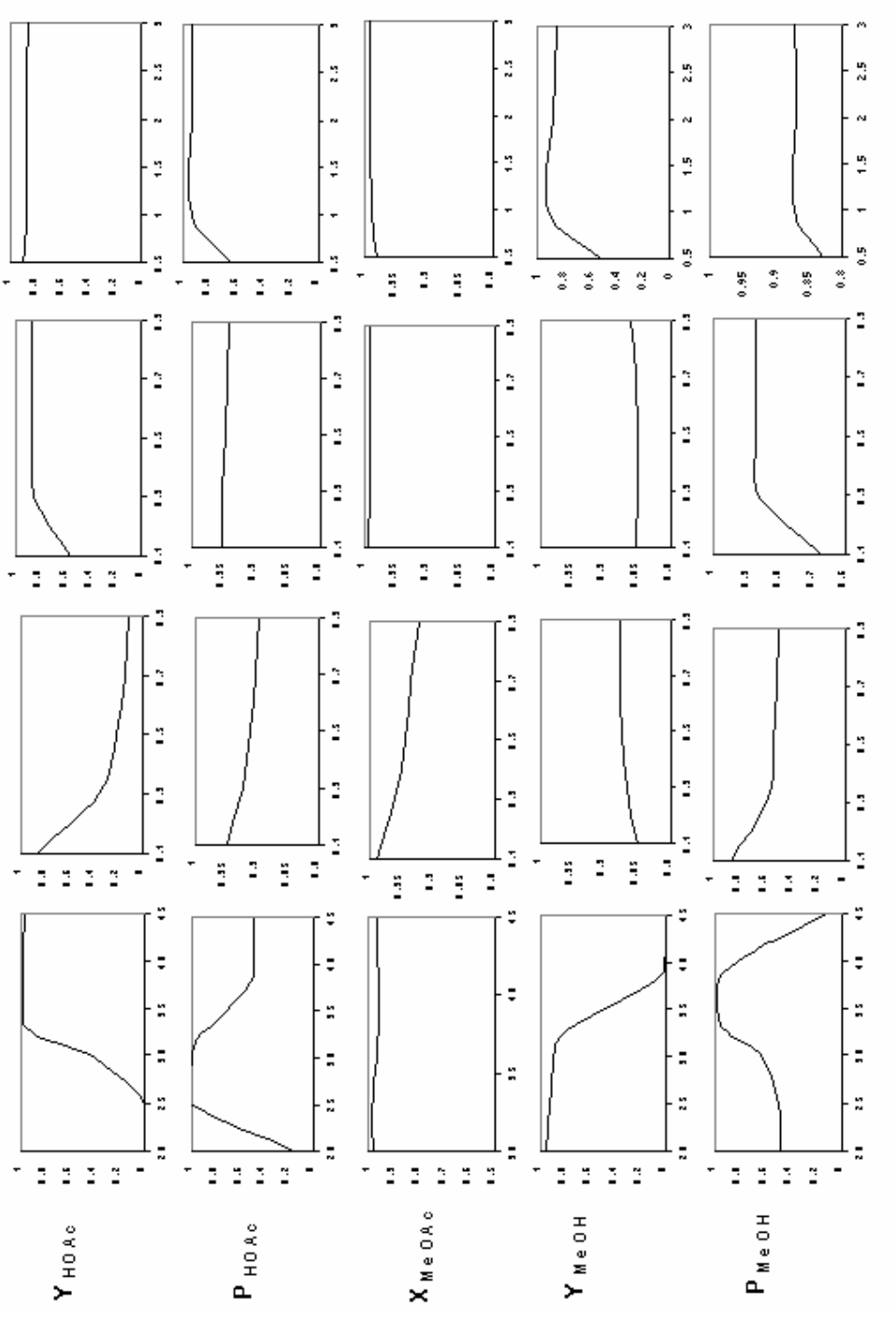

Reference: p=2,q=1,r=1,s=2, Q_P = 1 ml/min, L = 25 cm, ε = 0.4, $C_{HOAc,F}$ = 1 mol/l, α = 0.1, β = 0.5, γ = 3

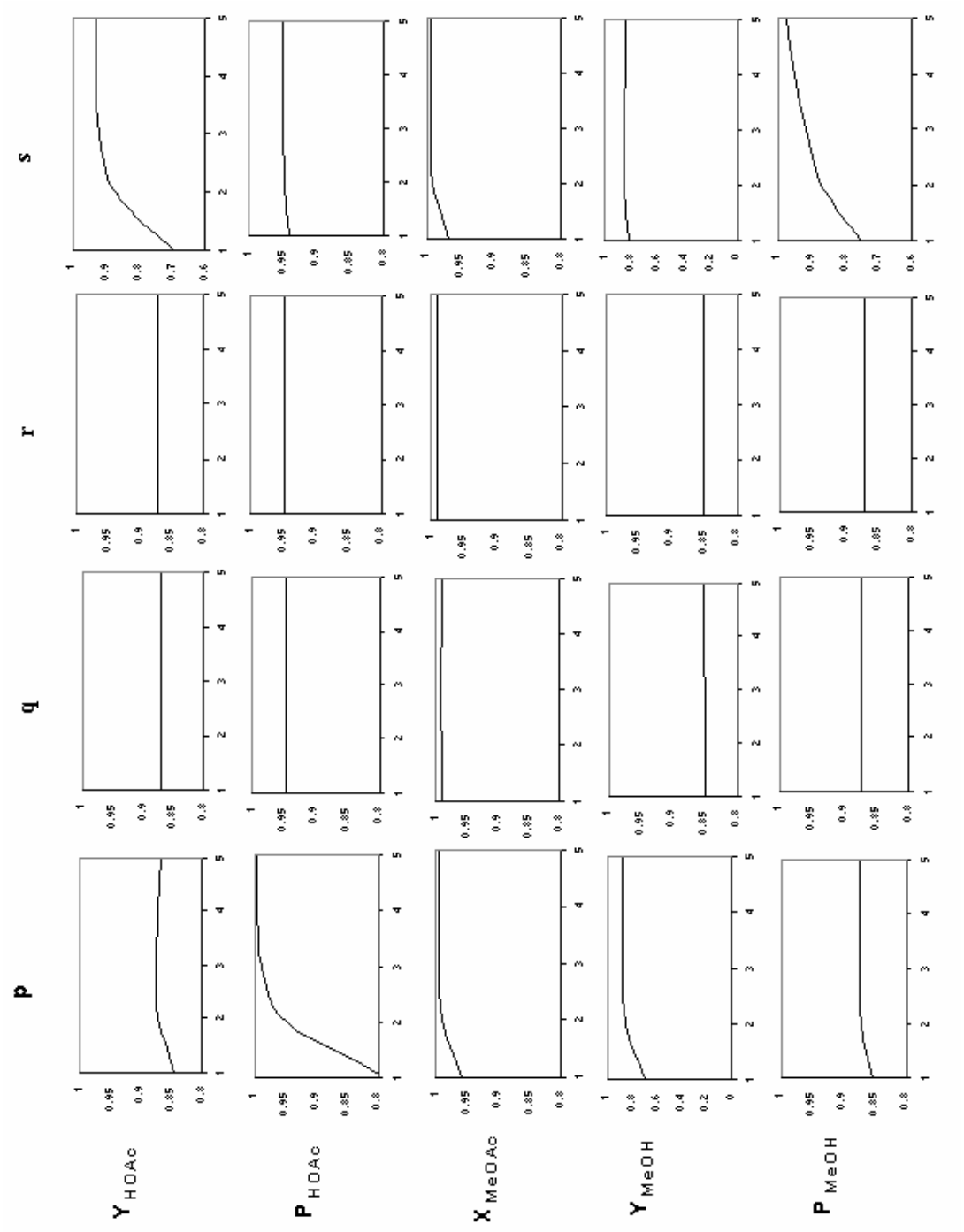
p
q
r
s
Y_{HOAc}
P_{HOAc}
X_{MeOAc}
Y_{MeOH}
P_{MeOH}

Table 7.2 Description of the multiobjective optimization problems solved together with constraints, bounds of decision variables, and fixed parameters

Case	Objective	Constraint	Decision variables	Fixed parameters
1	Max P_{HOAc} Max P_{MeOH}	$X_{MeOAc} \geq 90\%$ $P_{HOAc} \geq 80\%$ $P_{MeOH} \geq 80\%$	$30 \leq t_s \leq 60$ min, $3 \leq \gamma \leq 5$ [-] $0.1 \leq \beta \leq 0.9$ [-], $20 \leq L \leq 100$ cm $1 \leq s \leq 3$, $1 \leq q \leq 2$, $1 \leq r \leq 2$	$d_{col} = 0.94$ cm, $N_{col} = 7$ $Q_P = 1$ ml/min, $\alpha = 0.1$ $C_{HOAc}^{feed} = 1$ mol/l, T = 318 K
1a			$10 \leq t_s \leq 60$ min, $3 \leq \gamma \leq 5$ [-] $0.1 \leq \beta \leq 0.9$ [-], $1 \leq s \leq 3$	Same as case 1 except L = 20, 30, 50 cm q =1, r = 1
1b			$10 \leq t_s \leq 30$ min, $3 \leq \gamma \leq 5$ [-]	Same as case 1 except L =30 cm, p=2, q=1, r=1, s =3 $\beta = 0.4, 0.6, 0.8$ [-]
1c			$10 \leq t_s \leq 30$ min	Same as case 1b except $\beta = 0.8$ [-], $\gamma = 1.0, 1.5, 2.0, 3.0$ [-]

1d	Max P_{HOAc} Max P_{MeOH}	$X_{MeOAc} \geq 90\%$ $P_{HOAc} \geq 80\%$ $P_{MeOH} \geq 80\%$	$1 \times 10^{-4} \leq \alpha_1$, α_2, $\alpha_3 \leq 0.3$ [-]	Same as Case 1 except Point 1: $\beta = 0.44$ [-], $\gamma = 3.15$ [-], $t_s = 19.5$ min Point 2: $\beta = 0.75$ [-], $\gamma = 4.25$ [-], $t_s = 19.8$ min p = 3, s =2 Point 3: $\beta = 0.69$ [-], $\gamma = 3.40$ [-], $t_s = 19.5$ min p =2, s =3 $\alpha_4 = 4\,\alpha - (\alpha_1 + \alpha_2 + \alpha_3)$, L = 30 cm, q =1, r =1
1e			$10 \leq t_s \leq 30$ min $3 \leq \gamma \leq 5$ [-], $0.1 \leq \beta \leq 0.9$ [-] $1 \leq s \leq 4$ (for 8-column SMBR) χ (see Table 7.4, for Varicol)	Same as Case 1 except L=30 cm, N_{col} =6, 7, 8 q = 1, r =1
1f			$10 \leq t_s \leq 30$ min $3 \leq \gamma \leq 5$ [-], $0.1 \leq \beta \leq 0.9$ [-] χ (see Table 7.4)	Same as Case 1 except L =30 cm, $N_{subinterval}$ = 3, 4, 5
2	Max Y_{HOAc} Max Y_{MeOH}	$X_{MeOAC} \geq 90\%$ $P_{HOAc} \geq 80\%$ $P_{MeOH} \geq 80\%$	$10 \leq t_s \leq 30$ min $1.0 \leq \gamma \leq 3.0$, $0.1 \leq \beta \leq 0.9$, $1 \leq s \leq 3$, $1 \leq q \leq 2$, $1 \leq r \leq 2$	Same as Case 1 except L=30 cm
2a			$10 \leq t_s \leq 30$ min $1.0 \leq \gamma \leq 3.0$, $0.1 \leq \beta \leq 0.9$, χ (see Table 7.4)	Same as Case 2

The Pareto optimal solutions with respect to maximization of purity of both raffinate and extract streams and corresponding decision variables are illustrated in Figure 7.1. From Figure 7.1a, it can be observed that P_{HOAc} in raffinate stream increases at the cost of decreasing P_{MeOH} in extract stream, which is in agreement with the result obtained from the sensitivity study. It can be seen from Figure 7.1d and Figure 7.1e that eluent and raffinate flow rates are scattered, indicating that they are not important variables in deciding the Pareto solutions, as long as they are sufficiently large for the regeneration of adsorbent in section R and retention of HOAc in section Q respectively. This is validated later by investigating the effects of raffinate and eluent flow rates on the shift of Pareto solutions. Figure 7.1b shows that when switching time is slightly increased, P_{MeOH} in extrect stream increases, and it is also evident from Figure 7.1f that more columns are needed in section S in order to improve the purity of MeOH in extract stream.

Figure 7.2 compares the cyclic steady state concentration profiles for two points in the Pareto set indicated in Figure 7.1a, it is evident from this figure that the concentration fronts of HOAc and MeOH in section S are better separated as more columns are present in section S and with slightly greater switching time, leading to higher purity of MeOH in extract stream. The optimal number of columns in section Q and R are both equal to 1, which is expected since section P and S are the main sections for complete conversion and separation while section Q and R are mainly responsible for regeneration of solvent and adsorbent respectively. The optimal length of column was found to be about 87 cm.

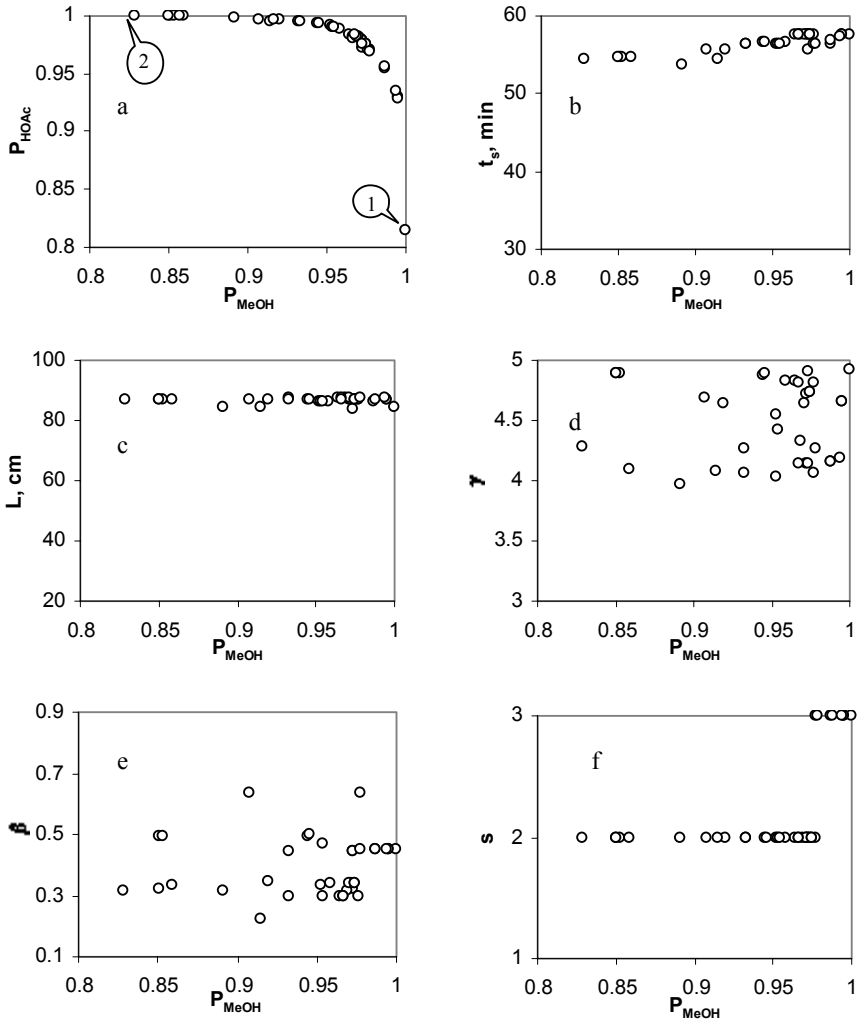

Figure 7.1 Optimal solutions and corresponding decision variables for maximization of P_{HOAc} in raffinate and P_{MeOH} in extract

7.4.1.1 Effect of the Column Length, L_{col}

The effect of column length on the Pareto optimal solutions was studied. The optimization problem was formulated by fixing the length of column as 20, 30 and 50 cm. The formulation of the optimization problem is given in Table 7.2 (Case 1a). Figure 7.3 shows that the performance of 7-column SMBR unit is satisfying when each of the columns is 30 cm long, as both of the purity of raffinate and extract streams can reach 90%. Therefore, in all the following cases, the column length is fixed as 30 cm.

7.4.1.2 Effect of Raffinate Flow Rate, β

In Case 1, it was observed that raffinate flow rate is relatively insensitive in deciding the optimal solutions. In this section, the Pareto solutions are determined for three different values of raffinate flow rates. The optimization formulation is provided in Table 7.2 (Case 1b). It is shown by Figure 7.4 that there is no significant shift of Paretos when the raffinate flow rate is reduced from 0.8 to 0.4. This is in agreement with the results obtained in Case 1.

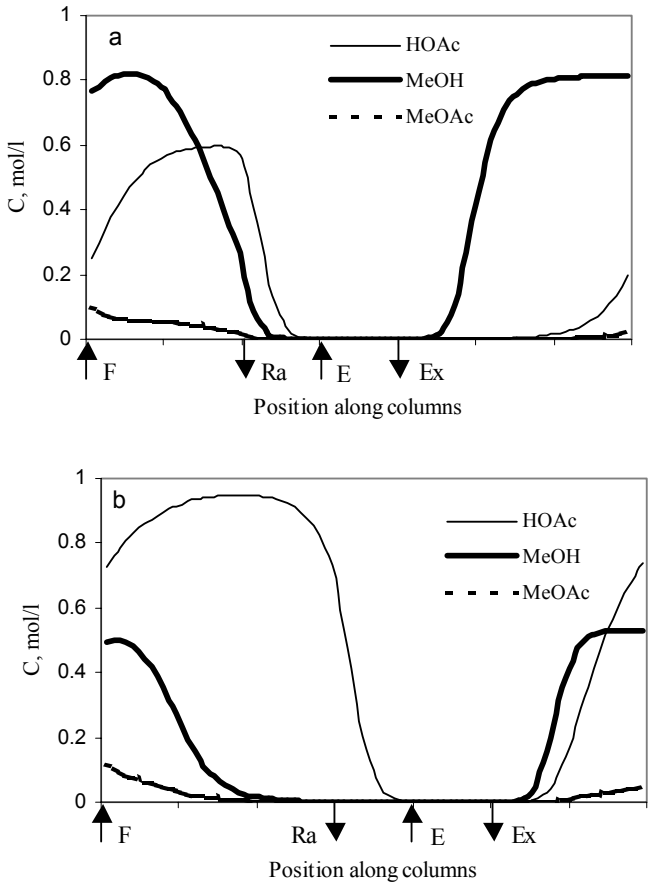

Figure 7.2 Concentration profiles of MeOAc-HOAc-MeOH at the end of 100 switching

a) Corresponding to point 1 in Figure 7.1a

b) Corresponding to point 2 in Figure 7.1a

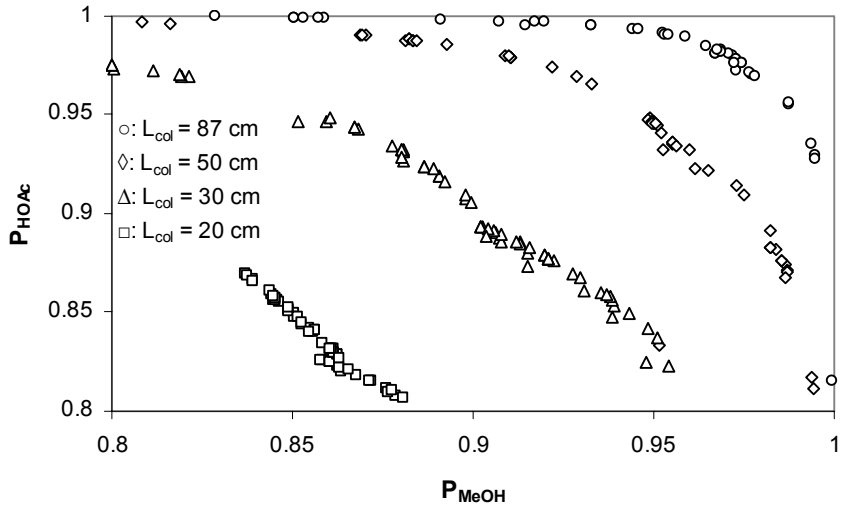

Figure 7.3 Comparison of Pareto solutions for different length of column

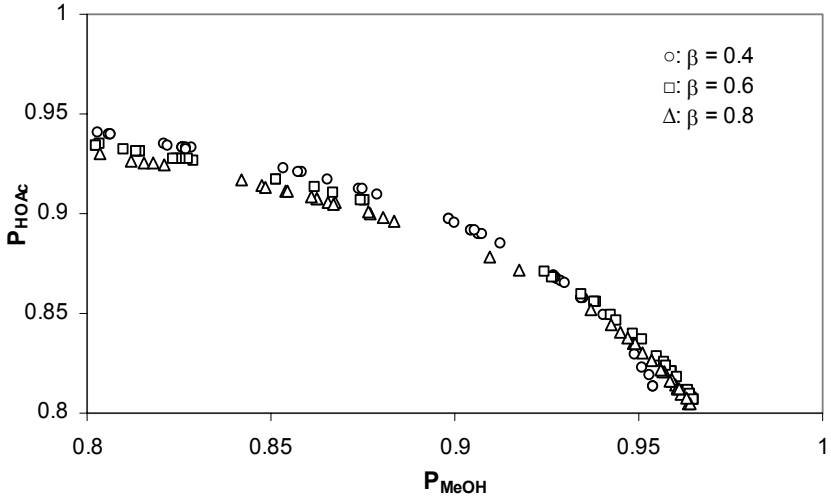

Figure 7.4 Effect of raffinate flow rate on the optimal solutions

7.4.1.3 Effect of Eluent Flow Rate, γ

The effect of eluent flow rate on the performance of SMBR is also investigated. The optimization formulation is described in Table 7.2 (Case 1c). Figure 7.5 compares the optimal solutions in terms of maximization of purity of both raffinate and extract streams for four different eluent flow rates. When the eluent flow rate is increased from 1.0 to 1.5, a 6.5% improvement in the purity of HOAc in raffiante stream is obtained for a given P_{MeOH} of about 90%. However, there is no significant improvement when the eluent flow rate is increased further from 1.5 to 2 and 3. This can be explained by comparing the cyclic steady state concentration profiles for eluent flow rate as 1.0, 1.5 and 3 as shown in Figure 7.6. It is observed that the solid adsorbent is not completely regenerated when the eluent flow rate is 1.0 and the remaining MeOH will later contaminate the purity of raffinate stream. When eluent flow rate is increased to 1.5, the complete regeneration of adsorbent is achieved in section R, leading to improvement in the purity of HOAc in raffinate stream.

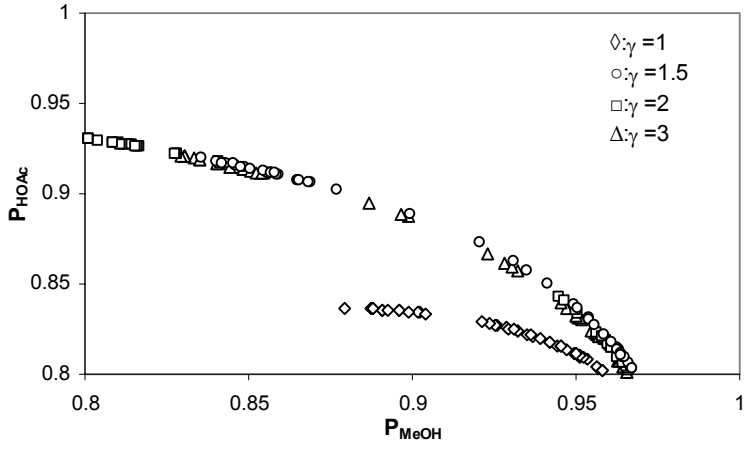

Figure 7.5 Effect of desorbent flow rate on the optimal solutions

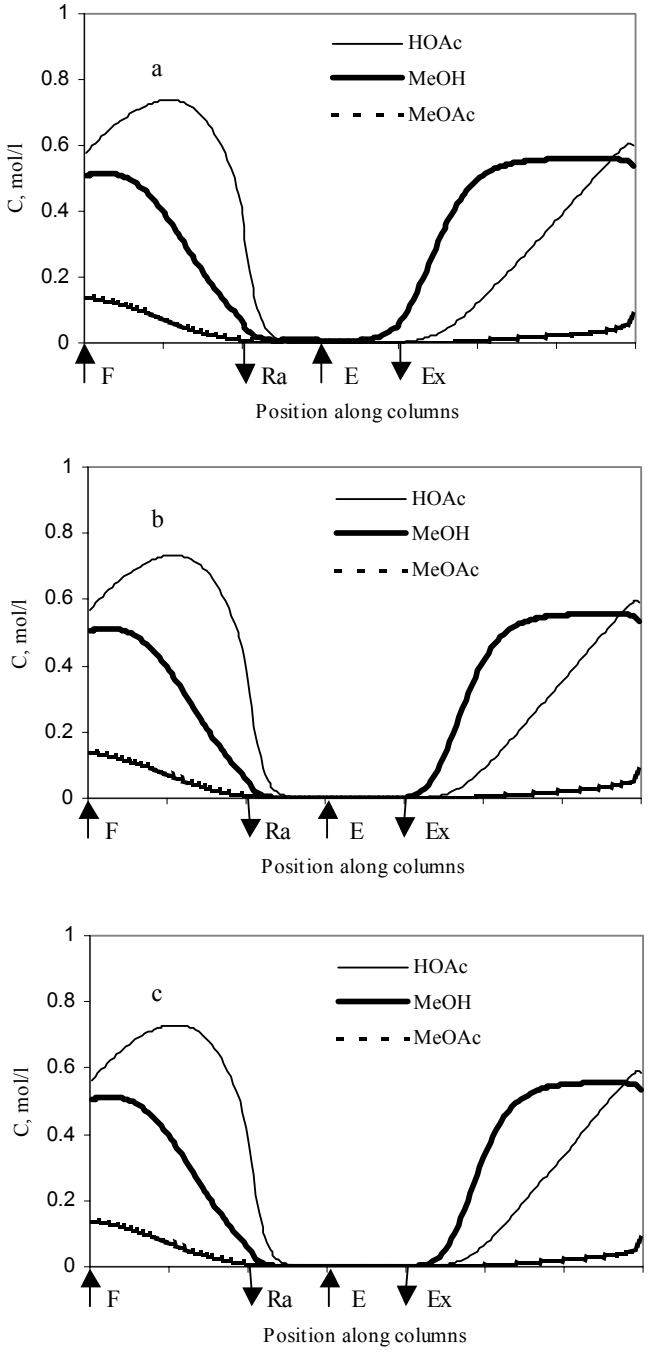

Figure 7.6 Concentration profiles of MeOAc-HOAc-MeOH at the end of 100 switching

a) $\gamma = 1.0$; b) $\gamma = 1.5$; c) $\gamma = 3.0$

7.4.1.4 Effect of Distributed Feed Flow

One of the limitations of the SMB is that during much of the operation, the stationary phase in some of the columns are either completely free of solutes, or contains only product so that the separation capacity is significantly reduced. One way to improve SMB efficiency is to use non-synchronous switching like in Varicol, which is considered later. Alternative option that could improve the effective utilization of adsorbent phase would be to vary the feed flow rate during a global switching interval. In order to evaluate the efficacy of this approach, and to determine the extent to which the performance of SMBR could be improved by using variable feed flow rate, the following optimization problem for the SMBR with four sub-feed interval is formulated and solved:

Maximize $$I_1 = P_{HOAc}(\alpha_1, \alpha_2, \alpha_3) \quad (7.13a)$$

Maximize $$I_2 = P_{MeOH}(\alpha_1, \alpha_2, \alpha_3) \quad (7.13b)$$

Subject to $$X_{MeOAc} \geq 90\%, P_{HOAc} \geq 80\%, P_{MeOH} \geq 80\% \quad (7.14a)$$

$$1 \times 10^{-4} \leq \alpha_1, \alpha_2, \alpha_3 \leq 0.3 \quad (7.14b)$$

$$\alpha_4 = 4\alpha - (\alpha_1 + \alpha_2 + \alpha_3) \quad (7.14c)$$

The fixed parameters are listed in Table 7.2 (Case 1d).

The operating conditions for the above problem is identical to the optimum solution obtained corresponding to Case 1a (L =30 cm) in Table 7.2 except that the feed flow rate was not kept constant at $\alpha = 0.1$ for the entire switching interval instead allowed to vary according to Eqs. 7.14b. Eqs. 7.14c is used to ensure that total feed flow rate is same as that of the constant feed flow case (case 1a in Table 7.2), and

therefore, the optimum results can be compared as shown in Figure 7.7, and it is evident from the figure that by varying the feed flow rate (although keeping the total

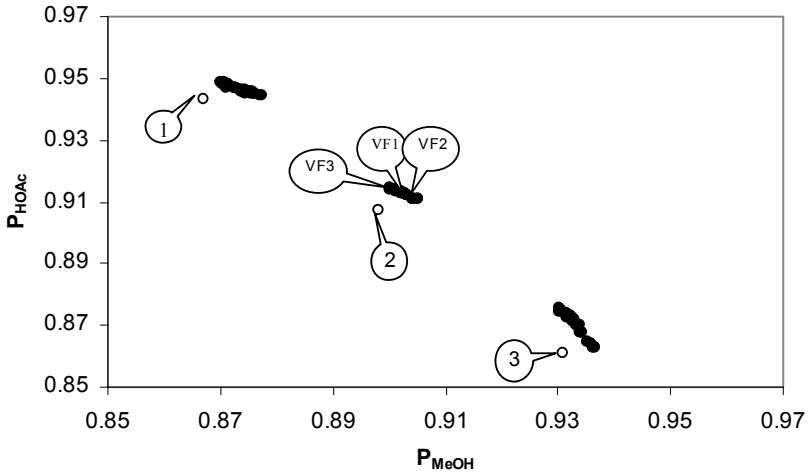

Figure 7.7 Comparison of optimal solutions of constant and distributed feed flow

Table 7.3 Comparison of objective function values for constant and variable feed flow

Point in Figure 7.7	P_{HOAc} [%]	P_{MeOH} [%]	α_1	α_2	α_3	α_4
VF1	91.3	90.2	5.8×10^{-4}	0.132	0.259	7.7×10^{-4}
VF2	91.1	90.5	4.8×10^{-4}	0.174	0.223	3.5×10^{-3}
VF3	91.3	90.2	4.8×10^{-4}	0.128	0.269	2.0×10^{-3}
2	90.7	89.8	$\alpha = 0.1$			

feed flow rate constant), both of the purity of raffinate and extract streams can be improved. Table 7.3 compares the objective function values and the corresponding optimal feed flow rates at the four sub-time intervals for three optimal points with the reference point 2 shown in Figure 7.7. It can be observed that the distribution of the feed flow rate for all the optimal solutions represents a uniform cyclic (periodic) behavior. The feed flow rate (α_1) is extremely small during the first sub-interval, then increases to a higher value for the second and the third time interval, and finally decreases to a lower value.

The advantage of this particular cyclic behavior for the performance of SMBR can be illustrated by comparing the concentration profiles for constant (point 2) and variable feed flow rate (VF_1) at the end of each of the four sub-time intervals as shown in Figure 7.8. The figure shows that the concentration fronts of MeOH and unreacted MeOAc move faster toward the raffinate port and tend to breakthrough from section P during the last time interval when the feed flow rate is constant. This gives rise to lower purity of HOAc (P_{HOAc}) in raffinate stream compared to variable feed flow. Likewise, the smaller feed flow rates in the first interval help to improve the purity of MeOH in extract stream, since HOAc and unreacted MeOAc tend to breakthrough from section S in the first time interval. The forced periodic feed flow rate could improve the performance SMBR for other operating conditions also and the extent of improvement varies depending on the specific reaction system, column configuration, and numbers of sub-time intervals employed.

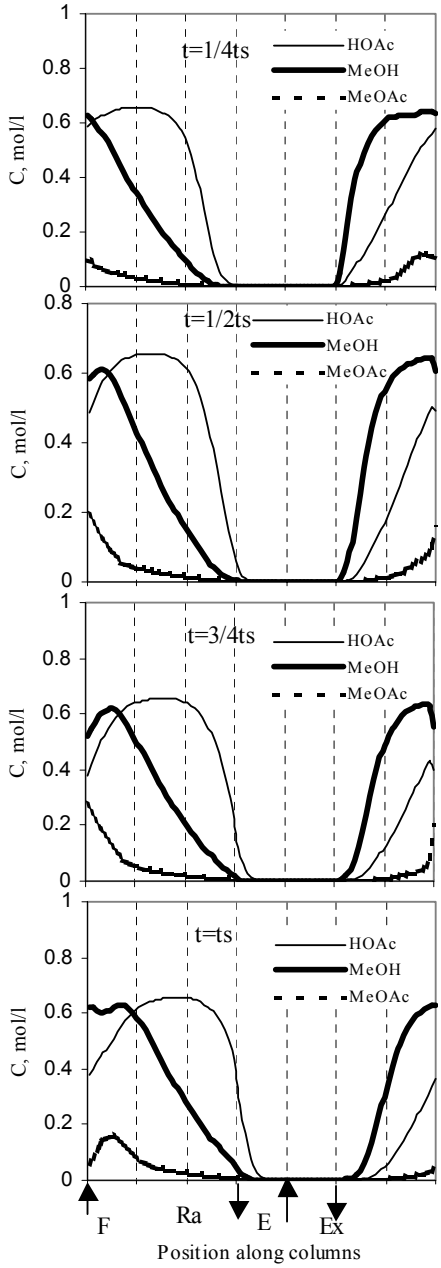

Figure 7.8a

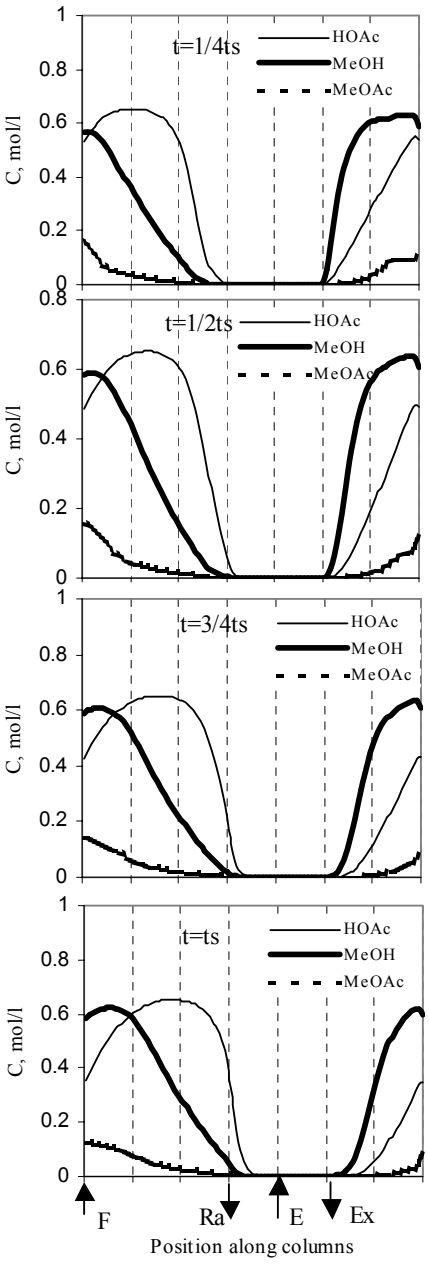

Figure 7.8b

Figure 7.8 Concentration profiles for constant and variable feed at the end of sub-time intervals

a) Variable feed flow rate; b) Constant feed flow rate (point 2 in Figure 7.7)

7.4.1.5 Comparison of the Performance of SMBR and Reactive Varicol Systems

In order to improve the process efficiency, SMB was recently modified into Varicol by introducing the non-synchronous shift of the inlet and outlet ports during a global switching period. It has been reported (Ludemann-Hombourger et al., 2000) that Varicol system performs better than its equivalent SMB system due to the flexibility in column distribution. Thus, in this section, the optimization study is carried out to determine what extend improvement can be obtained in a 4-subinterval 7-column reactive Varicol process over an equivalent SMBR unit. Furthermore, the performance of 7-column SMBR and reactive Varicol are compared with 6-column reactive Varicol and 8-column SMBR. For 6 and 7-column reactive Varicol, there can exist 10 and 20 possible column configurations respectively. Among these configurations, the possible optimal configurations selected from the simulation studies that lead to better performance of the system are listed in Table 7.4. The optimization problem is formulated as described in Table 7.2 (Case 1e).

The Pareto optimal solutions of the 6, 7-column reactive Varicol and 7, 8-column SMBR and corresponding switching times are illustrated in Figure 7.9. Slight improvement in both of the purity of raffinate and extract streams can be achieved in 7-column Varicol compared to an equivalent SMBR unit. However, 8-column SMBR performs better than 7-column Varicol while the performance of 6-column Varicol is worse than 7-column SMBR. The optimal column configurations for the 4-subinterval 6-column Varicol are C-C-C-A, A-A-C-C and for the 7-column Varicol are B-B-C-C, B-B-B-C, B-C-C-C. The optimal column configurations for 8-column SMBR are 2-1-1-4, 3-1-1-3 and 4-1-1-2. These optimal configurations imply that more columns are needed in section P or S in order to achieve as high purity of raffinate and extract

streams as possible since they are the main section for complete conversion and separation.

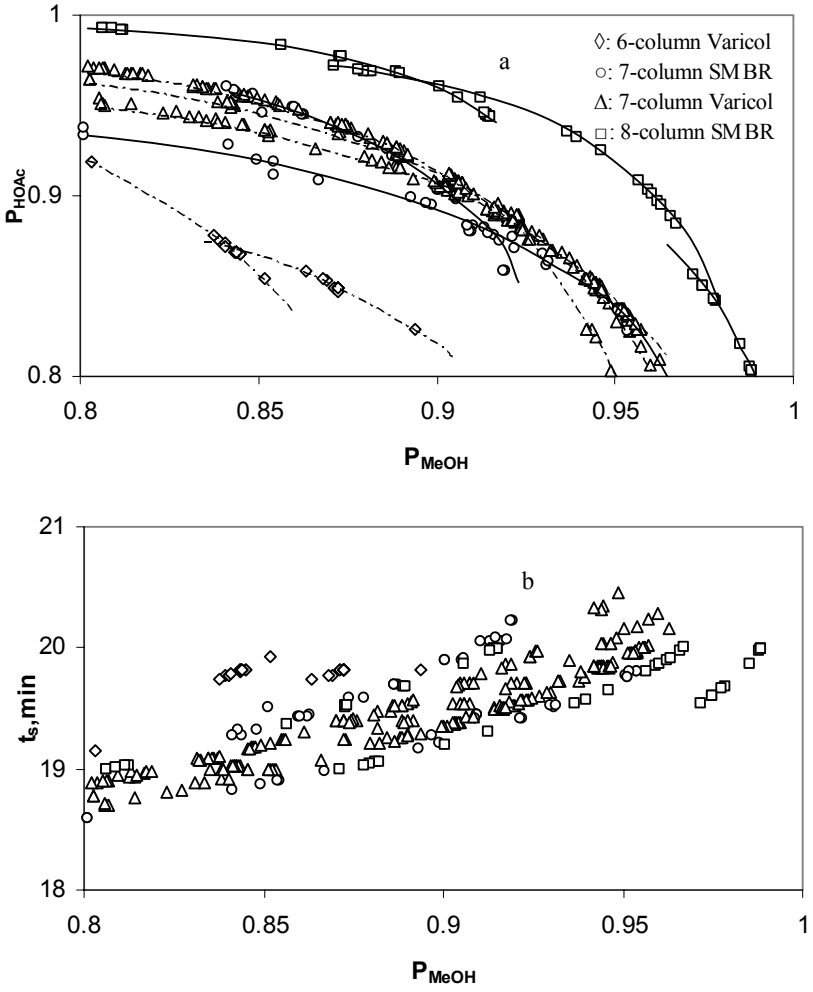

Figure 7.9 Comparison of Paretos for 6, 7-column Varicol and 7, 8-column SMBR

Table 7.4 List of possible optimal column configurations for 6 and 7- columnVaricol within a global switching period

N_{col} = 6			
χ	Column configuration[#]	χ	Column configuration
A	1/1/1/3	B	2/1/1/2
C	3/1/1/1	D	1/1/2/2
E	2/2/1/1	F	2/1/2/1
G	1/2/1/2	-	-
N_{col} = 7			
χ	Column configuration	χ	Column configuration
A	1/1/1/4	B	2/1/1/3
C	3/1/1/2	D	4/1/1/1
E	1/2/1/3	F	1/1/2/3
G	2/2/1/2	H	3/2/1/1
I	2/1/2/2	G	3/1/2/1

Column distribution 3/1/1/1 implies 3 columns in section P and one column each in sections Q to S.

7.4.1.6 Effect of Number of Sub-interval

In the previous section, 4-sub-interval switching within a global switching period was applied to 7-column Varicol system. It is expected that if the number of sub-intervals is increased, better performance could be achieved in Varicol due to additional flexibility in column distribution. Therefore, the effect of number of sub-interval switchings on the performance of Varicol is investigated by changing the subinterval from the reference value of 4 to 3 and 5. Figure 7.10 compares the optimal solutions in terms of maximization of P_{HOAc} in raffinate stream and P_{MeOH} in extract stream for the different number of sub-interval switching in 7-column Varicol. When the number of sub-intervals switching is increased from 3 to 4, a 2.3% improvement in the P_{HOAc} is obtained for a given P_{MeOH} of about 91%. However, there is not any significant improvement when the number of switching is increased further from 4 to

5, thus 4-subinterval is found to be sufficient for the effective operation of Varicol system for the hydrolysis of MeOAc. The optimal column configurations (χ) for the 3 and 5 sub-interval are B-C-C, C-C-B or C-C-C and B-C-C-C-C, B-B-C-C-C, B-B-B-C-C or B-B-B-B-C respectively.

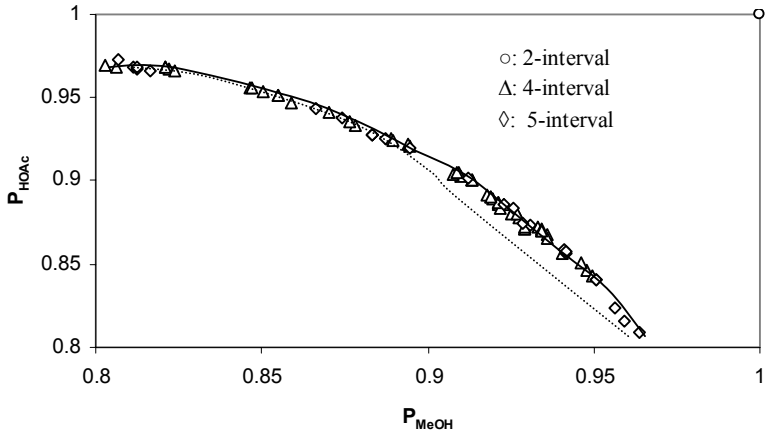

Figure 7.10 Effect of number of subinterval for 7-column Varicol

7.4.2 Case 2: Maximization of Y_{HOAc} in Raffinate Stream and Y_{MeOH} in Extract Stream

In this case, the optimization problem is formulated in order to obtain as high Y_{HOAc} in raffinate stream and Y_{MeOH} in Extract stream as possible while at the same maintaining the purity of raffinate and extract stream greater that 80%. The problem is described mathematically as follow:

Maximize $J_1 = Y_{HOAc}(t_s, \beta, \gamma, q, r, s)$ (7.15a)

Maximize $J_2 = Y_{MeOH}(t_s, \beta, \gamma, q, r, s)$ (7.15b)

Subject to $X_{MeOAc} \geq 90\%$, $P_{HOAc} \geq 80\%$, $P_{MeOH} \geq 80\%$ (7.16)

$10 \leq t_s \leq 30$ min; $1 \leq \gamma \leq 3$; $0.1 \leq \beta \leq 0.9$

$1 \leq s \leq 3$; $1 \leq q \leq 2$; $1 \leq r \leq 2$

Fixed parameters are given in Table 7.2 (Case2)

The optimal solutions with respect to maximization of Y_{HOAc} in raffinate and Y_{MeOH} in extract are illustrated in Figure 7.11. Figure 7.11a demonstrates that one cannot improve yield of HOAc in raffinate stream without sacrificing yield of MeOH in extract stream. When one is improved the other worsened, and therefore, it is not possible to maximize both at the same time.

Moreover, without violating the constraints on the purity of both raffinate and extract streams, the maximum Y_{HOAc} in raffinate and Y_{MeOH} in extract can be obtained are about 97% and 91% respectively, which are clearly illustrated by Figure 7.11e and Figure 7.11f.

Figure 7.11b shows that switching time is the key parameter in deciding the Pareto optimal solutions and it decreases when yield of MeOH in extract stream increases. The reduction of switching time increases the solid phase pseudo-velocity, and therefore, all components travel at a much faster rate with the solid phase, less amount of MeOH will breakthrough from section P, leading to higher yield of MeOH. Similiarly, when switching time increases, all components will travel at a faster rate with the fluid phase, less amount of HOAc will breakthrough from extract port and conversion also increases, resulting in higher yield of HOAc. This can be clearly illustrated by comparing the concentration profiles at different switching time, as shown in Figure 7.12.

It is observed from Figure 7.11c and Figure 7.11d that eluent flow rate and raffinate flow rate are insensitive in determining the Pareto solutions. The performance

of 7-column SMBR with respect of maximization of Y_{HOAc} and Y_{MeOH} was also compared with Varicol. Figure 7.13a shows that there is no significant improvement in the Varicol system. However, the eluent consumption in Varicol is less than that in an equivalent SMBR, which is shown in Figure 7.13b.

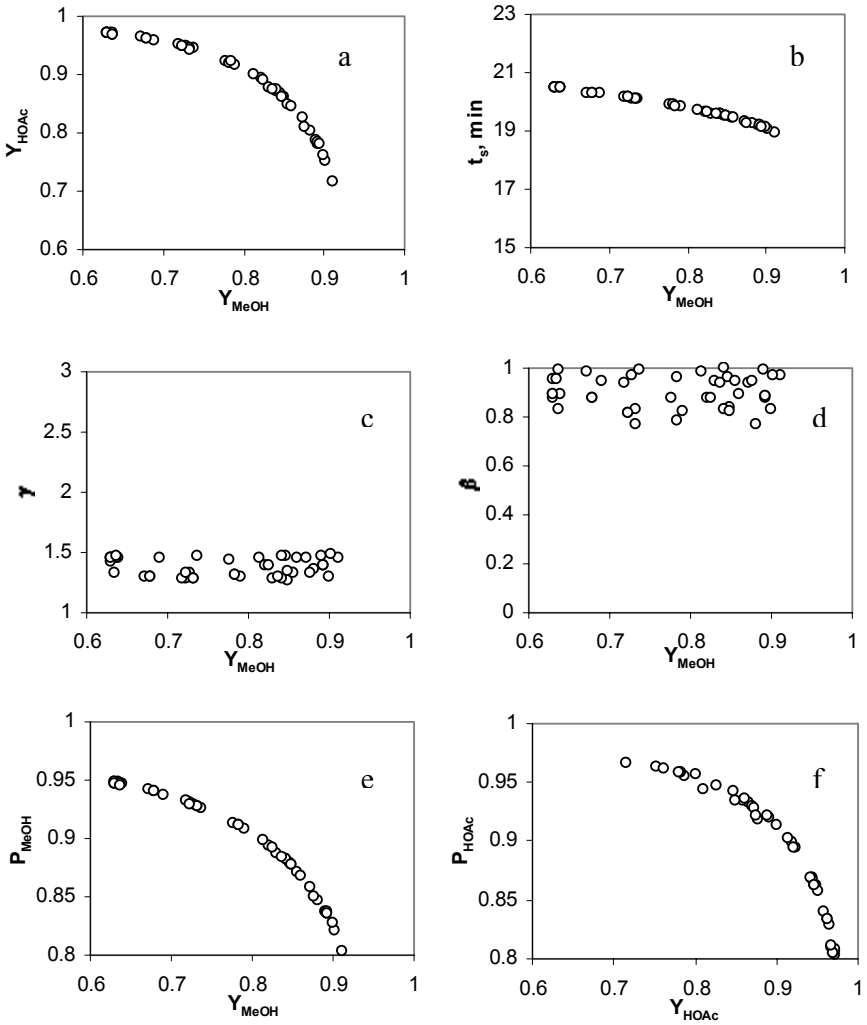

Figure 7.11 Pareto solutions and corresponding decision variables for maximization of Y_{HOAc} in raffinate and Y_{MeOH} in extract

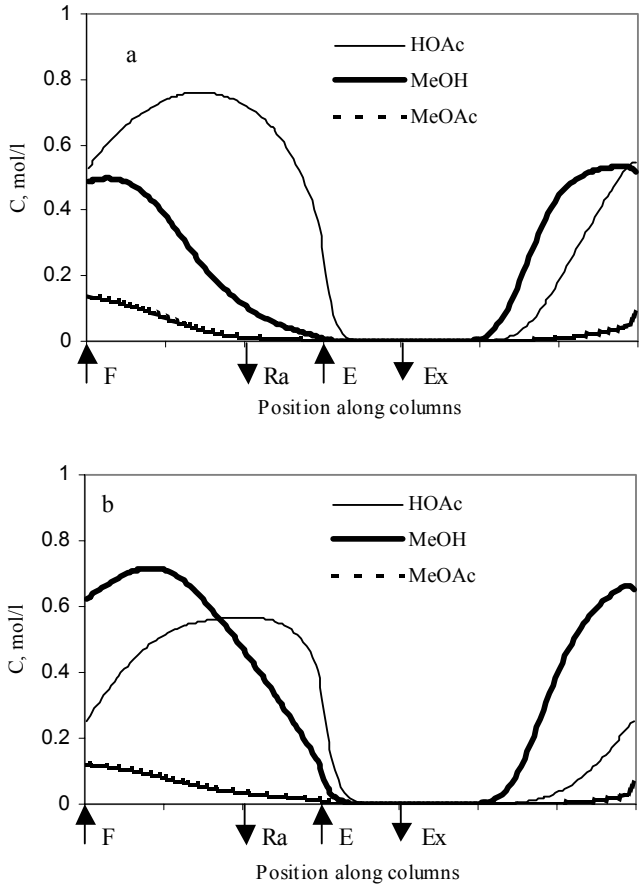

Figure 7.12 Concentration profile of MeOAc-HOAc-MeOH system at the end of 100 switching

a) t_s = 18 min; b) t_s = 20 min

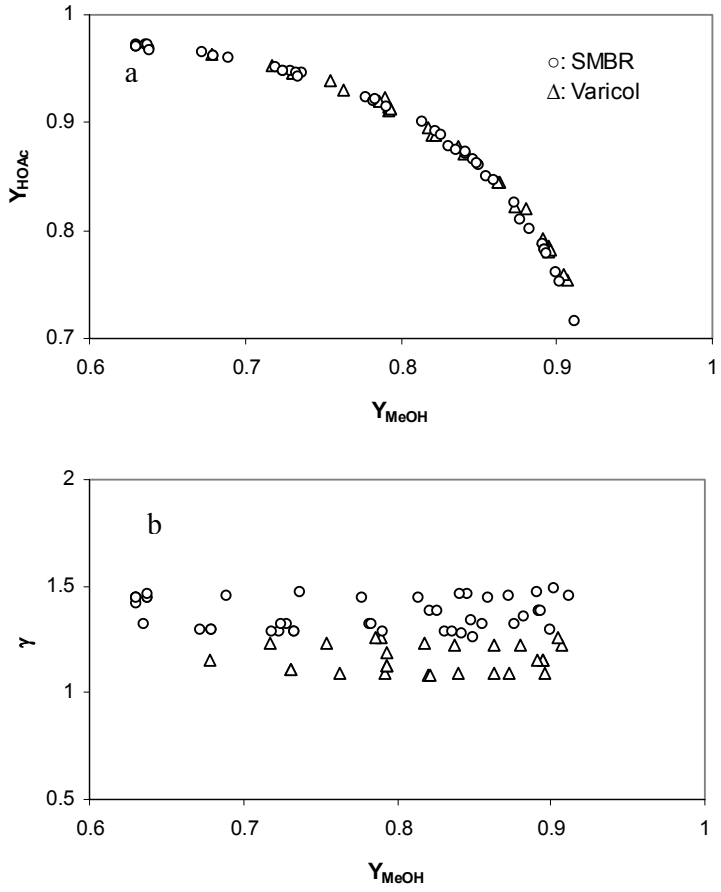

Figure 7.13 Comparison of optimal solutions of 7-column Varciol and an equivalent SMBR for Case2

7.5 Conclusions

In this chapter, a comprehensive multi-objective optimization study of SMBR and Varicol systems for the hydrolysis of MeOAc is reported. The Non-dominated Sorting Genetic algorithm (NSGA) was used in obtaining Pareto optimal solutions. The multi-objective optimization problems were formulated aiming at, a) simultaneous maximization of purity of both raffinate and extract streams, b) maximization of yield of HOAc in raffinate stream and that of MeOH in extract stream. The effects of colum length, raffinate flow rate, eluent flow rate and distributed feed flow rate on the Pareto optimal solutions in terms of maximization of purity of both raffinate and extract streams were investigated. The applicability of Varicol to reaction systems and the effect of number of sub-intervals on the performance of Varicol were also studied. It was observed that reactive Varicol performs better than SMBR due to its increased flexibility in column distribution. It is to be emphasized that there is no end of the variety of multi-objective optimization problems, which could be formulated and studied, and we have presented here, only a few simple examples, to illustrate the new optimization strategy and interpretation of results.

Chapter 8 Conclusions & Recommendations

8.1 Conclusions

This dissertation presents a systematic study of the performance of SMBR for the reversible reaction of acetic acid and methanol to methyl acetate. The adsorption equilibrium constants, dispersion coefficients and kinetic parameters were determined for the synthesis and hydrolysis of methyl acetate, corresponding to the different mobile phase, methanol or water. The mathematical model describing the dynamic behavior of the SMBR was developed based on equilibrium-dispersive model and verified experimentally at various operating conditions. Finally, a comprehensive multi-objective optimization study of SMBR and reactive Varicol was performed for the synthesis and hydrolysis of methyl acetate using the validated model in this study to determine the optimal design and operating parameters in order to successfully implement them on industrial scale. The comprehensive multi-optimization study also provides useful information that can guide in the understanding of SMBR potential, as well in its application to other systems.

8.1.1 Reaction Kinetics and Adsorption Isotherm Studies for Methyl Acetate Esterification and Hydrolysis

Reliable adsorption and kinetic parameters are very important for the design of reactors. In this work, the adsorption equilibrium constants, dispersion coefficients and kinetic parameters were first obtained for the two different applications of the reversible reaction of acetic acid and methanol catalyzed by Amberlyst 15 ion exchange resins, namely, the synthesis of methyl acetate, and the hydrolysis of methyl acetate. The quasi-homogeneous kinetic model and linear adsorption isotherm are

applicable in this study, since the solvent, methanol or water is present at a large excess concentration and the polymer resin is initially saturated with polar solvent (methanol or water). We assumed that the ion-exchange resin is completely swollen, the active sulfonic acid group is totally dissociated, and the solvated protons are evenly distributed in the polymer phase.

A mathematic model was developed to predict the elution profiles of the components in breakthrough experiments. The breakthrough curves of the reactants and products were experimentally measured at different temperatures, feed concentrations and flow rates. The adsorption and kinetic parameters were determined by minimizing an error function in order to fit the experimental results with the model predicted values using a state-of-the-art optimization technique, genetic algorithm.

It was also found that under the experimental conditions used, both external and internal mass resistances are negligible. The accuracy of the proposed mathematical model was further verified by comparing the experimental and predicted results at different feed concentrations and flow rates.

It was found that with increasing temperature, adsorption constants decrease, both the forward and backward reaction rate constants increase, and the reaction equilibrium constant for the forward reaction decreases while for the backward reaction increases. The computed adsorption and kinetic parameters were also compared with those reported in literature. It was found that the predicted breakthrough curves using the adsorption and kinetic constants reported in literature from batch reactor study could not predict our experimental results from packed bed plug flow reactor. However, our computed parameters obtained from a packed bed reactor can predict the experimental concentration profiles from a batch reactor reasonably well.

8.1.2 Optimization of SMBR for MeOAc Synthesis

The multi-objective optimization study for the synthesis of methyl acetate ester in a SMBR was carried out based on the numerical model modified from that reported by Lode et al. (2001). The non-dominated sorting genetic algorithm (NSGA) was used in obtaining the Pareto optimal solutions. Several two-objective functions and a three objective functions optimization were carried out to characterize the performance of SMBR. The optimization problems solved are (a) simultaneous maximization of productivity and purity of MeOAc, (b) simultaneous maximization of productivity and minimization of desorbent consumption, and (c) simultaneous maximization of productivity and purity of MeOAc together with minimization of desorbent consumption.

It was observed that productivity and purity of ester product at the raffinate port does not result in a global optimum solution instead a series of non-dominated (Pareto optimal) solutions were obtained. In all cases, switching time was the key parameter resulting in the Paretos while there exist unique optimal values for flow rate ratios m_2 and m_3. The optimal configuration for a 5-column SMBR unit was found to be 1-1-2-1 while the optimum mole fraction of acetic acid in the feed to be 0.79. Subsequently, the effects of conversion constraints and reaction rate constant on the Pareto optimal solutions were investigated. With the same purity requirement, the productivity is higher when the conversion constraint is lower, and the maximum productivity increases when the conversion requirement decreases. When the reaction rate constant increases, the productivity with the same purity requirement also increases. It was also found that the flow rate ratios in section 2 and section 3 control the available reactant (methanol) in the reactive section when pure acetic acid is used as feed. When the effect of m_1 on the performance of SMBR was investigated, it was found that when m_1

is small, the maximum productivity could be greatly improved at the cost of eluent flow. The three objective functions optimization results show that the productivity increases with decreasing purity and the desorbent consumption increases exponentially in order to achieve near 100% pure product.

8.1.3 Modeling, Simulation and Experimental Study of SMBR for MeOAc Synthesis

The synthesis of MeOAc in a simulated moving bed reactor was investigated by numerical simulation as well as experimentally. A rigorous mathematical model was developed to describe the dynamic behavior of SMBR and further validated by comparing the experimental results with model predictions at various operating conditions. It was observed that experimental results were in good agreement with that predicted from the model. The high yield and purity of MeOAc and near complete conversion of the limiting reactant, acetic acid, could be achieved in SMBR by selecting proper operating conditions. Parametric analysis was carried out based on the verified model to systematically investigate the effects of the process parameters on the performance of SMBR. It was found that there is a complex interaction of all these parameters on the reactor performance. Some of the operating parameters not only influence the purity, yield and selectivity of MeOAc significantly but also act in conflicting ways. This makes it extremely difficult to select length and number of columns in various sections, switching time and flow rates in different sections since desirable change in one performance criteria results in an unfavorable change in another desired variable. Therefore, one must carry out systematic multi-objective optimization study using the experimentally verified model developed in this study to determine appropriate design for successful implementation of SMBR on industrial scale

8.1.4 Optimization of Reactive SMB & Varicol for MeOAc Synthesis

The multi-objective optimization of reactive SMB and Varicol process for the synthesis of MeOAc were performed using NSGA. The optimal solutions in terms of maximization of purity and yield of MeOAc for the existing experimental setup were compared with the experimental results obtained by running the unit at the optimal operating conditions. The variation of feed flow rate during a global switching period on the performance of SMBR was investigated. It was found the both the purity and yield of MeOAc could be improved compare to the constant feed flow process. The effects of flow rates and total number of columns on the performance of reactive SMB were investigated. The applicability of Varicol to reaction systems is also evaluated by comparing the optimal results with that of SMBR. It was found that the performance of reactive Varicol could be better than that of reactive SMB due to the increased flexibility.

8.1.5 Optimization of Reactive SMB & Varicol for MeOAc Hydrolysis

A comprehensive multi-objective optimization study of SMBR and Varicol systems for the hydrolysis of MeOAc using NSGA is reported. The multi-objective optimization problems were formulated aiming at a) simultaneous maximization of purity of both raffinate and extract streams, b) maximization of yield of HOAc in raffinate stream and MeOH in extract stream. The effects of colum length, Raffinate flow rate, eluent flow rate and distributed feed flow rate on the Pareto optimal solutions in terms of maximization of purity of both Raffinate and extract streams were investigated. The effect of number of sub-intervals on the performance of Varicol was also studied. It was observed that reactive Varicol performs better than SMBR due to the better utilization of the solid adsorbent. It is to be emphasized here that there is no end of the variety of multi-objective optimization problems, which could be formulated

and studied, and we have presented here, only a few simple examples, to illustrate the new optimization strategy and interpretation of results.

8.2 Recommendations for Future Work

Due to the cyclic switching of the inlet and outlet ports, the SMBR process features a complex hybrid (mixed discrete/continuous) dynamics. It has high sensitivities to disturbances and a tendency to instability when the operating condition is close to the economic optimum. The development and implementation of a suitable control framework for SMBR process is necessary in order to exploit the full economic potential of the process. Therefore, the control of SMBR with respect to safe and economical operation while guaranteeing the product specifications at any time is naturally becomes the next task.

In this investigation, the non-dominated sorting genetic algorithm (NSGA) is used in obtaining the Pareto optimal solutions. NSGA is adequate for solving the multi-objective problems formulated in this study. However, its robustness is potentially affected when the complexity of the problems increases, such as increase in the number of the objective functions and/or decision variables. Hence, a better multi-objective optimization method is required to deal with such problems.

Furthermore, the concept of SMBR can be further developed, besides non-synchronous port switching and variable feed flow rate, proper column temperature and pressure gradient can also be introduced, such as SF-SMBR. These will introduce more freedom to the SMBR process, leading to better performance.

REFERENCES

Adam, P., R.-M. Nicoud, M. Bailly and O. Ludemann-Hombouger. Process and Device for Separation with Variable-Length, US Patent, 6, 136, 198. 1998.

Agreda,V.H., L.R. Partin, and W.H. Heise. High Purity Methyl Acetate via Reactive Distillation, Chem. Eng. Prog., *86*, pp. 40-46. 1990**.**

Azevedo, D.C.S. and A.E. Rodrigues. Design Methodology and Operation of a Simulated Moving Bed Reactor for the Inversion of Sucrose and Glucose-Fructose Separation, Chem. Eng. J., *82*, pp. 95-107. 2001.

Bhaskar, V., S.K. Gupta and A.K. Ray. Applications of Multiobjective Optimization in Chemical Engineering, Rev. Chem. Eng., *16*, pp. 1-54. 2000a.

Bhaskar, V., S.K. Gupta and A.K. Ray. Multiobjective Optimization of an Industrial Wiped-film Pet Reactor, AICHE J., *46*, pp. 1046-1058. 2000b.

Bhaskar, V., S.K. Gupta and A.K. Ray. Multiobjective Optimization of an Industrial Wiped-film Poly (Ethylene Terephthalate) Reactor: Some Further Insights, Comput. Chem. Eng., *25*, pp. 391-407. 2001.

Biressi, G., O. Ludemann-Hombourger, M. Mazzotti, R.-M. Nicoud and M. Morbidelli. Design and Optimization of a Simulated Moving Bed Unit: Role of Deviations from Equilibrium Theory, J. Chromatogr. A., *876*, pp. 3-15. 2000a.

Biressi, G., F. Quattrini, M. Juza, M. Mazzotti, V. Schurig and M. Morbidelli. Gas Chromatographic Simulated Moving Bed Separation of the Enantiomers of the Inhalation Anesthetic Enflurance, Chem. Eng. Sci., *55*, pp. 4537-4547. 2000b.

Broughton, D.B. and C.G. Gerhold. Continuous Sorption Process Employing Fixed Bed of Sorbent and Moving Inlets and Outlets, US Patent 2 985 589. 1961.

Carr, R.W. Continuous Reaction Chromatography. In Preparative and Production Scale Chromatography, ed by G. Ganetsos and P.E. Barker, pp. 421-447. New York: Marcel Dekker. 1993.

Chakrabarti, A. and M.M. Sharma. Cation Ion Exchange Resin as Catalyst, Reactive Polymers, *20*, pp. 1-45. 1993.

Chankong, V. and Y.Y. Haimes. Multiobjective Decision Making: Theory and Methodology. pp. 1-406, New York: North Holland. 1983.

Charton, F. and R.-M. Nicoud. Complete Design of a Simulated Moving-Bed, J. Chromatogr A., *702*, pp. 97-112. 1995.

Ching, C.B. and Z.P. Lu. Simulated Moving Bed Reactor: Application in Bioreaction and Separation, Ind. Eng. Chem. Res., *36*, pp. 152-159. 1997.

Cho, B.K., R.W. Carr and R. Aris. A Continuous Chromatographic Reactor, Chem. Eng. Sci., *35*, pp. 74-81. 1980.

Cho, B.K., R. Aris and R.W. Carr. The Mathematical Theory of a Counter-current Catalytic Reactor, Proc. Roy. Soc. Lond. A, *383*, pp. 147–189. 1982

Chu, C. and L.C. Tsang. The Behavior of a Chromatographic Reactor, Ind. Eng. Chem. Process Des. Dev., *10*, pp. 47-53. 1971.

Core, F. Performance of Chromatographic Reactors in Cyclic Operation, Ind. Eng. Chem. Process Des., *6*, pp. 10-16. 1967.

Deb, K. Optimization for Engineering Design: Algorithms and Examples. pp. 290-320. New Delhi: Prentice-Hall of India, India. 1995.

Deb, K. Multi-Objective Optimization Using Evolutionary Algorithms. UK: Wiley, Chichester. 2001.

DeGarmo, J.L., V.N. Parulekar and V. Pinjala. Consider Reactive Distillation, Chem. Eng. Prog., *88*, pp. 43-50. 1992.

Doherty, M.F. and G. Buzad. Reactive Distillation by Design, Trans. Inst. Chem. Eng., *70A*, pp. 448-458. 1992.

Dunnebier, G. and K.U. Klatt. Optimal Operation of Simulated Moving Bed Chromatographic Processes, Comput. Chem. Eng., *23*, pp. S195-S198. 1999.

Dunnebier, G., J. Fricke and K.U. Klatt. Optimal Design and Operation of Simulated Moving Bed Chromatographic Reactors, Ind. Eng. Chem. Res., *39*, pp. 2290-2304. 2000.

Dwivedi, P.N. and S.N. Upadhyay. Particle-Fluid Mass Transfer in Fixed and Fluidized Beds, Ind. Eng. Chem. Process Des. Dev., *16*, pp. 157-165. 1977.

Fish, B., R.W. Carr and R. Aris. The Continuous Countercurrent Moving Bed Chromatographic Reactor, Chem. Eng. Sci., *41*, pp. 661-668. 1986.

Fish, B.B., R.W. Carr and R. Aris. Computer Aided Experimentation in Countercurrent Reaction Chromatography and Simulated Countercurrent Chromatography, Chemical Engineering Science, *43*, pp. 1867-1873. 1988.

Fish, B.B., R.W. Carr and R. Aris. An Experimental Study of the Countercurrent Moving-bed Chromatographic Reactor, Chemical Engineering Science, *44*, pp. 1773-1783. 1989.

Fogler, H.S., Elements of Chemical Reaction Engineering. pp. 625-628, Englewood Cliffs, N.J.: Prentice Hall. 1992.

Fonseca, C.M. and P.J. Fleming. Multiobjective Optimization and Multiple Constraints Handling with Evolutionary Algorithms I: A Unified Formulation, IEEE Trans. Syst. Man. Cy. A, *28*, pp. 26-37. 1998.

Fricke, J., M. Meurer and H. Schmidt-Traub. Design and Layout of Simulated-Moving Bed Chromatographic Reactors, Chem. Eng. Technol., *22*, pp. 835-839. 1999a.

Fricke, J., M. Meurer, J. Dreisorner and H. Schmidt-Traub. Effect of Process Parameters on the Performance of a Simulated Moving Bed Chromatographic Reactor, Chem. Eng. Sci., *54*, pp. 1487-1492. 1999b.

Fuchigami,Y. Hydrolysis of Methyl Acetate in Distillation Column Packed with Reactive Packing of Ion Exchange Resin, J. Chem. Eng. Jpn., *23*, pp.354-358. 1990.

Gentilini, A., C. Migliorini, M. Mazzotti and M. Morbidelli. Optimal Operation of Simulated Moving-bed Units for Non-linear Chromatographic Separations II. Bi-Langmuir Isotherm, J. Chromatogr. A., *805*, pp. 37-44. 1998.

Goldberg, D.E. Genetic Algorithms in Search, Optimization, and Machine Learning. pp. 1-379, Reading, Mass.: Addison-Wesley. 1989.

Guiochon, G, S.G. Shirazi and A.M. Katti. Fundamentals of Preparative and Nonlinear Chromatography. pp. 1-701, Boston: Academic Press. 1994.

Han, S.J., Y. Jin and Z.Q. Yu. Application of a Fluidized Reaction-Distillation Column for Hydrolysis of Methyl Acetate, Chem. Eng. J., *66*, pp. 227-230. 1997.

Hashimoto, K., S. Adachi, H. Noujima and Y. Ueda. A New Process Combining Adsorption and Enzyme Reaction for Producing Higher Fructose Syrup, Biotechnol. Bioeng., *25*, pp. 2371-2393. 1983.

Holland, J.H. Adaptation in Natural and Artificial Systems: An Introductory Analysis with Applications to Biology, Control and Artificial Intelligence. pp. 1-183, Ann Arbor: University of Michigan Press. 1975.

Karlsson, S., F. Pettersson and T. Westerlund. A MILP-Method for Optimizing a Preparative Simulated Moving Bed Chromatographic Separation Process, Comput. Chem. Eng., *23*, pp. S487-S490. 1999.

Kawase, M., A. Pilgrim, T. Araki and K. Hashimoto. Lactosucrose Production Using a Simulated Moving Bed Reactor, Chem. Eng. Sci., *56*, pp. 453-458. 2001.

Kawase, M., T.B. Suzuki, K. Inoue, K. Yoshimoto and K. Hashimoto. Increased Esterification Conversion by Application of the Simulated Moving-Bed Reactor, Chem. Eng. Sci., *51*, pp. 2971-2976. 1996.

Kawase, M., Y. Inoue, T. Araki and K. Hashimoto. The Simulated Moving-Bed Reactor for Production of Bisphenol A, Catal. Today, *48*, pp. 199-209. 1999.

Klatt, K.U., F. Hanisch, G. Dünnebier and S. Engell. Model-based Optimization and Control of Chromatographic Processes, Comput. Chem. Eng., *24*, pp. 1119-1126. 2000.

Klatt, K.U., F. Hanisch and G. Dünnebier. Model-Based Control of a Simulated Moving Bed Chromatographic Process for the Separation of Fructose and Glucose, J. Process. Contr., *12*, pp. 203-219. 2002.

Kruglov, A. Methanol Synthesis in a Simulated Countercurrent Moving-Bed Adsorptive Catalytic Reactor, Chem. Eng. Sci., *49*, pp. 4699-4716. 1994.

Langer, S.H. and J.E. Patton. Chemical Reactor Applications of the Gas Chromatography Column. In New Developments in Gas Chromatography, ed by J. H. Purnell, pp. 293–373. New York: Wiley-Interscience. 1973.

Langer, S.H., J.K. Yurchak and J.E. Patton. The Gas Chromatography Column as a Chemical Reactor, Ind. Eng. Chem., *61*, pp.10–21. 1969.

Lode, F., M. Houmard, C. Migliorini, M. Mazzotti and M. Morbidelli. Continuous Reactive Chromatography, Chem. Eng. Sci., *56*, pp. 269-291. 2001.

Lode, F., M. Mazzotti and M. Morbidelli. Comparing True Countercurrent and Simulated Moving-Bed Chromatographic Reactors, AIChE J. *49(4)*, pp. 977-988. 2003.

Lode, F., M. Mazzotti and M. Morbidelli. Synthesis of Methylacetate in a Simulated Moving-Bed Reactor: Experiments and Modeling, AIChE J. *49(6)*, pp. 1516-1523. 2003.

Ludemann-Hombourger, O., R.-M. Nicoud and M. Bailly. The “VARICOL” Process: A New Multicolumn Continuous Chromatographic Process, Separation Science and Technology, *35*(12), pp. 1829-1862. 2000.

Ludemann-Hombourger, G. Pigorini, R.M. Nicoud, D.S. Ross and G. Terfloth. Application of the VARICOL Process to the Separation of the Isomers of the SB-553261 racemate, J. Chromatogr. A., *947*, pp. 59-68. 2002.

Ma, Z. and N.H.L. Wang. Standing Wave Analysis of SMB Chromatography: Linear Systems, AICHE J., *43*(10), pp. 2488-2508. 1997.

Magee, E.M. The Course of a Reaction in a Chromatographic Column, Ind. Eng. Chem. Fund., *2*, pp. 32-36. 1963.

Mallmann, T., B.D. Burris, Z. Ma and N.-H.L. Wang. Standing Wave Design of Nonlinear SMB Systems for Fructose Purification, AICHE J., *44*(12), pp. 2628-2646. 1998.

Mark C. Bjorklund, Alexey V. Kruglov and Robert W. Carr. Studies of the Oxidative Coupling of Methane to Ethane and Ethylene in a Simulated Countercurrent Moving Bed Chromatographic Reactor, Ind. Eng. Chem. Res., *40*, pp. 2236-2242. 2001.

Mazzotti, M., G. Storti and M. Morbidelli. Robust Design of Countercurrent Adsorption Separation Processes: 2. Multicomponent Systems, AICHE J., *40*(11), pp. 1825-1842. 1994.

Mazzotti, M., G. Storti and M. Morbidelli. Robust Design of Countercurrent Adsorption Separation: 3. Nonstoichiometric Systems, AICHE J., *42*(10), pp. 2784-2796. 1996a.

Mazzotti, M., A. Kruglov, B. Neri, D. Gelosa and M. Morbidelli. A Continuous Chromatographic Reactor: SMBR, Chem. Eng. Sci., *51*(10), pp. 1827-1836. 1996b.

Mazzotti, M., G. Storti and M. Morbidelli. Optimal Operation of Simulated Moving Bed Units for Nonlinear Chromatographic Separations, J. Chromatogr. A., *769*, pp. 3-24. 1997a.

Mazzotti, M., G. Storti and M. Morbidelli, Robust Design of Countercurrent Adsorption Separation Processes: 4. Desorbent in the Feed, AICHE J., *43*(1), pp. 64-72. 1997b.

Meurer, M., U. Altenhoner, J. Strube, A. Untiedt and H. Schmidt-Traub. Dynamic Simulation of a Simulated-Moving-Bed Chromatographic Reactor for the Inversion of Sucrose, Starch/Starke, *48*, pp. 452-457. 1996.

Meurer, M., U. Altenhoner, J. Strube and H. Schmidt-Traub. Dynamic Simulation of Simulated Moving Bed Chromatographic Reactors, J. Chromatogr. A., *769*, pp. 71-79. 1997.

Migliorini, C., M. Mazzotti and M. Morbidelli. Continuous Chromatographic Separation Through Simulated Moving Bed under Linear and Nonlinear Conditions, J. Chromatogr. A., *827*, pp. 161-173. 1998.

Migliorini, C., A. Gentilini, M. Mazzotti and M. Morbidelli. Design of Simulated Moving Bed Units under Nonideal Conditions, Ind. Eng. Chem. Res., *38*, pp. 2400-2410. 1999a.

Migliorini, C., M. Fillinger, M. Mazzotti and M. Morbidelli. Analysis of Simulated Moving-Bed Reactors, Chem. Eng. Sci., *54*, pp. 2475-2480. 1999b.

Oh, P.P., A.K. Ray and G.P. Rangaiah. Triple Objective Optimization of Industrial Hydrogen Plants, J. Chem. Eng. Japan, in press. 2001.

Petroulas, T., R. Aris and R.W. Carr. Analysis of the Countercurrent Moving Bed Chromatographic Reactor, Comp. & Maths. with Appls., *11*, pp. 5–34. 1985a.

Petroulas, T., R. Aris and R.W. Carr. Analysis and Performance of a Countercurrent Moving-bed Chromatographic Reactor, Chem. Eng. Sci., *40*, pp. 2233–2240. 1985b.

Pöpken, T., L. Götze and J. Gmehling. Reaction Kinetics and Chemical Equilibrium of Homogeneously and Heterogeneously Catalyzed Acetic Acid Esterification with Methanol and Methyl Acetate Hydrolysis, Ind. Eng. Chem. Res., *39*, pp.2601-2611. 2000.

Proll, T. and E. Kusters. Optimization Strategy for Simulated Moving Bed Systems. J. Chromatogr. A., *800*, pp. 135-150. 1998.

Rajesh, J.K., S.K. Gupta, G.P. Rangaiah and A.K. Ray. Multiobjective Optimization of Industrial Hydrogen Plants, Chem. Eng. Sci., *56*, pp. 999-1010. 2001.

Ravi, G., S.K. Gupta and M.B. Ray. Multiobjective Optimization of Cyclone Separators Using Genetic Algorithm, Ind. Eng. Chem. Res., *39*, pp. 4272-4286. 2000.

Ray, A.K., A. Tonkovich, R.W. Carr and R. Aris. The Simulated Countercurrent Moving-bed Chromatographic Reactor, Chem. Eng. Sci., *45*, pp. 2431-2437. 1990.

Ray, A.K. The Simulated Countercurrent Moving Bed Chromatographic Reactor: A Novel Reactor-Separator. Ph.D. Dissertation, University of Minnesota. 1992.

Ray, A.K., R.W. Carr and R. Aris. The Simulated Countercurrent Moving-Bed Chromatographic Reactor – a Novel Reactor Separator, Chem. Eng. Sci., *49*, pp. 469-480. 1994.

Ray, A.K. and R.W. Carr. Numerical Simulation of a Simulated Countercurrent Moving Bed Chromatographic Reactor, Chem. Eng. Sci., *50*, pp. 3033-3041. 1995a.

Ray, A.K. and R.W. Carr. Experimental Study of a Laboratory-Scale Simulated Countercurrent Moving Bed Chromatographic Reactor, Chem. Eng. Sci., *50*, pp. 2195-2202. 1995b.

Rehfinger, A. and U. Hoffmann. Kinetics of Methyl Tertiary Butyl Ether Liquid Phase Synthesis Catalyzed by Ion Exchange Resin-I. Intrinsic Rate Expression in Liquid Phase Activities, Chem. Eng. Sci., *45*, pp. 1605-1617. 1990.

Rev, E. Reactive Distillation and Kinetic Azeotropy, Ind. Eng. Chem. Res., *33*, pp. 2174-2179. 1994.

Roginskii, S.Z., M.I. Yanovskii and G.A. Gaziev. Chemical Reaction under Chromatographic Conditions, Dokl. Akad. Nauk SSSR (Engl. Transl.), *140*, pp. 771-776. 1961.

Roginskii, S.Z., M.I. Yanovskii and G.A. Gaziey. Catalytic Reaction and Catalysis under Chromatographic Conditions, Kinetics and Catalysis, *3*, pp. 529-540. 1962.

Sarmidi, M. R. and P. Barker. Saccharification of Modified Starch to Maltose in a Continuous Rotating Annular Chromatograph (CACR), Journal of Chemical Techniques in Biotechnology, *57*, pp. 229-235. 1993a.

Sarmidi, M. R. and P. Barker. Simultaneous Biochemical Reaction and Separation in a Rotating Annular Chromatograph, Chem. Eng. Sci., *48*, pp. 2615-2623. 1993b.

Schiesser, W.E. The Numerical Method of Lines. pp. 1-326, New York: Academic Press. 1991.

Schweich, D. and J. Villermaux. The Behavior of a Chromatographic Reactor: A New Theoretical Approach, Ind. Eng. Chem. Fundam., *17*, pp.1-7. 1978.

Schweich, D., J. Villermaux and M. Sardin. An Introduction to Nonlinear Theory of Adsorptive Reactors, AICHE J., *26*, pp. 477-486. 1980.

Schweich, D. and J. Villermaux. The Preparative Chromatographic Reactor Revisited, Chem. Eng. J., *24*, pp. 99-109. 1982.

Song, S.K. and Y.Y. Lee. Countercurrent Reactor in Acid Catalyzed Cellulose Hydrolysis, Chem. Eng. Commun., *17*, pp. 23–30. 1982.

Song, W., G. Venimadhavan, J.M. Manning, M.F. Malone and M.F. Doherty. Measurement of Residue Curve Maps and Heterogeneous Kinetics in Methyl Acetate Synthesis, Ind. Eng. Chem. Res., *37*, pp. 1917-1928. 1998

Srinivas, N. and K. Deb. Multiobjective Function Optimization using Non-dominated Sorting Genetic Algorithms, Evolutionary Computing, *2*, pp. 221-248. 1995.

Storti, G., M. Masi, R. Paludetto, M. Morbidelli and S. Carra. Adsorption Separation Processes: Countercurrent and Simulated Countercurrent Operations, Comput. Chem. Eng., *12*, pp. 475-482. 1988.

Storti, G., M. Mazzotti, M. Morbidelli and S. Carra. Robust Design of Binary Countercurrent Adsorption Separation Processes, AICHE J., *39*, pp. 471-492. 1993.

Storti, G., R. Baciocchi, M. Mazzotti and M. Morbidelli. Design of Optimal Operating Conditions of Simulated Moving Bed Adsorptive Separation Units, Ind. Eng. Chem. Res., *34*, pp. 288-301. 1995.

Strube, J., A. Jupke, A. Epping, H. Schmidt-Traub, M. Schulte and R. Devant. Design, Optimization and Operation of SMB Chromatography in the Production of Enatiomerically pure pharmaceuticals, Chirality, *11*, pp. 440-450, 1999.

Takeuchi, K. and Y. Uraguchi. Separation Conditions of the Reactant and the Product with a Chromatographic Moving Bed Reactor, J. chem. Eng. Jap., *9*, pp.164–166. 1976a.

Takeuchi, K. and Y. Uraguchi. Basic Design of Chromatographic Moving Bed Reactors for Product Refining, J. chem. Eng. Jap., *9*, pp. 246–248. 1976b.

Takeuchi, K. and Y. Uraguchi. The Effect of the Exhausting Section on the Performance of a Chromatographic Moving Bed reactor, J. chem. Engng Jap., *10*, pp. 72–74. 1977.

Takeuchi, K. and Y. Uraguchi. Computational Studies of a Chromatographic Moving Bed Reactor for Consecutive and Reversible Reactions, J. chem. Engng Jap., *11*, pp. 216–220. 1978.

Tonkovich, A.L., R.W. Carr and R. Aris. Enhanced C_2 Yields from Methane Oxidative Coupling by Means of a Separative Chemical Reactor, Science, *262*, pp. 221-223. 1993.

Tonkovich, A.L. and R.W. Carr. A Simulated Countercurrent Moving-bed Chromatographic Reactor for the Oxidative Coupling of Methane: Experimental Results, Chem. Eng. Sci., *49*(24a), pp. 4647-4657. 1994a.

Tonkovich, A.L. and R.W. Carr. Modeling of the Simulated Countercurrent Moving-bed Chromatographic Reactor Used for the Oxidative Coupling of Methane. Chem. Eng. Sci., *49*(24a), pp. 4657-4665. 1994b.

Toumi, A. F. Hanisch and S. Engell. Optimal Operation of Continuous Chromatographic Processes: Mathematical Optimization of the VARICOL Process. Ind. Eng. Chem. Res., 41, pp. 4328-4337. 2002

Van Deemter, J. J., F. J. Zuiderweg and A. Klinkenberg. Longitudinal Diffusion and Resistance to Mass Transfer as Causes of Nonideality in Chromatography, Chem. Eng. Sci., *5*, pp. 271-289. 1956.

Viswanathan, S. and R. Aris. Countercurrent Moving Bed Chromatographic Reactors, Proc. 3rd ISCRE, Adv. Chem. Ser., *133*, pp.191–204. 1974a.

Viswanathan, S. and R. Aris. An Analysis of the Countercurrent Moving Bed Reactor, SIAM-AMS Proc., *8*, pp.99–124. 1974b.

Wetherold, R.G., E. Wissler and K. Bischoff. An Experimental and Computational Study of the Hydrolysis of Methyl Formate in Chromatographic Reactor, Adv. Chem. Ser., *133*, pp.181-190. 1974.

Wooley, R., Z. Ma and N.H.L. Wang. A Nine-Zone Simulated Moving Bed for the Recovery of Glucose and Xylose from Biomass Dydrolyzate, Ind. Eng. Chem. Res., *37*(9), pp. 3699-3709. 1998.

Wu, D.J., Z. Ma and N.H.L. Wang. Optimization of Throughput and Desorbent Consumption in Simulated Moving-Bed Chromatograph for Paclitaxel Purification, J. Chromatogr. A., *855*, pp. 71-89. 1999.

Xu, Z.P. and K.T. Chuang. Kinetics of Acetic Acid Esterification over Ion Exchange Catalysts, Can. J. Chem. Eng., *74*, pp.493-550. 1996.

Zhang, Z. Multi-objective Optimization of Simulated Moving Bed (SMB) Systems. Ph. D. Dissertation, National University of Singapore. 2001.

Zhang, Z., K. Hidajat and A.K. Ray. Determination of Adsorption and Kinetic Parameters for Methyl Tert-Butyl Ether Synthesis from Tert-Butyl Alcohol and Methanol, J. Catal., *200*, pp. 209-221. 2001a.

Zhang, Z., K. Hidajat and A.K. Ray. Application of Simulated Countercurrent Moving Bed Chromatographic Reactor for MTBE Synthesis, Ind. Eng. Chem. Res., *40*(9), pp. 5305-5316. 2001b.

Zhang, Z., K. Hidajat, A. K. Ray, Multiobjective Optimization of Simulated Countercurrent Moving Bed Chromatographic Reactor (SCMCR) for MTBE Synthesis, Ind. Eng. Chem. Res., *41*, pp. 3213-3232. 2002a.

Zhang, Z., K. Hidajat, A. K. Ray, M. Morbidelli, Multi-objective Optimization of Simulated Moving Bed system and Varicol process for Chiral Separation, AIChE J., *48*(12), pp. 2088-2816. 2002.

Zhong, G. and G. Guiochon. Simulated Moving Bed Chromatography: Comparison between the Behaviors under Linear and Nonlinear Conditions, Chem. Eng. Sci., *52*, pp. 4403-4418. 1997.

Publications

Yu, Weifang, K. Hidajat & A.K. Ray. Optimal Operation of Reactive Simulated Moving Bed and Varicol Systems, *J. Chem. Technol. Biot.*, *78(2-3)*, pp. 287-293. 2003.

Yu, Weifang, K. Hidajat & A.K. Ray. Reaction Kinetics and Adsorption Isotherm Studies for Methyl Acetate Esterification and Hydrolysis, *Applied Catalysis A: General*, in press.

Yu, Weifang, K. Hidajat & A.K. Ray. Modeling, Simulation and Experimental Study of the Simulated Moving Bed Reactor for the Synthesis of Methyl Acetate Ester, *Ind. Eng. Chem. Res*., in press.

Yu, Weifang, K. Hidajat & A.K. Ray. Application of Multi-objective Optimization in the Design and Operation of Reactive SMB and Varicol Systems, *Ind. Eng. Chem. Res*., in press.

Yu, Weifang, K. Hidajat & A.K. Ray. Application of multi-objective optimization in the design of SMB in chemical process industry, *J. of Chemical Institute of Chemical Engineers*, in press.

Yu, Weifang, K. Hidajat & A.K. Ray. Optimization of Hydrolysis of Methyl Acetate in Simulated Moving Bed Reactor and Varicol Systems, submitted to *Chem. Eng. J.*, 2003.

Appendix A A note on Genetic Algorithm

GA is a search technique developed by Holland (1975), which mimics the process of natural selection and natural genetics. In this algorithm, a set of decision variables are first coded in the form of a set of randomly generated binary numbers (0 and 1), called *strings* or *chromosomes,* thereby creating a 'population (gene pool)' of such binary strings. Each chromosome is then mapped into a set of *real* values of the decision variables, using the upper and lower bounds of each of these. A model of the process is then used to provide values of the objective function for each chromosome. The value of the objective function of any chromosome reflects its 'fitness'. The Darwinian principle of 'survival of the fittest' is used to generate a new and improved gene pool (new generation). This is done by preparing a 'mating pool', comprising of copies of chromosomes, the number of copies of any chromosome being proportional to its fitness (Darwin's principle). Pairs of chromosomes are then selected randomly, and pairs of daughter chromosomes generated using operations similar to those in genetic reproduction. The gene pool evolves, with the fitness improving over the generations.

Three common operators are used in GA [called *s*imple GA (SGA), to distinguish it from its various adaptations] to obtain an improved (next) generation of chromosomes. These are referred to as reproduction, crossover and mutation. Reproduction is the generation of the mating pool, where the chromosomes are copied probabilistically based on their fitness values. However, no new strings are formed in the reproduction phase. *New* strings are created using the crossover operator by exchanging information among pairs of strings in the mating pool. A pair of daughter chromosomes are produced by selecting a crossover site (chosen randomly) and exchanging the two parts of the pair of parent chromosomes (selected randomly from

the mating pool). The effect of crossover may be detrimental or beneficial. It is hoped that the daughter strings are superior. If they are worse than the parent chromosomes, they will slowly die a natural death over the next few generations (the Darwinian principle at work). In order to preserve some of the good strings that are already present in the mating pool, not all strings in the pool are used in crossover. A crossover probability, P_{cross}, is used, where only $100P_{cross}$ percent of the strings in the mating pool are involved in crossover while the rest continue unchanged to the next generation. After a crossover is performed, mutation takes place. The mutation operator changes a binary number at *any* location in a chromosome from a 1 to a 0 and vice versa, with a small probability, P_{mute}. Mutation is needed to create a point in the neighborhood of the current point, thereby achieving a local search around the current solution and to maintain diversity in the population. The entire process is repeated till some termination criterion is met (the specified maximum number of generations is attained, or the improvements in the values of the objective functions become lower than a specified tolerance).

The optimal solutions to a multiobjective function optimization problem are non-dominated (or Pareto-optimal) solutions. In order to handle multiple objective functions and find Pareto-optimal solutions, the simple genetic algorithm (SGA) has been modified. The new algorithm, Non-dominated Sorting Genetic Algorithm (NSGA), differs from SGA only in the way the selection operator works.

NSGA uses a ranking selection method to emphasize the good points and a niche method to create diversity in the population without losing a stable sub-population of good points. In the new procedure, several groups of non-dominated chromosomes from among all the members of the population at any generation are identified and classified into 'fronts'. Each of the members in a particular front is

assigned a large, common, front fitness value (a dummy value) arbitrarily. To distribute the points in this (or any other) front evenly in the decision variable domain, the dummy fitness value is then modified according to a sharing procedure by dividing it by the niche count of the chromosome. The niche count is a quantity that represents the number of neighbors around it, with distant neighbors contributing less than those nearby. The niche count, thus, gives an idea of how crowded the chromosomes are in the decision variable space. Use of the shared fitness value for reproduction, thus, helps spread out the chromosomes in the front since crowded chromosomes are assigned lower fitness values. This procedure is repeated for all the members of the first front. Once this is done, these chromosomes are temporarily removed from consideration, and all the *remaining* ones are tested for non-dominance. The non-dominated chromosomes in *this* round are classified into the next front. These are all assigned a dummy fitness value that is a bit lower than the *lowest* shared fitness value of the previous front. Sharing is performed thereafter. The sorting and sharing is continued till all the chromosomes in the gene pool are assigned shared fitness values. The usual operations of reproduction, crossover and mutation are now performed. It is clear that the non-dominated members of the first front that have fewer neighbors, will get the highest representation in the mating pool. Members of later fronts, which are dominated, will get lower representations (they are still assigned some low fitness values, rather than 'killed', in order to maintain the diversity of the gene pool). Sharing forces the chromosomes to be spread out in the decision variable space. The population is found to converge very rapidly to the Pareto set. It is to be noted that any number of objectives (both minimization and maximization problems) can be solved using this procedure. A flowchart describing this technique is presented below. A more elaborate

description of GA is available in Holland (1975), Goldberg (1989) and Bhaskar *et al.* (2000a).

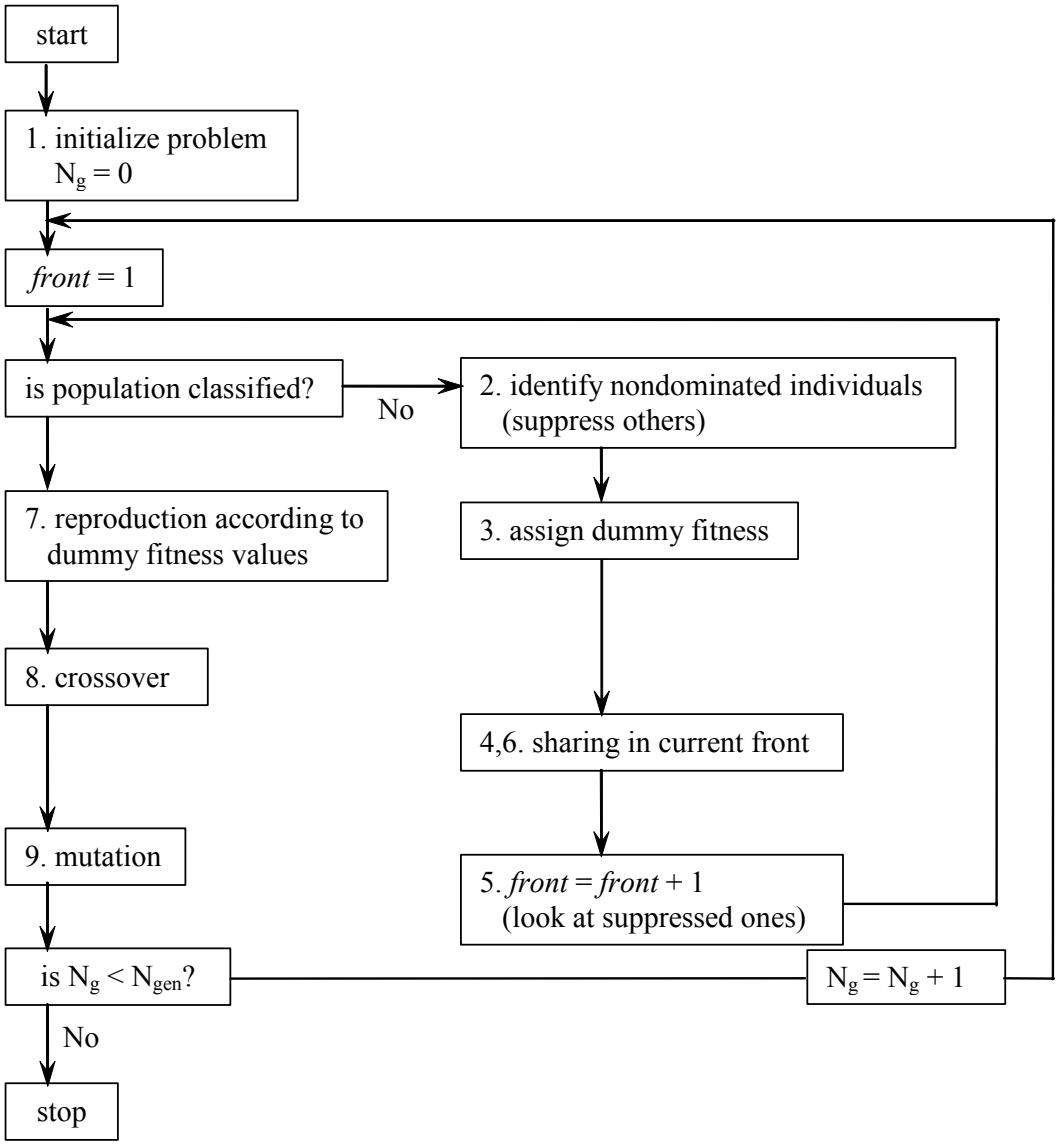

Figure A.1 A flowchart describing NSGA (Bhaskar et al., 2000a)

Appendix B Experimental Data for MeOAc Synthesis in the SMBR

Table B.1 Effect of switching time

t_s (min)	Concentration (mol/l)					
	Raffinate			Extract		
	MeOAc	H_2O	HOAc	MeOAc	H_2O	HOAc
12	0.177	0.045	0.0	0.106	0.167	0.0
16	0.391	0.016	0.0	0.008	0.174	0.0
20	0.389	0.012	0.0	0.001	0.180	0.0
24	0.416	0.023	0.0	0.001	0.179	0.0

Table B.2 Effect of eluent flow rate

Q_E (ml/min)	Concentration (mol/l)					
	Raffinate			Extract		
	MeOAc	H_2O	HOAc	MeOAc	H_2O	HOAc
1.5	0.414	0.146	0.0	0.004	0.378	0.0
2.0	0.436	0.072	0.0	0.002	0.256	0.0
3.0	0.389	0.012	0.0	0.001	0.180	0.0
4.0	0.403	0.0	0.0	0.001	0.128	0.0

Table B.3 Effect of feed flow rate

Q_F (ml/min)	Concentration (mol/l)					
	Raffinate			Extract		
	MeOAc	H_2O	HOAc	MeOAc	H_2O	HOAc
0.1	0.196	0.006	0.0	0.001	0.090	0.0
0.2	0.389	0.012	0.0	0.001	0.180	0.0
0.3	0.595	0.024	0.0	0.002	0.251	0.0
0.4	0.776	0.043	0.0	0.012	0.314	0.0

Table B.4 Effect of flow rate in section P

Q_p (ml/mi)	Concentration (mol/l)					
	Raffinate			Extract		
	MeOAc	H_2O	HOAc	MeOAc	H_2O	HOAc
0.5	0.104	0.062	0	0.130	0.160	0
1.0	0.389	0.012	0	0.001	0.180	0
1.5	0.392	0.079	0	0.0004	0.152	0
2.0	0.382	0.31	0.015	0.0005	0.045	0.0001